



**MONASH** University

# **Towards harmonious downscaled soil moisture maps from the SMAP and SMOS satellites**

**Sabah Sabaghy**

A thesis submitted for the degree of Doctor of Philosophy at  
Monash University in 2019

Faculty of Engineering, Department of Civil Engineering



## **Copyright notice**

© Sabah Sabaghy (2019). Except as provided in the Copyright Act 1968, this thesis may not be reproduced in any form without the written permission of the author.

I certify that I have made all reasonable efforts to secure copyright permissions for third party content included in this thesis and have not knowingly added copyright content to my work without the owner's permission.



# Synopsis

Recent advances in space-borne remote sensing provides an unprecedented opportunity to monitor soil moisture at global scale. The European Space Agency (ESA), and National Aeronautics and Space Administration (NASA) have developed dedicated soil moisture monitoring missions with a repeat time intervals of 3 days. Both the missions the Soil Moisture and Ocean Salinity (SMOS) and the Soil Moisture Active Passive (SMAP) use L-band passive microwave (radiometer) remote sensing technology, which is widely accepted as the most accurate technique to retrieve soil moisture dynamics in time and space. However, the coarse spatial scale ( $\sim 40$  km) of the SMOS and SMAP radiometer-only soil moisture products places a limitation on their application. While the 40 km spatial resolution is satisfactory for hydro-climatological studies, to satisfy the requirements of hydro-meteorological and agricultural applications soil moisture maps required a spatial resolution finer than 10 km and 1 km, respectively.

Use of fine resolution data on land surface features has been proposed as a solution to disaggregate the coarse passive microwave soil moisture into high to medium resolutions. This technique, called downscaling or disaggregation, takes advantage of the strengths of both passive microwave observations of soil moisture of low spatial resolution and the spatially detailed information on land surface features that either influence or represent soil moisture variability. Currently, a variety of downscaling techniques exist including radar-, optical-, radiometer-, oversampling-, soil surface attributes-, data assimilation-, and machine learning-based methods. These techniques have typically been developed and tested under differing weather and climate conditions, with no clear guidance on which technique performs the best.

Varying accuracy of downscaling techniques was found in literature, with studies indepen-

---

dently analysing the performance of each downscaling technique using different reference data sets. Until now, there has been no single study testing the performance of these downscaling techniques against a common reference data set. Therefore, this thesis has inter-compared the performance of existing radar-, optical-, radiometer-, and oversampling-based downscaled products against an extensive data set representative of south-eastern Australia, including the Soil Moisture Active Passive Experiment (SMAPEX) airborne soil moisture maps and OzNet *in situ* soil moisture measurements. This comparison revealed the relative strengths and limitations of each downscaled soil moisture. Moreover, this study has shown that the oversampling-based soil moisture downscaling technique was superior to other downscaled products in capturing the heterogeneity of reference soil moisture in space and time. The possible improvement (or deterioration) of each downscaled product was also assessed by benchmarking their accuracy against the radiometer-only retrievals of SMAP and SMOS.

The usefulness of merging these products for yielding a better estimate of soil moisture has been investigated by evaluating different combination scenarios. This has explored the potential of combining downscaled soil moisture products in generating a more temporally complete accurate sequence of soil moisture estimates than downscaled products alone. While the merging scheme improved the temporal representativeness of soil moisture products, the analysis found no improvement of combined products in terms of the spatial representativeness of soil moisture.

# **Declaration**

This thesis contains no material which has been accepted for the award of any other degree or diploma at any university or equivalent institution and that, to the best of my knowledge and belief, this thesis contains no material previously published or written by another person, except where due reference is made in the text of the thesis.

Sabah Sabaghy

June 2019



# Acknowledgements

I would like to thank my supervisors for their invaluable guidance and encouragement during the completion of my PhD journey. My sincere gratitude goes to my primary supervisor Prof. Jeffrey Walker who has offered me this PhD position. Jeff's guidance, insightful criticism and advice enabled me to create the boundary of my thesis project. The discussions I had with Jeff, and his comments on my paper and/or thesis drafts gave me real insight into the study. I would also like to thank my second supervisor, Dr. Luigi Renzullo, for his advice which widened my perspective, and his motivation which encouraged me to work harder.

To all my friends and colleagues at Monash University that made this study period an amazing experience, I would like to say a big thank you. Stefania, Ying, Valentina and Ashkan, I have experienced a great friendship with you. You were always there for me and I greatly benefited from your invaluable attitude towards research and life.

Last but by no means least, I am grateful to my family. My parents, Zahra and Mahmoud, and my siblings, Leyla and Hamed, have always provided me continuous emotional support. I owe them my strength and confidence to pursue my dreams. Then, there was my husband Maziar, my inspiration to not give up and stay strong during toughest challenges. Maziar, my research would have been impossible without your continuous love, encouragement and patience.



# Contents

<b>Synopsis</b>	<b>III</b>
<b>Declaration</b>	<b>V</b>
<b>Acknowledgments</b>	<b>VI</b>
<b>List of abbreviations</b>	<b>IX</b>
<b>List of figures</b>	<b>XIV</b>
<b>List of tables</b>	<b>XX</b>
<b>1 Introduction</b>	<b>1</b>
1.1 Importance of soil moisture . . . . .	1
1.2 Importance of high resolution moisture measurement . . . . .	2
1.3 Statement of problems related to high resolution soil moisture mapping . . .	3
1.4 Objectives and scope . . . . .	5
1.5 Outline of approach . . . . .	5
1.6 Thesis organization . . . . .	10
<b>2 Review of spatially enhanced passive microwave derived soil moisture</b>	<b>13</b>
2.1 Soil moisture measurement techniques . . . . .	13
2.2 Review of soil moisture downscaling methods . . . . .	19
2.2.1 Microwave-based downscaling techniques . . . . .	19

---

2.2.2	Optical-based downscaling techniques . . . . .	48
2.2.3	Soil surface attributes-based downscaling techniques . . . . .	58
2.2.4	Model/Data-based downscaling techniques . . . . .	62
2.3	Assessment of the strengths and weaknesses of downscaling techniques . . .	68
2.4	Unresolved challenges to soil moisture downscaling . . . . .	71
2.5	Chapter summary . . . . .	73
<b>3</b>	<b>Study area and data sets</b>	<b>75</b>
3.1	Study area . . . . .	75
3.2	The SMAPEX-4 and -5 airborne field campaigns . . . . .	77
3.2.1	Airborne sampling . . . . .	78
3.2.2	Ground sampling . . . . .	78
3.3	Airborne PLMR soil moisture maps . . . . .	82
3.4	Downscaled soil moisture products . . . . .	84
3.4.1	Radar-based . . . . .	88
3.4.2	Optical-based . . . . .	90
3.4.3	Radiometer-based . . . . .	92
3.4.4	Oversampling-based . . . . .	93
3.5	Chapter summary . . . . .	95
<b>4</b>	<b>Inter-comparison of alternative downscaled products</b>	<b>97</b>
4.1	Introduction . . . . .	97
4.2	Evaluation methodology . . . . .	101
4.2.1	Evaluation against the OzNet in situ soil moisture measurements . . .	102
4.2.2	Evaluation against the SMAPEX-4 and -5 PLMR soil moisture maps	102

---

4.3	Results . . . . .	104
4.3.1	Temporal analysis against the OzNet . . . . .	105
4.3.2	Temporal analysis against airborne PLMR soil moisture . . . . .	112
4.3.3	Spatial analysis against the airborne PLMR soil moisture . . . . .	117
4.4	Discussion . . . . .	122
4.5	Chapter summary . . . . .	126
<b>5</b>	<b>Combined downscaled soil moisture products</b>	<b>127</b>
5.1	Introduction . . . . .	127
5.2	Combining methodology . . . . .	128
5.3	Results . . . . .	132
5.3.1	Temporal analysis against the OzNet . . . . .	137
5.3.2	Temporal analysis against the airborne PLMR soil moisture . . . . .	138
5.3.3	Spatial analysis against the airborne PLMR soil moisture . . . . .	144
5.4	Discussion . . . . .	145
5.5	Chapter summary . . . . .	150
<b>6</b>	<b>Conclusions and future work</b>	<b>153</b>
6.1	Conclusions . . . . .	153
6.1.1	Review of spatially enhanced passive microwave derived soil moisture	153
6.1.2	Inter-comparison of alternative downscaled soil moisture products .	155
6.1.3	Combined downscaled soil moisture products . . . . .	156
6.1.4	Comparison of results from this study with literature . . . . .	156
6.2	Future work . . . . .	157
	<b>References</b>	<b>161</b>



## List of abbreviations

AACES	Australian Airborne Cal/val Experiments for SMOS
ALADIN	Aire Limitée Adaptation Dynamique développement InterNational
ALEXI	Atmosphere Land EXchange Inversion
AMSR-E	Advanced Microwave Scanning Radiometer-Earth observing system
AMSR2	Advanced Microwave Scanning Radiometer-Earth Observing System
ANN	Artificial Neural Network
ASAR	Advanced Synthetic Aperture Rada
ASCAT	Advanced SCATterometer
ASTER	Advanced Scanning Thermal Emission and Reflection
AVHRR	Advanced Very High Resolution Radiometer
BPNN	Back-Propagation Neural Network
CAP	Combined active-passive
CATDS	Centre Aval de Traitement des Données SMOS
CCI	Climate Change Initiative
CDF	Cumulative Distribution Function
CLASS	Canadian LAnd Surface Scheme
ComRad	Combined Radar Radiometer
DEM	Digital Elevation Model
DisPATCh	Disaggregation based on Physical And Theoretical scale Change
ECs	expansion coefficients
EMT	Equilibrium Moisture from Topography
EMT + VS	Equilibrium Moisture from Topography, Vegetation, and Soil

---

EnBKF-2	Ensemble Bias corrected Kalman Filter-2
EOF	Empirical Orthogonal Function
ESA	European Space Agency
EVI	Enhanced Vegetation Index
GEOS-5	Goddard Earth Observing System version 5
GIS	Geographic Information System
HDAS	Hydraprobe Data Acquisition System
IFOV	Instantaneous Field of View
ISBA	Interactions between Surface, Biosphere, and Atmosphere
IWS	Interferometric Wide Swath
LAI	Leaf Area Index
LDAS	Land Data Assimilation System
LSP-DSSAT	Land Surface Process-Decision Support System for Agrotechnology Transfer
LST	Land Surface Temperature
MDPI	Microwave Polarization Difference Index
METOP	METEorological OPERational
MODIS	MODerate resolution Imaging Spectro-radiometer
MOEA	Multi-Objective Evolutionary Algorithm
MSG SEVIRI	METEOSAT Second Generation Spinning Enhanced Visible and Infrared Imager
MSR	Multi Spectral Radiometer
NAFE'05	National Airborne Field Experiment held in Australia in 2005
NAFE'06	National Airborne Field Experiment held in Australia in 2006
NASA	National Aeronautics and Space Administration
NDVI	Normalized Difference Vegetation Index
NDWI	Normalized Difference Water Index
NIR	Near InfraRed
NIR-Red	Near InfraRed-Red

---

NLDAS	North American Land Data Assimilation System
NMDI	Normalized Multiband Drought Index
NRSD	NIR-Red Spectral-based Disaggregation
NSMI	Normalized Soil Moisture Index
NWP	Numerical Weather Prediction
OSSE	synthetic data from an Observation System Simulation Experiment
PALS	Passive-Active L-/S-band
PET	Potential EvapoTranspiration
PLMR	Polarimetric L-band Multi-beam Radiometer
PR	Precipitation Radar
PRI	Principle of Relevant Information
RMSD	Root Mean Square Deviation
RVM	Relevance Vector Machine
SAR	Synthetic Aperture Radar
SEE	Soil Evaporative Efficiency
SEKF	Simplified Ensemble Kalman Filter
SFIM	Smoothing Filter-based Intensity Modulation
SGP97	Southern Great Plains 1997
SGP99	Southern Great Plains Experiment in 1999
SMAP	Soil Moisture Active Passive
SMAPEX	Soil Moisture Active Passive Experiment
SMIs	Soil Moisture Indices
SMOS	Soil Moisture and Ocean Salinity
SMTMN	Soil Moisture/Temperature Monitoring Network
SRRMs	Self-Regularized Regressive Model
SSM/I	Special Sensor Microwave Imager
SWI	Soil Wetness Index
SWIR	Short-Wave InfraRed

---

TIR	Thermal InfraRed
TMI	TRMM Microwave Imager
TRMM	Tropical Rainfall Measuring Mission
TVDI	Temperature Vegetation Drought Index
TWI	Topography-based Wetness Index
ubRMSD	unbiased RMSD
VIS	Visible
VTCI	Vegetation Temperature Condition Index

# List of Figures

1.1	Summary of spatial and temporal resolution requirement of soil moisture for a range of applications (Dr. Thomas Jackson and Prof. Dara Entekhabi, personal communication). . . . .	3
1.2	Schematic of the evaluation procedure of downscaled soil moisture retrievals and their combination against airborne PLMR and OzNet <i>in situ</i> soil moisture measurements. . . . .	6
2.1	Schematic of the downscaling concept using spatially detailed information on land surface features to distribute coarse scale soil moisture to fine scale.	18
2.2	Schematic diagram of the SMAP active/passive baseline algorithm (adapted from Dr. Xiaoling Wu personal communication). . . . .	45
2.3	Schematic of the SFIM technique for downscaling coarse passive microwave brightness temperature to yield a medium resolution soil moisture retrieval.	48
2.4	Triangle/Trapezoid concept of the LST/VI feature space (adapted from Petropoulos et al., 2015 and Merlin et al., 2012). . . . .	49
2.5	Schematic of the downscaling model structure developed by Piles et al. (2012). . . . .	52
2.6	Schematic of DisPATCH downscaling method which combines accurate but coarse passive microwave observations with high resolution optical observations. . . . .	54
2.7	Summary of accuracy statistics from different downscaling techniques presented as boxplot that contains the interquartile ranges, the sample median (bar), and outliers associated with the mean (dot). * n indicates the number of validation studies that reported the accuracy of retrieval in terms of R or R <sup>2</sup> and RMSD for the particular downscaling approach, and were thus used to make this figure. . . . .	69

---

3.1	The study areas for (a) SMAPE <sub>x</sub> -4 and (b) SMAPE <sub>x</sub> -5 airborne field campaigns conducted in the Yanco region in south east of Australia. Landuse is shown along with red rectangles which delineate the coverage of airborne measurements of each campaign, being 71 km × 85 km for SMAPE <sub>x</sub> -4 and 71 km × 89 km for SMAPE <sub>x</sub> -5. Blue rectangles show the locations of the intense ground samplings and black dots are the OzNet <i>in situ</i> monitoring stations. . . . .	76
3.2	Time series of the OzNet top 5 cm <i>in situ</i> soil moisture and rainfall measurements for the period between 1st April and 1st November 2015 used in this study. The light blue line and dashed gray lines show the median and interquartile range of soil moisture measurements, respectively. The dark blue bars show the mean daily rainfall over the Yanco region. . . . .	77
3.3	The aircraft equipped with PLMR L-band passive microwave instrument.	79
3.4	The viewing configuration of PLMR on-board the aircraft (adapted from SMAPE <sub>x</sub> -1 work-plan). . . . .	79
3.5	Vegetation sampling, including: a) surface spectral reflectance measurement, b) leaf area measurement, c) destructive vegetation sampling, and d) vegetation height measurement. . . . .	80
3.6	A sample photo taken of the pin profiler that was here used to characterise the roughness profile (top), and a post-processed experimental profile extracted from this photo (bottom). . . . .	81
3.7	An Example of HDAS intensive soil moisture measurements over one of the focus farms on 17 September 2015 during the SMAPE <sub>x</sub> -5 airborne field campaign. . . . .	82
3.8	An example of the airborne PLMR soil moisture maps derived from the PLMR radiometric brightness temperature observed on 22 May 2015 during the SMAPE <sub>x</sub> -4 airborne field campaign. . . . .	83
3.9	Example of vegetation water content maps for the SMAPE <sub>x</sub> -4 and -5 airborne field campaigns. . . . .	84
3.10	Comparison of SMAPE <sub>x</sub> -4 and -5 PLMR soil moisture estimates at 3 km against aggregated intense HDAS soil moisture measurements to 3 km. Horizontal whiskers in red show the standard deviation of aggregated HDAS measurements to 3 km, while vertical whiskers in blue show the standard deviation of aggregated PLMR soil moisture estimates to 3 km. .	85

---

3.11	The coarse SMOS and SMAP passive microwave soil moisture estimates for the Yanco region during the SMAPEX-4 and -5 airborne field campaigns period. The date is written on soil moisture plots for the nearest available observations to PLMR flight days when coincident overpass data are not available. Notes: missing data are shown in white colour and, A and D stand for ascending and descending overpasses, respectively. . . . .	89
3.12	An example of the SMAP A/P soil moisture map observed on 17 April 2015.	90
3.13	An example of the SMAP MOEA soil moisture map observed on 15 April 2015. . . . .	91
3.14	Examples of the SMOS DisPATChA and DisPATChD soil moisture maps observed on 3 April 2015. . . . .	92
3.15	Examples of the SMAP VTCI and SMOS VTCI soil moisture maps observed on 1 and 2 September 2015, respectively. . . . .	92
3.16	An example of the SMAP SFIM soil moisture map observed on 09 April 2015. . . . .	93
3.17	An example of the SMAP EnhancedA and EnhancedD soil moisture maps observed on 03 July 2015. . . . .	94
4.1	Schematic of the procedure used for evaluation of the downscaled soil moisture retrievals against the airborne PLMR and the OzNet <i>in situ</i> soil moisture measurements. . . . .	101
4.2	Schematic of the downscaled soil moisture product grids at (a) 9 km and (b) 10 km. The SMAPEX-4 and -5 flight coverage and location of the OzNet stations are highlighted in magenta rectangles and red dots, respectively. The cyan rectangle shows the common analysis area for both airborne field campaigns. Green squares show the chosen pixels for analysis of soil moisture products against the OzNet measurements. These pixels contain the largest number of the OzNet stations (more than four); the number of available stations is written in the pixel. . . . .	103
4.3	Time series plots of PLMR observed reference soil moisture estimates and the range of the downscaled soil moisture estimates for the Yanco region during the SMAPEX-4 period. DisPATCh, VTCI-based and PLMR soil moisture maps are presented at their original scale of 1 km as well as 9 km after aggregation. The date is written on soil moisture plots for the nearest available observations to PLMR flight days when coincident overpass data are not available. Note: missing data are shown in white colour. . . . .	106

---

4.4	As for Figure 4.3 but for the SMAPEx-5 period. . . . .	107
4.5	Sample of the temporal evolution of PLMR observed reference soil moisture estimates, the median of measurements from the OzNet stations, coarse SMAP and SMOS at 9 km without any downscaling technique being applied, and the range of the downscaled soil moisture estimates for the Yanco region during the period between 1 April and 1 November 2015; d indicates the number of days for which the downscaled soil moisture products were available over the SMAPEx-4 and -5 flight area. . . . .	108
4.6	Summary of results obtained from temporal analysis of soil moisture products at (a) 1 km and (b) 9 km against the OzNet. For 9 km products, only pixels with the largest number of stations were chosen. Each boxplot displays the distribution of the accuracy statistics of different downscaled soil moisture products based on the interquartile range, the maximum and minimum range, and the statistics median (bar) associated with the mean (dot). d indicates the number of the downscaled soil moisture products that were used in this analysis and n indicates the number of statistical parameters that are summarized in this figure. . . . .	110
4.7	As for Figure 4.6 but for the comparison against airborne PLMR soil moisture at 1 km in which analysis was carried out for all the pixels covering the study area. These results are from different scenarios including: a) the equal number of downscaled soil moisture products captured during the SMAPEx-4, b) all available products during the SMAPEx-4, and c) products captured over the entire SMAPEx-4 and -5 airborne field campaigns' period. Here s stands for the dimension of analysis area arranged in row $\times$ column. Note: the performance analysis of the VTCI-based products was not possible for the SMAPEx-4 period as only one SMOS VTCI and two SMAP VTCI soil moisture maps were available. . . . .	113
4.8	As for Figure 4.7 but for the comparison against airborne PLMR soil moisture at 9 km. . . . .	116
4.9	Summary of results obtained from spatial analysis of soil moisture products at 1 km against airborne PLMR soil moisture in which analysis was carried out for all the pixels covering the study area. These results are from different scenarios including: a) the equal number of the downscaled soil moisture products captured during the SMAPEx-4, b) all available products during the SMAPEx-4, and c) products captured over the entire SMAPEx-4 and -5 airborne field campaigns' period. . . . .	119
4.10	As for Figure 4.9 but for the spatial analysis at 9 km. . . . .	120
5.1	Schematic diagram showing the combination procedure. . . . .	129

---

5.2	Error variance maps used for merging the downscaled soil moisture products during the SMAPEX-4 airborne field campaign. . . . .	131
5.3	Averaged spatial auto-correlation analysis of relative uncertainty of downscaled soil moisture products. . . . .	132
5.4	Time sequence plots of the combinations of downscaled soil moisture products from the five different combination scenarios described in Table 5.2 across the SMAPEX-4 airborne field campaign. Note: Missing data are shown in white colour. . . . .	134
5.5	As for Figure 5.4 but across the SMAPEX-5 airborne field campaign. . . .	135
5.6	Sample of PLMR airborne time series of soil moisture estimates for the 9 km pixel having the largest number of OzNet stations (shown in Figure 4.2). Shown here is the median of measurements from the OzNet stations, coarse SMAP and SMOS soil moisture retrievals posted to 9 km without any downscaling technique being applied, and combination scenarios for the Yanco region during the SMAPEX-4 and -5 airborne field campaigns' period. This temporal evolution is generated for 9 and 10 km pixels (shown in Figure 4.2) having the largest <i>in situ</i> monitoring stations. Note: d indicates the number of days for which soil moisture products were available over the SMAPEX-4 and -5 flight area. . . . .	136
5.7	Boxplots summarising the interquartile range, the maximum and minimum range, and the median (bar) associated with the mean (dot) of statistical results obtained from temporal analysis of combined soil moisture products at (a) 1 km and (b) 9 km against OzNet <i>in situ</i> measurements for the SMAPEX-4 airborne field campaign. For 9 and 10 km products, only pixels with largest number of stations (see Figure 4.2) were chosen. d indicates the number of downscaled soil moisture products that were used in this analysis and n indicates the number of statistical parameters that are summarised in this figure. . . . .	138
5.8	As for Figure 5.7 but for the SMAPEX-5 airborne field campaign flight dates.	139
5.9	As for Figure 5.7 but for the comparison against airborne PLMR soil moisture at 1 km in which analysis was carried out for all the pixels covering the study area. These results are from the different scenarios including: a) combined products across 5 days when all downscaled soil moisture products were available on the same date during the SMAPEX-4, b) all available products during the SMAPEX-4, and c) all available products during the SMAPEX-5. Here s stands for the dimension of analysis area arranged in rows $\times$ column. Please be noted that the maximum RMSD obtained for S4 and S5 products during the SMAPEX-5 was 0.55 and 0.56 $\text{m}^3 \text{m}^{-3}$ , respectively . . . . .	142

---

5.10	As for Figure 5.9 but for the comparison of combined products at 9 km against airborne PLMR soil moisture. . . . .	143
5.11	Boxplots summarising the interquartile range, the maximum and minimum range, and the statistics median (bar) associated with the mean (dot) of statistical results obtained from spatial analysis of combined soil moisture products at 1 km. These results are from the different scenarios including: a) combined products across 5 days when all downscaled soil moisture product were available on the same date during the SMAPEX-4, b) all available products during the SMAPEX-4, and c) all available products during the SMAPEX-5. . . . .	146
5.12	As for Figure 5.11 but for the comparison of combined products at 9 km against airborne PLMR soil moisture. . . . .	147
5.13	The correlation coefficient maps generated between time series of error estimates of downscaled soil moisture products at 1 km during the SMAPEX-4 airborne field campaign. Note: missing data shown in white colour are pixels for which less than 5 pairs of coincident error estimates were available.	149
5.14	As for Figure 5.13 but for the downscaled soil moisture products originally at 9 km or mapped into a 9 km grid. . . . .	149
5.15	Boxplots summarising the interquartile range, the maximum and minimum range, and the statistics median and average (bar and dot, respectively) associated with the mean of correlation coefficients obtained from comparison of error estimates of downscaled soil moisture products at a) 1 km and b) 9 km. . . . .	150

# List of Tables

2.1	Summary of the strengths and weaknesses of each downscaling method listing all the methods and pros/cons. . . . .	20
2.2	Summary table on accuracy of soil moisture downscaling methods including the list of methods, references, and main inputs. . . . .	22
3.1	Summary table on the downscaled and non-downscaled soil moisture products used in the inter-comparison according to the downscaling techniques and approaches. Included is the product definition, key references, and main downscaling inputs as applicable. . . . .	86
4.1	Averaged accuracy of the downscaled and non-downscaled soil moisture products at 9 km, evaluated against the airborne PLMR soil moisture and the OzNet <i>in situ</i> soil moisture measurements. Notes: i) the evaluation of SMAP MOEA and A/P was only carried out during the short SMAPEX-4 period due to radar availability, and ii) gray cells indicate the accuracy of products with superior performance to the other downscaled soil moisture products. . . . .	123
5.1	Availability of downscaled soil moisture products used for combination. . .	129
5.2	List of downscaled soil moisture product combination scenarios tested. . . .	131
5.3	Averaged accuracy of the combined products at 1 km, evaluated against the airborne PLMR soil moisture and OzNet <i>in situ</i> soil moisture measurements. Gray cells indicate the accuracy of products with slightly better performance than the other combined products. . . . .	141
5.4	Comparison of results from the combined products with the downscaled soil moisture products based on literature review. . . . .	144



# Chapter 1

## Introduction

This thesis explored the most appropriate downscaling methodology(ies) for the low resolution soil moisture products of the Soil Moisture Active Passive (SMAP) and the Soil Moisture and Ocean Salinity (SMOS) satellite missions for soil moisture mapping at higher spatial resolution. It also evaluated the potential for producing a combination of downscaled soil moisture retrievals. The aim is to achieve a spatial resolution finer than 10 km with a target accuracy of approximately  $0.04 \text{ m}^3 \text{ m}^{-3}$ .

Existing downscaling techniques for high resolution soil moisture mapping were first systematically and critically reviewed. This review provides the reported accuracy of each downscaling techniques, which have been independently derived using different data sets. Consequently, a quantitative assessment of the existing radar-, optical-, oversampling-, and radiometer-based downscaling approaches was undertaken using an extensive data set collected specifically for that purpose, being the Soil Moisture Active Passive Experiment (SMAPEX)-4 and -5 airborne field campaigns, and the OzNet *in situ* stations. Combinations of soil moisture retrievals from these different downscaling algorithms were then tested as a step towards harmonious multi-sensor high resolution soil moisture retrieval for a typical Australian landscape.

### 1.1 Importance of soil moisture

Land-atmosphere interactions are affected by soil moisture on a global scale (e.g. Entekhabi et al., 1996, 2010; Petropoulos et al., 2015), thus exerting an impact upon the climate and

weather (e.g. Entekhabi, 1995; Jung et al., 2010; Lakshmi, 2013; Seneviratne et al., 2010; Taylor, 2015; Western et al., 2002) by influencing the partitioning of the incoming radiant energy at the land surface into sensible and latent heat fluxes (Xia et al., 2014). Soil moisture variation also controls the water and energy cycle components through the amount of evapotranspiration, which affects the soil surface wet and dry patterns that in turn affect precipitation (Hirschi et al., 2011; Koster et al., 2004). The volume of surface run-off and groundwater recharge also depends upon the soil moisture by way of the precipitation infiltration rate into the soil (Tuttle and Salvucci, 2014). Regional characterization of soil moisture variability at short time intervals would therefore greatly assist understanding of the land-atmosphere system.

## **1.2 Importance of high resolution moisture measurement**

Obtaining accurate information on soil moisture at an appropriate temporal and spatial scales is challenging to achieve with global coverage using traditional approaches, due to the high spatial and temporal variability of soil moisture. This variation is caused by the heterogeneous nature of soil properties, topography, land cover, and meteorology (e.g. rainfall and evapotranspiration) that vary as a function of scale (e.g. Crow et al., 2012; Vereecken et al., 2008). Meteorological forcing has a dominant control on the soil moisture spatial pattern at watershed, regional and continental scales (Crow et al., 2012; Jana, 2010), unlike the field and point scales where the soil moisture varies due to land cover, topography and soil properties. Accordingly, fine-scale soil moisture measurements can provide a vital piece of information for economic, social and environmental planning. Development of field and watershed scale soil moisture measurements is therefore of benefit to agricultural production and better understanding of rainfall-runoff responses, respectively (Robinson et al., 2008). Moreover, measurement of soil moisture at regional and continental scales is important for interpreting land-surface-atmosphere interactions (Kerr et al., 2001; Robinson et al., 2008). Figure 1.1 summarizes the temporal and spatial resolution requirements of soil moisture in a range of application areas.

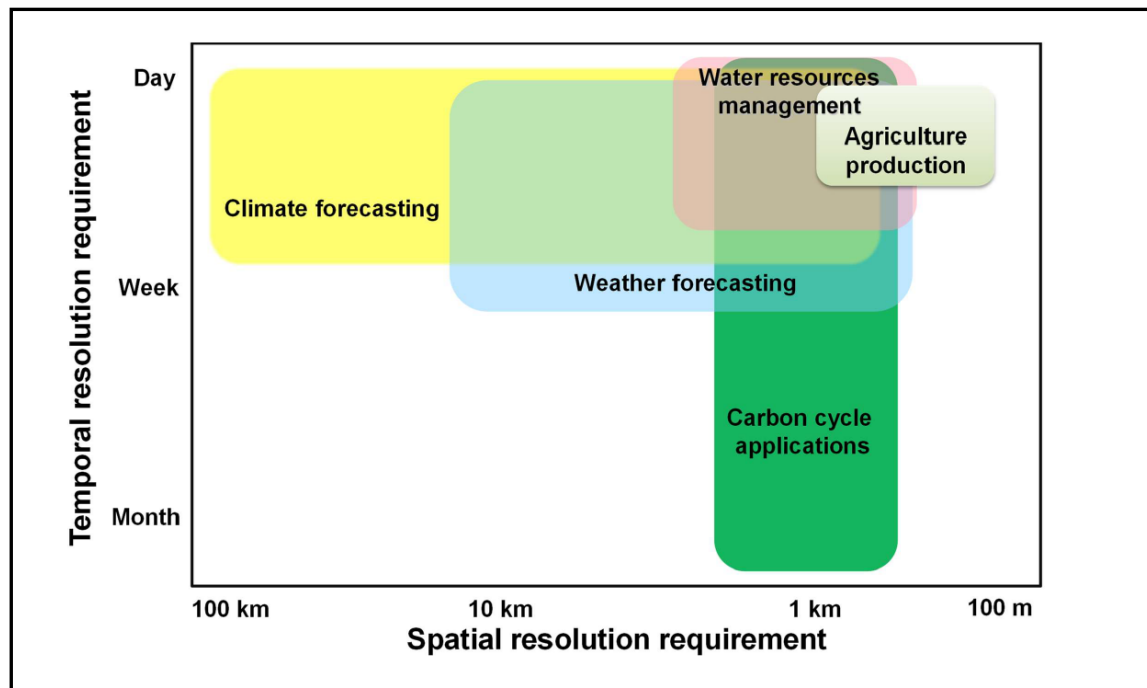


Figure 1.1: Summary of spatial and temporal resolution requirement of soil moisture for a range of applications (Dr. Thomas Jackson and Prof. Dara Entekhabi, personal communication).

### 1.3 Statement of problems related to high resolution soil moisture mapping

Remote sensing can capture spatial and temporal patterns of soil moisture in the landscape, with low frequency passive microwave remote sensing a proven technology for providing soil moisture estimates. Particularly useful are passive microwave observations at L-band because of their high sensitivity to soil moisture, and their favourable signal-to-noise ratio (Njoku and Entekhabi, 1996). The ESA as well as the NASA have launched L-band passive microwave instruments on board the Soil Moisture and Ocean Salinity (SMOS) and Soil Moisture Active Passive (SMAP) satellites in 2009 and 2015, respectively. However, L-band radiometers monitor global surface soil moisture at approximately 40 km spatial resolution, and it is this coarse spatial scale that restricts the range of application of the retrievals to only hydro-climatological studies (Entekhabi et al., 2008b). Development of a consistent time series of soil moisture maps at moderate spatial resolution (1 to 10 km) is vital for SMOS and SMAP soil moisture to be used across a wider range of applications (Entekhabi et al., 2010), including agricultural production, water resources management and carbon

cycle studies.

Downscaling, otherwise known as disaggregation, has been proposed as the solution to spatially enhance these coarse resolution soil moisture observations, through association with complementary observations, or ancillary information about the land surface features at higher spatial resolution. Such information includes solar reflectance, thermal emission, passive microwave emissions at a higher frequency, radar backscatter, soil or surface attributes such as topography and soil properties, and land surface modelling. Each of these ancillary data sources has its own strengths and limitations in terms of, for example, sensitivity to surface soil moisture dynamics and availability.

While a variety of downscaling techniques, otherwise known as disaggregation, have been proposed to improve the spatial scale of passive microwave derived soil moisture (Peng et al., 2017), there has been no rigorous test to assess the relative strengths and weaknesses of their performance. Moreover, combination of the different downscaled soil moisture products for a consistent time series and better temporal and spatial representation of soil moisture has not been tested. Consequently, this research first reviewed the strengths and weaknesses of downscaling techniques based on their pros and cons as well as the accuracy of each downscaling techniques based on its published, derived from comparison against typically different reference data sets. The lack of information about the performance of different downscaled soil moisture products for a specific set of reference conditions stimulated an evaluation of the radar-, optical-, radiometer-, and oversampling-based downscaling methodologies available, for a typical Australian climate and landscape. These investigations have helped identify the best downscaling algorithm(s) for application to the SMAP and SMOS satellites. This research ultimately proposes a combination of the different downscaled soil moisture products, demonstrating the potential for a better representation of soil moisture than from the individual downscaled products alone to produce a consistent time series of downscaled soil moisture retrievals at a resolution finer than 10 km,

## 1.4 Objectives and scope

The principal objective of this research was to determine the most appropriate downscaling methodology(ies) which yields the best overall soil moisture estimation at higher resolution based on literature, and direct comparison against each other using a common reference data set. A technique for combination of downscaled soil moisture retrievals was also developed for testing the performance of a merged disaggregated soil moisture product, with the aim to provide a more accurate soil moisture map than that form any of the individual downscaled products alone. Additional objectives included benchmarking the performance of down-scaled products against the radiometer-only soil moisture retrievals of SMAP and SMOS. The intention of this comparison was to reveal if downscaled soil moisture products could surpass the coarse passive soil moisture estimates in terms of accuracy, and to quantify the extent of possible improvement (or deterioration).

Reference data used for assessment of radiometer-only products, downscaled products and combinations include ground measured near-surface soil moisture content from the OzNet stations (Smith et al., 2012) in the Murrumbidgee catchment and experimental airborne soil moisture maps collected from the SMAPEX-4 and -5 airborne field campaigns. Coincident use of airborne and ground based soil moisture measurements for evaluation represents a significant contribution to address unresolved questions in the soil moisture remote sensing community regarding the reliability of remotely sensed soil moisture evaluation against sparse *in situ* soil moisture measurements.

## 1.5 Outline of approach

This thesis was conducted following three main steps, including: i) systematic review and comparison of current downscaling techniques based on literature review, ii) inter-comparison of soil moisture products based on direct comparison of them against each other, and iii) combination of soil moisture retrievals from different downscaled products to increase the accuracy of soil moisture maps at finer resolution than 10 km. Steps (i) to (iii) are described as below and a diagram of the approach is outlined in Figure 1.2.

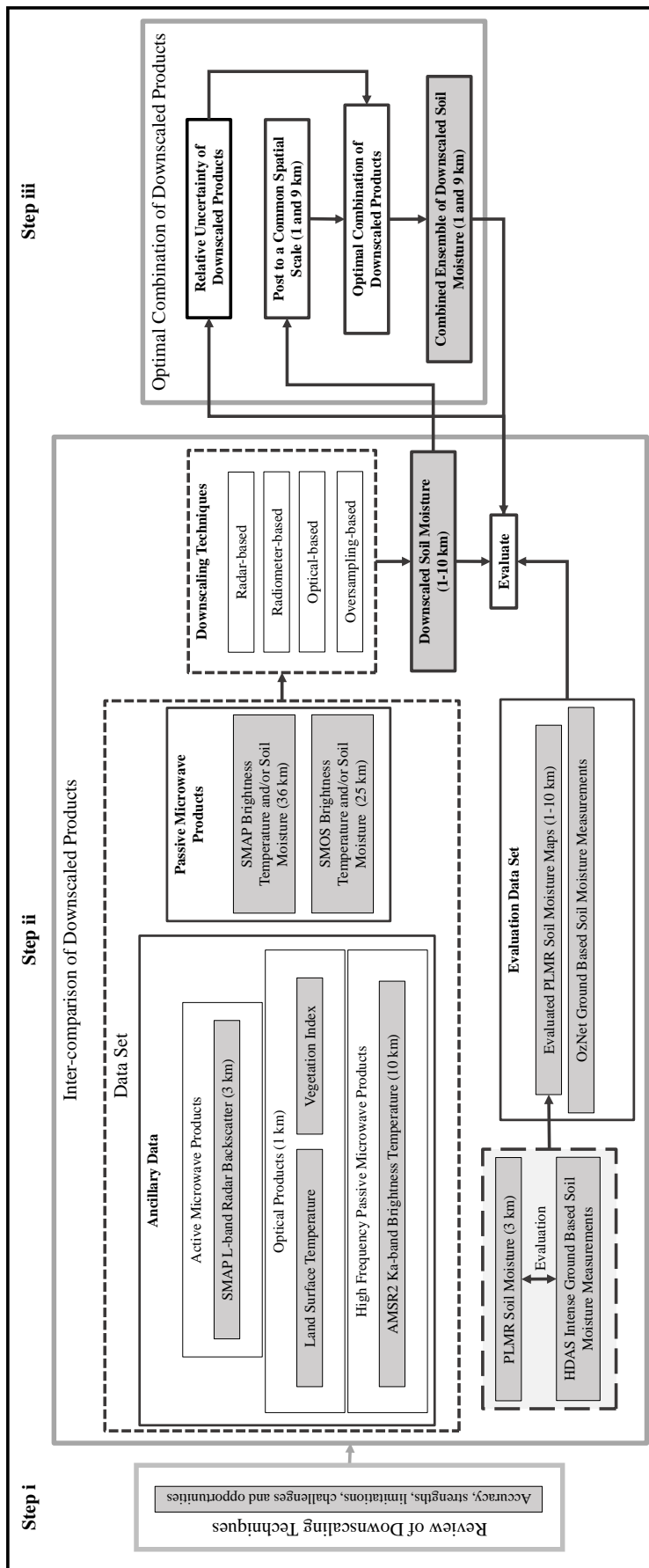


Figure 1.2: Schematic of the evaluation procedure of downscaled soil moisture retrievals and their combination against airborne PLMR and OzNet *in situ* soil moisture measurements.

**Step i)** Existing downscaling techniques for high resolution soil moisture mapping were systematically and critically reviewed. This review revealed the strengths and limitations associated with each technique, specifically in relation to the suitability and/or applicability in terms of the accuracy of soil moisture products, and availability of the land surface feature data, which are the key components in mapping accurate soil moisture. This work involved preparation of a comprehensive literature survey of downscaling methods and how they operate to improve soil moisture spatial scale. Subsequently, an overview and discussion on the advantages, drawbacks and knowledge gaps related to each approach was provided to highlight the opportunities and challenges related to the research in this field.

**Step ii)** Airborne L-band passive microwave brightness temperature were collected during the SMAPEX-4 and -5 airborne field campaigns, using the PLMR instrument concurrent with the SMAP and SMOS satellite overpasses. The Polarimetric L-band Multi-beam Radiometer (PLMR) radiometric brightness temperature observations were used to derive a reference airborne soil moisture data set. The accuracy of the reference airborne PLMR soil moisture maps were then quantified using INTENSIVE ground soil moisture sampling data that were conducted concurrent to flight acquisitions. The involvement of this thesis candidate in the SMAPEX-4 and -5 airborne field campaigns included intensive *in situ* measurement of soil moisture by Hydraprobe Data Acquisition System (HDAS) , collecting and post-processing the surface roughness measurements, producing daily vegetation water content maps and evaluation of derived PLMR airborne soil moisture maps.

A range of different radar-, optical-, radiometer-, and oversampling-based downscaling methods were benchmarked with SMOS and SMAP coarse passive microwave observations, as well as the data mentioned above to consistently evaluate their performance. This inter-comparison was undertaken over the Yanco region using the SMAPEX-4 and 5 field campaign data including the evaluated airborne-derived 1 km resolution PLMR soil moisture maps, and OzNet *in situ* soil moisture measurements as evaluation references. The coarse SMAP and SMOS passive soil moisture products were evaluated against each other and reference data including airborne PLMR soil moisture maps and OzNet *in situ* measurements. This was to: i) understand to what extent SMAP and SMOS coarse soil moisture are correlated, and ii) indicate the improvement of downscaled soil moisture products over

the coarse passive microwave soil moisture products. The methods assessed as part of this thesis are as outlined below.

The SMAP soil moisture was downscaled from 36 to 9 km using the radar-based downscaling techniques, including: i) the baseline active/passive method of SMAP (Das et al., 2014) and, ii) the Multi-Objective Evolutionary Algorithm (MOEA) by Akbar et al. (2016). The SMAP baseline active/passive algorithm downscales the SMAP Level 2 brightness temperature (SPL2SMP) using a linear correlation between SMAP Level 2 Radar backscatter (SPL2SMA) and brightness temperature. Soil moisture is then estimated by applying the radiative transfer model (single channel algorithm, Jackson, 1993) to the downscaled brightness temperature. These estimates are available at the NASA National Snow and Ice Data Center Distributed Active Archive Center (NSIDC DAAC) website as SMAP Level 3 Radar/Radiometer Global Daily 9 km EASE-Grid Soil Moisture, Version 3 (SPL3SMAP). The core of the MOEA technique is a joint cost function which optimizes accuracy and spatial scale of soil moisture retrieval through giving more weight to the most accurate soil moisture retrievals from either radar backscatter or brightness temperature. The MOEA technique was applied to the SMAP Level 2 Radiometer Half-Orbit 36 km EASE-Grid Soil Moisture, Version 2 and SMAP Level 1C Radar Half-Orbit High-Resolution backscatter Data on 1 km Swath Grid, Version 1 (SPL1CS0) pairs.

Two types of physically based optical downscaling techniques were applied to the daily global SMOS Level 3 radiometric soil moisture retrievals, obtained from i) the SMOS observations at mean spatial scale of 43 km and posted on the 25 km grid (SMOS operational MIR CLF31A/D, version 3.00 obtained from the Centre Aval de Traitement des Données SMOS (CATDS) website) and ii) the SMAP Level 3 Radiometer Global Daily soil moisture posted on the 36 km EASE-Grid, in order to achieve a 1 km spatial resolution; the Disaggregation based on Physical And Theoretical scale Change (DisPATCH; Merlin et al., 2013) and the Vegetation Temperature Condition Index (VTCI) (Peng et al., 2015, 2016) approaches were applied.

The DisPATCH model utilizes the SMOS L3 radiometric soil moisture (SMOS operational, version 2.8 obtained from the Centre Aval de Traitement des Données SMOS (CATDS) web-

site) as background, and a high resolution approximation of the Soil Evaporative Efficiency (SEE) – produced using the MODerate resolution Imaging Spectroradiometer (MODIS) soil temperature and vegetation index data – to downscale soil moisture to a resolution of 1 km. This technique was applied to the ascending and descending SMOS soil moisture observations resulting in two DisPATCh products, the ascending DisPATCh (DisPATChA) and descending DisPATCh (DisPATChD).

The VTCI technique uses the high resolution VTCI as the downscaling factor. The VTCI is a thermal based proxy which is used as a drought monitoring index (Wang et al., 2001). It is calculated based on the triangular/trapezoidal feature space constructed from 4 day composite MODIS Leaf Area Index (LAI, MCD15A3) at 1 km resolution and the daily Aqua MODIS day-and night-time land surface temperature difference (MYD11A1).

Downscaled SMAP soil moisture retrievals were also produced at 10 km using the radiometer-based Smoothing Filter-based Intensity Modulation (SFIM) model applied by Gevaert et al. (2015). In the SFIM procedure, SMAP Level 2 brightness temperature (SPL2SMP) is down-scaled to the resolution of the Advanced Microwave Scanning Radiometer-Earth Observing System (AMSR2) Ka-band observations (~10 km), using a weighting factor. This weighting factor was derived from a ratio between the Ka-band brightness temperature value for each grid cell at approximately 10 km and the average of Ka-band brightness temperature across the coarse scale of SMAP brightness temperature observations. From downscaled SMAP brightness temperature, soil moisture content was estimated through application of the Land Parameter Retrieval Model (LPRM, Owe et al., 2008).

An oversampling-based technique (Chan et al., 2018) which is based on the Backus-Gilbert interpolation method (Backus and Gilbert, 1970, 1967) was also used to enhance not only the spatial scale of SMAP brightness temperature but also its accuracy. The Backus-Gilbert is a theory of interpolation which provides brightness temperature at 9 km by averaging brightness temperature centered near a particular radius with a relatively short length of intervals. Soil moisture was then derived by applying a radiative transfer model to the brightness temperature posted onto the 9 km grid. This technique was applied to the morning/descending and afternoon/ascending SMAP level 1B Radiometer Half-Orbit Time-Ordered brightness

Temperature products at  $47 \text{ km} \times 36 \text{ km}$  and resulted in two series of products, the EnhancedD and EnhancedA, respectively.

**Step iii)** The final stage of this research was to examine the performance of combined down-scaled soil moisture products from the various merging scenarios, with a particular expectation of capturing the spatio-temporal dynamic of ground based and airborne soil moisture more accurately. A Gaussian merging approach, which is also known as the inverse variance weighted averaging approach (Lee et al., 2016), was used to combine the different sources of downscaled retrievals. The ESA Climate Change Initiative (CCI) program uses this same merging scheme to produce the ESA CCI soil moisture data, which is a combination of various single-sensor active and passive microwave soil moisture products (Dorigo et al., 2017).

Applying this merging technique to the downscaled soil moisture products is based on assuming the soil moisture retrieval error to be independent and that it can be approximated by normal random variables. Taking the statistical uncertainties in downscaled soil moisture contents into the soil moisture retrieval procedure, the precision of final retrievals was expected to depend to a great extent on the accuracy of the initial soil moisture content guess, the error estimates and the available downscaled data.

## 1.6 Thesis organization

The research included in this thesis is organized into six chapters. **Chapter 2** is a review of the soil moisture measurement techniques, the importance of soil moisture downscaling, and existing downscaling techniques for spatial resolution improvement of coarse passive microwave soil moisture products. This chapter presents a summary of the strengths and weaknesses of each downscaling technique and a quantitative assessment of their performances based on the reported accuracy in current literatures. This work has been published in the journal *Remote Sensing of Environment* as a review paper:

**Sabaghy, S.,** Walker, J. P., Renzullo, L. J., and Jackson, T. J. (2018). Spatially enhanced passive microwave derived soil moisture: Capabilities and opportunities. 209:551

– 580, 2018

**Chapter 3** gives the description of the study area and key reference data sets used for evaluation of the downscaled and combined soil moisture products in this thesis. It concludes with an evaluation of the PLMR airborne soil moisture maps against intensive ground sampling of soil moisture and description of the downscaled soil moisture products used in evaluation and combining method. This work has been submitted to the journal Remote Sensing of Environment as a data paper. My involvement in this paper was: i) producing the daily vegetation water content maps used for PLMR airborne soil moisture retrieval, and ii) evaluating the derived PLMR airborne soil moisture maps. I was also responsible for intensive HDAS *in situ* measurement of soil moisture and surface roughness sampling during the SMAPEX-4 and -5 airborne field campaigns, and post-processing the surface roughness measurements after the SMAPEX experiments.

Ye, N., Walker, J. P., Wu, X., Jeu, R. de, Entekhabi, D., Gao, Y., Jackson, T. J., Jonard, F., Kim, E., Merlin, O., Pauwels, V., Renzullo, L., Rüdiger, C., **Sabaghy, S.**, von Hebel, C., Yueh, S. H., and L. Zhu. The Soil Moisture Active Passive Experiments: Towards calibration and validation of the SMAP mission. In review.

The inter-comparison of downscaled products benchmarked with the PLMR airborne soil moisture maps and *in situ* OzNet measurements is provided in **Chapter 4**. Preliminary results from this work were published as an invited peer-reviewed conference paper, with the full results submitted to the journal Remote Sensing of Environment for review. My role in this co-authored paper was to set up the collaboration with the relevant research groups around the world to provide me with downscaled soil moisture products so that I could play the role of independent broker in doing the comparison. I undertook all the evaluation analysis (including temporal analysis against the OzNet *in situ* soil moisture measurements and PLMR airborne observations, and spatial analysis against the PLMR airborne soil moisture maps), all the writings and interpretation of results.

**Sabaghy, S.**, Walker, J.P., Renzullo, L.J., Akbar, R., Chan, S., Chaubell, J., Das, N., Dunbar, R.S., Entekhabi, D., Gevaert, A., Jackson, T.J., Merlin, O., Moghaddam, M., Loew, A., Peng J., Piepmeier, J., Rüdiger, C., Stefan, V., Wu, X., Ye, N., and Yueh, S..

Comprehensive analysis of alternative downscaled soil moisture products. In review.

**Sabaghy, S.**, Walker, J.P., Renzullo, L.J., Akbar, R., Chan, S., Chaubell, J., Das, N., Dunbar, R.S., Entekhabi, D., Gevaert, A., Jackson, T.J., Merlin, O., Moghaddam, M., Peng J., Piepmeier, J., Piles, M., Rüdiger, C., Stefan, V., Wu, X., Ye, N., and Yueh, S. (2017). Comparison of downscaling techniques for high resolution soil moisture mapping, In Proceedings of IEEE International Geoscience and Remote Sensing Symposium (IGARSS), Fort Worth, Texas, USA, 23-28 July, 2017.

**Chapter 5** develops a combination of downscaled products to examine the performance of an integrated downscaled product in terms of accuracy, compared to the individual downscaled products alone. **Chapter 6** presents the conclusions of this research and discusses the direction for future work and research identified based on this research.

## Chapter 2

# Review of spatially enhanced passive microwave derived soil moisture

This chapter provides background knowledge about the soil moisture measurement techniques and importance of soil moisture downscaling, followed by a systematic and critical review of existing downscaling techniques for high resolution soil moisture mapping. Strengths and limitations associated with each technique are discussed, specifically in relation to the suitability and/or applicability in terms of the accuracy of soil moisture products, and availability of the land surface feature data, which are the key component in mapping accurate soil moisture. A detailed background of the downscaling methods and how they operate to improve soil moisture spatial scale are also provided. Subsequently, there is an overview and discussion on the advantages, drawbacks and knowledge gaps related to each approach to highlight the opportunities and challenges related to the research in this field. This review provides a detailed description of the limitations of the various downscaling techniques, so as to move forward the development of high resolution soil moisture mapping from coarse passive microwave observations and summarising the accuracy of the different approaches. The work in this chapter has been published in Remote Sensing of Environment (Sabaghy et al., 2018) .

### 2.1 Soil moisture measurement techniques

Historically, ground sampling was the only possible approach to measuring soil moisture. However, the sparseness of point measurement stations makes the use of *in situ* measurements for capturing the spatially variable nature of soil moisture impractical due to their

high maintenance and operation expenses. The need for global soil moisture monitoring that compliments the sparsely distributed ground measurements has led to the development of space-borne remote sensing (e.g. Entekhabi et al., 1999, 2010; Kerr et al., 2012; Njoku et al., 2002), covering the Earth's surface with a temporal frequency of a few days. Consequently, a number of sensors have been launched on space-borne platforms over the past four decades to acquire the electromagnetic emission, reflection and/or scattering from the land surface, but not necessarily designed for soil moisture.

Sensors are classified according to the electromagnetic spectrum in which they monitor the Earth's surface. The regions of the spectrum of greatest interest for soil moisture are the optical and microwave. Optical remote sensing measures the solar reflective (Visible (VIS), Near InfraRed (NIR), and Short-Wave InfraRed (SWIR) bands) and/or thermal emissive (Thermal InfraRed (TIR) band) regions of the electromagnetic spectrum. These measurements have been used to determine spatial soil moisture variations by monitoring changes in surface albedo (e.g. Dalal and Henry, 1986; Leone and Sommer, 2000; Liu et al., 2002) and soil heat capacity (Petropoulos et al., 2015). While this information can be observed at a 1 km or better spatial resolution on a (cloud-free) daily basis, the signal is directly related to only the very top millimetres of the soil surface for bare soil, or to the surface of the leaves if vegetated. Moreover, the relationship to soil moisture typically depends on evaporative demand and/or vegetation variation across seasons, which limits the potential application of optical observations for direct soil moisture retrieval (Petropoulos et al., 2015). These optical observations also suffer from being attenuated by the atmosphere, and are unable to provide useful data under cloudy skies. This makes the interpretation of optically-based soil moisture predictions complicated because data on the surface micro-meteorological and atmospheric information is required for corrections (Zhang and Wegehenkel, 2006). Access to such data is limited at global scale, thus restricting the application of optical remote sensing for direct soil moisture estimation.

The conversion of remotely sensed solar reflection/albedo data to soil moisture is primarily based on the color of the soil or vegetation. Thus, information about soil mineral composition, organic matter, local incidence angle and vegetation type is required (e.g. Wang and Qu, 2009). For bare soil the determination of soil moisture is limited to observing and in-

terpreting changes in soil color, with moist soil being darker than dry soil. When there is a layer of vegetation, observations primarily reflect changes in vegetation color and/or water in the vegetation. Several land surface indices e.g. Normalized Difference Vegetation Index (NDVI) by Rouse et al. (1974), Normalized Difference Water Index (NDWI) by Gao (1996), and Normalized Multiband Drought Index (NMDI) by Wang and Qu (2007) were developed to suppress vegetation and/or plant color impact. However, their application is limited by the factors mentioned previously.

The utility of TIR remote sensing for soil moisture mapping has been demonstrated in several studies (e.g. Anderson et al., 2007; Friedl and Davis, 1994; Muller and Décamps, 2001; Schmugge et al., 1980; Verhoef et al., 1996). These studies have shown that while there is a negative correlation between the diurnal range in surface soil temperature and the surface soil moisture content, moist soil is cooler in daytime and warmer at night-time than dry soil. This is because the presence of water, which has a greater heat capacity, leads to moist soil having a greater resistance to temperature change than dry soil. These TIR techniques, which use the thermal inertia concept for estimation of soil moisture, are often based on using the TIR imagery in energy balance calculations (e.g. Goward et al., 2002) or hydrological models (e.g. Coppola et al., 2007; Minacapilli et al., 2009). The thermal inertia principle correlates changes of soil temperature to changes of soil moisture as well as heat capacity (e.g. Mallick et al., 2009; van Doninck et al., 2011). Moreover, the TIR data is either used alone or combined with vegetation indices to adjust for the vegetation impact on the degree of heat transferred into the soil (Carlson et al., 1994). For example, Hain et al. (2009) used the TIR-based Atmosphere Land EXchange Inversion (ALEXI) surface energy balance model (Anderson et al., 1997, 2007; Mecikalski et al., 1999) to estimate available water fraction, from which volumetric soil moisture was indirectly derived.

Microwave emission (collected by passive sensors) and backscatter (from active sensors, otherwise known as radars) are directly related to near surface soil moisture ( $\leq 5$  cm) through the dielectric contrast between that of liquid water ( $\sim 80$ ) and dry soil ( $\sim 4$ ) (Schmugge et al., 1974). The observations can be made under almost all-weather conditions due to the atmosphere being transparent at the wavelengths most suitable for soil moisture (X- to L-band). The difference between the active and passive microwave techniques lies in the

source of the signal; radar observations measure the proportion of a transmitted signal being backscattered to the sensor proportional to the surface reflectivity and roughness, while the radiometer observations are measurements of a natural emission proportional to the surface emissivity and physical temperature (Ulaby et al., 1981).

Active microwave remote sensing of soil moisture has the advantage of being at high spatial resolution, especially Synthetic Aperture Radar (SAR) which has the capability of observing the earth's surface at resolutions as high as 10 m Torres et al. (2012). However, this high spatial resolution results in a revisit time of 35 days or longer. The temporal repeat issue has been recently addressed through a constellation of sensors by the ESA; Sentinel-1 consists of two polar orbiting satellites having a global coverage of at least once every 6 to 12 days in Interferometric Wide Swath (IWS) mode (Wagner et al., 2009). The higher temporal resolution of Sentinel-1 SAR observations compared to that of previous SAR missions improves the feasibility of using SAR radar backscatter for a wider range of soil moisture applications. Nevertheless, its narrow imaging swath cannot achieve the temporal resolution of 3 days or better that is required for many soil moisture mapping needs (e.g. Walker and Houser, 2004; the National Research Council's Decadal Survey). Radar imagery is also highly sensitive to surface roughness, vegetation biomass and vegetation water content, making the direct soil moisture retrieval from radar backscatter alone a complex process. One solution proposed to overcome this problem is to use temporal change detection approach (Engman and Chauhan, 1995; Moran et al., 2000; Njoku et al., 2002; Wagner et al., 1999), which assumes that factors such as surface roughness remain fixed with only the soil moisture varying. However, to date accurate and global soil moisture retrieval from SAR backscatter remains a challenge.

Passive microwave emissions at L-band (e.g. Jackson, 1993; Njoku and Entekhabi, 1996; Schmugge et al., 1974, 2002; Ulaby et al., 1996) have been of great interest because of their better sensitivity to soil moisture dynamics (Ulaby et al., 1982) than radar and optical observations, and their favourable signal-to-noise ratio. Consequently, the ESA and NASA have launched dedicated soil moisture missions using L-band passive microwave instruments aboard the SMOS satellite in 2009 and SMAP satellite in 2015, respectively, to monitor global surface soil moisture at a temporal resolution of at least 3 days. SMOS

uses an interferometric radiometer with aperture synthesis by which multi-angular brightness temperature data sets are collected. In contrast, the SMAP radiometer has a scanning real aperture antenna which provides single angle ( $\sim 40^\circ$ ) but high accuracy brightness temperature observations. Both the SMOS and SMAP satellites have an approximately 40 km resolution of their brightness temperature measurements, due to the trade-offs in antenna (aperture) size needed for high resolution and the technical challenge of launching and operating a large antenna in space. As the 40 km spatial resolution restricts the applications to hydro-climatological studies Entekhabi et al. (2008b), spatial enhancement approaches are required if the passive microwave missions are to satisfy hydro-meteorological and agricultural applications Entekhabi et al. (2010). Figure 1.1 summarizes the temporal and spatial resolution requirements of soil moisture in a range of application areas.

No remote sensing technique utilizing a single electromagnetic region or approach can by itself satisfy the accuracy, spatial and temporal resolution requirements. While L-band passive microwave can yield accurate estimates of soil moisture content at low resolution, the radar and optical imagery are capable of high spatial resolution but low accuracy soil moisture; the decreased accuracy of the radar- and optical-based remote sensing of soil moisture is due to the high impact by features such as surface roughness and vegetation canopy. Consequently, the SMAP satellite had included a radar in its design, to produce an approximately 10 km resolution soil moisture by merging the active and passive microwave data sets and permitting a compromise on accuracy. But due to a hardware anomaly, the radar transmitter failed on 7th of July 2015, making the SMAP combination of active and passive microwave observations no longer possible.

Apart from the SMAP active/passive baseline approach (Das et al., 2014), there have been a number of other studies that have proposed leveraging the strengths of passive microwave with that of radar and/or optical observations. This leveraging is possible through a process called downscaling or disaggregation. Downscaling methods combine coarse passive microwave observations with high spatial resolution features obtained from: microwave remote sensing backscatter observations from active microwave sensors (e.g. Akbar and Moghaddam, 2015; Das et al., 2011, 2014; Piles et al., 2009b) higher frequency radiometric observations from passive microwave sensors (e.g. Gevaert et al., 2015; Santi, 2010); visi-

ble, SWIR and/or TIR observations from optical sensors (e.g. Muller and Décamps, 2001; Verhoef et al., 1996); and/or soil surface attributes (e.g. Ines et al., 2013; Pellenq et al., 2003). More recently, data assimilation has been used to combine coarse passive microwave data into a high resolution hydrological/land surface model (e.g. Reichle et al., 2001, 2017; Sahoo et al., 2013), and a hydrological/land surface model has been used to train machine learning techniques for soil moisture downscaling (e.g. Chai et al., 2011; Chakrabarti et al., 2015, 2016; Srivastava et al., 2013). One advantage of these model-based prediction approaches is that there is no need for concurrent overpass by other satellites or concern about lost data due to cloud coverage.

There are also statistical-based downscaling approaches (e.g. Kaheil et al., 2008; Loew and Mauser, 2008; Mascaro et al., 2010, 2011; Parada and Liang, 2003; Shi et al., 2014b; Verhoest et al., 2015), which provide the possible behaviour of the soil moisture using copula probability distributions and/or wavelet coefficients. Camps et al. (2008) and Piles et al. (2009a) have also developed mathematical-based downscaling techniques, which also estimate the possible behaviour of the soil moisture using the Fourier domain. However, such techniques are out of scope of this review, which provides an overview of downscaling techniques that derive a deterministic pattern of soil moisture at higher resolution.

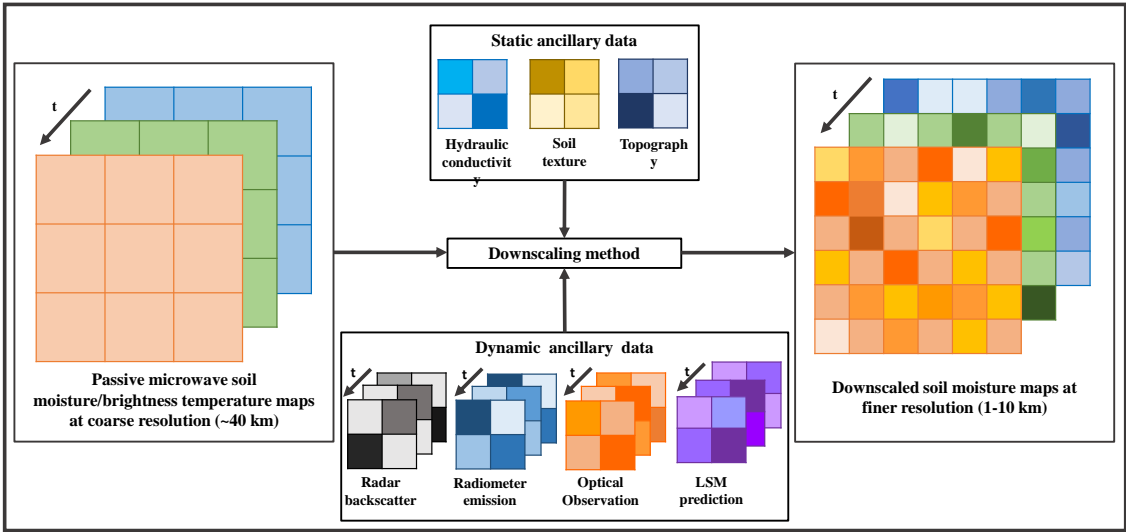


Figure 2.1: Schematic of the downscaling concept using spatially detailed information on land surface features to distribute coarse scale soil moisture to fine scale.

## 2.2 Review of soil moisture downscaling methods

Accurate soil moisture maps at moderate spatial resolutions (1-10 km) are required for regional and local earth system applications. Various downscaling techniques have been proposed for meeting the user requirements on spatial scale and accuracy of soil moisture measurements. A schematic of the general approach to downscaling soil moisture is shown in Figure 2.1, with Table 2.1 providing a concise overview of the strengths and weaknesses of each downscaling method by listing each method with its pros/cons. Table 2.2 provides the reported accuracy of each downscaling technique together with the list of methods, references, main inputs, and improvement of downscaled products over the radiometer-only measurements, as suggested by Merlin et al. (2015).

### 2.2.1 Microwave-based downscaling techniques

The capability of active and passive microwave observations has been verified for soil moisture mapping since the 80's (e.g. Dobson and Ulaby, 1986; Ulaby et al., 1982). The Advanced SCATterometer (ASCAT) aboard the European METeorological OPERational (METOP) satellite is an example of an operational microwave radar which maps soil moisture globally at coarse resolution of 25 and 50 km Wagner et al. (2013). The ESA CCI active microwave soil moisture data, which is a merged product created from C-band scatterometers (ERS-1/2 scatterometer, METOP Advanced Scatterometer), is available at 12.5 km. However, these products cannot satisfy the spatial resolution requirement of the soil moisture applications presented in Figure 1.1. Advanced Synthetic Aperture Radar (ASAR) also maps soil moisture at 1 km, but this product is only available over Australia, southern and central Africa, and parts of Argentina for the time period between January 2005 and May 2010 (see: <https://www.geo.tuwien.ac.at/mrs/data-viewers/>). Accordingly, active microwave observations alone have not been able to routinely provide accurate high resolution soil moisture estimates (e.g. Paloscia et al., 2013; Walker et al., 2004) globally, but can contribute valuable information about the geophysical properties of the target scenes (e.g. Chauhan, 1997; Mohanty et al., 2017). Reliable soil moisture retrieval from passive microwave remote sensing is limited to the lower frequencies, namely L-band ( $\sim 1.4$  GHz),

Table 2.1: Summary of the strengths and weaknesses of each downscaling method listing all the methods and pros/cons.

Downscaling Techniques	Approaches	Pros	Cons
<b>Radar-based</b>	Complimentary radar and radiometer	<ul style="list-style-type: none"> <li>• Applicable under all-weather condition</li> </ul>	<ul style="list-style-type: none"> <li>• Lack of concurrent radar and radiometer observations at the same temporal repeat and on the same platforms</li> </ul>
	Change detection of radar	<ul style="list-style-type: none"> <li>• Independent from meteorological and land surface information</li> </ul>	<ul style="list-style-type: none"> <li>• Low temporal coverage of radar imagery</li> </ul>
	Fractal interpolation	<ul style="list-style-type: none"> <li>• Better sensitivity of radar backscatter to soil moisture dynamics than optical observations</li> </ul>	<ul style="list-style-type: none"> <li>• Active microwave observations are sensitive to vegetation cover and surface roughness</li> </ul>
	Bayesian		
	Combined radar and radiometer		
<b>Radiometer-based</b>	Combined high and low frequency radiometer	<ul style="list-style-type: none"> <li>• Applicable under all-weather condition</li> </ul>	<ul style="list-style-type: none"> <li>• Spatial scale of soil moisture retrievals is limited to the scale of high frequency radiometric observations</li> </ul>
		<ul style="list-style-type: none"> <li>• Direct relationship of radiometric emissions to soil moisture dynamics</li> </ul>	<ul style="list-style-type: none"> <li>• High frequency microwave observations are sensitive to vegetation cover and rainfall events</li> </ul>
		<ul style="list-style-type: none"> <li>• Availability of radiometric emissions at higher frequency and at regular repeat coverage</li> </ul>	
<b>Optical-based</b>	Physical		<ul style="list-style-type: none"> <li>• No availability of optical observations under cloudy sky</li> </ul>
	Thermal inertia	<ul style="list-style-type: none"> <li>• High spatial resolution of optical observations</li> </ul>	<ul style="list-style-type: none"> <li>• Impacts of vegetation cover on the optical observations makes relating these observations to soil moisture difficult</li> </ul>
	Semi-empirical	<ul style="list-style-type: none"> <li>• High temporal resolution of optical observations</li> </ul>	<ul style="list-style-type: none"> <li>• Indirect relationship of optical observations to soil moisture variations</li> </ul>
<b>Soil surface attributes-based</b>	Statistical	<ul style="list-style-type: none"> <li>• Reflects soil water dynamic and storage capacity impact/control on soil moisture space-time scaling behaviour</li> </ul>	<ul style="list-style-type: none"> <li>• Limited access to global data on attributes including topography, soil surface properties and their possible rate of change</li> </ul>
<b>Data assimilation-based</b>	High resolution model predictions combined with low resolution radiometric observations	<ul style="list-style-type: none"> <li>• Accounts for both model and measurement uncertainties</li> <li>• No need to have concurrent overpass by other satellites</li> </ul>	<ul style="list-style-type: none"> <li>• Requires information on meteorological and land surface parameters at high resolution</li> </ul>

Table 2.1 (continued).

Downscaling Techniques	Approaches	Pros	Cons
Machine learning-based	Relationship with surface parameters	<ul style="list-style-type: none"> <li>No need to have concurrent overpass by other satellites</li> <li>No need for continuous data</li> <li>No lost data due to cloud coverage</li> </ul>	<ul style="list-style-type: none"> <li>Needs parameter optimization</li> <li>Computationally demanding</li> <li>Training globally</li> </ul>

Table 2.2: Summary table on accuracy of soil moisture downscaling methods including the list of methods, references, and main inputs.

Downscaling Techniques	Approaches	References	Main inputs	Accuracy	Improvement over the radiometer only measurements	Range of accuracy parameters
<b>Radar-based</b>	Complimentary radar and radiometer	Ulabay et al. (1983) Theis et al. (1986)	<ul style="list-style-type: none"> <li>NASA C-130 airborne L-band scatterometer data</li> <li>NASA C-130 airborne L- and C-band radiometric data</li> </ul>	+/- 30% of truth soil moisture C-band V-pol $R^2=0.65$ , C-band H-pol $R^2=0.65$ , L-band H-pol $R^2=0.95$	- C-band V-pol $\Delta R^2=0.42$ , C-band H-pol $\Delta R^2=0.43$ , L-band H-pol $\Delta R^2=0.26$	RMSD $\in$ (0.01,0.029) $m^3 m^{-3}$ $R^2 \in$ (0.65,0.99)
		O'Neill et al. (1992)	<ul style="list-style-type: none"> <li>MACHYDRO '90 experimental AIRSAR L-band radar data</li> <li>MACHYDRO '90 experimental PBMR L-band radiometric data</li> </ul>	RMSD=0.029 $m^3 m^{-3}$	-	
		O'Neill et al. (1996)	<ul style="list-style-type: none"> <li>MACHYDRO '90 experimental data set including PBMR L-band radiometric and AIRSAR L-band radar data</li> <li>Washita '92 experimental ESTAR L-band radiometric and GSFC's L-band truck-mounted radar data</li> </ul>	MACHYDRO '90: RMSD=0.028 $m^3 m^{-3}$ $R^2=0.93$ (on average) Washita '92: $\alpha = 0$ : RMSD=0.016 $m^3 m^{-3}$ , $R^2=0.99$ (on average) $\alpha \neq 0$ : RMSD=0.01 $m^3 m^{-3}$ , $R^2=0.99$ (on average)	-	
		Chauhan et al. (1997)	<ul style="list-style-type: none"> <li>MACHYDRO '90 experimental data</li> </ul>	Absolute bias on average < 0.05 $m^3 m^{-3}$	-	
Change detection of radar		Njoku et al. (2002)	<ul style="list-style-type: none"> <li>SGP99 L- and S-band PALS experimental data</li> </ul>	No report on retrievals analysis, just proposing a method for downscaling	-	RMSD $\in$ (0.028,0.052) $m^3 m^{-3}$ $R^2 \in$ (0.31,0.85)
		Narayan et al. (2006)	<ul style="list-style-type: none"> <li>SMEX02 PALS L-band radiometer data</li> <li>SMEX02 AIRSAR L-band radar data</li> </ul>	RMSD=0.046 $m^3 m^{-3}$ , $R^2=0.7$ (on average) After removing outliers: RMSD=0.028 $m^3 m^{-3}$ , $R^2=0.85$ (on average)	-	
		Narayan and Lakshmi (2008)	<ul style="list-style-type: none"> <li>AMSR-E C-band radiometric data</li> <li>TMI X-band brightness temperature</li> <li>TRMM-PR Ku-band backscatter data</li> </ul>	AMSR-E & TRMM-PR: RMSD=0.052 $m^3 m^{-3}$ , $R^2=0.31$ TMI & TRMM-PR: RMSD=0.049 $m^3 m^{-3}$ , $R^2=0.45$	AMSR-E & TRMM-PR: $\Delta$ RMSD=0.025 $m^3 m^{-3}$ , $\Delta R^2=0.14$ TMI & TRMM-PR: $\Delta$ RMSD=0.031 $m^3 m^{-3}$ , $\Delta R^2=0.08$	

Table 2.2 (continued)

Downscaling Techniques	Approaches	References	Main inputs	Accuracy	Improvement over the radiometer only measurements	Range of accuracy parameters
Fractal interpolation		Bindlish and Barros (2002)	<ul style="list-style-type: none"> <li>SGP '97 ESTAR L-band radiometric data</li> </ul>	RMSD= 0.028 m <sup>3</sup> m <sup>-3</sup>	ΔRMSD= 0.004 m <sup>3</sup> m <sup>-3</sup>	
	Bayesian	Zhan et al. (2006)	<ul style="list-style-type: none"> <li>SIR-C/X-SAR L-, C-, and X-band data</li> <li>L-band OSSE experimental data set</li> </ul>	3 km: RMSD=0.028 m <sup>3</sup> m <sup>-3</sup> (Low noise data) RMSD=0.038 m <sup>3</sup> m <sup>-3</sup> (High noise data) 9 km: RMSD=0.027 m <sup>3</sup> m <sup>-3</sup> (Low noise data) RMSD=0.044 m <sup>3</sup> m <sup>-3</sup> (High noise data)	3 km: ΔRMSD=0.013 m <sup>3</sup> m <sup>-3</sup> (Low noise data) ARMSD=0.022 m <sup>3</sup> m <sup>-3</sup> (High noise data) 9 km: ΔRMSD=0.012 m <sup>3</sup> m <sup>-3</sup> (Low noise data) ARMSD=0.028 m <sup>3</sup> m <sup>-3</sup> (High noise data)	RMSD ∈ (0.013,0.044) m <sup>3</sup> m <sup>-3</sup> R <sup>2</sup> ∈ (0.1,0.55)
Combined radar and radiometer		Wu et al. (2017)	<ul style="list-style-type: none"> <li>SMAPEX-3 L-band PLMR and PLIS observations</li> </ul>	1 km: RMSD= 0.020 m <sup>3</sup> m <sup>-3</sup> , R <sup>2</sup> =0.1 3 km: RMSD=0.017 m <sup>3</sup> m <sup>-3</sup> , R <sup>2</sup> =0.3 9 km: RMSD=0.013 m <sup>3</sup> m <sup>-3</sup> , R <sup>2</sup> =0.55	1 km: ΔRMSD= 0.041 m <sup>3</sup> m <sup>-3</sup> , ΔR <sup>2</sup> =0.01 3 km: ΔRMSD=0.023 m <sup>3</sup> m <sup>-3</sup> , ΔR <sup>2</sup> =0.18 9 km: ΔRMSD=0.014 m <sup>3</sup> m <sup>-3</sup> , ΔR <sup>2</sup> =0.35	
		Piles et al. (2009b)	<ul style="list-style-type: none"> <li>SMEX02 L-band PALS experimental data set</li> </ul>	RMSD=0.027 m <sup>3</sup> m <sup>-3</sup> (H pol) RMSD=0.023 m <sup>3</sup> m <sup>-3</sup> (V pol)	ΔRMSD=0.02 m <sup>3</sup> m <sup>-3</sup>	RMSD ∈ (0.019,0.12) m <sup>3</sup> m <sup>-3</sup>
		Das et al. (2011)	<ul style="list-style-type: none"> <li>L-band OSSE experimental data set</li> </ul>	PALS: RMSD=0.035 m <sup>3</sup> m <sup>-3</sup> OSSE: RMSD=0.028 to 0.033 m <sup>3</sup> m <sup>-3</sup>	ΔRMSD ∈ (0.015-0.02) m <sup>3</sup> m <sup>-3</sup>	
		Das et al. (2014)		PALS: RMSD=0.033 m <sup>3</sup> m <sup>-3</sup>	ΔRMSD > 0.02 m <sup>3</sup> m <sup>-3</sup>	
		Akbar et al. (2015)	<ul style="list-style-type: none"> <li>MEX02 L-band PALS experimental data set</li> </ul>	Low noise level: RMSD=0.039 m <sup>3</sup> m <sup>-3</sup> (on average)	ΔRMSD=0.006 m <sup>3</sup> m <sup>-3</sup> (Low noise level, on average)	
			<ul style="list-style-type: none"> <li>Truck mounted ComRad data</li> </ul>	High noise level: RMSD=0.047 m <sup>3</sup> m <sup>-3</sup> (on average)	ΔRMSD=0.002 m <sup>3</sup> m <sup>-3</sup> (High noise level, on average)	
		van der Velde et al. (2015)	<ul style="list-style-type: none"> <li>AMSR-E VUA-NASA C-band soil moisture products</li> <li>PALSAR L-band radar backscatter</li> </ul>	1 km: RMSD=0.067 m <sup>3</sup> m <sup>-3</sup> , R <sup>2</sup> =0.37 (on average) 5 km: RMSD=0.068 m <sup>3</sup> m <sup>-3</sup> , R <sup>2</sup> =0.36 (on average) 10 km: RMSD=0.069 m <sup>3</sup> m <sup>-3</sup> , R <sup>2</sup> =0.36 (on average)	1 km: ΔRMSD=0.126 m <sup>3</sup> m <sup>-3</sup> , ΔR <sup>2</sup> =0.02 (on average) 5 km: ΔRMSD=0.125 m <sup>3</sup> m <sup>-3</sup> , ΔR <sup>2</sup> =0.01 (on average) 10 km: ΔRMSD=0.124 m <sup>3</sup> m <sup>-3</sup> , ΔR <sup>2</sup> =0.01 (on average)	

Table 2.2 (continued)

Downscaling Techniques	Approaches	References	Main inputs	Accuracy	Improvement over the radiometer only measurements	Range of accuracy parameters
		Wu et al. (2016)	<ul style="list-style-type: none"> <li>• SMAPEX-3 L-band PLMR and PLIS observations</li> </ul>	<p>The baseline active-passive algorithm by Das et al. (2014):</p> <p>1 km: RMSD=0.038 m<sup>3</sup> m<sup>-3</sup>                      3 km: RMSD=0.028 m<sup>3</sup> m<sup>-3</sup>                      9 km: RMSD=0.019 m<sup>3</sup> m<sup>-3</sup></p> <p>The active/passive retrieval algorithm by Das et al. (2011):</p> <p>1 km: RMSD=0.042 m<sup>3</sup> m<sup>-3</sup>                      3 km: RMSD=0.030 m<sup>3</sup> m<sup>-3</sup>                      9 km: RMSD=0.021 m<sup>3</sup> m<sup>-3</sup></p> <p>The change detection approach by Piles et al. (2009b):</p> <p>1 km: RMSD=0.044 m<sup>3</sup> m<sup>-3</sup>                      3 km: RMSD=0.033 m<sup>3</sup> m<sup>-3</sup>                      9 km: RMSD=0.026 m<sup>3</sup> m<sup>-3</sup></p>	<p>ΔRMSD=0.01 m<sup>3</sup> m<sup>-3</sup> (For each type of downscaling algorithm)</p>	
		Rüdiger et al. (2016)	<ul style="list-style-type: none"> <li>• AACES L-band PLMR observations</li> </ul>	RMSD=0.06 to 0.12 m <sup>3</sup> m <sup>-3</sup>	-	
		Montzka et al. (2016)	<ul style="list-style-type: none"> <li>• ASAR C-band radar data</li> <li>• PLMR brightness temperature</li> <li>• F-SAR radar backscatter</li> </ul>	<p>The active/passive retrieval algorithm by Das et al. (2011):</p> <p>Juelich: RMSD=0.083 m<sup>3</sup> m<sup>-3</sup>                      Monschau: RMSD=0.094 m<sup>3</sup> m<sup>-3</sup></p> <p>The baseline active-passive algorithm by Das et al. (2014):</p> <p>Juelich: RMSD=0.066 m<sup>3</sup> m<sup>-3</sup>                      Monschau: RMSD=0.077 m<sup>3</sup> m<sup>-3</sup></p> <p>The alternative active-passive algorithm by Montzka et al. (2016):</p> <p>Juelich: RMSD=0.078 m<sup>3</sup> m<sup>-3</sup>                      Monschau: RMSD=not available</p>	-	
<b>Radiometer-based</b>	Combined high and low	Santi, (2010)	<ul style="list-style-type: none"> <li>• AMSR-E LPRM C-band soil moisture product</li> <li>• AMSR-E Ka-band radiometric data</li> </ul>	Just proposing a method for downscaling/no analysis	-	RMSD ∈ (0.054,0.13) m <sup>3</sup> m <sup>-3</sup>

Table 2.2 (continued)

Downscaling Techniques	Approaches	References	Main inputs	Accuracy	Improvement over the radiometer only measurements	Range of accuracy parameters
frequency radiometer		Gevaert et al. (2015)		RMSD=0.13 m <sup>3</sup> m <sup>-3</sup> , R <sup>2</sup> =0.41*	ΔRMSD=0.01 m <sup>3</sup> m <sup>-3</sup> , ΔR <sup>2</sup> =0.01*	R <sup>2</sup> ∈ (0.28,0.41)
		de Jeu et al. (2014)		Std. Dev.=0.05 m <sup>3</sup> m <sup>-3</sup>	ΔStd. Dev.=-0.016 m <sup>3</sup> m <sup>-3</sup>	
		Parinussa et al. (2014)**	<ul style="list-style-type: none"> <li>• AMSR-E LPRM C-band soil moisture product</li> <li>• ALEXI TIR soil moisture products</li> <li>• ASCAT C-band soil moisture products</li> <li>• AMSR-E Ka-band radiometric data</li> </ul>	Downscaled ALEXI: RMSD=0.054 m <sup>3</sup> m <sup>-3</sup> , R <sup>2</sup> =0.34*	Downscaled ALEXI: ΔRMSD=0 m <sup>3</sup> m <sup>-3</sup> , ΔR <sup>2</sup> =-0.01*	
			Downscaled AMSRE: RMSD=0.06 m <sup>3</sup> m <sup>-3</sup> , R <sup>2</sup> =0.35*	Downscaled AMSRE: ΔRMSD=0 m <sup>3</sup> m <sup>-3</sup> , ΔR <sup>2</sup> =-0.02*		
			Downscaled ASCAT: RMSD=0.066 m <sup>3</sup> m <sup>-3</sup> , R <sup>2</sup> =0.28*	Downscaled ASCAT: ΔRMSD=0.002 m <sup>3</sup> m <sup>-3</sup> , ΔR <sup>2</sup> =-0.02*		
Optical-based	Physical	Merlin et al. (2005)	<ul style="list-style-type: none"> <li>• SGP '97 ESTAR L-band radiometric data</li> <li>• AVHRR optical data set</li> </ul>	Std. Dev.=0.054 m <sup>3</sup> m <sup>-3</sup>	-	RMSD ∈ (0.003,0.211) m <sup>3</sup> m <sup>-3</sup>
		Merlin et al. (2008a)	<ul style="list-style-type: none"> <li>• Monsoon '90 PMBR L-band radiometric data</li> <li>• MODIS products including NDVI and LST</li> </ul>	EF based: RMSD=0.03 m <sup>3</sup> m <sup>-3</sup> , R <sup>2</sup> =0.62*	-	R <sup>2</sup> ∈ (0.0,0.81)
		Merlin et al. (2008b)	<ul style="list-style-type: none"> <li>• NAFE'06 L-band airborne radiometer observations</li> <li>• MODIS products including NDVI and LST</li> </ul>	AEF based: RMSD=0.02 m <sup>3</sup> m <sup>-3</sup> , R <sup>2</sup> =0.66*	-	UbRMSD *** ∈ (0.039,0.102) m <sup>3</sup> m <sup>-3</sup>
		Merlin et al. (2010)		Uniform θ: RMSD=0.017 m <sup>3</sup> m <sup>-3</sup> , R <sup>2</sup> =0.42*	-	
				Non-uniform θ: RMSD=0.0153 m <sup>3</sup> m <sup>-3</sup> , R <sup>2</sup> =0.58*	-	
				RMSD=0.012 to 0.025 m <sup>3</sup> m <sup>-3</sup> , R <sup>2</sup> =0.55 to 0.81*	-	
		Merlin et al. (2009)	<ul style="list-style-type: none"> <li>• NAFE'06 L-band airborne radiometer observations</li> <li>• MODIS products including NDVI and LST</li> <li>• ASTER</li> </ul>	RMSD=0.062 m <sup>3</sup> m <sup>-3</sup> , R <sup>2</sup> =0.64	-	
		Merlin et al. (2012)	<ul style="list-style-type: none"> <li>• SMOS level-2 soil moisture product</li> </ul>	Austral summer: RMSD=0.057 m <sup>3</sup> m <sup>-3</sup> , R <sup>2</sup> =0.49*	-	

Table 2.2 (continued)

Downscaling Approaches Techniques	References	Main inputs	Accuracy	Improvement over the radiometer only measurements	Range of accuracy parameters
		<ul style="list-style-type: none"> <li>• MODIS products including NDVI and LST</li> </ul>	Austral winter: RMSD=0.138 m <sup>3</sup> m <sup>-3</sup> , R <sup>2</sup> =~0*		
Merlin et al. (2013)		<ul style="list-style-type: none"> <li>• SMOS level-2 soil moisture product</li> <li>• MODIS products including NDVI and LST</li> <li>• ASTER products including NDVI and LST</li> <li>• Landsat products including NDVI and LST</li> </ul>	3 km, used MODIS: RMSD=0.11 m <sup>3</sup> m <sup>-3</sup> , R <sup>2</sup> =0.45* 100 m, used ASTER: RMSD=0.0815 m <sup>3</sup> m <sup>-3</sup> , R <sup>2</sup> =0.50* 100 m, used Landsat: RMSD=0.1 m <sup>3</sup> m <sup>-3</sup> , R <sup>2</sup> =0.72*	3 km, used MODIS: ΔRMSD=0.01 m <sup>3</sup> m <sup>-3</sup> , ΔR <sup>2</sup> =0.1* 100 m, used ASTER: ΔRMSD=0.0385 m <sup>3</sup> m <sup>-3</sup> , ΔR <sup>2</sup> =0.15* 100 m, used Landsat: ΔRMSD=0.2 m <sup>3</sup> m <sup>-3</sup> , ΔR <sup>2</sup> =0.37*	
Djamaï et al. (2015)		<ul style="list-style-type: none"> <li>• SMOS level-2 soil moisture product</li> <li>• MODIS products including NDVI and LST</li> </ul>	Against ground data: RMSD=0.03 to 0.05 m <sup>3</sup> m <sup>-3</sup> , R <sup>2</sup> =0.09 to 0.27* Against airborne soil moisture: R <sup>2</sup> =0.24 to 0.64*	-	
Fan et al. (2015)		<ul style="list-style-type: none"> <li>• Airborne PLMR soil moisture at 700 m resolution</li> <li>• ASTER products including NDVI and LST at 100 m</li> </ul>	RMSD=0.048 m <sup>3</sup> m <sup>-3</sup> , R <sup>2</sup> =0.37*	ΔRMSD=-0.08 m <sup>3</sup> m <sup>-3</sup> , ΔR <sup>2</sup> =N/A	
Malbêteau et al. (2016)		<ul style="list-style-type: none"> <li>• AMSR-E level-3 LPRM soil moisture product</li> <li>• SMOS level-3 daily soil moisture product</li> <li>• MODIS products including NDVI and LST</li> <li>• DEM data (gtopo30)</li> </ul>	AMSR-E: Ascending: RMSD=0.076m <sup>3</sup> m <sup>-3</sup> , R <sup>2</sup> =0.61* Descending: RMSD=0.092 m <sup>3</sup> m <sup>-3</sup> , R <sup>2</sup> =0.61* SMOS: Ascending: RMSD=0.079 m <sup>3</sup> m <sup>-3</sup> , R <sup>2</sup> =0.53* Descending: RMSD=0.068 m <sup>3</sup> m <sup>-3</sup> , R <sup>2</sup> =0.5*	AMSR-E: Ascending: ΔRMSD=0.019 m <sup>3</sup> m <sup>-3</sup> , ΔR <sup>2</sup> =-0.08* Descending: ΔRMSD=0.025 m <sup>3</sup> m <sup>-3</sup> , ΔR <sup>2</sup> =-0.12* SMOS: Ascending: ΔRMSD=0.011 m <sup>3</sup> m <sup>-3</sup> , ΔR <sup>2</sup> =-0.04* Descending: ΔRMSD=0.016 m <sup>3</sup> m <sup>-3</sup> , ΔR <sup>2</sup> =-0.02*	
Molero et al. (2016)		<ul style="list-style-type: none"> <li>• SMOS level-3 daily soil moisture product</li> </ul>	Averaged results from ascending and descending overpasses	Yanco: AurbRMSD=-0.018 m <sup>3</sup> m <sup>-3</sup> , AR <sup>2</sup> =-0.08*	

Table 2.2 (continued)

Downscaling Techniques	Approaches	References	Main inputs	Accuracy	Improvement over the radiometer only measurements	Range of accuracy parameters
	<ul style="list-style-type: none"> <li>MODIS products including NDVI and LST</li> <li>DEM data (gropo30)</li> </ul>			Yanco: ubRMSD**= $-0.093 \text{ m}^3 \text{ m}^{-3}$ , $R^2=0.12^*$ Murrumbidgee: ubRMSD= $0.102 \text{ m}^3 \text{ m}^{-3}$ , $R^2=0.1^*$ Little Washita: ubRMSD= $0.076 \text{ m}^3 \text{ m}^{-3}$ , $R^2=0^*$ Walnut Gluch: ubRMSD= $0.039 \text{ m}^3 \text{ m}^{-3}$ , $R^2=0.01^*$	Murrumbidgee: $\Delta \text{ubRMSD}=-0.021 \text{ m}^3 \text{ m}^{-3}$ , $\Delta R^2=0.06^*$ Little Washita: $\Delta \text{ubRMSD}=-0.014 \text{ m}^3 \text{ m}^{-3}$ , $\Delta R^2=-0.01^*$ Walnut Gluch: $\Delta \text{ubRMSD}=-0.007 \text{ m}^3 \text{ m}^{-3}$ , $\Delta R^2=0.01^*$	
Djamaï et al. (2016)	<ul style="list-style-type: none"> <li>SMOS level-2 soil moisture product</li> <li>MODIS products including NDVI and LST</li> <li>OURANOS geophysical data</li> <li>NARR atmospheric forcing data</li> </ul>			Linear: Ascending: RMSD= $0.06 \text{ m}^3 \text{ m}^{-3}$ , $R^2=0.58^*$ Descending: RMSD= $0.05 \text{ m}^3 \text{ m}^{-3}$ , $R^2=0.66^*$ Non-linear: Ascending: RMSD= $0.06 \text{ m}^3 \text{ m}^{-3}$ , $R^2=0.49^*$ Descending: RMSD= $0.06 \text{ m}^3 \text{ m}^{-3}$ , $R^2=0.52^*$	Linear: Ascending: $\Delta \text{RMSD}=0.04 \text{ m}^3 \text{ m}^{-3}$ , $\Delta R^2=0.13^*$ Descending: $\Delta \text{RMSD}=0.06 \text{ m}^3 \text{ m}^{-3}$ , $\Delta R^2=-0.03^*$ Non-linear: Ascending: $\Delta \text{RMSD}=0.04 \text{ m}^3 \text{ m}^{-3}$ , $\Delta R^2=0.04^*$ Descending: $\Delta \text{RMSD}=0.05 \text{ m}^3 \text{ m}^{-3}$ , $\Delta R^2=-0.17^*$	
Chen et al. (2017)	<ul style="list-style-type: none"> <li>SMAP radiometer-derived soil moisture products</li> <li>MODIS land surface reflectance products</li> </ul>			May: NRSD: RMSD= $0.04 \text{ m}^3 \text{ m}^{-3}$ , $R^2=0.15^*$ DisPATCh: RMSD= $0.07 \text{ m}^3 \text{ m}^{-3}$ , $R^2=0.13^*$ September: NRSD: RMSD= $0.12 \text{ m}^3 \text{ m}^{-3}$ , $R^2=0.06^*$ DisPATCh: RMSD= $0.17 \text{ m}^3 \text{ m}^{-3}$ , $R^2=0.04^*$	May: NRSD: $\Delta \text{RMSD}=0 \text{ m}^3 \text{ m}^{-3}$ DisPATCh: $\Delta \text{RMSD}=-0.03 \text{ m}^3 \text{ m}^{-3}$ September: NRSD: $\Delta \text{RMSD}=0.02 \text{ m}^3 \text{ m}^{-3}$ DisPATCh: $\Delta \text{RMSD}=-0.03 \text{ m}^3 \text{ m}^{-3}$	
Kim and Hogue (2012)	<ul style="list-style-type: none"> <li>AMSR-E Level 3 soil moisture product from NSIDC</li> <li>MODIS products including NDVI and LST</li> </ul>			RMSD= $0.051 \text{ m}^3 \text{ m}^{-3}$ , $R^2=0.073^*$	$\Delta \text{RMSD}=0.003 \text{ m}^3 \text{ m}^{-3}$ , $\Delta R^2=0.067^*$	

Table 2.2 (continued)

Downscaling Approaches Techniques	References	Main inputs	Accuracy	Improvement over the radiometer only measurements	Range of accuracy parameters
	Zhou et al. (2015)	<ul style="list-style-type: none"> <li>AMSR2 Level 3 soil moisture products</li> <li>MODIS products including NDVI and LST</li> </ul>	Merlin et al. (2008;2009): RMSD=0.032 m <sup>3</sup> m <sup>-3</sup> , R <sup>2</sup> =0.55* Kim and Hogue, (2012): RMSD=0.038 m <sup>3</sup> m <sup>-3</sup> , R <sup>2</sup> =0.58*		
	Peng et al. (2015)	<ul style="list-style-type: none"> <li>ESA CCI multi-mission soil moisture product</li> <li>MODIS products including NDVI and LST</li> <li>MSG SEVIRI data</li> </ul>	MODIS based: RMSD=0.076 m <sup>3</sup> m <sup>-3</sup> , ubRMSD**=0.042 m <sup>3</sup> m <sup>-3</sup> , R <sup>2</sup> =0.34* SEVIRI based: RMSD=0.072 m <sup>3</sup> m <sup>-3</sup> , ubRMSD=0.04 m <sup>3</sup> m <sup>-3</sup> , R <sup>2</sup> =0.38*	MODIS based: ΔRMSD=0.034 m <sup>3</sup> m <sup>-3</sup> , ΔubRMSD=0.008 m <sup>3</sup> m <sup>-3</sup> , ΔR <sup>2</sup> =0.06* SEVIRI based: ΔRMSD=0.038 m <sup>3</sup> m <sup>-3</sup> , ΔubRMSD=0.01 m <sup>3</sup> m <sup>-3</sup> , ΔR <sup>2</sup> =0.1*	
	Peng et al. (2016)	<ul style="list-style-type: none"> <li>ESA CCI multi-mission soil moisture products</li> <li>MODIS products including NDVI/EVI and LST</li> </ul>	LST/NDVI: RMSD=0.099 m <sup>3</sup> m <sup>-3</sup> , R <sup>2</sup> =0.38* LST/EVI: RMSD=0.103 m <sup>3</sup> m <sup>-3</sup> , R <sup>2</sup> =0.36* LST <sub>day-night</sub> /NDVI: RMSD=0.078 m <sup>3</sup> m <sup>-3</sup> , R <sup>2</sup> =0.56* LST <sub>day-night</sub> /EVI: RMSD=0.091 m <sup>3</sup> m <sup>-3</sup> , R <sup>2</sup> =0.45*	LST/NDVI: ΔRMSD=0.042 m <sup>3</sup> m <sup>-3</sup> , ΔR <sup>2</sup> =0.23* LST/EVI: ΔRMSD=-0.046 m <sup>3</sup> m <sup>-3</sup> , ΔR <sup>2</sup> =0.25* LST <sub>day-night</sub> /NDVI: ΔRMSD=-0.021 m <sup>3</sup> m <sup>-3</sup> , ΔR <sup>2</sup> =0.05* LST <sub>day-night</sub> /EVI: ΔRMSD=-0.034 m <sup>3</sup> m <sup>-3</sup> , ΔR <sup>2</sup> =0.16*	
	Kim et al. (2017)**	<ul style="list-style-type: none"> <li>Merged active-passive ESA CCI soil moisture products</li> <li>MODIS 16-day NDVI composite</li> </ul>	REMEDHUS: RMSD=0.11 m <sup>3</sup> m <sup>-3</sup> , ubRMSD**=0.05 m <sup>3</sup> m <sup>-3</sup> , R <sup>2</sup> =0.24* CONUS: Arid: RMSD=0.074 m <sup>3</sup> m <sup>-3</sup> , ubRMSD=0.054 m <sup>3</sup> m <sup>-3</sup> , R <sup>2</sup> =0.29* (median values) Temperate: RMSD=0.105 m <sup>3</sup> m <sup>-3</sup> , ubRMSD=0.079 m <sup>3</sup> m <sup>-3</sup> , R <sup>2</sup> =0.14* (median values) Cold: RMSD=0.091 m <sup>3</sup> m <sup>-3</sup> , ubRMSD=0.074 m <sup>3</sup> m <sup>-3</sup> , R <sup>2</sup> =0.23* (median values)	REMEDHUS: ΔRMSD=0 m <sup>3</sup> m <sup>-3</sup> , ΔubRMSD=0.01 m <sup>3</sup> m <sup>-3</sup> , ΔR <sup>2</sup> =0.1* CONUS: Arid: ΔRMSD=0 m <sup>3</sup> m <sup>-3</sup> , ΔubRMSD=-0.003 m <sup>3</sup> m <sup>-3</sup> , ΔR <sup>2</sup> =0.03* Temperate: ΔRMSD=-0.006 m <sup>3</sup> m <sup>-3</sup> , ΔubRMSD=-0.008 m <sup>3</sup> m <sup>-3</sup> , ΔR <sup>2</sup> =-0.01*	

Table 2.2 (continued)

Downscaling Techniques	Approaches	References	Main inputs	Accuracy	Improvement over the radiometer only measurements	Range of accuracy parameters
		Wang et al. (2016)	<ul style="list-style-type: none"> <li>Microwave products of soil moisture produced by Dorigo et al. (2012)</li> <li>MODIS products including EVI and LST</li> </ul>	On average: RMSD=0.211 m <sup>3</sup> m <sup>-3</sup>	On average: ΔRMSD=-0.022 m <sup>3</sup> m <sup>-3</sup>	Cold: ARMSD=-0.002 m <sup>3</sup> m <sup>-3</sup> , ΔubRMSD=-0.004 m <sup>3</sup> m <sup>-3</sup> , ΔR <sup>2</sup> =0 <sup>*</sup>
		Hemakumara et al. (2004)	<ul style="list-style-type: none"> <li>AMSR-E C-band radiometric data</li> <li>MODIS and AVHRR LST and NDVI</li> </ul>	No report on retrievals analysis, just proposing a method for downscaling	-	
Thermal inertia		Fang and Lakshmi (2014b)	<ul style="list-style-type: none"> <li>AMSR-E soil moisture estimated using the single channel algorithm (SCA)</li> <li>SMOS Daily Level-3 soil moisture product</li> <li>MODIS products including NDVI and land surface temperature</li> <li>AVHRR and SPOT NDVI</li> <li>NLDAS model outputs including LST and soil moisture</li> </ul>	SMOS: RMSD=0.042 m <sup>3</sup> m <sup>-3</sup> , ubRMSD <sup>***</sup> =0.045 m <sup>3</sup> m <sup>-3</sup> (on average) AMSR-E: RMSD=0.0385 m <sup>3</sup> m <sup>-3</sup> , ubRMSD=0.045 m <sup>3</sup> m <sup>-3</sup> (on average)	SMOS: ARMSD=0.001 m <sup>3</sup> m <sup>-3</sup> , ΔubRMSD=-0.002 m <sup>3</sup> m <sup>-3</sup> (on average) AMSR-E: ARMSD=0.006 m <sup>3</sup> m <sup>-3</sup> , ΔubRMSD=-0.003 m <sup>3</sup> m <sup>-3</sup> (on average)	RMSD ∈ (0.027,0.146) m <sup>3</sup> m <sup>-3</sup> UbrRMSD <sup>***</sup> ∈ (0.026,0.045) m <sup>3</sup> m <sup>-3</sup> R <sup>2</sup> ∈ (0.22,0.56)
		Malliek et al. (2009)	<ul style="list-style-type: none"> <li>MODIS and ASTER optical data set</li> <li>AMSR-E C-band radiometric product</li> </ul>	Fractional vegetation cover < 0.5: RMSD=0.027 m <sup>3</sup> m <sup>-3</sup> , R <sup>2</sup> =0.56 <sup>*</sup> Fractional vegetation cover > 0.5: RMSD=0.06 m <sup>3</sup> m <sup>-3</sup> , R <sup>2</sup> =0.22 <sup>*</sup>	-	
		Fang et al. (2013)	<ul style="list-style-type: none"> <li>AMSR-E C-band radiometric data</li> <li>NLDAS model outputs including LST and soil moisture</li> <li>MODIS products including NDVI and LST</li> <li>AVHRR NDVI</li> </ul>	Mesonet data: RMSD=0.146 m <sup>3</sup> m <sup>-3</sup> , ubRMSD <sup>***</sup> =0.042 m <sup>3</sup> m <sup>-3</sup> Micronet data: RMSD=0.063 m <sup>3</sup> m <sup>-3</sup> , ubRMSD=0.026 m <sup>3</sup> m <sup>-3</sup>	Mesonet data: ARMSD=-0.005 m <sup>3</sup> m <sup>-3</sup> , ΔubRMSD=0.0 m <sup>3</sup> m <sup>-3</sup> Micronet data: ARMSD=-0.015 m <sup>3</sup> m <sup>-3</sup> , ΔubRMSD=-0.001 m <sup>3</sup> m <sup>-3</sup>	
		Fang and Lakshmi (2014a)	<ul style="list-style-type: none"> <li>AMSR-E C-band radiometric data</li> <li>NLDAS model outputs including LST and soil moisture</li> </ul>	NP89: RMSD=0.056 m <sup>3</sup> m <sup>-3</sup> , ubRMSD <sup>***</sup> =0.039 m <sup>3</sup> m <sup>-3</sup>	NP89: ΔRMSD=-0.001 m <sup>3</sup> m <sup>-3</sup> , ΔubRMSD=-0.001 m <sup>3</sup> m <sup>-3</sup>	



Table 2.2 (continued)

Downscaling Techniques	Approaches	References	Main inputs	Accuracy	Improvement over the radiometer only measurements	Range of accuracy parameters
		Sanchez-Ruiz et al. (2014)		<p>Morning orbits:                      RMSD=0.07 m<sup>3</sup> m<sup>-3</sup>, ubRMSD<sup>***</sup>=0.043 m<sup>3</sup> m<sup>-3</sup>, R<sup>2</sup>=0.37 (on average)                      Afternoon orbits:                      RMSD=0.051 m<sup>3</sup> m<sup>-3</sup>, ubRMSD=0.04 m<sup>3</sup> m<sup>-3</sup>, R<sup>2</sup>=0.52 (on average)</p>	<p>Morning orbits:                      ΔRMSD=0.0 m<sup>3</sup> m<sup>-3</sup>                      ΔubRMSD=0.003 m<sup>3</sup> m<sup>-3</sup>,                      ΔR<sup>2</sup>=0.1* (on average)                      Afternoon orbits:                      ΔRMSD=0.0 m<sup>3</sup> m<sup>-3</sup>,                      ΔubRMSD=0.004 m<sup>3</sup> m<sup>-3</sup>,                      ΔR<sup>2</sup>=0.11* (on average)</p>	
		Song et al. (2014)	<ul style="list-style-type: none"> <li>AMSR-E Ku-band brightness temperature</li> </ul>	RMSD=0.091 m <sup>3</sup> m <sup>-3</sup> , R <sup>2</sup> =0.62 (on average)	-	
		Song et al. (2012)	<ul style="list-style-type: none"> <li>MODIS NDVI and LST products</li> </ul>	RMSD=0.047 m <sup>3</sup> m <sup>-3</sup> , R <sup>2</sup> =0.74	-	
		Pablos et al. (2016)	<ul style="list-style-type: none"> <li>SMOS BEC level-3 soil moisture product</li> <li>MODIS products including NDVI and LST</li> </ul>	<p>LST day: ubRMSD<sup>***</sup>=0.04 to 0.06 m<sup>3</sup> m<sup>-3</sup>, R<sup>2</sup>=0.3 to 0.72* (on average)                      LST night: ubRMSD=0.04 to 0.07 m<sup>3</sup> m<sup>-3</sup>, R<sup>2</sup>=0.2 to 0.64* (on average)                      Ensemble of day and night LST:                      ubRMSD=0.04 to 0.07 m<sup>3</sup> m<sup>-3</sup>, R<sup>2</sup>=0.3 to 0.72* (on average)</p>		
		Piles et al. (2016)	<ul style="list-style-type: none"> <li>SMOS BEC level-3 soil moisture product</li> <li>MSG SEVIRI products including NDVI and LST</li> </ul>	<p>REMEDHUS:                      Instant: RMSD=0.043 m<sup>3</sup> m<sup>-3</sup>,                      ubRMSD<sup>***</sup>=0.04 m<sup>3</sup> m<sup>-3</sup>, R<sup>2</sup>=0.67*                      Daytime: RMSD=0.063 m<sup>3</sup> m<sup>-3</sup>,                      ubRMSD=0.06 m<sup>3</sup> m<sup>-3</sup>, R<sup>2</sup>=0.45*                      SMOSMANIA:                      Instant: RMSD=0.1 m<sup>3</sup> m<sup>-3</sup>,                      ubRMSD=0.051 m<sup>3</sup> m<sup>-3</sup>, R<sup>2</sup>=0.41*                      Daytime: RMSD=0.109 m<sup>3</sup> m<sup>-3</sup>,                      ubRMSD=0.062 m<sup>3</sup> m<sup>-3</sup>, R<sup>2</sup>=0.26*                      VAS:                      Instant: RMSD=0.065 m<sup>3</sup> m<sup>-3</sup>,                      ubRMSD=0.031 m<sup>3</sup> m<sup>-3</sup>, R<sup>2</sup>=0.79*</p>	<p>REMEDHUS:                      Instant: ΔRMSD=0.013 m<sup>3</sup> m<sup>-3</sup>,                      ΔubRMSD=-0.04 m<sup>3</sup> m<sup>-3</sup>,                      ΔR<sup>2</sup>=0.06*                      Daytime: ΔRMSD=-0.007 m<sup>3</sup> m<sup>-3</sup>,                      ΔubRMSD=-0.024 m<sup>3</sup> m<sup>-3</sup>,                      ΔR<sup>2</sup>=-0.16*                      SMOSMANIA:                      Instant: ΔRMSD=-0.021 m<sup>3</sup> m<sup>-3</sup>,                      ΔubRMSD=-0.01 m<sup>3</sup> m<sup>-3</sup>,                      ΔR<sup>2</sup>=-0.18*</p>	

Table 2.2 (continued)

Downscaling Techniques	Approaches	References	Main inputs	Accuracy	Improvement over the radiometer only measurements	Range of accuracy parameters
				Daytime: RMSE=0.072 m <sup>3</sup> m <sup>-3</sup> , ubRMSE=0.051 m <sup>3</sup> m <sup>-3</sup> , R <sup>2</sup> =0.45*	Daytime: ΔRMSE=-0.03 m <sup>3</sup> m <sup>-3</sup> , ΔubRMSE=-0.021 m <sup>3</sup> m <sup>-3</sup> , ΔR <sup>2</sup> =-0.33*, VAS: Instant: ΔRMSE=0.005 m <sup>3</sup> m <sup>-3</sup> , ΔubRMSE=0.014 m <sup>3</sup> m <sup>-3</sup> , ΔR <sup>2</sup> =-0.09* Daytime: ΔRMSE=-0.002 m <sup>3</sup> m <sup>-3</sup> , ΔubRMSE=-0.006 m <sup>3</sup> m <sup>-3</sup> , ΔR <sup>2</sup> =-0.26*	
		Knipper et al. (2017)	<ul style="list-style-type: none"> <li>SMOS CATDS Level 3 soil moisture products</li> <li>SMAP Level 3 (L3_SM_P) soil moisture products</li> <li>MODIS products including LST, EVI and Albedo</li> </ul>	<p>Chauhan et al. (2003) :</p> <p>SMOS : ubRMSE**=0.042 m<sup>3</sup> m<sup>-3</sup>, R<sup>2</sup>=0.31</p> <p>SMAP: ubRMSE=0.036 m<sup>3</sup> m<sup>-3</sup>, R<sup>2</sup>=0.39</p> <p>Piles et al. (2011) :</p> <p>SMOS : ubRMSE=0.043 m<sup>3</sup> m<sup>-3</sup>, R<sup>2</sup>=0.31</p> <p>SMAP: ubRMSE=0.037 m<sup>3</sup> m<sup>-3</sup>, R<sup>2</sup>=0.35</p> <p>Chauhan et al. (2003) :</p> <p>SMOS : ubRMSE=0.046 m<sup>3</sup> m<sup>-3</sup>, R<sup>2</sup>=0.32</p> <p>SMAP: ubRMSE=0.037 m<sup>3</sup> m<sup>-3</sup>, R<sup>2</sup>=0.37</p>	<p>Chauhan et al. (2003) :</p> <p>SMOS : ΔubRMSE=0.008 m<sup>3</sup> m<sup>-3</sup>, ΔR<sup>2</sup>=-0.06</p> <p>SMAP: ΔubRMSE=-0.004 m<sup>3</sup> m<sup>-3</sup>, ΔR<sup>2</sup>=-0.13</p> <p>Piles et al. (2011) :</p> <p>SMOS : ΔubRMSE=0.007 m<sup>3</sup> m<sup>-3</sup>, ΔR<sup>2</sup>=-0.06</p> <p>SMAP: ΔubRMSE=-0.005 m<sup>3</sup> m<sup>-3</sup>, ΔR<sup>2</sup>=-0.17</p> <p>Chauhan et al. (2003) :</p> <p>SMOS : ΔubRMSE=0.004 m<sup>3</sup> m<sup>-3</sup>, ΔR<sup>2</sup>=-0.05</p> <p>SMAP: ΔubRMSE=-0.005 m<sup>3</sup> m<sup>-3</sup>, ΔR<sup>2</sup>=-0.15</p>	
Soil surface attributes-based	Statistical	Kim and Barros (2002a)	<ul style="list-style-type: none"> <li>SGP '97 experimental ESTAR L-band radiometric data</li> <li>DEM and rainfall data set</li> <li>AVHRR NDVI products</li> <li>Soil texture derived from AVHRR observations</li> </ul>	Variance=0.24 m <sup>3</sup> m <sup>-3</sup> (On average)	-	<p>RMSE ∈ (0.0224,0.033)</p> <p>m<sup>3</sup> m<sup>-3</sup></p> <p>R<sup>2</sup> ∈ (0.023,0.86)</p>

Table 2.2 (continued)

Downscaling Techniques	Approaches	References	Main inputs	Accuracy	Improvement over the radiometer only measurements	Range of accuracy parameters
		Pellenq et al. (2003)	<ul style="list-style-type: none"> <li>• High resolution DEM data</li> <li>• High resolution soil moisture maps from time domain reflectometry</li> <li>• Soil temperature profile measurements</li> <li>• Soil heat flux and meteorological measurements including rainfall</li> <li>• Surface roughness measurements</li> <li>• Soils information including field saturated hydraulic conductivity and soil depth</li> </ul>	$R^2=0.67^*$		
		Wilson et al. (2005)	<ul style="list-style-type: none"> <li>• High resolution soil moisture data</li> <li>• Terrain attributes</li> </ul>	Std. Dev.=0.027 m <sup>3</sup> m <sup>-3</sup> (On average)	$\Delta$ Std. Dev.=0.011 m <sup>3</sup> m <sup>-3</sup> (On average)	
		Perry and Niemann (2007)	<ul style="list-style-type: none"> <li>• Soil and vegetation properties</li> </ul>	RMSD and R <sup>2</sup> are not reported as measures of agreement.		
		Busch et al. (2012)	<ul style="list-style-type: none"> <li>• High resolution DEM data</li> <li>• Topographic attributes including wetness index and variables that are contained in the wetness index (slope and lnSCA)</li> </ul>			
		Coleman and Niemann (2013)	<ul style="list-style-type: none"> <li>• High resolution DEM</li> <li>• Topographic indices</li> <li>• Vegetation and soil properties</li> </ul>			
		Ranney et al. (2015)	<ul style="list-style-type: none"> <li>• High resolution DEM</li> <li>• Topographic indices</li> <li>• High resolution vegetation and soil properties</li> </ul>	Topography: EMT: RMSD=0.028 m <sup>3</sup> m <sup>-3</sup> EOF: RMSD=0.027 m <sup>3</sup> m <sup>-3</sup> Topography and soil: EMT+VS: RMSD=0.029 m <sup>3</sup> m <sup>-3</sup> EOF: RMSD=0.027 m <sup>3</sup> m <sup>-3</sup>		
		Cowley et al. (2017)	<ul style="list-style-type: none"> <li>• High resolution DEM</li> </ul>	RMSD and R <sup>2</sup> are not reported as measures of agreement.		

Table 2.2 (continued)

Downscaling Approaches Techniques	References	Main inputs	Accuracy	Improvement over the radiometer only measurements	Range of accuracy parameters
	Hoehn et al. (2017)	<ul style="list-style-type: none"> <li>Topographic indices</li> <li>High resolution vegetation and soil properties</li> <li>Precipitation and potential evapotranspiration data</li> </ul>	The accuracy of downscaled soil moisture products is not provided at fine resolution, but at the resolution of coarse soil moisture after averaging the values within the scale of coarse soil moisture.		
	Temimi et al. (2010)	<ul style="list-style-type: none"> <li>AMSR-E Ka-band radiometric data</li> <li>MODIS LAI product</li> <li>Topographic attributes from STRM Digital Elevation Model</li> </ul>	Fort Chipewyan A: Dynamic TWI: $R^2=0.49^*$ (on average) Classic TWI: $R^2=0.14^*$ (on average) Prairie River: Dynamic TWI: $R^2=0.18^*$ (on average) Classic TWI: $R^2=0.023^*$ (on average)	Fort Chipewyan A: Dynamic TWI: $\Delta R^2=0.24^*$ Classic TWI: $\Delta R^2=-0.11^*$ Prairie River: Dynamic TWI: $\Delta R^2=-0.09^*$ Classic TWI: $\Delta R^2=-0.0247^*$	
	Ines et al. (2013)	<ul style="list-style-type: none"> <li>SGP97 experimental ESTAR L-band radiometric data</li> <li>Synthetic data set (Walnut Creek WC11)</li> <li>Soil hydraulic properties of Mualem-van Genuchten functions</li> </ul>	FD bottom-boundary conditions: RMSD=0.0224 $m^3 m^{-3}$ , $R^2=0.86^*$ (on average) Variable groundwater conditions: RMSD=0.0327 $m^3 m^{-3}$ , $R^2=0.74^*$ (on average)		
	Shin and Mohanty (2013)	<ul style="list-style-type: none"> <li>SGP97 experimental ESTAR L-band radiometric data</li> <li>Synthetic data set (Little Washita-LW 13 and 21, Oklahoma)</li> <li>Soil hydraulic properties of Mualem-van Genuchten functions</li> </ul>	LW 13: MBE=-0.203 to -0.169 $m^3 m^{-3}$ , $R^2=0.52$ to $0.83^*$ LW 21: MBE=-0.165 to -0.122 $m^3 m^{-3}$ , $R^2=0.12$ to $0.76^*$		
<b>Data assimilation-based</b>	Reichle et al. (2001)	<ul style="list-style-type: none"> <li>SGP97 experimental ESTAR L-band radiometric data</li> <li>Synthetic L-band radiometric data</li> <li>Outputs of a land surface hydrologic model by (Reichle, 2000)</li> </ul>	RMSD=0.03 to $0.038 m^3 m^{-3}$		RMSD $\in (0.03, 0.09) m^3 m^{-3}$ $R^2 \in (0.07, 0.86)$

Table 2.2 (continued)

Downscaling Approaches Techniques	References	Main inputs	Accuracy	Improvement over the radiometer only measurements	Range of accuracy parameters
low resolution radiometric observations	Draper et al. (2009)	<ul style="list-style-type: none"> <li>LPRM AMSR-E C-band soil moisture</li> <li>Outputs of ISBA model</li> </ul>	RMSD > 0.09 m <sup>3</sup> m <sup>-3</sup>	-	ubRMSD*** ∈ (0.0012, 0.083)
	Sahoo et al. (2013)	<ul style="list-style-type: none"> <li>AMSR-E X-band radiometer data</li> <li>Outputs of Noah land surface model by Mahrt and Pan (1984)</li> </ul>	RMSD = 0.03 m <sup>3</sup> m <sup>-3</sup> , R <sup>2</sup> = 0.69*	ΔRMSD = 0.02 m <sup>3</sup> m <sup>-3</sup> , ΔR <sup>2</sup> = 0.25*	
	Kornelsen et al. (2015)	<ul style="list-style-type: none"> <li>Simulated brightness temperature using CMEM</li> <li>Dense soil moisture measurements from experimental watersheds</li> </ul>	Little River: RMSD = 0.04 m <sup>3</sup> m <sup>-3</sup> Little Washita: RMSD = 0.06 m <sup>3</sup> m <sup>-3</sup>	Little River: ΔRMSD = 0.01 m <sup>3</sup> m <sup>-3</sup> Little Washita: ΔRMSD = 0.03 m <sup>3</sup> m <sup>-3</sup>	
	Lievens et al. (2015)	<ul style="list-style-type: none"> <li>SMOS Level 3 CATDS soil moisture</li> <li>Outputs of VIC model</li> <li>Precipitation, 2-meter air temperature, pressure, vapour pressure, wind speed, and incoming shortwave and longwave radiation</li> </ul>	Mean: RMSD = 0.076 m <sup>3</sup> m <sup>-3</sup> , R <sup>2</sup> = 0.51* SD: RMSD = 0.078 m <sup>3</sup> m <sup>-3</sup> , R <sup>2</sup> = 0.47* CDF: RMSD = 0.077 m <sup>3</sup> m <sup>-3</sup> , R <sup>2</sup> = 0.48*	Mean: ΔRMSD = -0.001 m <sup>3</sup> m <sup>-3</sup> , ΔR <sup>2</sup> = -0.02* SD: ΔRMSD = -0.004 m <sup>3</sup> m <sup>-3</sup> , ΔR <sup>2</sup> = -0.06* CDF: ΔRMSD = -0.004 m <sup>3</sup> m <sup>-3</sup> , ΔR <sup>2</sup> = -0.05*	
	Draper and Reichle (2015)	<ul style="list-style-type: none"> <li>Level 3 LPRM AMSR-E X-band soil moisture products</li> <li>Outputs of the NASA's Catchment Land Surface Model</li> </ul>	ubMSE*** = 0.0012 m <sup>3</sup> m <sup>-3</sup> (on average)	-	
	Reichle et al. (2017)	<ul style="list-style-type: none"> <li>SMAP L1C_TB brightness temperature observations</li> <li>Surface meteorological forcing data from the GEOS-5 atmospheric assimilation system. Corrected with precipitation observation</li> </ul>	All sites: ubRMSD*** = 0.038 m <sup>3</sup> m <sup>-3</sup> REMEDHUS: ubRMSD = 0.034 m <sup>3</sup> m <sup>-3</sup> Reynolds Creek: ubRMSD = 0.03 m <sup>3</sup> m <sup>-3</sup> Yanco: ubRMSD = 0.05 m <sup>3</sup> m <sup>-3</sup> Carman: ubRMSD = 0.05 m <sup>3</sup> m <sup>-3</sup> Walnut Gulch: ubRMSD = 0.032 m <sup>3</sup> m <sup>-3</sup>	-	

Table 2.2 (continued)

Downscaling Techniques	Approaches	References	Main inputs	Accuracy	Improvement over the radiometer only measurements	Range of accuracy parameters
	<ul style="list-style-type: none"> <li>Outputs of the NASA's Catchment Land Surface Model</li> </ul>			Little Washita: ubRMSE=0.034 m <sup>3</sup> m <sup>-3</sup> Fort Cobb: ubRMSE=0.038 m <sup>3</sup> m <sup>-3</sup> Little River: ubRMSE=0.038 m <sup>3</sup> m <sup>-3</sup> St Josephs: ubRMSE=0.05 m <sup>3</sup> m <sup>-3</sup> South Fork: ubRMSE=0.048 m <sup>3</sup> m <sup>-3</sup> Monte Buey: ubRMSE=0.029 m <sup>3</sup> m <sup>-3</sup> Tonzi Ranch: ubRMSE=0.037 m <sup>3</sup> m <sup>-3</sup> Kenaston: ubRMSE=0.038 m <sup>3</sup> m <sup>-3</sup> Valencia: ubRMSE=0.023 m <sup>3</sup> m <sup>-3</sup> Niger: ubRMSE=0.033 m <sup>3</sup> m <sup>-3</sup> Benin: ubRMSE=0.047 m <sup>3</sup> m <sup>-3</sup> Yanco: ubRMSE=0.041 m <sup>3</sup> m <sup>-3</sup>		
	<ul style="list-style-type: none"> <li>SMAP L1C TB brightness temperature observations</li> <li>Sentinel-1 C-band backscatter</li> <li>Surface meteorological forcing data from the GEOS-5 atmospheric assimilation system, Corrected with precipitation observation</li> <li>Outputs of the NASA's Catchment Land Surface Model</li> </ul>	Lievens et al. (2017)		Radiometer only assimilation: Core sites: ubRMSE**=0.048 m <sup>3</sup> m <sup>-3</sup> , R <sup>2</sup> =0.44* REMEDHUS: ubRMSE=0.037 m <sup>3</sup> m <sup>-3</sup> , R <sup>2</sup> =0.28* Yanco: ubRMSE=0.049 m <sup>3</sup> m <sup>-3</sup> , R <sup>2</sup> =0.85* Twente: ubRMSE=0.083 m <sup>3</sup> m <sup>-3</sup> , R <sup>2</sup> =0.27* Little Washita: ubRMSE=0.035 m <sup>3</sup> m <sup>-3</sup> , R <sup>2</sup> =0.64* Fort Cobb: ubRMSE=0.038 m <sup>3</sup> m <sup>-3</sup> , R <sup>2</sup> =0.55* South Fork: ubRMSE=0.052 m <sup>3</sup> m <sup>-3</sup> , R <sup>2</sup> =0.38* Valencia: ubRMSE=0.024 m <sup>3</sup> m <sup>-3</sup> , R <sup>2</sup> =0.24* Niger: ubRMSE=0.049 m <sup>3</sup> m <sup>-3</sup> , R <sup>2</sup> =0.22*	-	

Table 2.2 (continued)

Downscaling Techniques	Approaches	References	Main inputs	Accuracy	Improvement over the radiometer only measurements	Range of accuracy parameters
				Benind: ubRMSE=0.056 m <sup>3</sup> m <sup>-3</sup> , R <sup>2</sup> =0.55*		
				TxSON: ubRMSE=0.039 m <sup>3</sup> m <sup>-3</sup> , R <sup>2</sup> =0.69*		
				HOBE: ubRMSE=0.051 m <sup>3</sup> m <sup>-3</sup> , R <sup>2</sup> =0.53*		
				Sparse networks: ubRMSE=0.054 m <sup>3</sup> m <sup>-3</sup> , R <sup>2</sup> =0.44*		
				SCAN: ubRMSE=0.056 m <sup>3</sup> m <sup>-3</sup> , R <sup>2</sup> =0.41*		
				USCRNF: ubRMSE=0.053 m <sup>3</sup> m <sup>-3</sup> , R <sup>2</sup> =0.44*		
				Oklahoma Mesonetg: ubRMSE=0.058 m <sup>3</sup> m <sup>-3</sup> , R <sup>2</sup> =0.45*		
				OzNet: ubRMSE=0.062 m <sup>3</sup> m <sup>-3</sup> , R <sup>2</sup> =0.71*		
				SMOSMANIA: ubRMSE=0.045 m <sup>3</sup> m <sup>-3</sup> , R <sup>2</sup> =0.38*		
				Complementary radar and radiometer assimilation:		
				Core sites: ubRMSE=0.046 m <sup>3</sup> m <sup>-3</sup> , R <sup>2</sup> =0.49*		
				REMEDHUS: ubRMSE=0.035 m <sup>3</sup> m <sup>-3</sup> , R <sup>2</sup> =0.36*		
				Yanco: ubRMSE=0.049 m <sup>3</sup> m <sup>-3</sup> , R <sup>2</sup> =0.86*		
				Twente: ubRMSE=0.08 m <sup>3</sup> m <sup>-3</sup> , R <sup>2</sup> =0.38*		
				Little Washita: ubRMSE=0.035 m <sup>3</sup> m <sup>-3</sup> , R <sup>2</sup> =0.62*		
				Fort Cobb: ubRMSE=0.037 m <sup>3</sup> m <sup>-3</sup> , R <sup>2</sup> =0.55*		

Table 2.2 (continued)

Downscaling Techniques	Approaches	References	Main inputs	Accuracy	Improvement over the radiometer only measurements	Range of accuracy parameters	
				South Fork: ubRMSD=0.05 m <sup>3</sup> m <sup>-3</sup> , R <sup>2</sup> =0.45* Valencia: ubRMSD=0.024 m <sup>3</sup> m <sup>-3</sup> , R <sup>2</sup> =0.26* Niger: ubRMSD=0.045 m <sup>3</sup> m <sup>-3</sup> , R <sup>2</sup> =0.29* Benind: ubRMSD=0.056 m <sup>3</sup> m <sup>-3</sup> , R <sup>2</sup> =0.58* TxSON: ubRMSD=0.039 m <sup>3</sup> m <sup>-3</sup> , R <sup>2</sup> =0.67* HOBE: ubRMSD=0.046 m <sup>3</sup> m <sup>-3</sup> , R <sup>2</sup> =0.69* Sparse networks: ubRMSD=0.053 m <sup>3</sup> m <sup>-3</sup> , R <sup>2</sup> =0.46* SCAN: ubRMSD=0.055 m <sup>3</sup> m <sup>-3</sup> , R <sup>2</sup> =0.41* USCRNF: ubRMSD=0.053 m <sup>3</sup> m <sup>-3</sup> , R <sup>2</sup> =0.44* Oklahoma Mesonetg: ubRMSD=0.057 m <sup>3</sup> m <sup>-3</sup> , R <sup>2</sup> =0.45* OzNet: ubRMSD=0.061 m <sup>3</sup> m <sup>-3</sup> , R <sup>2</sup> =0.72* SMOSMANIA: ubRMSD=0.042 m <sup>3</sup> m <sup>-3</sup> , R <sup>2</sup> =0.44*			
<b>Machine-learning-based</b>	Relationship with surface parameters	Srivastava et al. (2013)	<ul style="list-style-type: none"> <li>SMOS L-band radiometric data</li> <li>MODIS LST product</li> </ul>	ANN: RMSD=0.011 m <sup>3</sup> m <sup>-3</sup> , R <sup>2</sup> =0.75 RVM: RMSD=0.013 m <sup>3</sup> m <sup>-3</sup> , R <sup>2</sup> =0.69 SVM: RMSD=0.013 m <sup>3</sup> m <sup>-3</sup> , R <sup>2</sup> =0.69 GLM: RMSD=0.013 m <sup>3</sup> m <sup>-3</sup> , R <sup>2</sup> =0.69	ANN: ΔRMSD=0.006 m <sup>3</sup> m <sup>-3</sup> , ΔR <sup>2</sup> =0.33 RVM: ΔRMSD=0.004 m <sup>3</sup> m <sup>-3</sup> , ΔR <sup>2</sup> =0.27 SVM: ΔRMSD=0.004 m <sup>3</sup> m <sup>-3</sup> , ΔR <sup>2</sup> =0.27 GLM: ΔRMSD=0.004 m <sup>3</sup> m <sup>-3</sup> , ΔR <sup>2</sup> =0.27	RMSD ∈ (0.006, 0.16) m <sup>3</sup> m <sup>-3</sup> R <sup>2</sup> ∈ (0.37, 0.96)	

Table 2.2 (continued)

Downscaling Techniques	Approaches	References	Main inputs	Accuracy	Improvement over the radiometer only measurements	Range of accuracy parameters
		Chai et al. (2011) Chai and Goh (2013)	<ul style="list-style-type: none"> <li>NAFE05 experimental PLMR L-band radiometric data</li> <li>MODIS products including surface reflectance, LST and emissivity</li> </ul>	RMSD=0.018 to 0.035 m <sup>3</sup> m <sup>-3</sup> RMSD=0.0233 m <sup>3</sup> m <sup>-3</sup> , R <sup>2</sup> =0.89	-	
		Chakrabarti et al. (2015) Chakrabarti et al. (2016)	<ul style="list-style-type: none"> <li>MicroWEXs meteorological forcing data</li> <li>Land cover map</li> <li>Synthetic data set simulated by using a coupled LSP-DSSAT model</li> </ul>	PRI method: RMSD=0.006 m <sup>3</sup> m <sup>-3</sup> UTD method: RMSD=0.079 m <sup>3</sup> m <sup>-3</sup> RMSD<0.02 m <sup>3</sup> m <sup>-3</sup>	-	
		Park et al. (2015)	<ul style="list-style-type: none"> <li>AMSR2 C-band LPRM daily soil moisture products</li> <li>MODIS products including surface albedo, LST, NDVI, EVI, LAI and evapotranspiration</li> </ul>	Random forest: RMSD=0.06 m <sup>3</sup> m <sup>-3</sup> , R <sup>2</sup> =0.96 Ordinary least square: RMSD=0.16 m <sup>3</sup> m <sup>-3</sup> , R <sup>2</sup> =0.47	-	
		Im et al. (2016)	<ul style="list-style-type: none"> <li>AMSR-E C-band LPRM Level 3 daily soil moisture products</li> <li>MODIS products including surface albedo, LST, NDVI, EVI, LAI and evapotranspiration</li> </ul>	Random forest: South Korea: RMSD=0.049 m <sup>3</sup> m <sup>-3</sup> , R <sup>2</sup> =0.50* Australia: RMSD=0.057 m <sup>3</sup> m <sup>-3</sup> , R <sup>2</sup> =0.71* Boosted regression trees: South Korea: RMSD=0.052 m <sup>3</sup> m <sup>-3</sup> , R <sup>2</sup> =0.56* Australia: RMSD=0.078 m <sup>3</sup> m <sup>-3</sup> , R <sup>2</sup> =0.59* Cubist: South Korea: RMSD=0.051 m <sup>3</sup> m <sup>-3</sup> , R <sup>2</sup> =0.49* Australia: RMSD=0.063 m <sup>3</sup> m <sup>-3</sup> , R <sup>2</sup> =0.37*	Random forest: South Korea: ΔRMSD=0.059 m <sup>3</sup> m <sup>-3</sup> , ΔR <sup>2</sup> =0.28* (on average) Australia: ΔRMSD=-0.004 m <sup>3</sup> m <sup>-3</sup> , ΔR <sup>2</sup> =0.45* (on average) Boosted regression trees: South Korea: ΔRMSD=0.056 m <sup>3</sup> m <sup>-3</sup> , ΔR <sup>2</sup> =0.34* (on average) Australia: ΔRMSD=-0.025 m <sup>3</sup> m <sup>-3</sup> , ΔR <sup>2</sup> =0.33* (on average) Cubist: South Korea: ΔRMSD=-0.057 m <sup>3</sup> m <sup>-3</sup> , ΔR <sup>2</sup> =0.27* (on average)	

Table 2.2 (continued)

Downscaling Approaches Techniques	References	Main inputs	Accuracy	Improvement over the radiometer only measurements	Range of accuracy parameters
	Jiang et al. (2017)	<ul style="list-style-type: none"> <li>LPRM, JAXA, and NASA AMSR-E soil moisture products</li> <li>JAXA AMSR2 soil moisture products</li> <li>SMOS CATDS Level 3 soil moisture products</li> </ul>	NASA AMSR-E: RMSD=0.15 m <sup>3</sup> m <sup>-3</sup> , R <sup>2</sup> =0.55* LPRM AMSR-E: RMSD=0.12 m <sup>3</sup> m <sup>-3</sup> , R <sup>2</sup> =0.69* JAXA AMSR-E: RMSD=0.081 m <sup>3</sup> m <sup>-3</sup> , R <sup>2</sup> =0.72* JAXA AMSR2: RMSD=0.055 m <sup>3</sup> m <sup>-3</sup> , R <sup>2</sup> =0.86* Ascending SMOS: RMSD=0.081 m <sup>3</sup> m <sup>-3</sup> , R <sup>2</sup> =0.41* Descending SMOS: RMSD=0.047 m <sup>3</sup> m <sup>-3</sup> , R <sup>2</sup> =0.77*	Australia: ΔRMSD=-0.01 m <sup>3</sup> m <sup>-3</sup> , ΔR <sup>2</sup> =0.11* (on average)  NASA AMSR-E: ΔRMSD=-0.012 m <sup>3</sup> m <sup>-3</sup> , ΔR <sup>2</sup> =0.18* LPRM AMSR-E: ΔRMSD=-0.001 m <sup>3</sup> m <sup>-3</sup> , ΔR <sup>2</sup> =-0.02* JAXA AMSR-E: ΔRMSD=0.037 m <sup>3</sup> m <sup>-3</sup> , ΔR <sup>2</sup> =-0.05* JAXA AMSR2: ΔRMSD=0.071 m <sup>3</sup> m <sup>-3</sup> , ΔR <sup>2</sup> =0.11* Ascending SMOS: ΔRMSD=0.01 m <sup>3</sup> m <sup>-3</sup> , ΔR <sup>2</sup> =0.1* Descending SMOS: ΔRMSD=0.004 m <sup>3</sup> m <sup>-3</sup> , ΔR <sup>2</sup> =0.09*	

\*The R<sup>2</sup> (coefficient of determination) has been calculated by squaring values in R (correlation coefficient).

\*\*Indicates studies where their accuracy parameters have been obtained from digitizing the results shown in figure.

\*\*\*ubRMSD and ubMSE values are not included in the summary and discussion section. They are added to this table for the information of readers.

Note: negative values of both ΔR<sup>2</sup> and ΔRMSD means that coarse passive microwave observations have provided better estimates of soil moisture than the downscaled products.

C-band ( $\sim 6.9$  GHz) and X-band ( $\sim 10$  GHz). The higher frequencies such as Ka-band are not as sensitive to soil moisture as lower frequencies and respond to a very shallow layer of soil (Calvet et al., 2011; Yee et al., 2017). Conversely, the Ka-band provides observations at much higher resolution than lower frequencies because the Instantaneous Field of View (IFOV) which is a spatial resolution measure of the remote sensing system is proportional to wavelength (Salvia et al., 2011). Therefore, while direct retrieval is unlikely, Ka-band could be a potential source of information about the surface spatial heterogeneity (e.g. Gevaert et al., 2015; Neale et al., 1990; Santi, 2010).

The multi-source concept, in which the strengths of each sensor type are utilized, could potentially improve the soil moisture estimation in terms of both accuracy and spatial scale. Several studies have therefore suggested that the remotely sensed soil moisture from the passive microwave observations at lower (L-and C-band) frequencies be combined with backscatter or passive microwave emission at higher (Ka-band) frequency. These combination techniques are briefly introduced in the radar-and radiometer-based subsections below.

The combination of active/passive microwave observations has been a preferred approach to downscaling because both sensors respond to changes in the dielectric properties of the soil. Ulaby et al. (1983) conducted one of the first investigations based on this approach using L-band radiometer and C-band radar soil moisture estimates over bare soil and corn fields. They found that it could reduce the estimation error by up to 30% of the reference soil moisture value. Findings from this pioneering work motivated Theis et al. (1986), O'Neill and Chauhan (1992), O'Neill et al. (1996) and Chauhan (1997) to propose approaches using active and passive microwave techniques in compliment to each other, to optimize the accuracy of the final soil moisture estimates. Theis et al. (1986) used L-band scatterometer data to compensate for the surface roughness impact on the response of L-and C-band radiometers to soil moisture. This complimentary combination significantly improved the passive microwave remote sensing of soil moisture over bare fields, especially for L-band soil moisture retrievals, with  $R^2$  equal to 0.95. In order to utilize active and passive microwave data sets in combination, O'Neill and Chauhan (1992) retrieved soil moisture from a radiative transfer model with radar-derived ancillary data on the vegetation attenuation parameter. This analysis, which was made for a single field covered by corn, demonstrated

that the radar derived vegetation attenuation could increase the accuracy of radiometric remote sensing of soil moisture. In another study, O'Neill et al. (1996) used L-band radar determination of vegetation transmissivity and scattering in a radiative transfer model to estimate soil moisture. They reported successful retrieval of soil moisture within about  $0.02 \text{ m}^3 \text{ m}^{-3}$  of the ground measurements. A dielectric-soil moisture relation was also employed by Chauhan (1997) to estimate soil moisture from Fresnel reflectivity, derived from radar-based estimation of vegetation and surface roughness parameters. The capability of passive microwave remote sensing in delivering soil moisture maps consequently improved, with an averaged absolute bias of less than  $0.05 \text{ m}^3 \text{ m}^{-3}$ .

### **Radar-based downscaling techniques**

Besides using combined passive and active microwave observations as a means of improving the retrieval of soil moisture measurement, investigations were made for combined radar-radiometer downscaling techniques. This technique attempts to recover the spatial detail of the coarse soil moisture/brightness temperature through the association of the sub-pixel distribution of land surface features embedded in the radar imagery. However, the sensitivity of backscatter to surface roughness and vegetation is the key limitation for applying this technique to radiometric soil moisture downscaling (Njoku et al., 2001). To explore this concept, a radar-radiometer data set was collected by the Passive-Active L-/S-band (PALS) sensor during the Southern Great Plains Experiment in 1999 (SGP99). This data set was used by Njoku et al. (2002) to design a change detection based downscaling algorithm that employed a linear relationship between the backscatter and volumetric soil moisture (e.g. Dobson and Ulaby, 1986). The use of relative changes in backscatter reduces the impact of surface roughness and vegetation on radar signals, and thus on soil moisture estimates (e.g. Moran et al., 2000; Quesney et al., 2000; Wagner and Scipal, 2000). Narayan et al. (2006) modified the Njoku et al. (2002) method by using the relative radar response to soil moisture suggested by Du et al. (2000).

In order to conduct an assessment of the algorithm's applicability, coincident active microwave observations and passive microwave derived soil moisture products were simulated to mimic the gradual wetting and drying conditions. The spatial variability in soil mois-

ture and vegetation water content were assumed to be the only factors influencing temporal changes in the radar signals. This method was used by Narayan and Lakshmi (2008) to downscale space-borne soil moisture estimates from the Advanced Microwave Scanning Radiometer (AMSR-E) and Tropical Rainfall Measuring Mission (TRMM) Microwave Imager (TMI) with backscatter from the Precipitation Radar (PR). This study demonstrated the applicability of the radar-based downscaling technique to represent soil moisture spatial variability. Through inter-comparison between downscaled TMI and AMSR-E, temporal coincidence between radar and radiometer observations was found to exist, providing credence to this approach; soil moisture products from the TMI sensor on the same platform as the TRMM-PR radar were much better enhanced spatially than those from the AMSR-E.

Research on the integration of radar and radiometer observations for spatially enhanced soil moisture mapping has not been limited to the physically based approach of Njoku et al. (2002). For example, Bindlish and Barros (2002) also produced sub-scale brightness temperature prior to soil moisture retrieval by applying a fractal interpolation methodology, combining radar and radiometric observations. In this approach, the ratio between high resolution HH-polarized backscatter, and aggregated backscatter to the scale of the coarse brightness temperature observation, was used as a weighting coefficient to estimate brightness temperature at the same resolution as the backscatter observations. In a further approach, Zhan et al. (2006) developed a Bayesian disaggregation method that merges radar and radiometer observations with an initial background soil moisture field. In this study, using synthetic data from an Observation System Simulation Experiment (OSSE), the background states of soil moisture were first derived using direct inversion of coarse brightness temperature. The uncertainties in the initial soil moisture estimate and the satellite observations were then used to merge observed and calculated brightness temperature and backscatter from the background soil moisture using emission and backscatter models, to get an updated soil moisture field. Wu et al. (2017) subsequently applied this technique to a time series of experimental aircraft-based radar/radiometer observations collected during the SMAPEX-3 field campaign Panciera et al. (2014) in south-eastern Australia to produce 1, 3 and 9 km resolution soil moisture maps. Findings from this study revealed that: i) the performance of the Bayesian method depended on the accuracy of the radar model, and

that ii) the Bayesian merging technique performed best over grassland areas with the radar model used in that study.

The development of radar-based downscaling techniques entered a new phase with the announcement of a dedicated active/passive microwave satellite for soil moisture, SMAP, in response to the National Research Council's Decadal Survey. The SMAP satellite was designed to measure temporally coincident surface emission and backscatter from a radiometer/radar using a single large mesh antenna with a conical scan configuration. The concept of having a radar and radiometer integrated into a single system was first introduced by Njoku et al. (2000). The conical scan provides measurements of the Earth's surface at constant incidence angle and antenna pattern characteristics across the entire swath. Accordingly, the data processing, interpretation, and geophysical retrieval become simplified. The SMAP mission aimed to combine the strengths of the respective radar and radiometer observations - high spatial resolution for the radar and high sensitivity to soil moisture for the radiometer - to estimate soil moisture content at an intermediate resolution.

The change detection method of Piles et al. (2009b) was among the first alternative techniques to derive active/passive microwave merged products. Piles et al. (2009b) made use of the linear correlation between backscatter and soil moisture content for formulating a disaggregation algorithm which derived relative changes of soil moisture. This approach produced the spatial variability of soil moisture by updating the radiometer soil moisture retrieval from the previous observation with the corresponding temporal changes in high resolution backscatter. The approach was applied to airborne data from PALS for the SMEX02 campaign, and to an OSSE. The change detection approach revealed superiority to radiometer-only estimations in terms of both the accuracy and spatial heterogeneity of soil moisture products.

The active/passive optional algorithm developed by Das et al. (2011) is an extension to the Piles et al. (2009b) change detection approach. This technique was also developed based on the linear regression between backscatter and volumetric soil moisture. The major enhancement of the active/passive retrieval method over the change detection technique was the estimation of an absolute soil moisture. Being based on the linear relationship between

backscatter and passive-based soil moisture products, the successful application of these techniques depends to a great extent on how well backscatter and soil moisture are correlated (Wu et al., 2014), and how sensitive they are to soil moisture changes.

The SMAP active/passive baseline algorithm by Das et al. (2014), which established a linear regression between backscatter and brightness temperature for estimation of absolute soil moisture at 9 km, was an extension of the active/passive optional retrieval algorithm developed by Das et al. (2011). The baseline algorithm downscaled observed brightness temperature and then performed the soil moisture retrieval, as opposed to the optional active/passive retrieval algorithm that downscaled derived soil moisture at coarse resolution as described above. An important aspect of the baseline algorithm is that it considers vegetation and surface roughness heterogeneity in time and space when calibrating the main downscaling factor  $\beta$  [K/dB] as an added value to the active/passive retrieval algorithm. The processing steps of the baseline model currently used by the SMAP science team are described in Figure 2.2.

Wu et al. (2016) applied the active/passive optional (Das et al., 2011), baseline (Das et al.,

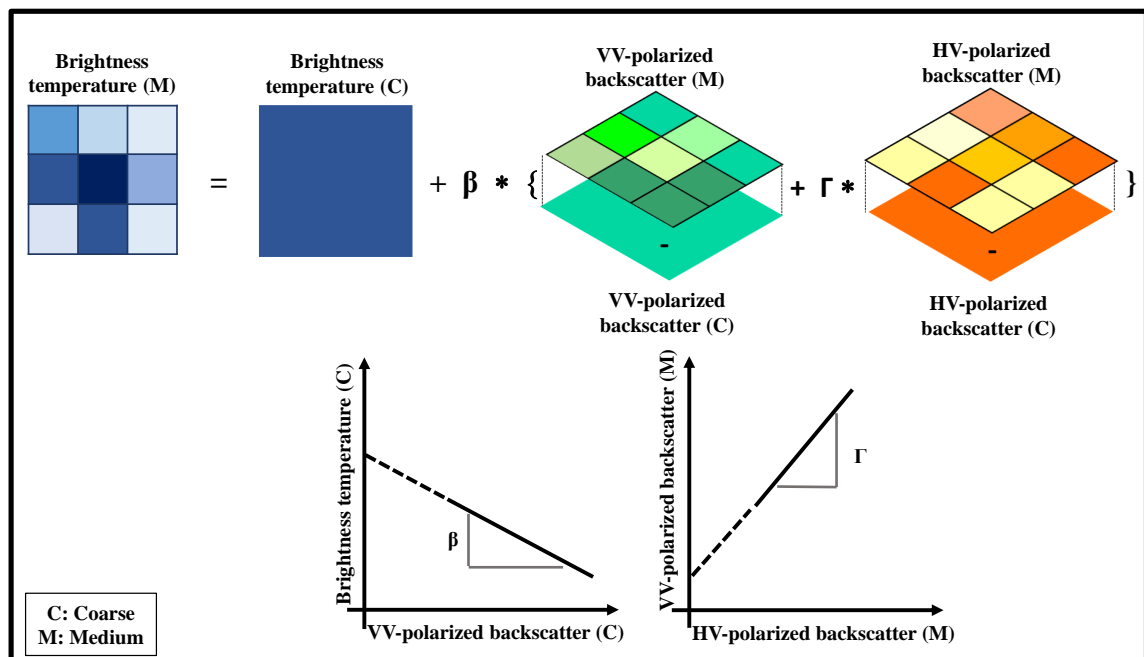


Figure 2.2: Schematic diagram of the SMAP active/passive baseline algorithm (adapted from Dr. Xiaoling Wu personal communication).

2014) and change detection (Piles et al., 2009b) retrieval algorithms to the SMAPEX-3 airborne simulation (Wu et al., 2015) of the SMAP data stream to test the robustness of alternate radar-radiometer combination algorithms over a semi-arid region. Findings of this study revealed that all the alternate algorithms had only small differences in average Root Mean Square Deviation (RMSD) and could effectively increase the spatial resolution of soil moisture retrievals from 36 to 9 km. However, the active/passive retrieval algorithm by Das et al. (2011) showed the best correlation with the reference soil moisture map. Consequently, Wu et al. (2016) recommended application of the optional active/passive retrieval algorithm by Das et al. (2011) for global soil moisture mapping.

Montzka et al. (2016) developed a linear relationship between radar-and radiometer-only soil moisture estimates for calibrating a disaggregation algorithm which enhances the spatial resolution of passive-based soil moisture retrievals. This approach was applied to L-band radar and radiometer airborne data from the Tereno campaign (Montzka et al., 2012). Performance of this method was compared against the active/passive optional (Das et al., 2011) and baseline (Das et al., 2014) retrieval algorithms. This analysis revealed superiority of the baseline algorithm in delivering more accurate high resolution soil moisture to the optional technique and the new combined radar/radiometer-only soil moisture technique by Montzka et al. (2016). However, the spatial pattern of retrieved soil moisture from the new combined radar/radiometer-only soil moisture technique by Montzka et al. (2016) was reported to be similar to that of the baseline retrievals.

Recently, Rüdiger et al. (2016) downscaled an airborne simulation of the coarse scale L-band brightness temperature at 50 km using ESA's C-band ASAR backscatter aggregated to 2 km. This technique included two changes to the active/passive optional algorithm: i) calibration of the downscaling factor at higher resolution than the coarse scale of L-band observations in order to have an adequate number of regression points for establishing a linear relationship, ii) the establishment of a linear regression between the radiometric emissivities and radar backscatter sensitivities instead of between soil moisture and radar backscatter. The intention of using backscatter sensitivities and radiometric emissivities was to preserve the information of vegetation heterogeneity in the downscaling products and to remove the surface temperature impacts, respectively. This downscaling approach resulted in soil moisture

estimates with errors of 0.06 to 0.12 m<sup>3</sup> m<sup>-3</sup>, which are comparable to other downscaling techniques.

Akbar and Moghaddam (2015) proposed a Combined Active-Passive (CAP) algorithm based on a joint cost function with adaptive regularization by Monte Carlo numerical simulations. To increase the reliability of soil moisture retrievals in terms of accuracy, CAP gave more weight to radiometric soil moisture but without discarding the complimentary radar-based soil moisture estimates. The novelty of the CAP model was the merging of the same-scaled and coincident radar and radiometric soil moisture. This approach was demonstrated using airborne PALS and tower Combined Radar Radiometer (ComRad) acquisitions, resulting in soil moisture retrievals with accuracy of 0.038 m<sup>3</sup> m<sup>-3</sup> for low noise level measurement scenario.

### **Radiometer-based downscaling techniques**

The downscaling of coarse passive microwave data has not been limited to the use of backscatter. The use of passive microwave observations at higher frequencies has also been introduced, with several systems using the same antenna for multi-frequency measurements; higher spatial resolutions are available from the higher frequencies. One such methodology is based on the multi-sensor image fusion technique known as SFIM by Liu (2000), initially applied for increasing the spatial resolution of multi-spectral optical data. The approach was subsequently applied by Santi (2010) for downscaling brightness temperature observations from the AMSR-E. Applying the SFIM on pairs of simultaneous Ka- and C-band acquisitions from the AMSR-E sensor, Santi (2010) reported on the SFIM's potential for disaggregating approximately 50 km resolution C-band (6.9 GHz) brightness temperature to 10 km. Unravelling of spatial variability in soil moisture using this technique is through heterogeneity captured by the Ka-band (36.5 GHz) brightness temperature at 10 km resolution in the disaggregation procedure.

The performance of this method for soil moisture downscaling was further evaluated by de Jeu et al. (2014) and Parinussa et al. (2014). While these studies reported on the algorithm success in enhancing the spatial variability of soil moisture and in capturing dry and wet

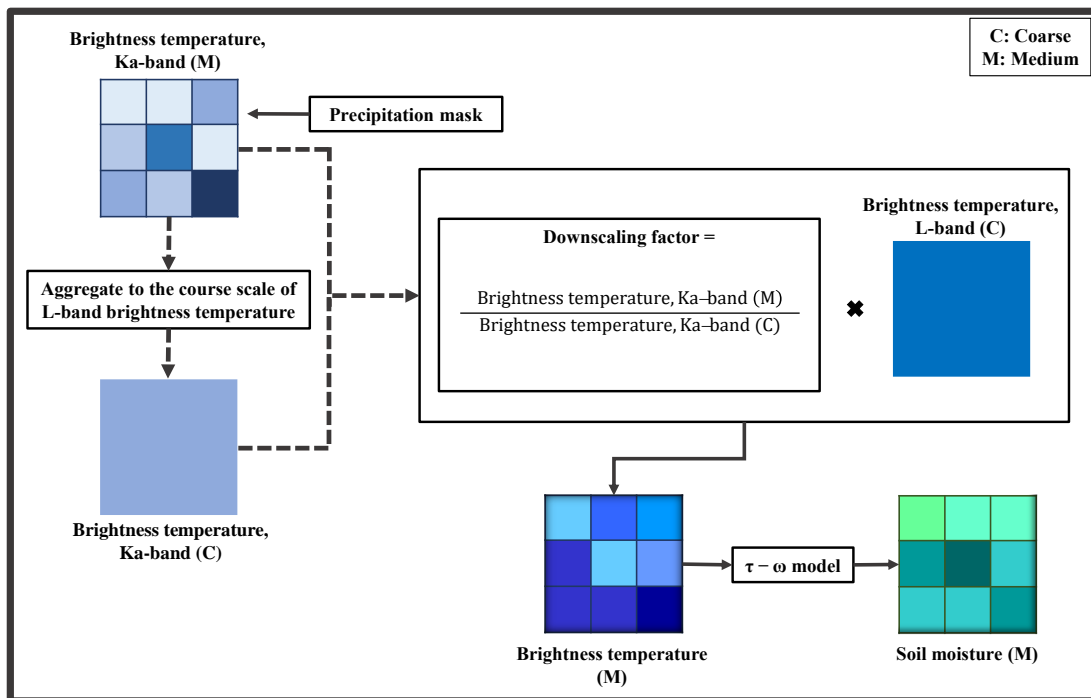


Figure 2.3: Schematic of the SFIM technique for downscaling coarse passive microwave brightness temperature to yield a medium resolution soil moisture retrieval.

regions, their analysis revealed that geophysical accuracy of the high resolution products remained on the same level as that of coarse AMSR-E soil moisture products. Their analysis also revealed that rainfall impacts on the Ka-band observations could diminish the accuracy of downscaled soil moisture products. Gevaert et al. (2015) recently corrected the Ka-band observations for precipitation prior to their use in the SFIM method. This modification involved the application of a precipitation mask to the Ka-band observations to remove them from the processing. Disaggregated soil moisture products at 10 km resolution were subsequently retrieved from the downscaled brightness temperature (see Figure 2.3).

## 2.2.2 Optical-based downscaling techniques

The association of land surface temperature and vegetation parameters with soil moisture conditions (Nemani et al., 1993) provides the basis for optical downscaling. Carlson et al. (1994) and Gillies and Carlson (1995) developed the universal triangle concept (Figure 2.4) which relates VIS/IR parameters, such as the NDVI and Land Surface Temperature (LST), to the soil moisture status. The sensitivity of surface temperature change in response

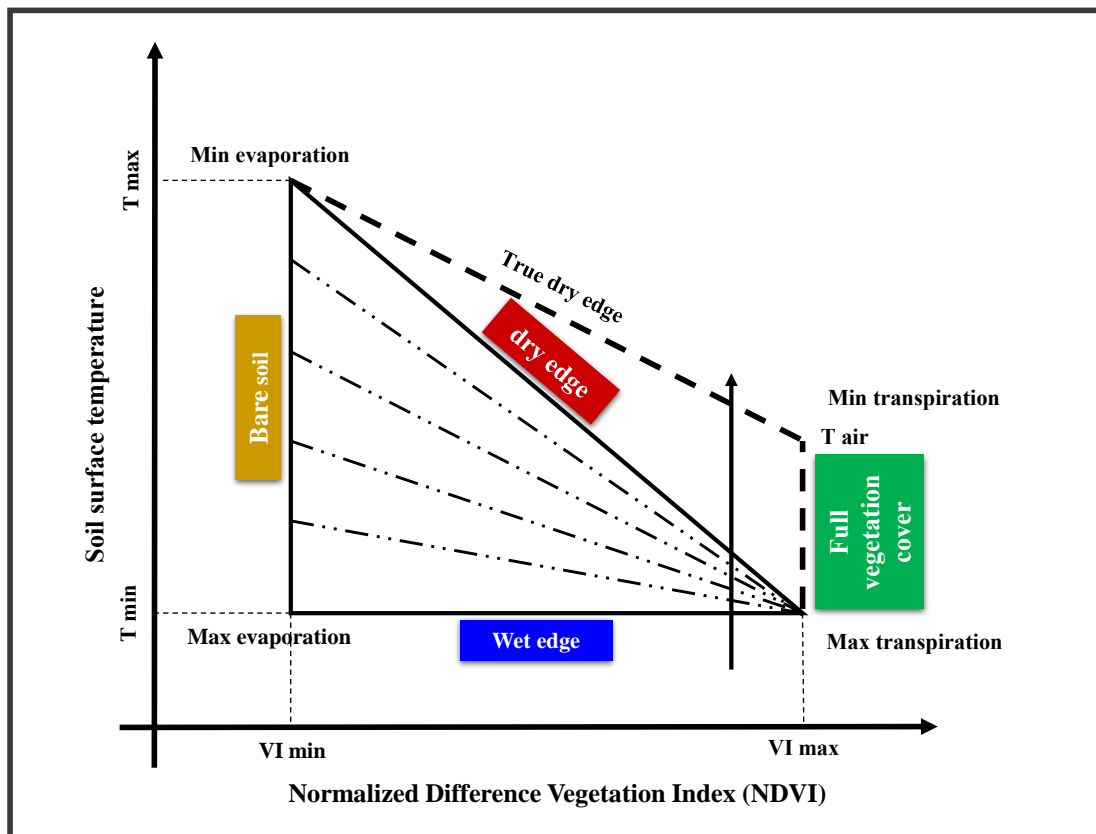


Figure 2.4: Triangle/Trapezoid concept of the LST/VI feature space (adapted from Petropoulos et al., 2015 and Merlin et al., 2012).

to soil moisture is considered to be different depending upon the surface conditions (e.g. canopy type, density of vegetation cover). This linkage creates a scatter plot of vegetation index-surface temperature in the shape of a triangle (or a four-sided polygon in the case that wet and dry edges cross beyond the maximum NDVI value), yielding boundaries of the wet and dry conditions. However, this concept cannot act as a direct methodology for soil moisture retrieval, due to attenuation of reflected solar radiation from the soil surface by the opaque overlaying media (e.g. atmosphere and vegetation), lack of micro-meteorological and atmospheric information, and the optical observations being affected by clouds.

Several researchers have used the triangle concept as a tool to improve the scale of passive microwave based soil moisture products (e.g. Fang et al., 2013; Merlin et al., 2006, 2008a,b, 2012, 2013; Piles et al., 2011), with land surface temperature and vegetation parameters derived from optical observations at high resolution being the key factor in the downscaling process. These optical-based downscaling techniques combine the strengths of optical and

radiometric observations (i.e. high spatial resolution optical data and high accuracy passive microwave derived soil moisture). While the high spatial resolution of optical observations provides information on heterogeneity of surface features, they have limited application due to being highly affected by cloud coverage and vegetation.

To calculate soil moisture variations at 1 km resolution, Chauhan et al. (2003) used optical observations from the Advanced Very High Resolution Radiometer (AVHRR) to infer spatial variability of surface features for downscaling coarse soil moisture from the Special Sensor Microwave Imager (SSM/I), which is not a particularly good frequency to use, for the Southern Great Plains (SGP97) campaign. Chauhan et al. (2003) calibrated a model through which an ensemble of satellite-derived vegetation index, surface albedo and land surface temperature with soil moisture at the coarse scale of SSM/I, led to reasonable estimates of fine scaled soil moisture in terms of accuracy ( $0.05 \text{ m}^3 \text{ m}^{-3}$ ). In this model, which was based on the model by Zhan et al. (2002), a simple linear average equation was applied to the pixel values of AVHRR within the passive microwave grid scale. This model was then applied to high resolution surface feature parameters to retrieve soil moisture maps at 1 km resolution. The advantage of this approach was its modest requirement of ancillary data for disaggregation. Later, Choi and Hur (2012) applied this model to downscale AMSR-E soil moisture products from 25 to 1 km over a study area in Korea. Disaggregated soil moisture products in this study were reported to have slightly lower RMSD and higher correlation of coefficient to ground-based measurements than those of the coarse AMSR-E soil moisture. This technique was also used by Zhao and Li (2013a) to downscale AMSR-E soil moisture retrievals from 25 to 5 km using the METEOSAT Second Generation Spinning Enhanced Visible and Infrared Imager (MSG SEVIRI) geostationary satellite data. The fact that geostationary satellites continuously monitor the land surface, facilitates capturing of temporal variation of LST which was correlated to soil moisture instead of an absolute value of LST in this study. Use of change in LST over time was suggested by Stisen et al. (2008) as a solution for reducing the mean error in the thermal information and the impact it had on the accuracy of downscaled soil moisture products. The two LST temporal variation parameters used in this study were mid-morning temperature rising rate and maximum temperature time, which are strongly related to soil moisture (Zhao and Li, 2013b). Retrievals from this

downscaling technique revealed no improvement over the AMSR-E soil moisture products when compared against ground based measurements of soil moisture; however, they showed better agreement with *in situ* measurements than the retrievals from Chauhan et al. (2003) method. Piles et al. (2014) expanded the approach to use the polarimetric multi-angular brightness temperature observations of SMOS to reflect precipitation impact on changes in soil moisture. An early version of the Piles et al. (2014) downscaling scheme was presented in Piles et al. (2011) to downscale SMOS derived soil moisture maps to 1 km resolution. Piles et al. (2011) recommended: i) to capitalize the synergy between SMOS and Moderate resolution Imaging Spectro-radiometer (MODIS) observations instead of other optical observations such as the AVHRR and Landsat, and ii) to average pixel values of MODIS within the SMOS grid scale that were not masked by clouds. While Piles et al. (2011) suggested the use of brightness temperature for better estimates of high resolution soil moisture maps, it was Piles et al. (2012) that added polarimetric and multi-angular brightness temperature into the model. This adjustment made the downscaling algorithm more reliable by increasing the temporal correlation and reducing error retrievals from 0.05 to 0.03 m<sup>3</sup> m<sup>-3</sup>. A schematic of this downscaling model is shown in Figure 2.5. Sánchez-Ruiz et al. (2014) used MODIS NDWI at the higher spatial resolution of 500 m, rather than the 1 km NDVI in Piles et al. (2014), to derive a better agreement of downscaled soil moisture with *in situ* measurements, particularly during periods of high vegetation activities.

The work of Piles et al. (2014) is capable of downscaling SMOS soil moisture products from a spatial resolution of 25 km to 1 km. However, this technique lacks the ability to preserve the temporal resolution of passive microwave soil moisture data; the temporal resolution of its retrievals is hampered by the availability of MODIS observations and their cloudiness. The shortcomings of this model were overcome by using the MSG SEVIRI optical data in place of MODIS data (Piles et al., 2016). The Piles et al. (2016) model provided 3 km temporally averaged soil moisture estimates using MSG geostationary satellite observations, to provide instantaneous soil moisture estimates at time increments of 15 minutes. The proposed downscaling technique not only estimated high resolution soil moisture with a similar quality to SMOS soil moisture, but also minimised the impact of clouds by using observations throughout the daytime.

Merlin et al. (2005) proposed the use of a physical downscaling model to derive the spatial variability of the top 0-5 cm soil moisture at 1 km resolution. This model disaggregates the surface soil moisture according to fine-scale information provided by radiometric surface temperature and surface coverage condition. Merlin et al. (2006) tested this algorithm over a semi-arid area and found that the model performed best for high solar radiation and low vegetation density. Merlin et al. (2008a) then translated space-and time-based anomalies of soil moisture indices at fine-scale into high resolution soil moisture from SMOS, by establishing a linear relationship to calibrate a time-invariant slope at the SMOS scale. Evaporative Fraction (EF; the ratio of evapotranspiration to the total energy available at the surface) and Soil Evaporative Efficiency (SEE; the ratio of actual to potential evaporation), were chosen as the Soil Moisture Indices (SMIs) for downscaling. The choice of EF and SEE for soil moisture downscaling was not only because of their direct dependency on soil moisture dynamics, but also their constant diurnal characteristic. Both SMIs provided a fine-scale distribution of soil moisture; however, SEE resulted in more accurate estimates of 1 km scale soil moisture, due to the higher correlation with surface soil moisture. The superior performance of this algorithm was reported for dry-end soil moisture controls and clear sky only condition. An expansion of this algorithm was presented in Merlin et al. (2008b), whereby the relationship between SEE and surface soil moisture was considered

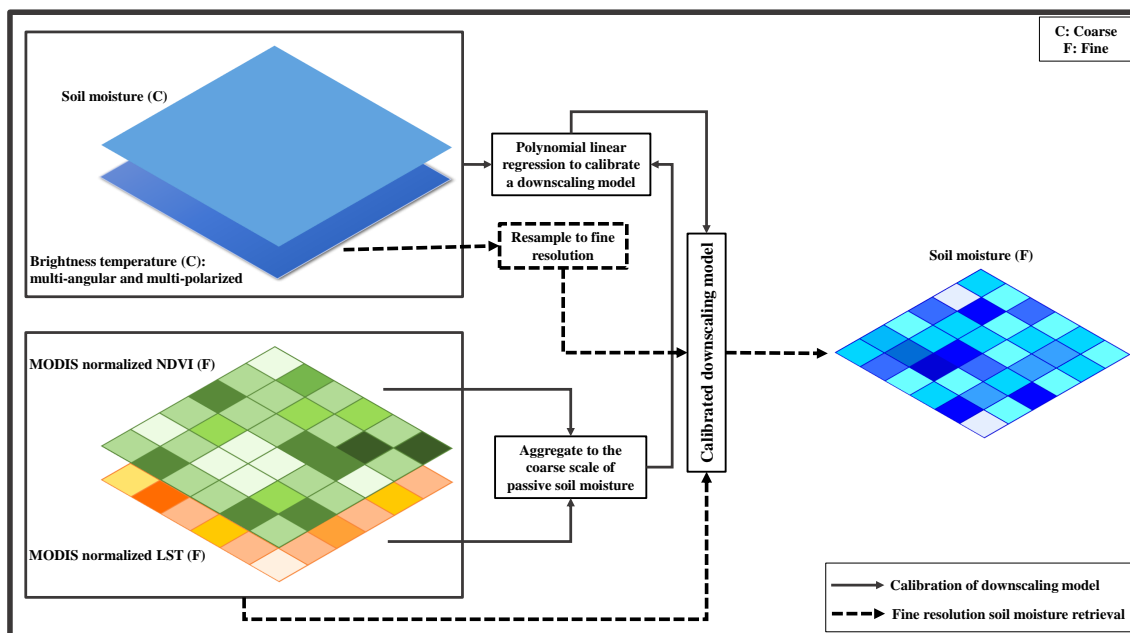


Figure 2.5: Schematic of the downscaling model structure developed by Piles et al. (2012).

to be variable and a function of soil type, wind speed, and SMOS-scale near surface soil moisture. Relating the spatially averaged MODIS thermal observations to 10 km, linearity of the SEE-soil moisture relationship was improved because sensitivity of coarse thermal observations to soil moisture was considerably higher. Merlin et al. (2009) introduced intermediate resolutions, with the range of 3 to 5 km being optimal for soil moisture products in terms of accuracy. They also suggested a sequential downscaling procedure with the use of multi-resolution thermal imagery. This procedure improved the spatial scale of SMOS retrievals from 40 km to 4 km resolution using the aggregated MODIS observations at 4 km, and subsequently used Advanced Scanning Thermal Emission and Reflection (ASTER) radiometer data to disaggregate retrievals to 500m soil moisture maps. However, application of this sequential downscaling model concept was not recommended since combined use of MODIS and ASTER increased uncertainty of soil moisture retrievals compared to MODIS only disaggregated soil moisture. The low temporal repeat of ASTER observations was another factor that reduced the functionality of this approach. Use of the exponential-based SEE model, as opposed to cosine-based suggested by Merlin et al. (2010), led to improved spatial representation of downscaled soil moisture. Developing a Taylor series of soil moisture with respect to projected SEE was also implemented to improve accuracy and robustness of the disaggregation model.

Ongoing efforts to improve performance of the SEE-based disaggregation model (Merlin et al., 2008b) led to the emergence of the DisPATCh model by Merlin et al. (2012), in which the use of the universal trapezoid (Figure 2.4) instead of the universal triangle concept was recommended for better soil moisture disaggregation. However, the DisPATCh model performance is still related to seasonal and climatic variations because the strength of the coupling between soil moisture and surface temperature varies on a seasonal basis. The strength of this coupling over semi-arid areas during summer resulted in a temporal correlation of 0.7 when compared to point-measurements. This result is in stark contrast to the correlation of downscaled soil moisture content over temperate climate during winter, which had a correlation of zero. The latest version of the DisPATCh model, including the use of vegetation water stress (Moran et al., 1994) and correction for elevation effects on temperature, was introduced by Merlin et al. (2013). That study contrasted the DisPATCh model with the linear

and non-linear behaviour of the SEE variable in relation to multi-resolution retrieval of soil moisture, and revealed preference for the SEE linear behaviour over non-linear for kilometer resolution. However, the assumption of a linear relationship between the SEE and soil moisture resulted in poorer performance at meter resolution. These results also confirmed that atmospheric evaporative demand with seasonal variation is the main factor controlling the quality of the DisPATCH downscaled soil moisture retrieval. This method is illustrated in Figure 2.6 to provide a clear understanding of how it works.

Using the DisPATCH technique to downscale AMSR-E and SMOS over the Murrumbidgee catchment in Australia, Malbêteau et al. (2016) reported that downscaled soil moisture could provide opportunities for reducing the negative impact of scale mismatch on validation of satellite soil moisture applications. Malbêteau et al. (2016) also showed that DisPATCH was efficient in increasing the correlation coefficient of satellite soil moisture retrievals, especially in semi-arid regions. For example, in the semi-arid region of Yanco, the correlation coefficient of SMOS for afternoon overpasses increased from 0.37 to 0.63 after disaggregation. Djamai et al. (2016) proposed combining DisPATCH derived soil moisture with the Canadian LAnd Surface Scheme (CLASS) simulations of soil moisture in order to estimate

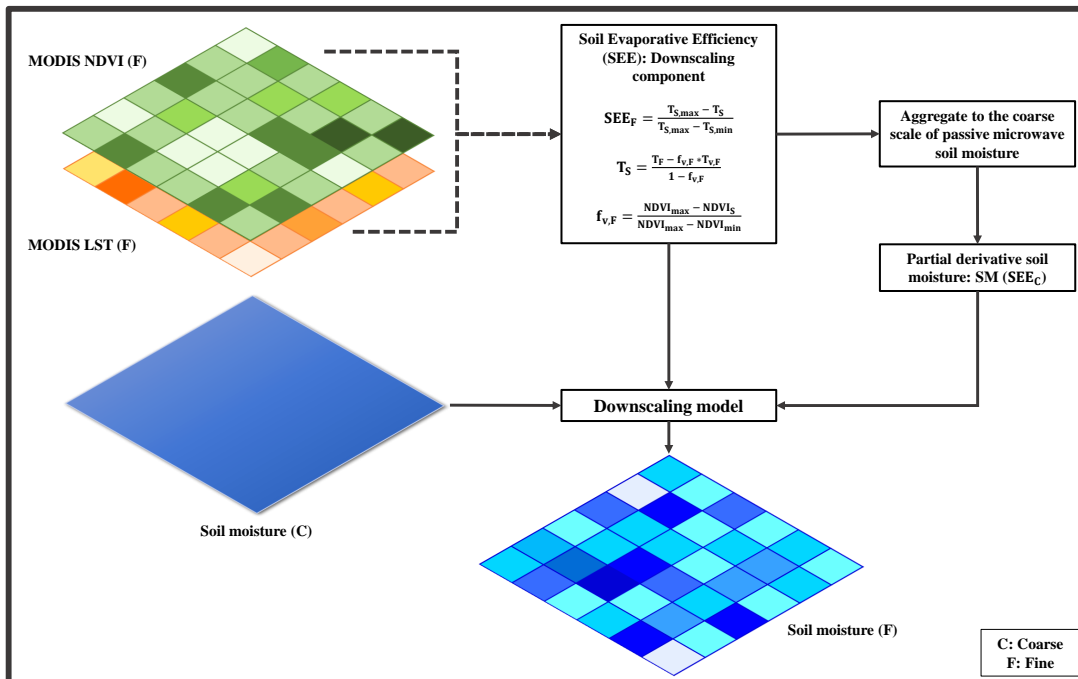


Figure 2.6: Schematic of DisPATCH downscaling method which combines accurate but coarse passive microwave observations with high resolution optical observations.

a continuous time series of 1 km soil moisture maps for cloudy and cloud-free days. In that study, the DisPATCH derived soil moisture was compared with the CLASS soil moisture simulation for cloud-free days to develop a robust slope correction function. Results from the application of this calibration function - assumed to be valid under cloudy sky - indicated the potential of a DisPATCH/CLASS combination for soil moisture retrieval under cloudy skies.

The soil evaporative efficiency has also been utilized in a different approach by Fang and Lakshmi (2014a), for downscaling AMSR-E soil moisture. In the first step of their soil moisture downscaling procedure, North American Land Data Assimilation System (NLDAS)-derived soil temperature was disaggregated to 1 km resolution using the MODIS LST and fractional vegetation cover. From the disaggregated NLDAS soil temperature, SEE was estimated using the model of Merlin et al. (2010). The 1 km SEE estimates were then converted to soil moisture maps at 1 km resolution using models developed by Noilhan and Planton (1989) and Lee and Pielke (1992). The difference between the AMSR-E derived soil moisture and up-scaled 1 km soil moisture to the resolution of AMSR-E were then added to each 1 km soil moisture pixel to estimate high resolution soil moisture.

Instead of the SEE, which was used in the physical-based downscaling technique by Merlin et al. (2010, 2012), Chen et al. (2017) used the Normalized Soil Moisture Index (NSMI) as a variance indicator of soil moisture in space. The dimensionless NSMI with resolution of 250 m was derived using the MODIS NIR and red-band land surface reflectance products. This downscaling technique, named Near InfraRed-Red (NIR-Red) Spectral-based Disaggregation (NRSD), was developed using a semi-physical relationship which related the NIR-Red triangle space (Huete et al., 1985; Richardson and Wiegand, 1977) to the soil moisture status. The NRSD technique was formalized to downscale 36 km SMAP radiometer-derived soil moisture to 250 m using the first-order Taylor series (Merlin et al., 2012) through which the SMAP soil moisture was corrected with respect to the converted variance of the NSMI to soil moisture. Accuracy, spatial resolution, and application scope of downscaled soil moisture products from the NRSD were reported to outperform the retrievals from DisPATCH.

The contribution of Soil Wetness Index (SWI) as a weighting factor to disaggregate coarse

AMSR-E surface soil moisture products was evaluated by Kim and Hogue (2012). The coarse C-band AMSR-E observations were multiplied by the ratio of the MODIS-scaled SWI to the mean of MODIS-based SWI over the AMSR-E footprints. To estimate SWI, the algorithm applied the Jiang and Islam (2003) model to MODIS temperature and Enhanced Vegetation Index (EVI) products. The selection of EVI over NDVI was intended to minimise the soil background interference in the vegetation index. The performance of this algorithm resulted in a better approximation of soil moisture than that of the coarse AMSR-E soil moisture over a semi-arid region in the San Pedro River basin. In addition, the model showed better performance than the triangle-based downscaling techniques developed by Chauhan et al. (2003) and Carlson et al. (1994). However, the correlation of estimates from Kim and Hogue (2012) approach with *in situ* soil moisture measurements was at lower level than products from the physical based model of Merlin et al. (2008b; and 2009).

By combining LST retrieval from passive microwave brightness temperature algorithm (McFarland et al., 1990) with an empirical relationship (Choudhury et al., 1987; Mao et al., 2012; Meesters et al., 2005) between the Microwave Polarization Difference Index (MDPI, Pampaloni and Paloscia, 1985) and NDVI, Song et al. (2014) developed a downscaling method which involved brightness temperature downscaling prior to soil moisture retrieval. This model was applied to the AMSR-E Ku-band observations available at 25 km to derive soil moisture maps at 1 km over the Maque monitoring network in China. Retrievals from this downscaling technique had a similar temporal trend to the *in situ* measurements with RMSD less than  $0.12 \text{ m}^3 \text{ m}^{-3}$ . This technique was suggested to have better performance over bare and sparsely vegetated soil surfaces where the soil has dry or moderately wet condition.

Hemakumara et al. (2004) and Peng et al. (2016) found that the VTCI had a positive correlation with soil moisture, and so developed a VTCI-based downscaling algorithm similar to Kim and Hogue (2012). Downscaled soil moisture from the VTCI-based algorithm showed spatially consistent agreement with *in situ* measurements and land cover, while maintaining the accuracy of coarse soil moisture products. To increase the operational efficiency of this approach, Peng et al. (2015) examined how the VTCI-based algorithm performed when the index is retrieved from a geostationary optical sensor such as the MSG SEVIRI. The capability of geostationary sensors to capture optical acquisitions at shorter time intervals increases

the chance of providing more cloud-free observations, thus leading to a greater continuity of downscaled soil moisture. However, it comes with a sacrifice on spatial resolution because the current geostationary optical observations are only available at the scale of 3 to 5 km. A new VI-based downscaling technique was recently developed by Kim et al. (2017), which established a linear relationship between NDVI and temporally averaged coarse passive microwave derived soil moisture data. For developing this downscaling model, Kim et al. (2017) used the ESA CCI merged active-passive microwave soil moisture data available at 25 km together with aggregated 1 km MODIS NDVI 16-day composite to 25 km. Validation results showed that NDVI can replace the required LST information for disaggregation when the LST product is not available or comes with a poor-quality due to cloud coverage. Therefore, use of the NDVI composite allows to downscale soil moisture without the cost of losing the temporal variability of coarse soil moisture due to lack of NDVI information under cloudy skies.

Wang et al. (2016) swapped the SWI downscaling parameter in the Kim and Hogue (2012) model for Temperature Vegetation Drought Index (TVDI, Sandholt et al., 2002) to downscale long time series of passive microwave observations of soil moisture produced by Dorigo et al. (2012a). The TVDI is a dryness index which was derived from MODIS LST and NDVI products (Patel et al., 2009). Compared with retrievals from the triangle based downscaling model by Carlson et al. (1994), the physical model by Merlin et al. (2009, 2010), and the Kim and Hogue (2012) model, TVDI-based downscaling retrievals showed superiority in terms of both accuracy and consistency of temporal variability with field measurements.

Another soil moisture disaggregation method is based on the thermal inertia principle, which correlated changes of soil temperature to changes of soil moisture as well as heat capacity (Mallick et al., 2009). This technique produced absolute volumetric soil moisture at 1 km resolution by converting SWI to soil moisture using prior knowledge on total water capacity and minimum soil moisture content based on soil type. Compared with a dry soil, water has a greater heat capacity and thus a greater resistance to temperature change. The presence of higher moisture content in the soil, therefore, leads to lower thermal conductivity, with wet soil having a lower day-night temperature difference than for dry soil. However, it is

easier to apply this linear relationship between soil moisture and diurnal change of surface temperature to bare soil conditions (Maltese et al., 2013). When the vegetation layer masks the soil surface, canopies interfere with fluctuations of soil moisture through water uptake.

Thermal inertia is also the basic concept behind the physically based optical-passive microwave combination technique developed by Fang et al. (2013). Relating a time series of daily averaged soil moisture estimates to diurnal changes of soil temperature, derived from NLDAS land surface modelling, Fang et al. (2013) calibrated a model for soil moisture downscaling. Calibration lines were fitted on a monthly basis to reduce the impact of varied vegetation biomass on retrievals. Increments of 0.3 in NDVI values were used for further modulation of the surface temperature and soil moisture relationship. Using this model, AMSR-E based soil moisture retrievals at 1 km were derived and corrected by applying the differences between the original coarse AMSR-E soil moisture products and high resolution retrievals within the AMSR-E grid scale. Fang and Lakshmi (2014b) adjusted the temperature difference between passive microwave and optical sensors (SMOS and MODIS, respectively), caused by different overpass time, to achieve better performance of this algorithm. For this purpose, a polynomial regression was fitted to diurnal changes of hourly NLDAS surface temperature and their corresponding time. The model was used to estimate surface temperature at MODIS and SMOS overpass time at NLDAS spatial scale to calculate temperature difference between them. MODIS LST was then adjusted by adding this temperature difference to MODIS LST pixels within each NLDAS pixel.

### **2.2.3 Soil surface attributes-based downscaling techniques**

The soil moisture state is determined by precipitation, but it also reflects space-time scaling behaviour in response to soil surface attributes and structure such as topography and soil properties (e.g. soil texture, and vegetation cover) (Kim and Barros, 2002b). Consequently, such information has been used in several disaggregation schemes (e.g. Kim and Barros, 2002a; Pellenq et al., 2003) to determine the spatial distribution of soil moisture. Topography provides information about soil water dynamics controlling soil moisture distribution, while soil properties provide information about soil water storage capacity and possible rates of change. However, the limited access to data on these properties at global scale imposes a

limitation on the development of these downscaling techniques for global application.

Findings by Kim and Barros (2002b) supported the idea that the fractal interpolation method proposed by Kim and Barros (2002a), which used topography, soil texture and vegetation cover, could be an effective downscaling method. An Empirical Orthogonal Function (EOF) analysis to assess the impact of ancillary data sets on downscaling results showed a close association of soil moisture variability with soil hydraulic conductivity. However, topography and vegetation cover were dominant in downscaling results during wet periods and persistence of dry-down, respectively. Through the coupling of a radiative transfer model to a hydrological model, Pellenq et al. (2003) developed a downscaling methodology that captured disaggregated soil moisture patterns as a function of topographic index and soil depth. Using the infiltration and evaporation concept, the soil moisture profile was simulated by a radiative transfer model and subsequently coupled with a hydrological model to explain how soil moisture behaviour in space is affected by the topography and soil depth. The estimation of soil moisture patterns based on this approach was in general satisfactory, but it revealed a weak point-scale correlation between simulations and observations.

Wilson et al. (2005) implicitly developed a topographic attribute-based downscaling technique for soil moisture estimation at 10 to 40 m from a spatially averaged ground based soil moisture. Using historic high resolution soil moisture measurement data, Wilson et al. (2005) first developed an empirical relationship between an ensemble of soil moisture, topographic attributes (such as elevation, specific contributing area, slope, wetness index, potential solar radiation index, lowness index, and a multi-resolution valley bottom flatness index), and the residuals patterns. Second, the topographic attributes and residuals were weighted based on the averaged soil moisture to map high resolution soil moisture for each day. However, such relationships were site specific.

Similarly, Perry and Niemann (2007) used the EOF analysis to decompose the priori high resolution soil moisture maps into spatial patterns of EOF covariation, time series of Expansion Coefficients (ECs) and the spatial-average soil moisture. Due to the existence of a strong relationship between ECs and spatial-average soil moisture, ECs were estimated from the spatial average soil moisture. A combination of spatial-average soil moisture, ECs,

and time-invariant EOFs was used to downscale soil moisture. Busch et al. (2012) further developed the Perry and Niemann (2007) EOF-based downscaling technique such that it did not require priori information about the high resolution soil moisture. Busch et al. (2012) deployed high resolution topographic attributes from a Digital Elevation Model (DEM) as the only source of information to estimate the EOF because findings by Perry and Niemann (2008) showed that EOFs were strongly related to topographic attributes. Such a relationship was constructed and applied to catchments, revealing that the relationships were site specific.

An Equilibrium Moisture from Topography (EMT; Coleman and Niemann, 2013) model, which is based on a conceptual water balance of the hydrologically active soil layer, is another downscaling technique using topographic indices for spatial resolution enhancement of soil moisture retrieval. This model performance outweighed the EOF method and required only a few soil moisture observations for calibration (Werbylo and Niemann, 2014). Vegetation and soil parameters were included in the EMT model for downscaling temporal soil moisture patterns over the Tarrawarra catchment; however, the fine resolution variations of these properties were not taken into account. Ranney et al. (2015) improved the performance of the EMT downscaling technique by including information about the spatial variation in vegetation and soil characteristics, and named it the Equilibrium Moisture from Topography, Vegetation, and Soil (EMT + VS). Vegetation data were found to be a valuable source of information for soil moisture downscaling. However, fine spatial scale soil data were able to further enhance the performance of EMT + VS downscaling technique. While this model showed good performance for a catchment with a topographic relief of less than 125 m, there is no evidence of its performance over regions with larger ranges of elevation. Large relief, which has impacts on spectral variation of precipitation (e.g. Cowley et al., 2017; Kyriakidis et al., 2001; Lloyd, 2005) and Potential EvapoTranspiration (PET, e.g. Cowley et al., 2017; Shevenell, 1999; Shi et al., 2014a; van der Linden et al., 2008) will also control the spatial patterns of soil moisture (Cowley et al., 2017). Accordingly, Cowley et al. (2017) added temporal average PET and precipitation downscaling methods to the Ranney et al. (2015) ETM model, in order to take the spatial patterns of both variables into account for enhancing the coarse soil moisture downscaling. In the process of

developing precipitation downscaling techniques the spatial heterogeneity of precipitation was assumed to be linearly related to topographic elevation (e.g. Castro et al., 2014) and topographic orientation (e.g. Franke et al., 2008). An interaction between precipitation, topographic elevation and topographic orientation was also assumed Hanson (1982). The PET downscaling method was based on a linear relationship between PET and air temperature (Blaney and Criddle, 1950) which decreases with altitude. Downscaling of PET, which has a predictable temporal pattern, showed more improvement in soil moisture estimates than precipitation downscaling did.

Values of fine scale parameters used in previous versions of the EMT + VS model were the same for all fine pixels lying within the coarse grid cell of soil moisture. Hoehn et al. (2017) used the shifting window to calculate fine scale parameters that vary over the coarse footprint of soil moisture to take development of the EMT + VS model a step further. The shifting window that provided the spatially varied fine scale parameters had the spatial scale of the coarse soil moisture and was centred on each fine grid cell to be calculated. The shifting window method estimated accurate fine resolution soil moisture for a situation where the generated errors of coarse soil moisture from a normal distribution had a standard deviation of  $0.01 \text{ m}^3 \text{ m}^{-3}$  or larger. Otherwise, the accuracy of soil moisture estimates from the original EMT + VS model - based on a fixed window method that applied the same value for all the fine pixels lying within the coarse grid - was higher than that of soil moisture estimates from the shifting window procedure. Unlike the fixed window procedure, the shifting window could not maintain the value of coarse soil moisture in its original state.

Using the temporally dynamic Topography-based Wetness Index (TWI) , Temimi et al. (2010) developed a new topography-based soil wetness downscaling solution. This study included, for the first time, a vegetation index at VIS wavelength (the MODIS Leaf Area Index product) in the TWI retrieval model, to capture its variation in time. This technique downscaled the soil wetness index derived from the AMSR-E 37-GHz observations having the greatest sensitivity to soil moisture changes (Temimi et al., 2007) to help improve estimation of the soil moisture spatial distribution. Temimi et al. (2010) used TWI as a wetness potential index to spatially disaggregate the soil wetness index and demonstrated that dynamic TWI is an effective index to increase the soil wetness correlation to precipitation

occurrence by 0.3, on average.

In studies by Ines et al. (2013) and Shin and Mohanty (2013), sub-pixel variation of remotely sensed soil moisture was estimated using the heterogeneity of soil texture and vegetation cover. The algorithm presented by Shin and Mohanty (2013) was inspired by the combined simulation-optimization approach of Ines et al. (2013), which downscaled remotely sensed soil moisture products using effective soil hydraulic properties (e.g. saturated soil moisture, saturated hydraulic conductivity, tortuosity in the soil) at sub-pixel scale, and fraction of soil/vegetation. The Shin and Mohanty (2013) inversion model produced soil moisture with satisfactory quality under various hydrologic and climate conditions using a genetic algorithm, which minimized the difference between observed and simulated soil moisture and evapotranspiration. For example, correlation coefficients of sub-pixel soil moisture to *in situ* measurements and mean bias error were reported to vary between 0.343 and 0.845, and -0.165 to -0.122 m<sup>3</sup> m<sup>-3</sup> for a silty loam soil covered by winter wheat and short native grass, respectively. While Ines et al. (2013) used soil characteristics and soil-vegetation fraction without assigning their location within a pixel, Shin and Mohanty (2013) specified the location of soil characteristics and vegetation cover. Shin and Mohanty (2013) also scaled evapotranspiration maps to infer soil moisture distribution, given that a strong correlation exists between evapotranspiration and soil moisture. While retrievals from this approach matched well with the *in situ* truth soil moisture content, qualified input data on the environmental factors (e.g. weather forcing, soil texture, and vegetation) were required under appropriate weather conditions to achieve such a performance.

#### **2.2.4 Model/Data-based downscaling techniques**

The downscaling of coarse resolution soil moisture observations has not been limited to the use of remote sensing data and/or soil surface attributes. Model predictions have also been used in model/data-based disaggregation schemes to spatially enhance soil moisture observations. These techniques, namely data assimilation-and machine learning-based, have no limitations related to the need for concurrent satellite overpasses or lost data due to cloud coverage. Descriptions of these techniques are briefly provided in the data assimilation-and machine learning-based sections below.

### **Data assimilation-based downscaling techniques**

Data assimilation has been used to improve profile soil moisture estimates (e.g. De Lannoy and Reichle, 2016b; Walker et al., 2001) from surface soil moisture observations. Moreover, the physically based hydrological models at the heart of data assimilation have been used to predict the spatial distribution of soil moisture at high resolution (Reichle et al., 2001). A four-dimensional (spatial update using multi-temporal observations) data assimilation, which can combine noisy high resolution model predictions with accurate low resolution observations, was first introduced by Reichle et al. (2001) as a quasi downscaling technique to overcome limitations in deriving fine-scaled information on soil moisture from passive microwave observations. Downscaling techniques based on the data assimilation concept are distinguished from other approaches by accounting for both model and satellite measurement uncertainties and their independence to either sources of information. Moreover, the philosophy behind this method is to use spatially coarse soil moisture observations to constrain a high resolution dynamic model. The RMSD of downscaled soil moisture products from the assimilation-based downscaling techniques is reported to be  $\sim 0.06 \text{ m}^3 \text{ m}^{-3}$  on average (see Table 2.2), which does not meet the accuracy requirement of soil moisture missions.

Draper et al. (2009) focused on AMSR-E C-band soil moisture assimilation into the Interactions between Surface, Biosphere, and Atmosphere (ISBA) model, which was the land surface scheme in Météo-France's Aire Limitée Adaptation Dynamique développement International (ALADIN) Numerical Weather Prediction (NWP) model. This model has an irregular spatial resolution, but its estimates were available at 9.5 km over most of European regions where this study was conducted. This two-dimensional (spatial update for a single soil layer) Simplified Ensemble Kalman Filter (SEKF) developed by Mahfouf et al. (2009) and Balsamo et al. (2006), yielded modelled high resolution surface soil moisture at  $\sim 9 \text{ km}$  and with RMSD values larger than  $0.09 \text{ m}^3 \text{ m}^{-3}$ .

Sahoo et al. (2013) disaggregated the 25 km gridded AMSR-E soil moisture products through assimilation into the 1 km resolution NOAH land surface model using a three-dimensional ensemble Kalman filter. Increasing the spatial correlation from 0.7 on average to 0.77, the

approach resulted in well matched surface soil moisture retrievals to the *in situ* data, including also lower RMSD values. Similar to the ,corrected Kalman Filter-2 (EnBKF-2) in De Lannoy et al. (2007), coarse satellite observations were rescaled to the model climatology prior to the assimilation. The RMSD of downscaled soil moisture without bias correction prior to data assimilation was reported to be in the range of 0.08 to 0.17 m<sup>3</sup> m<sup>-3</sup>, while with the bias correction was between 0.01 and 0.09 m<sup>3</sup> m<sup>-3</sup>.

As an extension to data assimilation systems that apply bias correction as a common practice, Kornelsen et al. (2015) developed a bias correction technique for soil moisture downscaling. In developing this downscaling procedure, precipitation and evapotranspiration were acknowledged as a derivative of soil moisture changes. The assumption of uniform precipitation over a radiometer scale was also made without making the distribution of soil moisture uniform in that scale. Having verified the temporal stability of brightness temperature and soil moisture, a simple mean-variance matching approach-a bias correction procedure-was applied to the simulated soil moisture over the SGP97's experimental watersheds. The analysis revealed the dependency of successful application of the bias correction technique to availability of priori information about the land surface conditions.

SMOS soil moisture products were also assimilated into the Variable Infiltration Capacity (VIC, Liang et al., 1994, 1996, 1999) by Lievens et al. (2015) to improve the accuracy and spatial resolution of SMOS soil moisture estimates from 25 to 12.5 km. This three-dimensional Ensemble Bias corrected Kalman Filter resulted in reduction of the RMSD of the simulated soil moisture from 0.058 m<sup>3</sup> m<sup>-3</sup> to 0.046 m<sup>3</sup> m<sup>-3</sup> and increase of the correlation from 0.56 to 0.71.

Being aware that assimilation can improve the surface soil moisture estimates at sub-seasonal time frame, Draper and Reichle (2015) assimilated a long record of AMSR-E X-band soil moisture at 25 km into the NASA's Catchment Land Surface Model (Koster et al., 2000), which was run on the 9 km EASE grid for North America. A one-dimensional bias-blind ensemble Kalman filter was used in this assimilation procedure by applying the coarse scale observations onto the higher resolution underlying model grid. Results from this study showed that for four test sites, assimilating a long record of soil moisture not only improved

the ability of the model to represent long-term events such as droughts, but also increased the spatial skill of the model.

Since 2015, SMAP has provided a Level 4 soil moisture product, which has surface and root-zone soil moisture values at 9 km. The Goddard Earth Observing System version 5 (GEOS-5) Land Data Assimilation System (LDAS, De Lannoy and Reichle, 2016a,b; Reichle et al., 2014) , which is a three-dimensional EnKF based assimilation technique, assimilates the SMAP 36 km brightness temperature (from L1C-TB; Chan et al. (2016)) into the NASA GEOS-5 Catchment Land Surface Model (Koster et al., 2000) for soil moisture estimation. The overall unbiased RMSD (ubRMSD) of the SMAP L4 surface soil moisture was reported by Reichle et al. (2017) to be  $0.037 \text{ m}^3 \text{ m}^{-3}$ , which meets the SMAP mission accuracy requirements. Results from this study are not included in the summary section, because they are not consistent with the other studies which reported regular RMSD values. Using this technique, Lievens et al. (2017) assimilated Sentinel-1 (Geudtner, 2012; Geudtner and Torres, 2012; Torres et al., 2012) C-band backscatter simultaneously with SMAP 36 km L-band brightness temperature to enhance the accuracy of soil moisture estimates. The complementary assimilation of radar backscatter and radiometer brightness temperature improved the performance, resulting in better surface soil moisture estimation than when only radiometer observations were assimilated.

### **Machine learning-based downscaling techniques**

The machine learning approach seeks to learn the relationship between the soil moisture and available information on surface parameters without requiring continuous data. This makes it a useful tool for integrating different sources of information about soil moisture (Notarnicola et al., 2008). Consequently, the way that artificial intelligence deals with noisy data from dynamic and non-linear systems (Remesan et al., 2009) makes it a potential technique to improve the scale of soil moisture Chai et al. (2009). Through a comprehensive analysis, Srivastava et al. (2013) demonstrated the feasibility of using the machine learning technique as a downscaling tool. The aim of this study was to derive a high spatial resolution soil moisture from SMOS using MODIS land surface temperature in a more functional way than optical-based downscaling, which its application is hampered by the sensitivity of optical

observations to clouds. They evaluated the performance of a variety of artificial intelligence techniques, including Artificial Neural Network (ANN) , Support Vector Machine (SVM), and Relevance Vector Machine (RVM) . Among these techniques, the ANN showed considerable potential for deriving accurate soil moisture at higher resolution, especially when applied to data sets divided based on growing and non-growing seasons.

Earlier, Chai et al. (2011) had also used the ANN model to downscale air-borne passive microwave observations from the National Airborne Field Experiment held in Australia in 2005 (NAFE'05) . Basing their ANN model on the linear downscaling algorithm (Merlin et al., 2008b), they acquired soil moisture retrievals with a root mean square error of 0.018 to 0.035  $\text{m}^3 \text{m}^{-3}$ . This accuracy, together with the fact that the approach does not rely on a large number of input data, was reported by Chai et al. (2011) to be the main advantages of the ANN model. Chai and Goh (2013) continued to explore the ANN performance for soil moisture disaggregation within an ensemble scheme. The ensemble scheme was recommended to reduce estimation errors through the combination of results from multiple neural network models. This finding concurred with the Hansen and Salamon (1990) suggestion that optimization of neural network models is possible by ensemble scheme.

Based on a machine learning approach called the Self-Regularized Regressive Models (SRRMs) , Chakrabarti et al. (2016) has delivered high resolution soil moisture maps at 1 km resolution with an RMSD of less than 0.02  $\text{m}^3 \text{m}^{-3}$ . Utilizing a regularized clustering and kernel regression, the SRRM technique was capable of deriving the desired variables for all pixels covering the study area. This technique was reported to be efficient in terms of computational time, number of required samples for training, and accuracy when compared to the earlier machine learning technique developed by Chakrabarti et al. (2015). It used a Bayesian transformation process which related the high resolution auxiliary information to coarse soil moisture through a probabilistic relationship on the basis of the Principle of Relevant Information (PRI) . Both SRRM and PRI techniques were developed and tested with the use of multi-scale synthetic data from a coupled Land Surface Process-Decision Support System for Agrotechnology Transfer (LSP-DSSAT) model .

Park et al. (2015) enhanced the spatial resolution of AMSR2 soil moisture products, re-

trieved using the VUA-NASA algorithm (Owe et al., 2001, 2008), from 25 km to 1 km using MODIS optical products in two different machine learning techniques: i) random forest and ii) ordinary least squares. Both approaches associated evapotranspiration and multiplication of LST and NDVI ( $LST \times NDVI$ ) in their process for soil moisture estimation. The random forest approach, which had flexibility in randomization and adopted an ensemble approach, outperformed this technique over the other machine learning approach. Similar to this study, Im et al. (2016) investigated the spatial downscaling of AMSR-E soil moisture data from 25 km to 1 km using MODIS 1 km products, including land surface temperature, surface albedo, NDVI, EVI, Leaf Area Index, and evapotranspiration. The intention of this study was to evaluate the performance of three different machine learning-based downscaling approaches including random forest, boosted regression trees, and Cubist approaches over two regions (South Korea and Australia). Among these techniques, the random forest showed superiority to the other techniques, yielding a higher correlation coefficient (0.71 and 0.84 for South Korea and Australia, respectively) of 1 km soil moisture with *in situ* measurements than that of the original AMSR-E soil moisture products.

The effective simulation of the non-linear relationship between soil moisture and LST/VI by Back-Propagation Neural Network (BPNN) motivated Jiang et al. (2017) to use it as a tool to improve the scale of coarse passive microwave soil moisture products. Assuming that the relationship between soil moisture and LST/VIs was scale-invariant, the BPNN was trained by taking different combinations of coarsely aggregated MODIS LST and VIs, including NDVI, EVI, and NDWI as the input, and the coarse soil moisture retrievals from AMSR-E, AMSR2, and SMOS as the output. The best trained BPNN model was then applied to the inputs at the MODIS scale to estimate fine scaled soil moisture. Optimal downscaled products, which showed significant correlation larger than 0.6 with *in situ* soil moisture data from the central Tibetan Plateau Soil Moisture/Temperature Monitoring Network (SMTMN) were achieved when the BPNN was trained using the combination of LST and EVI.

### 2.3 Assessment of the strengths and weaknesses of downscaling techniques

This chapter seeks to provide a critical review of the available soil moisture downscaling methods, including an evaluation of the strengths and weaknesses of their strategies. As presented, several downscaling methods exist for combining accurate passive microwave observations with high spatial resolution information on soil surface features which include vegetation coverage, soil surface attributes, soil temperature, etc. to derive high spatial resolution soil moisture. Some of the techniques are able to retrieve soil moisture estimates at an accuracy of  $0.04 \text{ m}^3 \text{ m}^{-3}$ , which is the soil moisture accuracy requirement - in the top 5 cm of the soil for vegetation water content  $\leq 5 \text{ kg.m}^{-2}$  - suggested by the SMAP science team for a wide range of applications (Entekhabi et al., 2008a).

Existing downscaling approaches are reported to have a range of accuracy under differing weather and climate conditions. A rigorous inter-comparison of different downscaling methods would be beneficial to clarify advantages and disadvantages of each downscaling method. However, until now there has been no study to thoroughly compare the various downscaling techniques for a specific set of conditions. Figure 2.7 presents a summary of Table 2.2 in order to give a concise overview of the performance of each downscaling technique in terms of reported accuracy. The performance variation of individual approaches may lie in the disparate characteristics of the data and field sites utilized for the soil moisture disaggregation evaluation. However, study domains and seasons are not distinguished in this study, as downscaling techniques should be applicable for a wide range of surface and climate conditions if they are to be applied operationally. Moreover, there is a wide variation between approaches, with each having its own advantages and limitations, and conditions where it works best. For example, the radar-radiometer microwave combination could be the most promising and/or robust technique to retrieve soil moisture values under homogeneous roughness and low vegetation density conditions as it is unaffected by meteorology, but the lack of concurrent radar and radiometer observations at the same frequency and platform currently limits its application.

The radar-based downscaling techniques have been shown to outperform the optical-based techniques (see Figure 2.7), in terms of RMSD ( $0.04 \text{ m}^3 \text{ m}^{-3}$  vs.  $0.072 \text{ m}^3 \text{ m}^{-3}$  on average

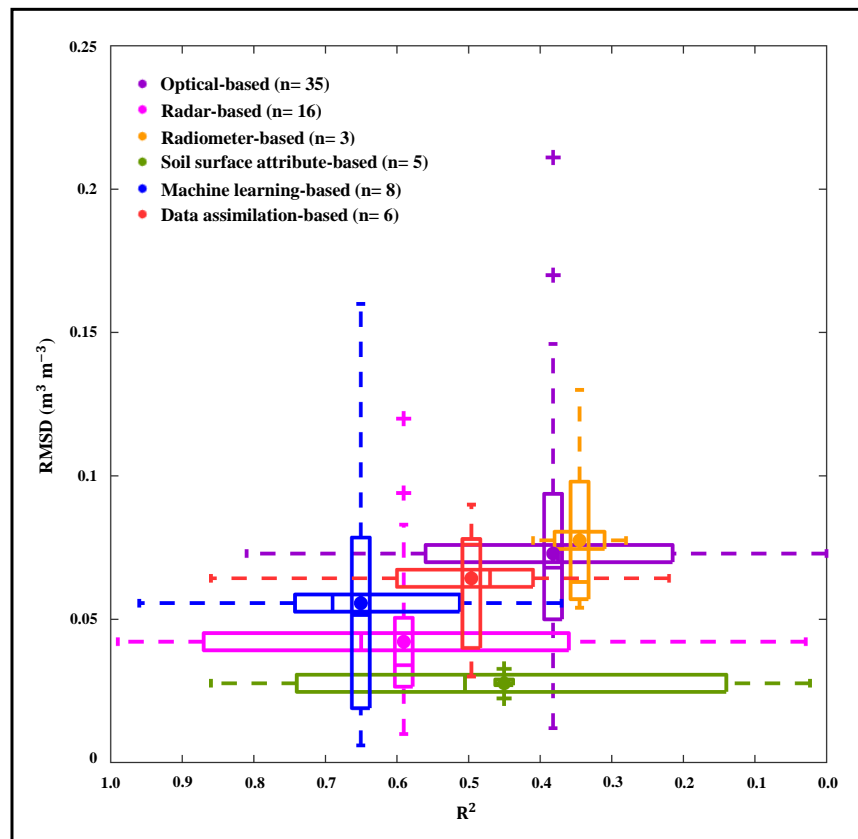


Figure 2.7: Summary of accuracy statistics from different downscaling techniques presented as boxplot that contains the interquartile ranges, the sample median (bar), and outliers associated with the mean (dot). \* n indicates the number of validation studies that reported the accuracy of retrieval in terms of R or  $R^2$  and RMSE for the particular downscaling approach, and were thus used to make this figure.

for radar-and optical-based downscaling techniques, respectively), due to the greater sensitivity of microwave observations to soil moisture dynamics under all-weather conditions. However, the trade-off between wavelength and temporal coverage of currently available radar imagery, and the impact of clouds on optical observations require consideration when evaluating their effectiveness in estimating accurate soil moisture from coarse passive microwave observations. The use of geostationary based optical sensors could alleviate some of the meteorological limitations of typical polar orbiting sensors due to high frequency optical acquisitions (0-30 minute), increasing the chance of obtaining cloud-free observations (Piles et al., 2016; Zhang et al., 2014). However, it comes at the cost of estimating soil moisture at the lower spatial scale of the geostationary based optical sensors (being on order of 3 to 5 km) than typical polar orbiting sensors (being on order of 1 km resolution).

Radiometric emissions at higher microwave frequencies (i.e. Ka-band) can penetrate through non-raining clouds similar to radar observations. Their advantage over the backscatter method is the availability at regular repeat coverage and reduced impact of surface roughness. These characteristics make them a potentially more reliable source of information on surface spatial heterogeneity for mapping variability of soil moisture compared with optical and radar observations. However, the radiometer-based downscaling technique has so far been found to result in less accurate soil moisture products than the radar-based technique. While the radiometer-based technique has shown similar performance to the optical-based downscaling techniques (Figure 2.7), optical observations have the advantage of producing disaggregated soil moisture at finer resolution (1 km) than currently available Ka-band passive microwave observations (10 km) when there is no cloud coverage. The superiority of radiometer-based to optical-based downscaling lies in the applicability of the radiometer-based technique under all-weather and climate conditions, unlike the optical-based techniques that are more applicable to areas where there is no such limitation (Garcia et al., 2014). Using a bigger antenna for scanning brightness temperature at Ka-band, or developing methods to resample the Ka-band observations to resolutions finer than 10 km while preserving the accuracy of medium scaled Ka-band brightness temperature observations, could be potential solutions to overcome this drawback and make the radiometer-based techniques operational.

Providing that spatially detailed information on soil surface attributes and a universal relationship was available at the global scale, the soil surface attributes-based downscaling technique could be a suitable alternative to the radar-based technique for disaggregation of soil moisture. This technique owes its performance to the information about soil water dynamics and soil water storage capacity, which are represented in the soil moisture downscaling process through the use of topography and soil properties, respectively. As shown in Figure 2.7, soil surface attributes-based downscaling technique is a more accurate technique in terms of RMSD than either the radiometer- or optical-based techniques, with an averaged accuracy of  $0.028 \text{ m}^3 \text{ m}^{-3}$ .

Use of high resolution land surface models together with data assimilation and/or machine learning could provide a more robust downscaling approach, as there are no limitations

related to the need for concurrent satellite overpasses, or lost data due to cloud coverage. Moreover, the advantages of a data assimilation-based downscaling technique may outweigh the machine learning-based technique because dynamically varying uncertainties of both the model predicted and satellite observed soil moisture, and the temporal interpolation of coarse soil moisture retrievals, are implicitly included. Data assimilation has the additional advantage of providing root zone soil moisture content. However, based on the available literature the machine learning technique (with RMSD of  $0.056 \text{ m}^3 \text{ m}^{-3}$  on average) seems not only to be superior to the data assimilation-based technique but also superior to the other currently available downscaling techniques, apart from radar-based techniques in terms of RMSD. The performance of the machine learning technique also appears to be superior to other downscaling techniques in terms of correlation between the downscaled and *in situ* soil moisture. However, further testing and research are required to increase the computational efficiency of this technique and to overcome its global training requirements before it could be considered for use operationally.

## 2.4 Unresolved challenges to soil moisture downscaling

There are several unresolved challenges facing soil moisture downscaling that need to be addressed. For example, in order to meet the spatial resolution requirement of agricultural production and efficient management of water resources, there is a need to improve the spatial scale of downscaled products to higher than 1 km (Figure 1.1). This highlights the need for high resolution ancillary data which usually dictates the spatial scale of downscaled products. These ancillary data should not only be at a high spatial resolution, but should also be precise in order to assure an accurate disaggregation of soil moisture. The large scale mismatch between coarse passive microwave observations and ancillary data may therefore allow for propagation of uncertainties, which needs to be addressed.

Reduction of uncertainty in the coarse passive microwave soil moisture retrieval process is another key factor for downscaled soil moisture improvement. The radiative transfer models used for soil moisture retrieval from passive microwave remote sensing has reached a mature level (Das et al., 2011). However, the variation of ancillary parameters (e.g. vegeta-

tion properties, surface roughness and scattering albedo) in space and time make the model parametrization and retrievals uncertain. Evaluation of the radiative transfer model across a wide range of climate and land surface conditions may assist in quantifying and clarifying such uncertainties.

A consistent inter-comparison of existing downscaling techniques for a specific set of conditions is essential for moving the development of downscaling techniques that are applicable across multi-satellite passive microwave observations forward. Accuracy and representativeness of evaluation reference data including *in situ* and airborne observations also set limitations to the adequate inter-comparison of existing downscaling techniques which require to be addressed. Yee et al. (2016) undertook a thorough assessment of this issue for the Yanco study site and suggested using intensive *in situ* measurements for evaluation of airborne soil moisture products, which together with temporal stability analysis could be used to identify representative stations for evaluation of satellite products at larger scale. However, in the presence of mixed land use, a weighting method was recommended.

For satisfactory application of high resolution soil moisture in agriculture and water resources management, continuous time series of soil moisture are required at temporal frequencies better than 3 days. The development of downscaling techniques that are applicable to multi-satellite coarse soil moisture data could potentially be a pragmatic solution to satisfying this demand. In this case, merged multi satellite soil moisture products could be developed, and be downscaled across all the low resolution passive microwave satellites using the best downscaling methodology. Multi satellite brightness temperature products could also be merged prior to the soil moisture retrieval and downscaling. However, the fusion of satellite soil moisture often outperforms the fusion of satellite products at brightness temperature level (Wagner et al., 2012). Consequently, in this study downscaled soil moisture products were merged. A harmonised ensemble of disaggregated soil moisture products from different retrieval algorithms might provide another solution, with the added value of providing more frequent soil moisture than the individual downscaled products alone. An ensemble of downscaled soil moisture products might also result in more accurate soil moisture products, recognising strengths of alternative products under varying climate and land surface conditions.

Therefore, this study seeks to rigorously compare the downscaling techniques that use remotely sensed data as either complementary or ancillary data for spatial resolution enhancement of L-band passive microwave observations. This research undertakes the first consistent assessment of the range of different radar-, optical-, radiometer-, and oversampling-based downscaled soil moisture products for typical Australian landscapes, using a specific set of evaluation data. Moreover, the combination of downscaled soil moisture products is developed to examine the impact of strengths recognition of alternative downscaled products on the accuracy of soil moisture products.

### **2.5 Chapter summary**

This chapter has provided a detailed description of alternative soil moisture downscaling techniques and their capabilities and opportunities. While the reasons and motivation for downscaling soil moisture and the concept behind each downscaling technique have been extensively described, this has also provided an overview of the resources required for each disaggregation technique and the expected accuracy of the approach. Moreover, an extensive quantitative comparison of the current soil moisture downscaling approaches was carried out, together with qualitative comparison of their pros and cons.

Some of the current challenges and/or knowledge gaps in soil moisture downscaling were described and this PhD thesis was set up to address two of the identified knowledge gaps, including: i) inter-comparison of different downscaling techniques against an extensive common data set collected for a specific set of condition, and ii) combination of downscaled soil moisture products. The performance of radiometer-only measurements, herein SMAP and SMOS passive L-band soil moisture products, were also assessed to reveal the extent of possible improvement or deterioration of both downscaled and combined products in terms of accuracy over the radiometer-only products. Data used for the assessment of downscaled, radiometer-only and combined soil moisture products were ground measured near-surface soil moisture content from the OzNet stations in Murrumbidgee catchment and experimental airborne soil moisture maps collected from the SMAPEX-4 and -5 airborne field campaigns described in Chapter 3.



# Chapter 3

## Study area and data sets

This chapter presents an overview of the study area and SMAPEX-4 and -5 airborne campaigns, which were carried out during the Australian autumn and spring 2015, respectively. A description of the PLMR airborne reference soil moisture maps derived from the PLMR radiometric brightness temperature is also presented here. An evaluation of the reference PLMR soil moisture maps against the soil moisture data measured by the HDAS is presented for all intense soil moisture ground sampling areas. The PLMR airborne soil moisture maps are subsequently used in Chapter 4 and Chapter 5 to evaluate the performance of the down-scaled, radiometer-only and merged soil moisture products. The downscaled soil moisture products used in the inter-comparison and combinations based on data availability, are also introduced. Components of this chapter have been contributed to the co-authored paper by Ye et al. (in review), which is submitted to Remote Sensing of Environment. My involvement in the SMAPEX-4 and -5 airborne field campaigns included intensive HDAS *in situ* measurement of soil moisture and surface roughness sampling. I was also responsible for post-processing the surface roughness measurements after the experiments, producing the daily vegetation water content maps and evaluating the derived airborne PLMR soil moisture maps.

### 3.1 Study area

The Yanco agricultural area in New South Wales, Australia, was chosen to conduct this research. Yanco has a landscape and climate that is representative of much of south-east Australia. The climate is classified as semi-arid based on the Köppen-Geiger climate classi-

fication system. An average annual amount of about 400mm precipitation falls in the Yanco area throughout the year, and its' minimum and maximum average annual temperature is 11°C and 24°C, respectively (Bureau of Meterology, 2018). The Yanco area is located on a flat plain in the Murrumbidgee River catchment and contains a network of soil moisture, temperature and rainfall monitoring stations known as OzNet (Smith et al., 2012). The locations of OzNet stations installed in the Yanco region are shown as black dots in Figure 3.1. The OzNet was established in 2001, covering the entire Murrumbidgee catchment with 38 monitoring sites that measure 90 cm soil moisture profile at depths of 0-5, 0-30, 30-60, and 60-90 cm. These data are available on <http://www.oznet.org.au>.

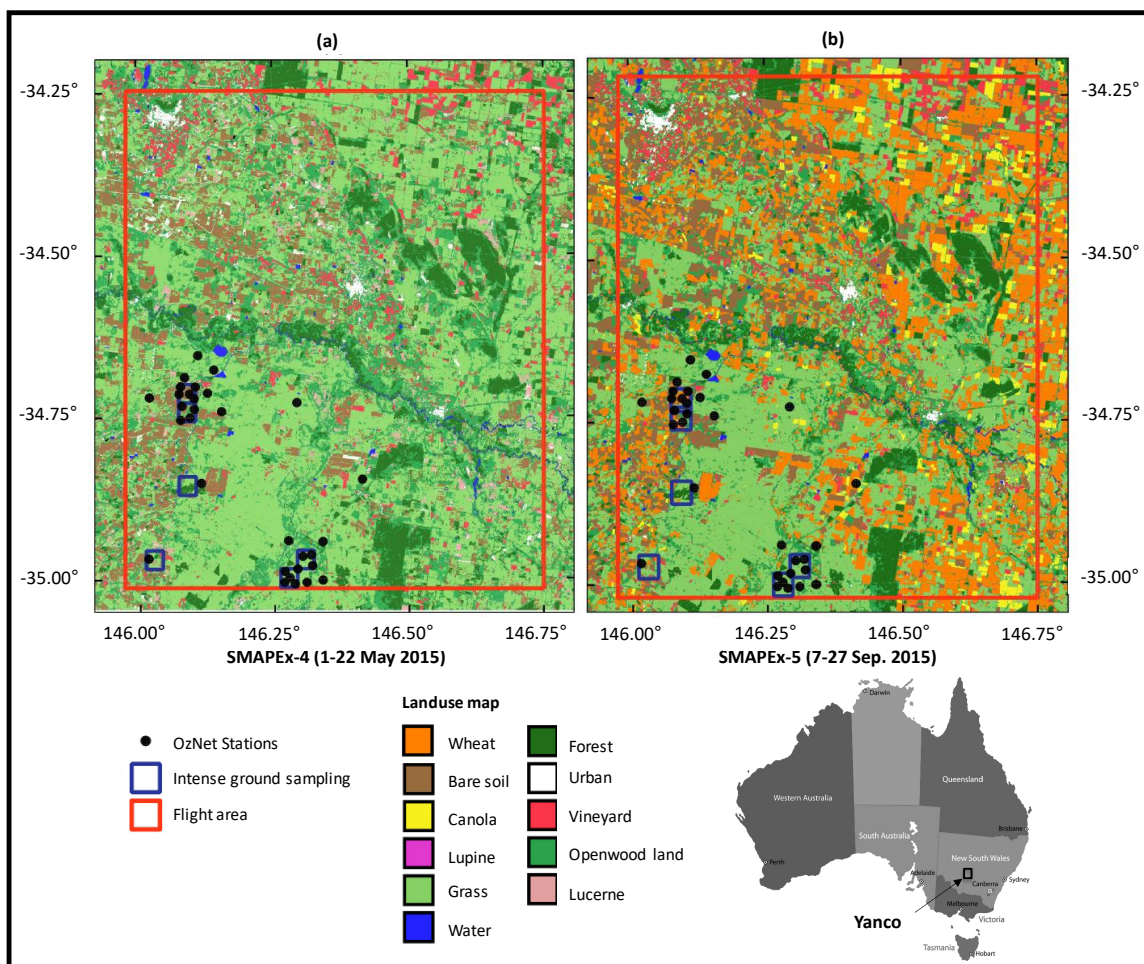


Figure 3.1: The study areas for (a) SMAPEx-4 and (b) SMAPEx-5 airborne field campaigns conducted in the Yanco region in south east of Australia. Landuse is shown along with red rectangles which delineate the coverage of airborne measurements of each campaign, being 71 km × 85 km for SMAPEx-4 and 71 km × 89 km for SMAPEx-5. Blue rectangles show the locations of the intense ground samplings and black dots are the OzNet *in situ* monitoring stations.

The temporal pattern of the OzNet soil moisture is consistent with the occurrence of precipitation events with wetting and drying cycles for the 1st April to 1st November 2015 study period as shown in Figure 3.2. The study area is relatively flat, with a variety of land use, soil and vegetation types, thus making Yanco an appropriate site for evaluation of downscaling algorithm performance.

### 3.2 The SMAPEX-4 and -5 airborne field campaigns

Over the Yanco region, the SMAPEX-4 and -5 airborne field campaigns were designed to cover an area of about  $71\text{ km} \times 89\text{ km}$  ( $145.98^\circ - 146.75^\circ\text{E}$  longitude and  $34.22^\circ - 35.03^\circ\text{S}$  latitude, see Figure 3.1). The SMAPEX-4 and -5 airborne field campaigns were designed for the purpose of calibration and validation of SMAP soil moisture products. These experiments were carried out during the Australian autumn (SMAPEX-4, from the 1st to 22nd May 2015) and spring (SMAPEX-5, from the 7th to 27th September 2015).

The flat topography, being equipped with the OzNet *in situ* soil moisture (Figure 3.1) and rainfall monitoring stations, and its representativeness of typical soil moisture, vegetation and land use conditions of Australian semi-arid climate condition, makes the Yanco region a

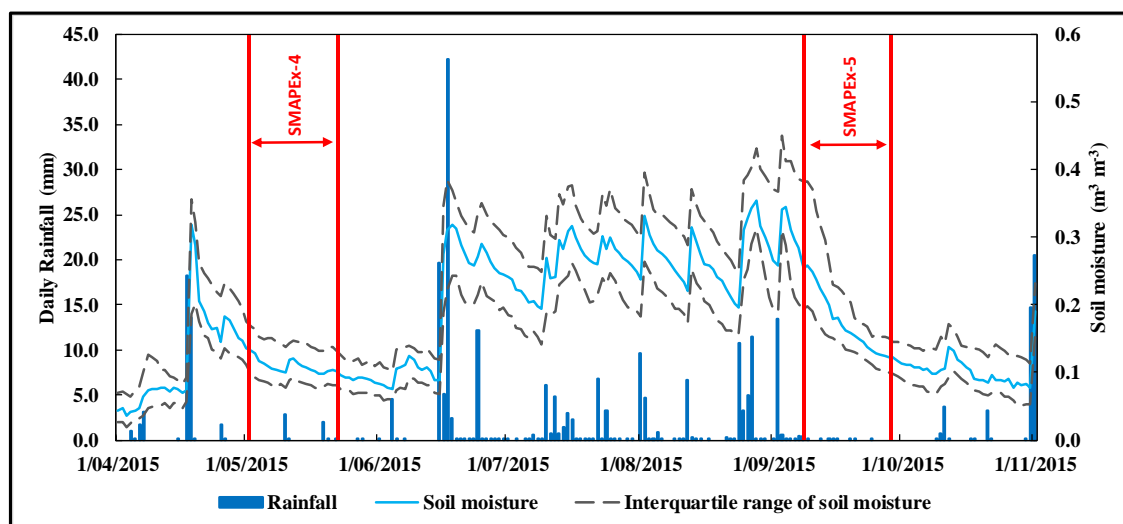


Figure 3.2: Time series of the OzNet top 5 cm *in situ* soil moisture and rainfall measurements for the period between 1st April and 1st November 2015 used in this study. The light blue line and dashed gray lines show the median and interquartile range of soil moisture measurements, respectively. The dark blue bars show the mean daily rainfall over the Yanco region.

unique study site for the SMAPEX project and inter-comparison of downscaled soil moisture products. The coverage of the SMAPEX-4 and -5 airborne observations corresponds to a complete SMAP radiometer 3dB footprint (SMAP L1B, brightness temperature product, approximately 39 km by 47 km).

### **3.2.1 Airborne sampling**

During the SMAPEX-4 and -5 airborne field campaigns, airborne L-band passive microwave brightness temperature were collected using the PLMR instrument (Figure 3.3) concurrent with the SMAP and SMOS satellite overpasses. The PLMR radiometer, having similar characteristics to that of the SMAP mission, operates at L-band (1.4 GHz frequency) to monitor brightness temperature at both vertical and horizontal polarization with 1 km resolution, when flown at 3 km altitude. It collected dual-polarized brightness temperature measurements with six-beams as shown in Figure 3.4, with across-track incidence angles of  $\pm 7^\circ$ ,  $\pm 21.5^\circ$ , and  $\pm 38.5^\circ$ , which were then angle normalized to  $\pm 38.5^\circ$  using the approach of Ye et al. (2015) before retrieval of the soil moisture.

### **3.2.2 Ground sampling**

The airborne L-band passive microwave observations were supported by ground sampling activities that were conducted concurrent to flight acquisitions across focus farms as shown in Figure 3.1, to provide information about vegetation (biomass, vegetation water content, leaf area index, etc.) and surface roughness, which were used for the soil moisture retrieval. Information about vegetation water content is required to model L-band passive microwave based land surface emissions. Such information was collected by destructive vegetation sampling of dominant vegetation types, which were present in the Yanco region. In order to map vegetation water content at larger scales using aircraft and satellite observations, surface spectral reflectance and leaf area data are required. Surface spectral reflectance was measured using a Multi Spectral Radiometer (MSR) developed by CROPSCAN, with the installed filters matched to MODIS spectral bands (ranging from 0.4  $\mu\text{m}$  to 14.4  $\mu\text{m}$  in terms of wavelength). Simultaneous to spectral observations, biomass sampling and leaf area measurement were made. Biomass, vegetation water content, and plant structure were



Figure 3.3: The aircraft equipped with PLMR L-band passive microwave instrument.

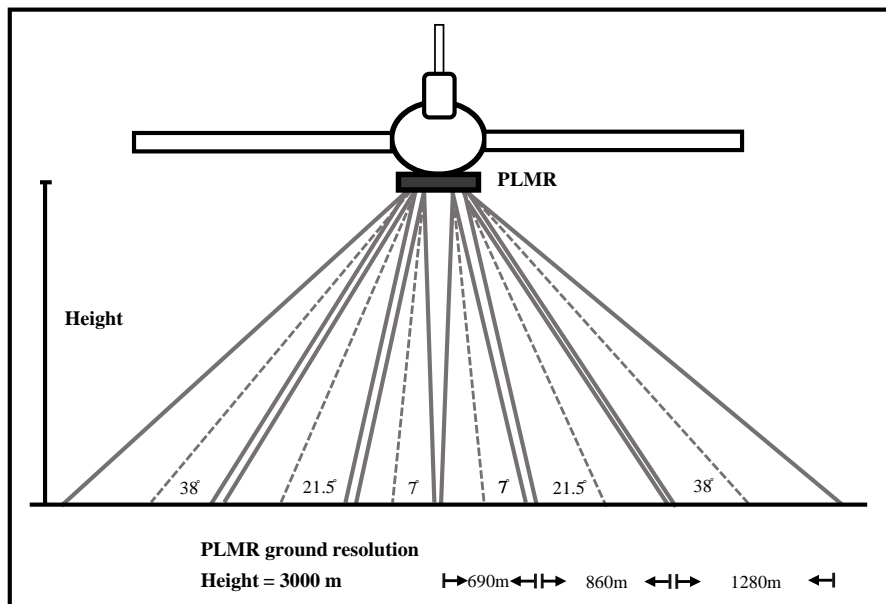


Figure 3.4: The viewing configuration of PLMR on-board the aircraft (adapted from SMAPEX-1 work-plan).

sampled assuming that they have insignificant changes within a week. These spatial and intensive vegetation sampling (Figure 3.5) took place to: i) provide insight into the maturity level and vegetation water content of dominant vegetation types, and ii) track the vegetation evolution across the campaign period.

Characterisation of surface roughness profiles was undertaken for major land cover types to capture the variability of surface conditions observed within the SMAPEX-4 and -5 airborne field campaigns. A 1m-long pin profiler (Figure 3.6) equipped with a digital camera, was used to acquire two 3m-long profiles. At each roughness sampling location, the

three consecutive readings were performed to simulate a 3m-long profile in the North-South and East-West orientations, or along and across the row direction of ploughed fields in the presence of cultivations. Previous SMAPEX campaigns revealed the stability of correlation length estimates for 3m-long profiles. In addition to the pin profiler, Figure 3.6 also shows a sample of the extracted roughness profile used to derive statistics from the post-processed images.

The HDAS system - a dielectric probe - was used to measure top 5 cm *in situ* soil moisture data on a 250 m grid spacing coincident with airborne sampling. Figure 3.7 shows an



Figure 3.5: Vegetation sampling, including: a) surface spectral reflectance measurement, b) leaf area measurement, c) destructive vegetation sampling, and d) vegetation height measurement.

example of HDAS soil moisture measurements in one of the focus farms. The use of intensive HDAS soil moisture measurements minimize the effect of random sampling errors at local scale, and were collected to evaluate the performance of airborne PLMR soil moisture retrievals. The HDAS system uses a Hydraprobe soil moisture sensor and a Geographic Information System (GIS) to collect information about location as well as soil moisture content (Merlin et al., 2007). The accuracy of HDAS measurements has been reported to be better than  $0.04 \text{ m}^3 \text{ m}^{-3}$  for individual HDAS measurements during the SMAPEX-4 and -5 airborne field campaigns, irrespective of soil type (Ye et al., in review). Earlier results of HDAS measurements accuracy has been reported to be  $\pm 0.039$  across the Murrumbidgee River catchment during the National Airborne Field Experiment held in Australia in 2006 (NAFE'06) , the Australian Airborne Cal/val Experiments for SMOS (AACES) and the

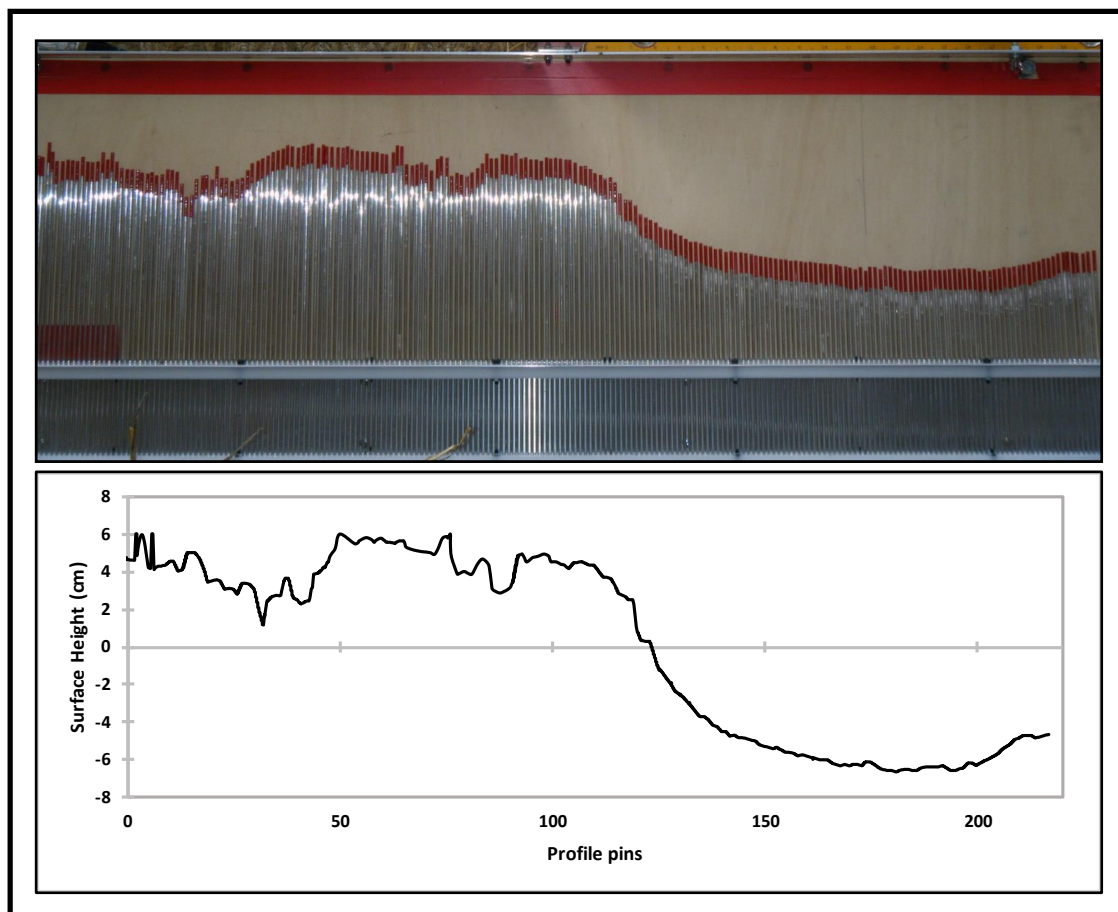


Figure 3.6: A sample photo taken of the pin profiler that was here used to characterise the roughness profile (top), and a post-processed experimental profile extracted from this photo (bottom).

SMAPEX-1 to -3 campaigns.

Apart from the OzNet sites in the Yanco area, six identical temporary monitoring stations were installed in the centre of each focus farm (Figure 3.1) to collect time series data on rainfall, skin temperature, leaf wetness, soil temperature at depths of 2.5 cm, 5 cm, 15 cm, and 40 cm, and soil moisture at depths of 0-5 cm and 20-25 cm during the SMAPEX-4 and -5 airborne field campaigns. The locations of temporary stations were chosen based on the cropping conditions during the SMAPEX-4 and -5 and logistical constraints. The supplementary data from these stations was used for the airborne brightness temperature temporal correction and the airborne PLMR soil moisture retrieval, and to confirm soil moisture variation during the course of each sampling day.

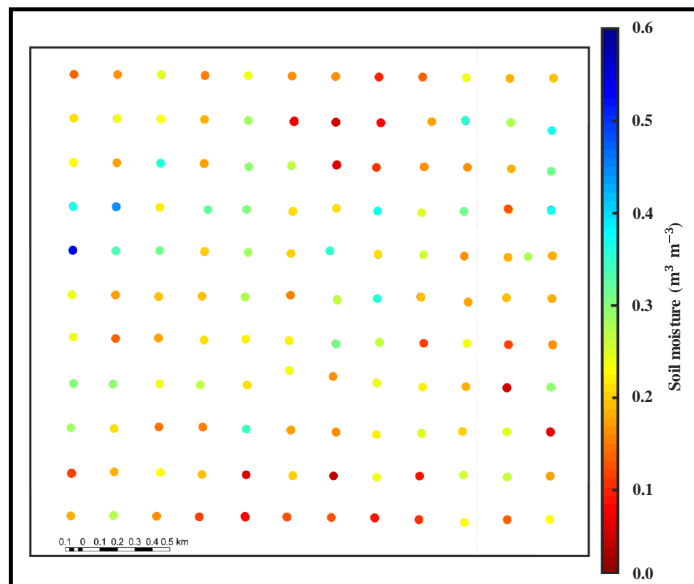


Figure 3.7: An Example of HDAS intensive soil moisture measurements over one of the focus farms on 17 September 2015 during the SMAPEX-5 airborne field campaign.

### 3.3 Airborne PLMR soil moisture maps

The PLMR radiometric brightness temperature observations were used to derive a reference airborne soil moisture data set. An example of airborne PLMR soil moisture map on 22 May 2015 is shown in Figure 3.8. This retrieval process included application of the L-band Microwave Emission of the Biosphere (L-MEB, Wigneron et al., 2007) radiative transfer model to the PLMR brightness temperature (Ye et al., in review). The vegetation water

content maps shown in Figure 3.9 used by the L-MEB model for soil moisture retrieval, were estimated using the relationships developed by Gao et al. (2015) which convert the NDVI (Rouse et al., 1974) from the daily 250 m MODerate resolution Imaging Spectroradiometer (MODIS) reflectance products (MOD09GQ) to vegetation water content. These data were used together with the surface roughness and vegetation parametrization of Panciera et al. (2008, 2009) and the land surface type specific parameters were collected from the studies by Grant et al. (2008) and Wigneron et al. (2007). In order to estimate the effective soil temperature, the average of soil temperature measurements at 2.5 and 40 cm depth were calculated using measurements from the six temporary monitoring stations over the Yanco area.

In order to quantify the accuracy of the reference airborne PLMR soil moisture maps and their propagation into the statistical parameters obtained from the downscaled soil moisture evaluation in Chapter 4 and Chapter 5, the airborne PLMR soil moisture retrievals were compared against the HDAS measurements over all intense soil moisture sampling areas for the SMAPEX-4 and -5 airborne field campaigns (Figure 3.10). The intensive HDAS soil moisture measurements were averaged to 3 km and the airborne PLMR soil moisture aggregated to 3 km. While overall evaluation of 3 km PLMR soil moisture pixels are reported

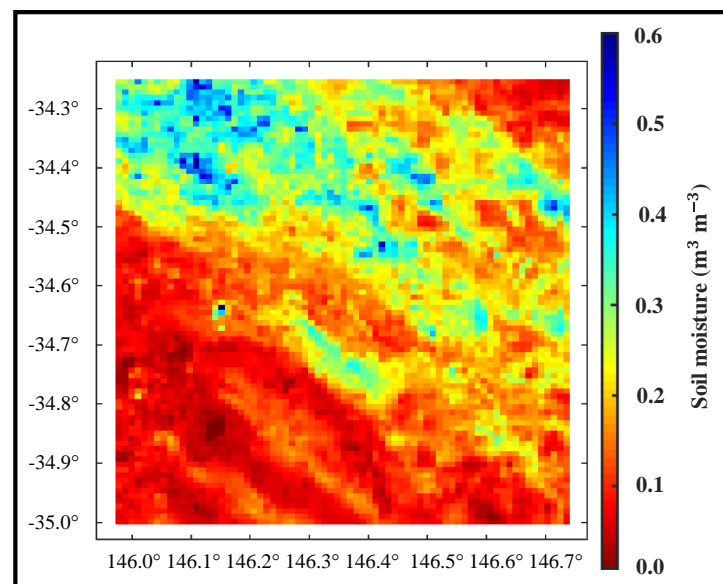


Figure 3.8: An example of the airborne PLMR soil moisture maps derived from the PLMR radiometric brightness temperature observed on 22 May 2015 during the SMAPEX-4 airborne field campaign.

in Figure 3.10, the accuracy assessment was also conducted for each dominant land surface type. An overall RMSD of  $0.04 \text{ m}^3 \text{ m}^{-3}$  and  $R^2$  of 0.76 was achieved for 3 km SMAPE<sub>x</sub>-4 and -5 soil moisture data, which shows the capability of airborne soil moisture being an adequate reference for the evaluation of downscaled soil moisture products. The PLMR soil moisture maps at 1 km were not evaluated in a similar way as there were only a few HDAS intense soil moisture measurements ( $\leq 4$ ) available within each 1 km footprint, yielding the analysis unreliable. In addition, the HDAS measurements within the 1 km scale had a large variability due to the range of moisture conditions.

### 3.4 Downscaled soil moisture products

This study evaluated the performance of soil moisture downscaled products against each other in terms of accuracy and capability to capture the variability of soil moisture in space and time. The products were derived from a variety of current downscaling techniques, categorized as either radar-, optical-, radiometer- and oversampling-based techniques. The soil

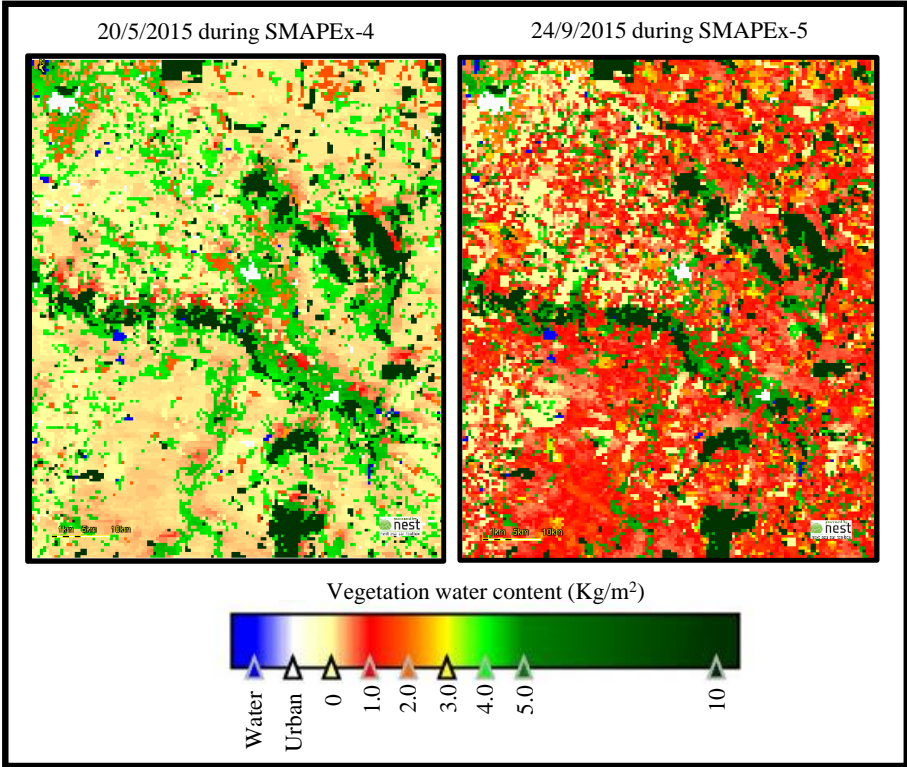


Figure 3.9: Example of vegetation water content maps for the SMAPE<sub>x</sub>-4 and -5 airborne field campaigns.

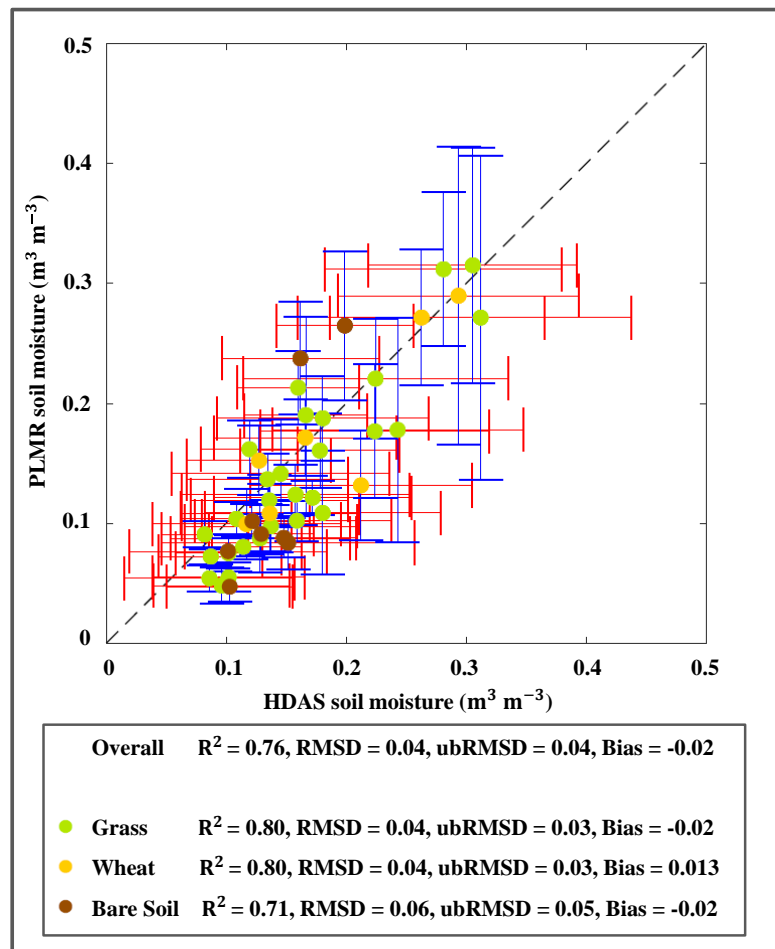


Figure 3.10: Comparison of SMAPE<sub>x</sub>-4 and -5 PLMR soil moisture estimates at 3 km against aggregated intense HDAS soil moisture measurements to 3 km. Horizontal whiskers in red show the standard deviation of aggregated HDAS measurements to 3 km, while vertical whiskers in blue show the standard deviation of aggregated PLMR soil moisture estimates to 3 km.

moisture products evaluated in this study are listed in Table 3.1 along with the downscaling techniques and approaches, product definitions, key references, and main downscaling inputs as applicable. The downscaling techniques were benchmarked against the SMOS and SMAP coarse passive microwave observations to provide insight about the impact of downscaling approaches on the accuracy of soil moisture retrievals, and inter-compared over the Yanco region using the airborne soil moisture maps collected during the SMAPE<sub>x</sub>-4 and-5 airborne field campaigns, as well as the OzNet *in situ* measurements for the period between 1st April and 1st November 2015. The intention of this comparison was to reveal if the

Table 3.1: Summary table on the downscaled and non-downscaled soil moisture products used in the inter-comparison according to the downscaling techniques and approaches. Included is the product definition, key references, and main downscaling inputs as applicable.

<b>Spatial Resolution</b>	<b>Downscaling Technique</b>	<b>Downscaling Approach</b>	<b>Product Definition</b>	<b>Product name</b>	<b>Key Reference</b>	<b>Main Downscaling Inputs</b>
1 km	Optical-based	Disaggregation based on Physical And Theoretical scale Change (DisPATCH)	Ascending DisPATCH product with Ascending SMOS	SMOS DisPATCHa	Merlin et al. (2013)	* SMOS Level 3 radiometric soil moisture retrievals on 25 km grid posting
			Descending DisPATCH product with Descending SMOS	SMOS DisPATCHd		* Daily MODIS land surface temperature * Digital Elevation Model (DEM) outputs * 16 day composite MODIS vegetation index products
1 km	Optical-based	Vegetation Temperature Condition Index (VTCI)	VTCI-based downscaled product with Descending SMAP	SMAP VTCI	Peng et al. (2015, 2016)	* SMAP Level 3 Radiometer Global Daily soil moisture on 36 km grid posting * 4 day composite MODIS Leaf Area Index at 1 km * Daily Aqua MODIS day and night time land surface temperature
			VTCI-based downscaled product with Descending SMOS	SMOS VTCI		* SMOS Level 3 radiometric soil moisture retrievals on 25 km grid posting * 4 day composite MODIS Leaf Area Index at 1 km * Daily Aqua MODIS day and night time land surface temperature
9 km	Oversampling-based	Backus-Gilbert interpolation method	Ascending Enhanced product with Ascending SMAP	SMAP Enhanceda	Chaubell et al. (2016)	* Ascending SMAP L1B Radiometer Half-Orbit Time-Ordered Temperatures at 47 kmx36 km

Table 3.1 (continued)

Spatial Resolution	Downscaling Technique	Downscaling Approach	Product Definition	Product name	Key Reference	Main Downscaling Inputs
9 km	Oversampling-based	Backus-Gilbert interpolation method	Descending Enhanced product with Descending SMAP	SMAP EnhancedID	Chaubell et al. (2016)	* Descending SMAP L1B Radiometer Half-Orbit Time-Ordered Brightness Temperatures at 47 km×36 km
		Radar-based	The SMAP active/passive baseline algorithm Multi-Objective Evolutionary Algorithm (MOEA)	SMAP A/P SMAP MOEA	Das et al. (2014) Akbar et al. (2016)	* SMAP radiometer brightness temperature on 36 km grid posting * SMAP radar backscatter at 3 km
10 km	Radiometer-based	Smoothing Filter-based Intensity Modulation (SFIM)	SFIM-based product with SMAP	SMAP SFIM	Gevaert et al. (2015)	* SMAP Level2 brightness temperature on 36 km grid posting * Advanced Microwave Scanning Radiometer-Earth Observing System (AMSR2) Ka-band brightness temperature at 10 km
			Ascending Passive SMOS Descending Passive SMOS	SMOS PassiveA SMOS PassiveD	Jacquette et al. (2013), ATBD	N/A
25 km	N/A		Ascending Passive SMAP Descending Passive SMAP	SMAP PassiveA SMAP PassiveD	O'Neill et al. (2018), ATBD	N/A
			Ascending Passive SMOS Descending Passive SMOS	SMOS PassiveA SMOS PassiveD	Jacquette et al. (2013), ATBD	N/A
36 km	N/A		Ascending Passive SMAP Descending Passive SMAP	SMAP PassiveA SMAP PassiveD	O'Neill et al. (2018), ATBD	N/A
			Ascending Passive SMOS Descending Passive SMOS	SMOS PassiveA SMOS PassiveD	Jacquette et al. (2013), ATBD	N/A

Note: ATBD stands for Algorithm Theoretical Basis Document.

downscaled soil moisture products surpassed the coarse passive soil moisture estimates in terms of accuracy, and to quantitate the extent of possible improvement (or deterioration) in Chapter 4 and Chapter 5. In this study, the SMAP Level 3 Radiometer Global Daily soil moisture (version 3) posted on the 36 km EASE-Grid and the daily global SMOS Level 3 radiometric soil moisture retrievals, obtained from the 43 km mean spatial scale SMOS observations posted on the 25 km grid (SMOS operational MIR CLF31A/D, version 3.00 obtained from the CATDS website) were evaluated for this purpose. Examples of the coarse SMOS and SMAP soil moisture products are shown in Figure 3.11 for the SMAPEX-4 and -5 airborne field campaigns.

### **3.4.1 Radar-based**

The SMAP soil moisture was downscaled from 36 to 9 km using the radar-based downscaling techniques, including: i) the baseline active/passive method of SMAP (Das et al., 2014), and ii) the Multi-Objective Evolutionary Algorithm (MOEA) by Akbar et al. (2016). The baseline active/passive combination technique is the main procedure used by the SMAP science team to produce the SMAP Radar/Radiometer soil moisture products at 9 km resolution prior to the radar failure. This downscaling algorithm was developed to take advantage of the strengths of passive and active microwave observations, being accurate and high resolution soil moisture mapping, respectively. The baseline algorithm disaggregated the SMAP radiometric brightness temperature through combination with SMAP radar backscatter. This procedure, which inherited background knowledge from the work of Piles et al. (2009b) and Das et al. (2011), includes: i) calibrating model parameters from a linear regression analysis of the time series of brightness temperature-radar backscatter pairs at the radiometric footprint (36 km), and ii) combination of the coarse resolution brightness temperature and medium resolution radar backscatter (9 km) using a linear function, which utilizes the calibrated slope from the predecessor step. Soil moisture is then estimated by applying the radiative transfer model (single channel algorithm, Jackson, 1993) to the downscaled brightness temperature. These estimates are available at the NASA National Snow and Ice Data Center Distributed Active Archive Center (NSIDC DAAC) website as SMAP Level 3 Radar/Radiometer Global Daily 9 km EASE-Grid Soil Moisture, Version

3 (SPL3SMAP). Figure 3.12 shows an example of the baseline active/passive combination technique retrievals, hereafter referred to as the SMAP A/P.

The MOEA is a physical-based downscaling technique Akbar et al. (2016), which implicitly disaggregates the radiometric soil moisture from the coarse scale of 36 km to the medium scale of 9 km using a multi-objective optimization approach . This technique is based on the combination of optimized radar- and radiometer-only soil moisture estimations and is developed to compromise on the performance of the forward electromagnetic emission and scattering models. The MOEA technique finds an optimum solution by including evaluation

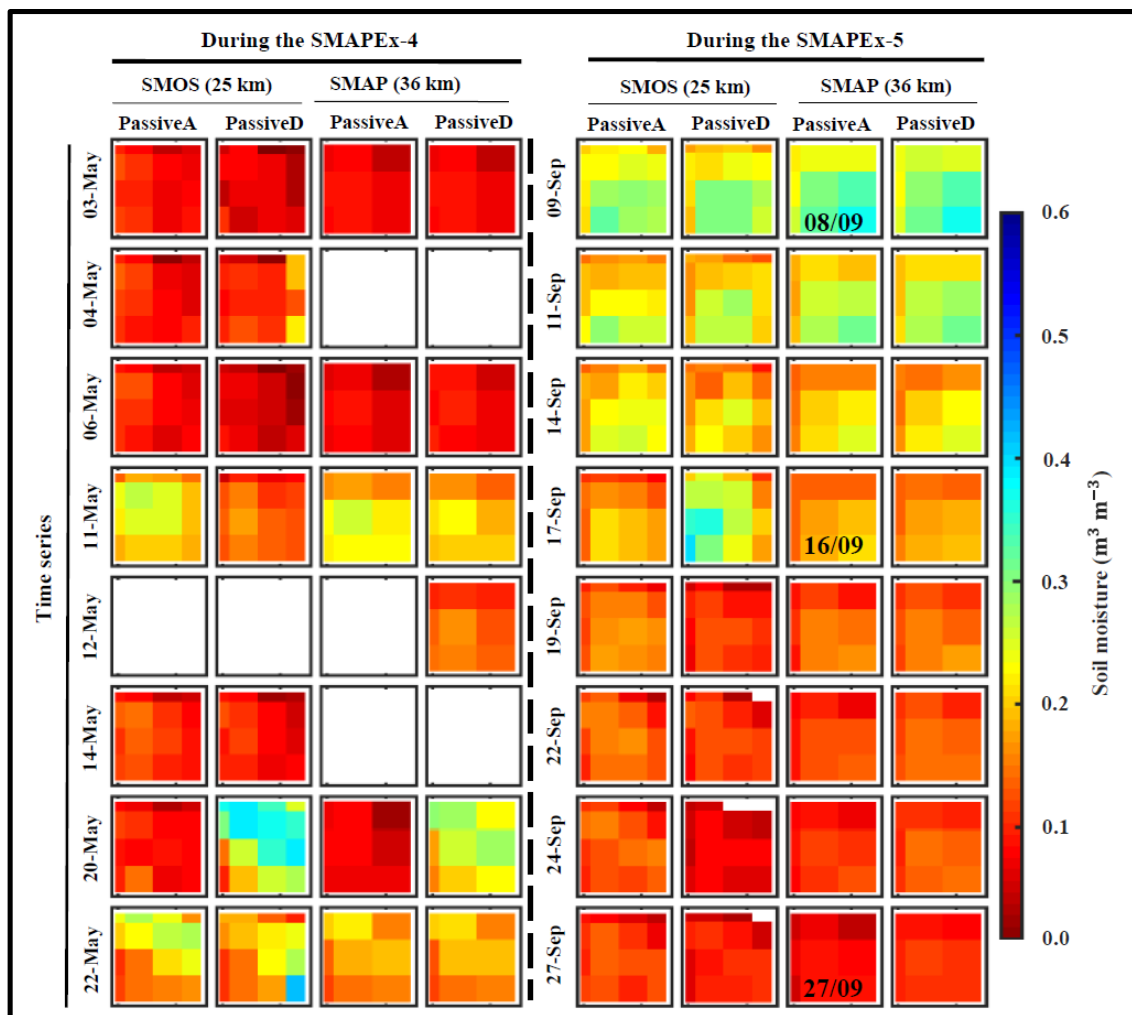


Figure 3.11: The coarse SMOS and SMAP passive microwave soil moisture estimates for the Yanco region during the SMAPEX-4 and -5 airborne field campaigns period. The date is written on soil moisture plots for the nearest available observations to PLMR flight days when coincident overpass data are not available. Notes: missing data are shown in white colour and, A and D stand for ascending and descending overpasses, respectively.

of multiple objective functions within each iteration. Based on stochastic operators, the MOEA procedure gives more weight to the most accurate soil moisture retrievals from either radar backscatter or brightness temperature. The MOEA technique was applied to the SMAP L2 Radiometer Half-Orbit 36 km EASE-Grid Soil Moisture, Version 2 and SMAP L1C Radar Half-Orbit High-Resolution  $\sigma^0$  Data on 1 km Swath Grid, Version 1 (SPL1CS0) pairs. An example of the SMAP MOEA is presented in Figure 3.13.

### 3.4.2 Optical-based

Two types of physically based optical downscaling techniques were applied to the daily global SMOS Level 3 radiometric soil moisture retrievals, posted on the 25 km grid (SMOS operational MIR CLF31A/D, version 3.00 obtained from the CATDS website) and SMAP Level 3 Radiometer Global Daily soil moisture posted on the 36 km EASE-Grid. Disaggregation was based on the Physical And Theoretical scale Change (DisPATCH; Merlin et al., 2013) and the Vegetation Temperature Condition Index (VTCI; Peng et al., 2015, 2016) approaches to achieve a 1 km spatial resolution.

The DisPATCH uses the Soil Evaporative Efficiency (SEE, i.e. ratio of actual to potential soil evaporation) derived from the daily MODIS land surface temperature (MOD11A1 and

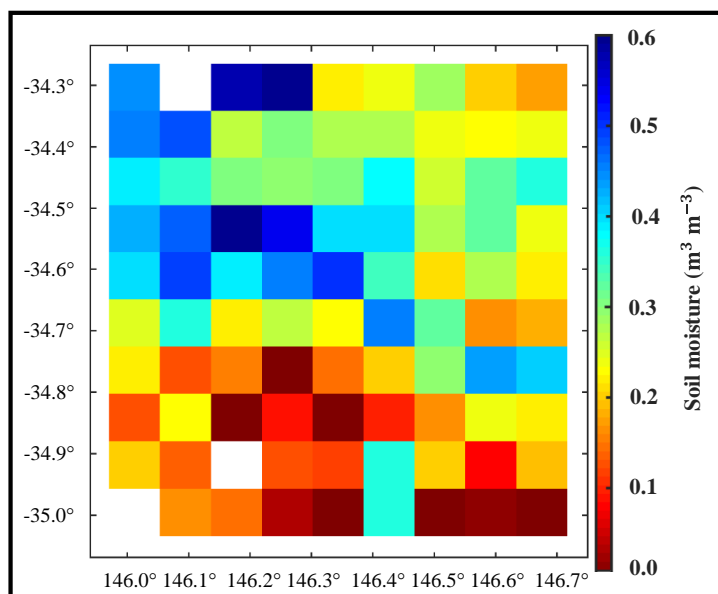


Figure 3.12: An example of the SMAP A/P soil moisture map observed on 17 April 2015.

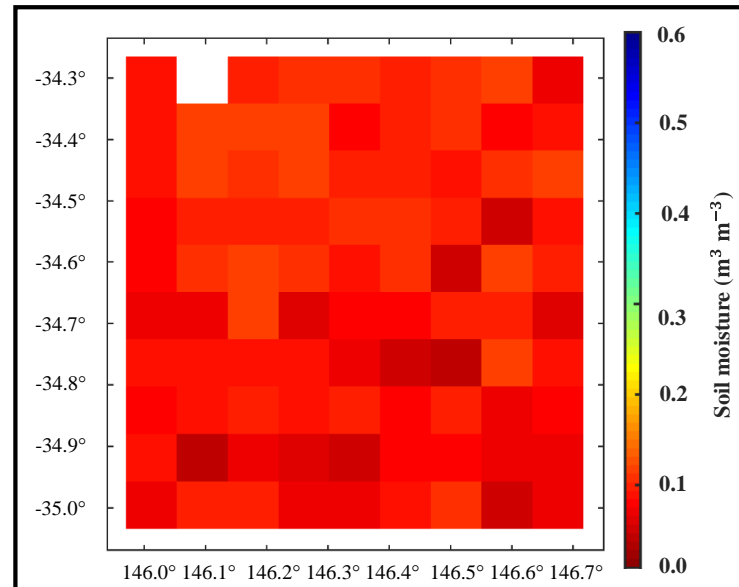


Figure 3.13: An example of the SMAP MOEA soil moisture map observed on 15 April 2015.

MYD11A1 products) and a 16 day composite MODIS vegetation index product (MOD13A2) at 1 km resolution, as the main soil moisture downscaling component. MODIS land surface temperature is decoupled in its soil and vegetation components based on a partitioning method (Moran et al., 1994) with the decoupled surface temperature corrected for the impact of elevation using an ancillary 1 km resolution Digital Elevation Model (DEM) according to Merlin et al. (2013). The SEE proxy is an appropriate downscaling index because: i) it has a relatively constant daily characterization for non-cloudy skies (Crago and Brutsaert, 1996) and ii) it corresponds well with soil moisture changes (Anderson et al., 2007). The DisPATCh technique was applied to the SMOS ascending and descending soil moisture observations resulting in two DisPATCh products, the morning/ascending DisPATCh (DisPATChA) and afternoon/descending DisPATCh (DisPATChD). An example of the SMOS DisPATChA and DisPATChD soil moisture maps during the SMAPEX-4 airborne field campaign are shown in Figure 3.14.

The VTCI technique uses the high resolution VTCI as the downscaling factor. The VTCI is a thermal based proxy which is used as a drought monitoring index (Wang et al., 2001). It is calculated based on the triangular/trapezoidal feature space constructed from 4 day composite MODIS Leaf Area Index (LAI, MCD15A3) at 1 km resolution and the daily Aqua MODIS day-and night-time land surface temperature difference ( $\Delta LST_{day-night}$ , MYD11A1).

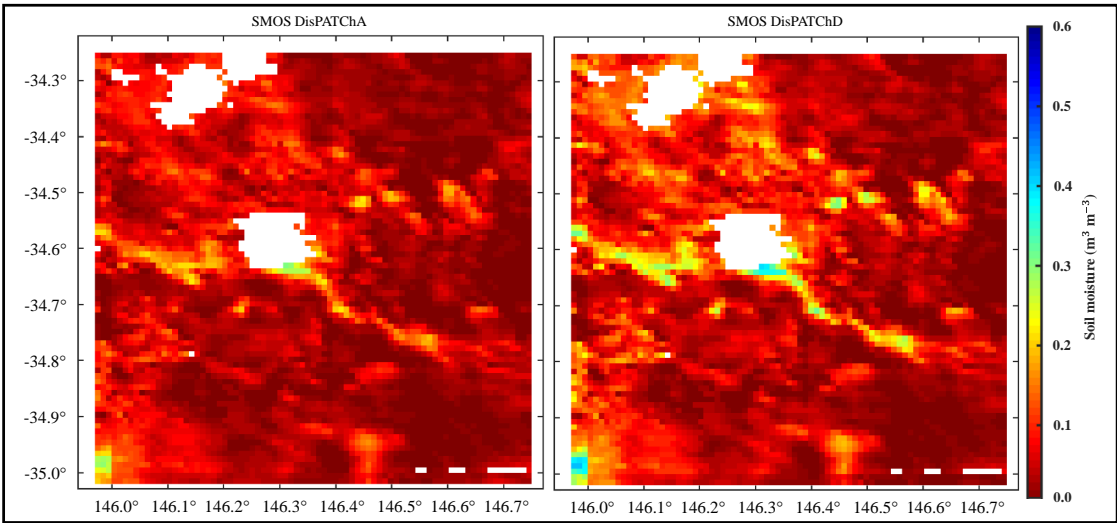


Figure 3.14: Examples of the SMOS DisPATChA and DisPATChD soil moisture maps observed on 3 April 2015.

The SMAP VTCI and SMOS VTCI soil moisture maps observed on 3rd April 2015 during the SMAPEX-4 airborne field campaign are shown in Figure 3.15.

### 3.4.3 Radiometer-based

Downscaled SMAP soil moisture retrievals were also produced at 10 km using the radiometer-based Smoothing Filter-based Intensity Modulation (SFIM) model developed by Gevaert

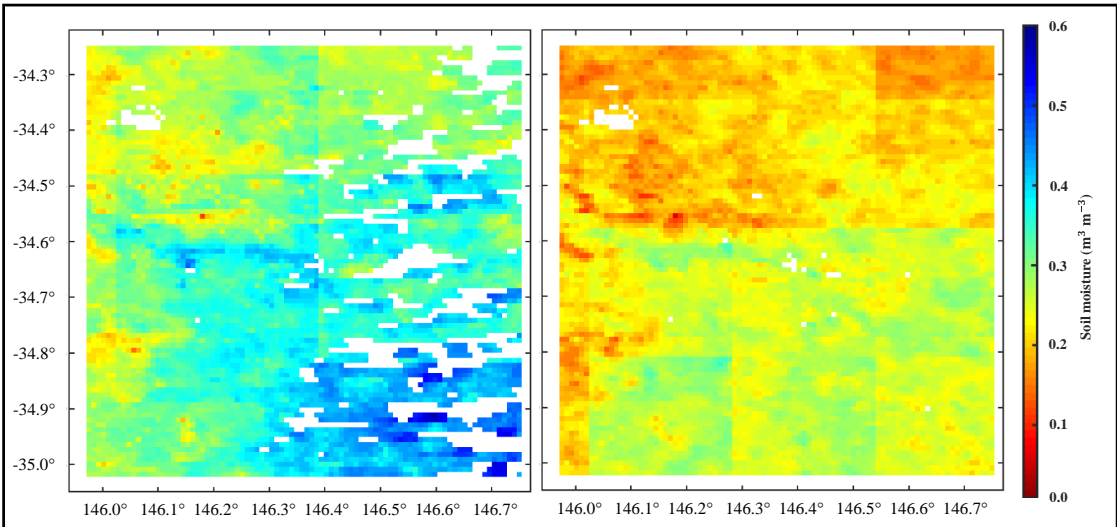


Figure 3.15: Examples of the SMAP VTCI and SMOS VTCI soil moisture maps observed on 1 and 2 September 2015, respectively.

et al. (2015). The SFIM methodology is based on the multi-sensor image fusion technique designed by (Liu, 2000). Success of this technique in producing downscaled Landsat Thematic Mapper data to a higher spatial resolution using the high resolution Satellite Pour l'Observation de la Terre images, motivated Santi (2010) to employ this technique for the purpose of soil moisture downscaling. In the SFIM procedure a weighting factor is used to downscale the 36 km SMAP Level 2 brightness temperature (SPL2SMP) to 10 km. The downscaling factor used here is the ratio between the Advanced Microwave Scanning Radiometer-Earth Observing System (AMSR2) Ka-band brightness temperature for each grid cell at 10 km and the average of Ka-band brightness temperature across the coarse scale of the SMAP brightness temperature observations. From downscaled SMAP brightness temperature, soil moisture content was estimated through application of the Land Parameter Retrieval Model (LPRM, Owe et al., 2001, 2008). An example of the SMAP SFIM soil moisture map during the SMAPEX-4 airborne field campaign is shown in Figure 3.16.

### 3.4.4 Oversampling-based

An oversampling-based technique (Chan et al., 2018; Chaubell, 2016), based on the Backus-Gilbert interpolation method (Backus and Gilbert, 1970, 1967), was also used to enhance

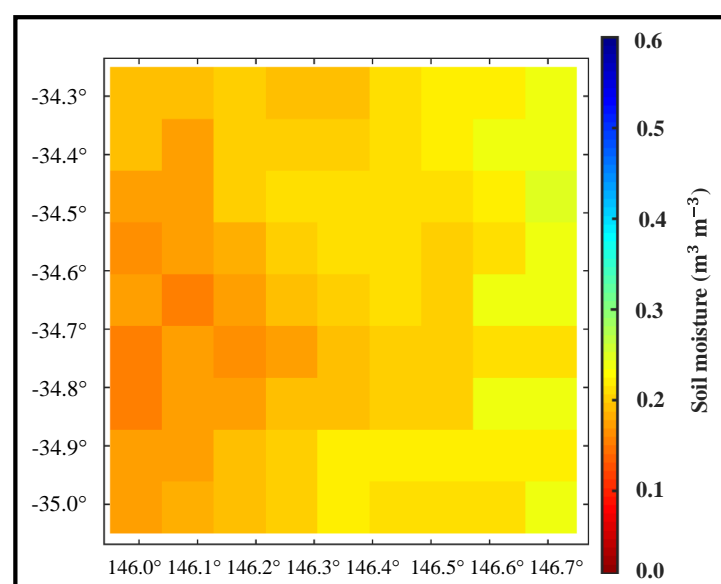


Figure 3.16: An example of the SMAP SFIM soil moisture map observed on 09 April 2015.

not only the spatial scale of SMAP brightness temperature but also its accuracy. Soil moisture was then derived by applying a radiative transfer model to the brightness temperature posted onto a 9 km grid. This technique was applied to the morning/descending (D) and afternoon/ascending (A) SMAP level 1B Radiometer Half-Orbit Time-Ordered brightness temperature products at  $47 \text{ km} \times 36 \text{ km}$ , resulting in two series of products: the EnhancedD and EnhancedA, respectively. The Backus-Gilbert is an optimal interpolation theory that provides the closest observation to what perhaps would be measured by the radiometric instrument at the interpolation point (Poe, 1990). To this aim, all the brightness temperature values that are centred near a particular radius within a relatively short length of intervals are aggregated to a spatial resolution higher than the resolution and/or footprint of observations. The extent of improvement of the spatial resolution is determined by the sampling density and overlap in the response functions of the instrument at measurement locations. Long and Daum (1998) found out that when the sampling pattern is denser there is a better opportunity for the spatial resolution enhancement of observations. The non-uniformity of overlapping measurement is another factor which facilitates better resolution enhancement (Long, 2003). Figure 3.17 shows an example of the SMAP EnhancedA and EnhancedD soil moisture maps observed on 11 May 2015 during the SMAPEX-4 airborne field campaign.

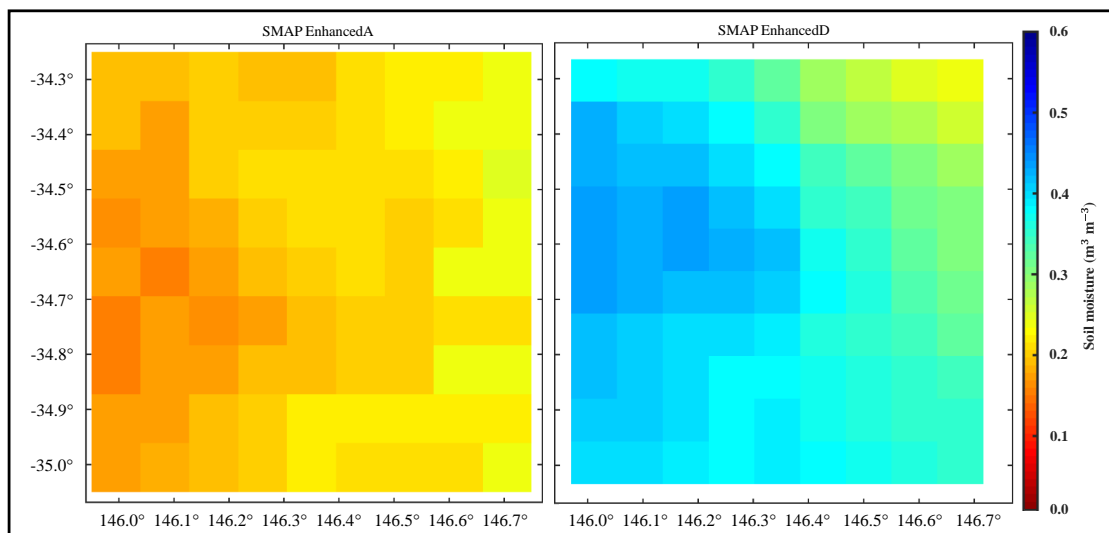


Figure 3.17: An example of the SMAP EnhancedA and EnhancedD soil moisture maps observed on 03 July 2015.

### 3.5 Chapter summary

This chapter provided an overview of the SMAPEX-4 and -5 data which was used together with *in situ* OzNet soil moisture measurements for inter-comparison of the performance of downscaled, radiometer-only and merged soil moisture products. For the purpose of calibration and validation of SMAP soil moisture products the SMAPEX-4 and -5 airborne campaigns were conducted, during which comprehensive data set including L-band passive microwave observations from PLMR, HDAS intensive soil moisture ground sampling, soil surface roughness and vegetation data were collected. These airborne campaigns were supported by the OzNet monitoring stations providing *in situ* soil moisture measurements.

Downscaled soil moisture products used in the inter-comparison and merging method were also described, outlining the downscaling techniques and approaches, product definitions, key references, and main downscaling inputs as applicable. The downscaled soil moisture products include retrievals of radar-, optical-, radiometer- and oversampling-based downscaling techniques. The SMOS and SMAP coarse passive microwave data sets used for benchmarking the downscaled soil moisture products against of, were also briefly introduced in this chapter.



## Chapter 4

# Inter-comparison of alternative downscaled products

Existing optical-, radiometer-, and oversampling-based downscaling methods could be an alternative to the radar-based approach for delivering downscaled soil moisture. Nevertheless, retrieval of accurate high resolution soil moisture remains a challenge, and there has been no test to assess which downscaling methodology yields the best overall soil moisture estimation at higher resolution against a common reference data set. Consequently, this chapter presents an inter-comparison of the radar-, optical-, radiometer-, and oversampling-based downscaling techniques against a common reference data set including the SMAPEX-4 and -5 airborne field campaigns and the OzNet *in situ* measurements from Chapter 3, to determine the relative strengths and weaknesses of their performances. The work in this chapter has been submitted to the journal Remote Sensing of Environment for publication.

### 4.1 Introduction

Soil moisture influences land-atmosphere interaction via fluxes of energy and water, and thus impacts weather and climate conditions (Seneviratne et al., 2010), hydrology (Corradini, 2014; Koster et al., 2004, 2010) and agricultural production (Bolten et al., 2010). The ability to provide reliable, spatially distributed and temporally consistent measurements of soil moisture will therefore be of great benefit. Key to providing such information economically across the globe has been the development of L-band passive microwave remote sensing technology (Entekhabi et al., 2010; Kerr et al., 2016). The passive L-band microwave approach is widely accepted as the optimum technology for soil moisture estimation (En-

tekhabi et al., 2010) because: i) it is highly sensitive to soil moisture dynamics (Ulaby et al., 1982), ii) it has a direct relationship to soil moisture (Jackson and Schmugge, 1989), iii) it is relatively unaffected by the vegetation and atmosphere (Ulaby et al., 1982), iv) it is independent of weather condition and daylight (Jackson, 1993), v) it has a large signal-to-noise ratio (Njoku and Entekhabi, 1996), and vi) it is able to see into the top approximately 5 cm of the soil (Owe and Van de Griend, 1998).

There are currently two L-band passive microwave satellite missions dedicated to monitoring the near surface soil moisture every 2 to 3 days: i) the ESA Soil Moisture and Ocean Salinity (SMOS), which was launched in November 2009 as the first ever dedicated satellite for soil moisture mapping, and ii) the NASA Soil Moisture Active Passive (SMAP), launched in January 2015 as the first ever satellite to combine a radar and radiometer to produce an enhanced resolution soil moisture product.

Each of these satellite is equipped with a specific antenna setup which makes their products disparate in terms of quality, spatial resolution and sampling density. The SMAP has a rotating real aperture antenna that conically scans the surface soil moisture, using an L-band radiometer, at approximately 40 km spatial resolution with 11 km along scan and 31 km across scan spacing, and at a constant incidence angle of 40 degree. This characteristic of SMAP simplifies data processing and interpretation, and increases the accuracy of repeat-pass soil moisture estimation (O'Neill et al., 2018). The SMOS radiometer is a 2D (interferometric) Microwave Imaging Radiometer with Aperture Synthesis (MIRAS) which collects multi-angular brightness temperature at the scale of about 40 km. While SMOS does not have the same sampling capability of SMAP, its overlapping snap shots with varying incidence angle across the swath allow for multi-incidence angle data for the same footprint. Together, the SMOS and SMAP missions provide the continuity of dedicated satellite soil moisture observations for the globe since 2010 (Kerr et al., 2016).

Soil moisture estimates at native resolution from both the SMOS and SMAP radiometers are only available at a coarse scale of approximately 40 km (provided on 25 km and 36 km grid spacing, respectively), which is not sufficient to meet the spatial resolution requirements of hydro-meteorological, agricultural and carbon cycle applications (e.g Entekhabi et al.,

2010; Molero et al., 2016). However, the SMAP satellite included an L-band radar which was to be combined with the L-band radiometer observations for spatial scale improvement of the radiometric observations, so as to allow accurate high resolution global near-surface soil moisture mapping (Entekhabi et al., 2010; O’Neill et al., 2010). The sensitivity of radar backscatter to soil moisture dynamics and the geophysical properties of the soil surface was expected to contribute to improvement of the retrievals’ accuracy and disaggregation of radiometric soil moisture estimates (Chauhan, 1997; Petropoulos et al., 2015). However, loss of coincident radar imaging in July 2015 due to a hardware anomaly meant that an alternative downscaling approach had to be sought. Moreover, there is no radar sensor aboard the SMOS. Consequently, alternative downscaling techniques have been applied to the two soil moisture missions, with the aim to accurately and efficiently increase the resolution of SMOS and SMAP passive L-band soil moisture (and/or brightness temperature).

Reviews of techniques for downscaling passive microwave data for high resolution soil moisture mapping have been recently published by Sabaghy et al. (2018) and Peng et al. (2017). Downscaling methods exploit both the accuracy of the passive L-band microwave observations and the high resolution spatial variability of the ancillary data. Accordingly, downscaling techniques include, but are not limited to, radar-, optical-, radiometer-, and oversampling-based methods.

The radar-based downscaling techniques (Akbar and Moghaddam, 2015; Bindlish et al., 2008; Das et al., 2011, 2014; Piles et al., 2009b; Zhan et al., 2006) are based on radar-radiometer combination algorithms which enhance the spatial detail of coarse radiometric soil moisture using the spatially varied information on land surface features provided by radar. The extent of correlation between backscatter and soil moisture, and sensitivity of backscatter to soil moisture changes determine the success of radar-based downscaling techniques in estimating the variation of soil moisture in space (Wu et al., 2014).

The basic concept behind the optical-based downscaling techniques (e.g. Fang et al., 2013; Merlin et al., 2006, 2008a,b, 2012, 2013; Piles et al., 2011, 2012, 2013) is the feature space between vegetation index and surface temperature in the shape of a triangle/trapezoid (e.g. Carlson et al., 1994; Gillies and Carlson, 1995) which indicates wet and dry conditions at its

edges. This feature space adjusts the sensitivity of land surface temperature to soil moisture as a function of vegetation cover density and canopy type.

The radiometer-based downscaling technique (e.g. Gevaert et al., 2015; Santi, 2010) uses radiometric emissions at higher frequency (Ka-band, 26 to 40 GHz) to provide information about spatial variability of the surface when there is no rainfall event (Gevaert et al., 2015). The advantage of the radiometer- (over the optical-) based approach lies in the capacity of radiometer imagery to deliver ancillary data under all weather conditions and being less affected by the soil surface condition. However, the radiometer-based technique is not able to improve the resolution of soil moisture content to the same extent as the optical-based techniques due to the coarser resolution of that data, as the resolution of downscaled soil moisture products is dictated by that of the ancillary data used for the downscaling.

The oversampling-based method (Chan et al., 2018; Chaubell, 2016) applies an interpolation technique which rescales the brightness temperature values to 30 km and posts onto a 9 km grid. Consequently, it creates the most optimal brightness temperature by aggregating brightness temperature values that are centred near a particular radius with a relatively short length of intervals. For the methods that downscale the brightness temperature (e.g. oversampling- and radiometer-based techniques), soil moisture retrieval is then conducted on the higher resolution brightness temperature using the same passive microwave soil moisture retrieval algorithm used with the coarse observations.

While a diversity of downscaling approaches exist, until now there has been no rigorous test to assess which downscaling methodology yields the best overall soil moisture estimation at higher resolution. Therefore, this chapter presents a consistent inter-comparison of the various downscaling techniques against each other and a reference data to determine the relative strengths and weaknesses of their performance. This is the first consistent assessment of the complete range of different radar-, optical-, radiometer-, and oversampling-based downscaled soil moisture products which are readily available using the same set of evaluation data, in order to take a step towards multi-sensor high resolution soil moisture retrieval for typical Australian landscapes. The performance of the downscaled soil moisture products was also benchmarked against the radiometer-only retrievals of SMAP and SMOS.

## 4.2 Evaluation methodology

This section describes the evaluation procedure that is summarised in Figure 4.1. Here the downscaled soil moisture products are evaluated against a consistent reference data set that includes the OzNet *in situ* soil moisture measurements and the SMAPEX-4 and -5 airborne PLMR soil moisture maps. The coarse passive SMAP and SMOS soil moisture products were also compared against the same reference data set providing a baseline scenario. This evaluation is meant to serve as a quantitative assessment of the improvement in the downscaled soil moisture products over the coarse soil moisture products, applied directly at the same spatial resolution as the comparable downscaled soil moisture product. Consequently, prior to the evaluation of coarse SMAP and SMOS soil moisture products, each product was mapped onto a 1 and 9 km grid, with the value of each coarse pixel assigned to each higher resolution pixel lying within the original pixel.

The evaluation against the OzNet measurements was conducted over the period between 1st April and 1st November 2015, while the time frame of the evaluation against airborne PLMR soil moisture was associated with the temporal extent of the SMAPEX-4 and -5 airborne field campaigns. The evaluation included a temporal analysis of the downscaled soil

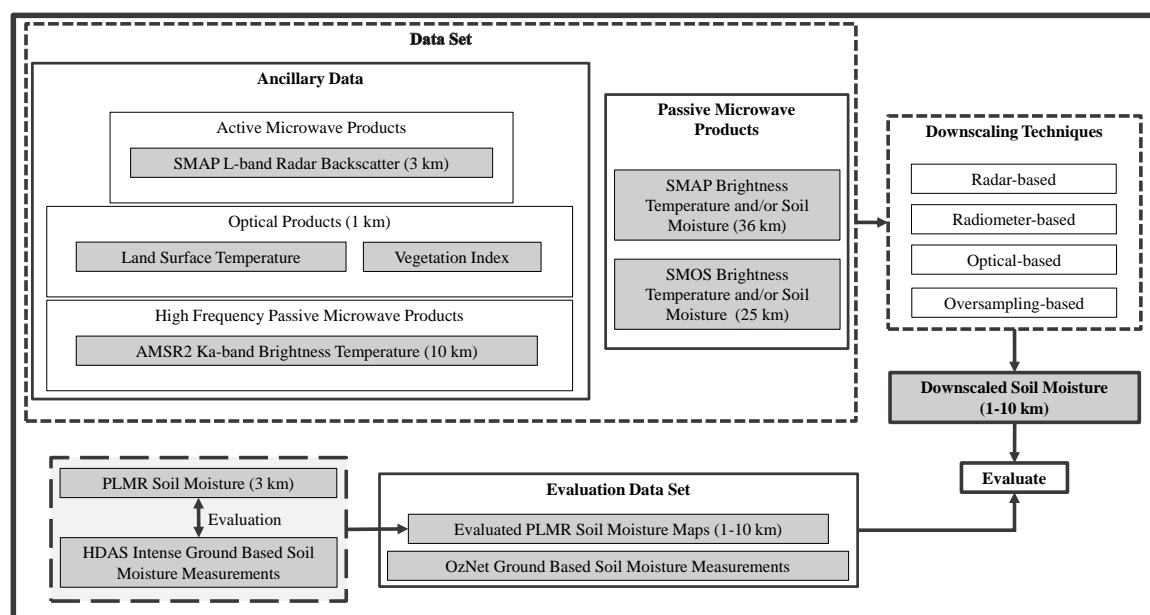


Figure 4.1: Schematic of the procedure used for evaluation of the downscaled soil moisture retrievals against the airborne PLMR and the OzNet *in situ* soil moisture measurements.

moisture products against both the OzNet and airborne PLMR soil moisture. In the temporal analysis, time series of soil moisture values from each pixel of modelled estimates were compared against corresponding values from the reference PLMR maps and/or aggregated OzNet measurements to the products pixel scale. Moreover, the spatial analysis was carried out against the airborne PLMR soil moisture. In the spatial analysis, daily maps of estimates were compared against the corresponding reference map. From the temporal and spatial match-ups mentioned above, the performance metrics were calculated, including bias, coefficient of determination ( $R^2$ ), Root Mean Square Deviation (RMSD), and unbiased RMSD (ubRMSD), and slope of linear regression.

The optical-based downscaled soil moisture products were evaluated at two different scales: i) 1 km being the original scale of the optical-based products, and ii) 9 km being the scale of radar- and oversampling-based retrievals. For the evaluation at 9 km, the optical-based products herein DisPATCh and VTCI were upscaled to the SMAP A/P scale of 9 km, using the arithmetic average. The evaluation at 9 km was conducted to make the comparison system consistent across the downscaled soil moisture products being mainly available at 9 km.

#### **4.2.1 Evaluation against the OzNet in situ soil moisture measurements**

To compare the downscaled soil moisture products against the OzNet, soil moisture measurements from individual stations were averaged within the grid cell of each product. For the grid scales larger than 1 km, comparisons were made across the pixels that had a large number of the OzNet stations (more than or equal to four) within their scale. Figure 4.2 shows the selected pixels at the medium scales of 9 and 10 km at which the downscaled soil moisture products were evaluated.

#### **4.2.2 Evaluation against the SMAPEX-4 and -5 PLMR soil moisture maps**

The evaluation of the downscaled soil moisture products against PLMR required pairing of the PLMR soil moisture maps with the nearest available downscaled soil moisture products to the PLMR flights, when coincident downscaled data were not available. The nearest

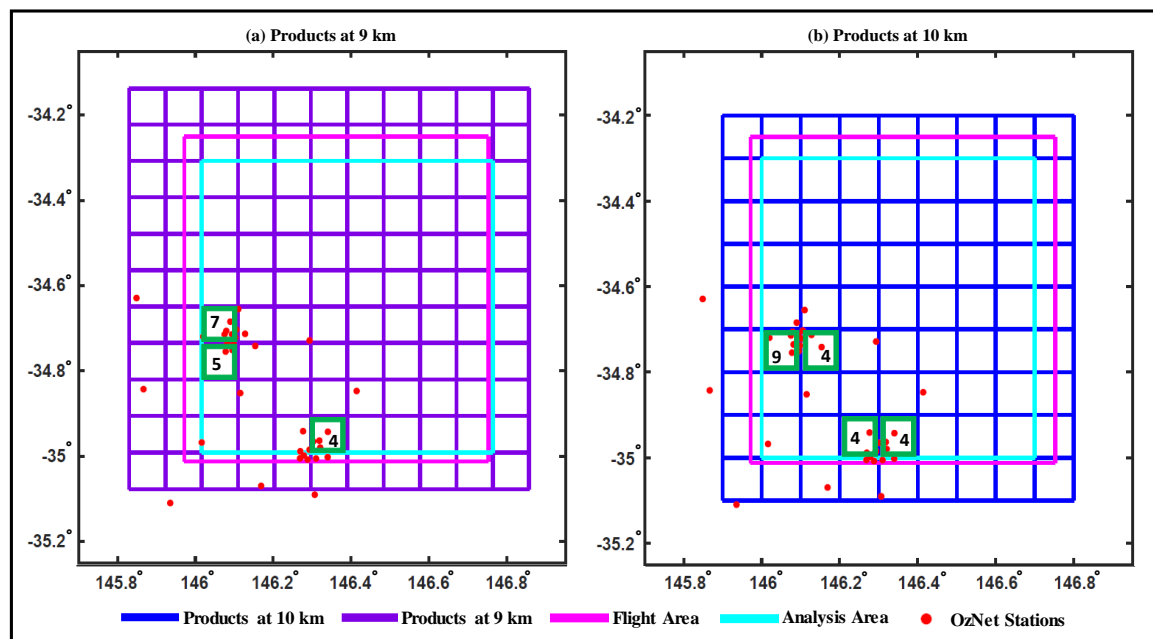


Figure 4.2: Schematic of the downscaled soil moisture product grids at (a) 9 km and (b) 10 km. The SMAPEX-4 and -5 flight coverage and location of the OzNet stations are highlighted in magenta rectangles and red dots, respectively. The cyan rectangle shows the common analysis area for both airborne field campaigns. Green squares show the chosen pixels for analysis of soil moisture products against the OzNet measurements. These pixels contain the largest number of the OzNet stations (more than four); the number of available stations is written in the pixel.

available products were selected based on information about the rainfall occurrence over the study area and minimal average absolute change ( $\leq 0.02 \text{ m}^3 \text{ m}^{-3}$ ) of the OzNet soil moisture measurements between the flight dates and those of the nearest available products in time. The date of the nearest available observations to PLMR flights is written on soil moisture thumbnail plots (Figure 4.3 and 4.4 provided in the results section) when data were not coincident. The main comparison scenario of the downscaled soil moisture products against the airborne PLMR soil moisture was developed to discard the seasonal performance of the downscaled soil moisture products because the operational application of the downscaled soil moisture products should be regardless of climate conditions (Sabaghy et al., 2018). The analysis herein used the entire downscaled soil moisture data captured during both the SMAPEX-4 and -5 airborne field campaigns. Moreover, the seasonal performance of the downscaled soil moisture products was examined for the Austral autumn (March-May, using the SMAPEX-4 data) and spring (September-November using the SMAPEX-5 data) as a complementary scenario, in order to understand the seasonal performance and uncertainties

of the soil moisture products.

Radar-based soil moisture products were only available for the period between 15 April and 7 July 2015 when the SMAP radar was still transmitting data. Thus, radar-based products were evaluated only for the SMAPE<sub>x</sub>-4 airborne field campaign. The seasonal evaluation of the performance of the other downscaled soil moisture products was conducted when enough (4 or more) coincident downscaled soil moisture maps were available. Accordingly, the performance analysis of the VTCI-based products was not possible for the SMAPE<sub>x</sub>-4 period as only one SMOS VTCI and two SMAP VTCI soil moisture maps were captured due to cloud.

In order to address the potential variation in number of different downscaled soil moisture products available for comparison, and eliminate the impact on evaluation, only the downscaled soil moisture products collected on 3, 6, 11, 20 and 22 May 2015 during the SMAPE<sub>x</sub>-4 were evaluated herein. This evaluation was undertaken for the SMAPE<sub>x</sub>-4 period only because the radar-, optical-, radiometer- and oversampling-based products were all available over this period.

### **4.3 Results**

Time series of the downscaled and observed airborne PLMR soil moisture maps during the SMAPE<sub>x</sub>-4 and -5 airborne field campaigns are shown in Figure 4.3 and Figure 4.4, respectively. These figures show the performance of the downscaled soil moisture products in capturing the spatio-temporal variability of soil moisture. The airborne PLMR soil moisture estimates at 1 km have consistency with the occurrence of precipitation events, mimicking the dry down cycle observed during the SMAPE<sub>x</sub>-5 and the rainfall interrupted drying spell during the SMAPE<sub>x</sub>-4 (Figure 3.2). There is no clear evidence from Figures 4.3 and 4.4 to show that any downscaling process is clearly superior to another for disaggregation of SMAP and/or SMOS, but among the downscaled soil moisture products available over the SMAPE<sub>x</sub>-4 period, DisPATCH and VTCI products- especially at 9 km- revealed the best visual agreement with the spatial and temporal pattern of airborne PLMR soil moisture compared to other products. However, a limitation of the optical approach is that it

cannot deliver any soil moisture downscaling under cloudy skies because of the lack of cloud free optical imagery, which is the key component or input in the optical downscaling process. This shortcoming of optical imagery resulted in the reduced availability of the VTCI-based downscaled soil moisture, which uses the difference of day and night land surface temperature in derivation of its downscaling index. The lack of access to optical observations, which is more pronounced for the SMAPEX-5 period, is unlike microwave-based approaches where there are no such gaps in data. The microwave-techniques are in general capable of soil moisture downscaling under all-weather conditions. This capability is due to microwave observations being able to pass through non-raining clouds unaffected. The success of DisPATCH and VTCI products in capturing the soil moisture spatio-temporal variability is followed by both of the radar-based downscaled soil moisture products, namely the SMAP MOEA and A/P products, which were only available for the SMAPEX-4 period.

The temporal evolution of the downscaled soil moisture products at 9 km was also compared with that of aggregated OzNet measurements to 9 km (Figure 4.5) showing a significant level of agreement between them. The majority of the downscaled soil moisture values do not match the median OzNet soil moisture closely, but are in the range of aggregated OzNet measurements. However, there are also a few days on which the downscaled soil moisture estimates laid outside the OzNet measurement range.

### **4.3.1 Temporal analysis against the OzNet**

Temporal analysis of soil moisture products was carried out against pixels containing multiple OzNet stations. In this analysis, time series of soil moisture values from the chosen pixels were compared against corresponding values from aggregated OzNet soil moisture measurements. A summary of accuracy statistics from different downscaled soil moisture products is presented as a boxplot in Figure 4.6, containing the minimum, maximum, median, and interquartile ranges together with the mean.

Comparison of products at 9 km resolution (Figure 4.6-b) shows that the SMAP VTCI soil moisture product had the best temporal agreement with the OzNet measurements, followed

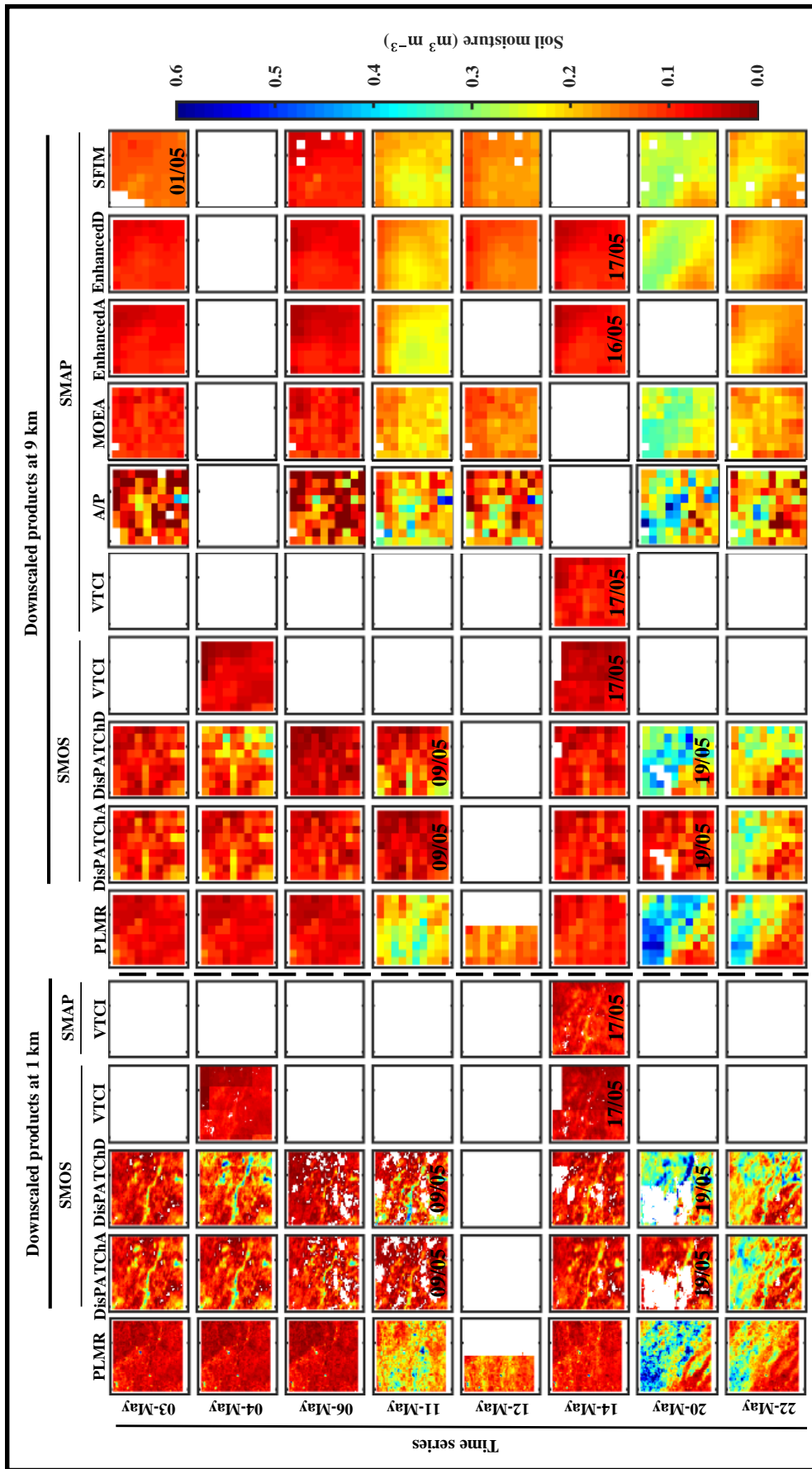


Figure 4.3: Time series plots of PLMR observed reference soil moisture estimates and the range of the downscaled soil moisture estimates for the Yanco region during the SMAPEX-4 period. DisPATCh, VTCl-based and PLMR soil moisture maps are presented at their original scale of 1 km as well as 9 km after aggregation. The date is written on soil moisture plots for the nearest available observations to PLMR flight days when coincident overpass data are not available. Note: missing data are shown in white colour.

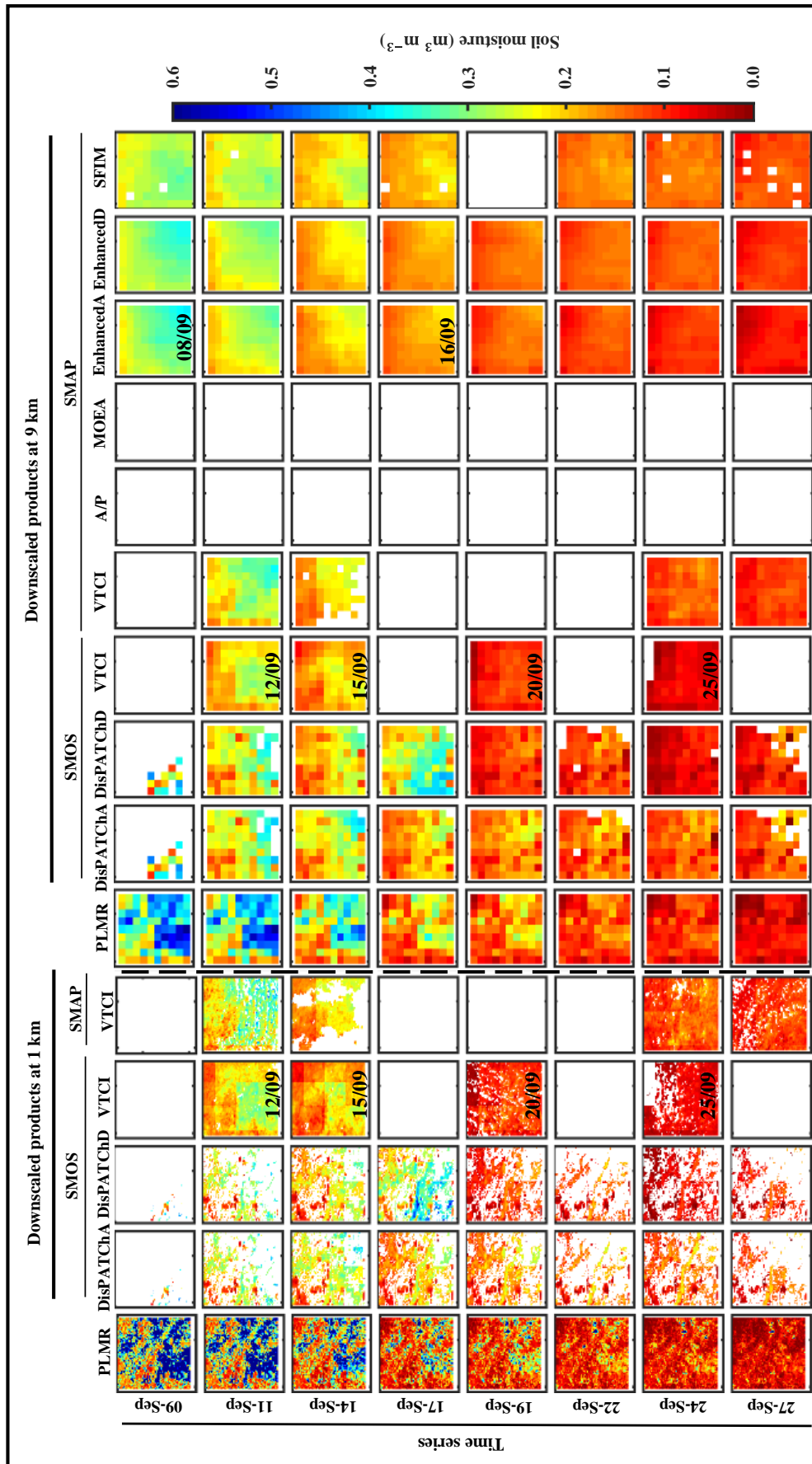


Figure 4.4: As for Figure 4.3 but for the SMAPEX-5 period.

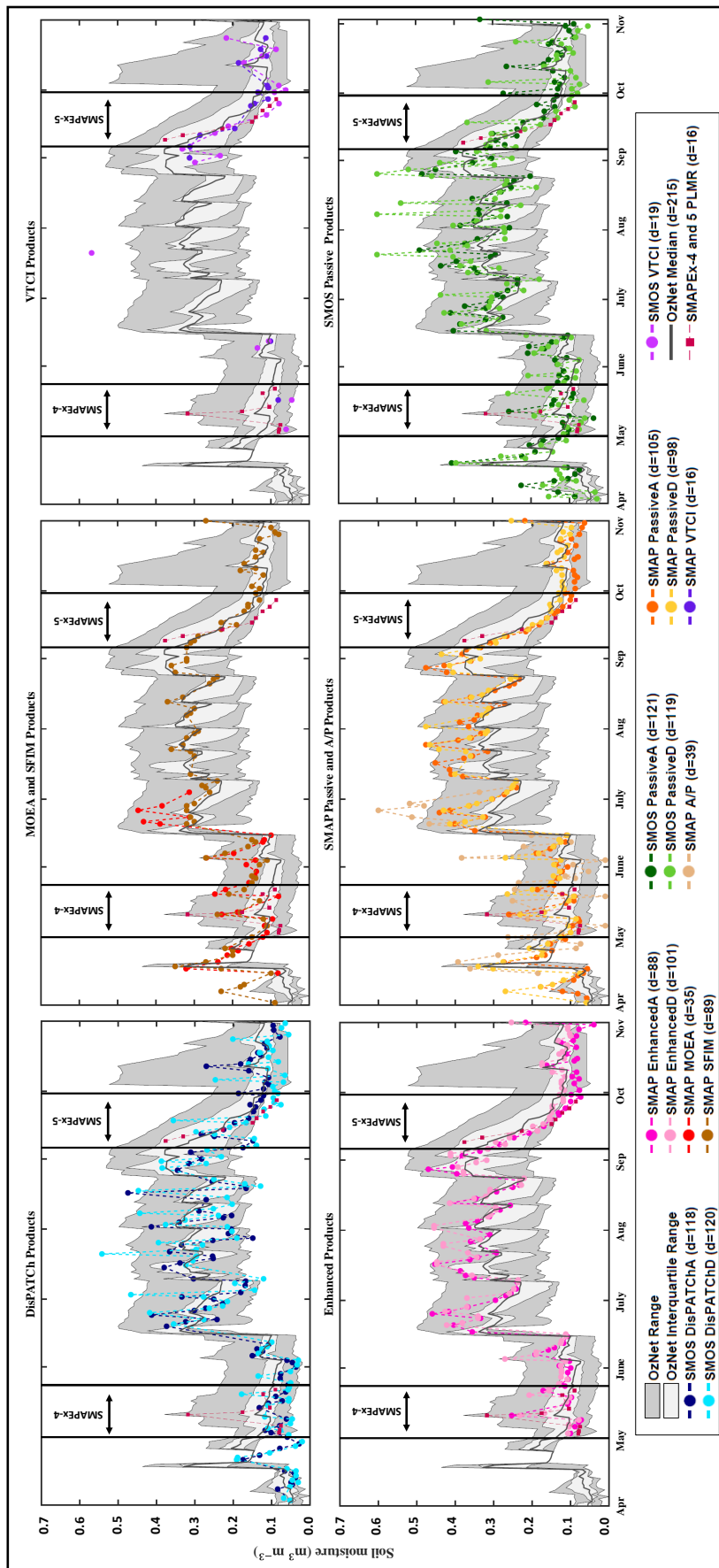


Figure 4.5: Sample of the temporal evolution of PLMR observed reference soil moisture estimates, the median of measurements from the OzNet stations, coarse SMAP and SMOS at 9 km without any downscaling technique being applied, and the range of the downscaled soil moisture estimates for the Yanco region during the period between 1 April and 1 November 2015; d indicates the number of days for which the downscaled soil moisture products were available over the SMAPEX-4 and -5 flight area.

by the SMAP EnhancedD and EnhancedA products. The SMOS VTCI, SMOS PassiveD and DisPATChD had the lowest agreement with the temporal pattern of the OzNet soil moisture compared to other products at 9 km, having an average  $R^2$  of  $\sim 0.6$ . The difference between the performance of the SMAP and SMOS VTCI is the result of the difference in the SMAP and SMOS PassiveD from which the SMAP and SMOS VTCI products were derived. The SMAP VTCI soil moisture had an overall bias of  $-0.011 \text{ m}^3 \text{ m}^{-3}$ , which explains the slight underestimation relative to the ground OzNet measurements. While the SMOS VTCI, DisPATChD and SMAP VTCI underestimated relative to the OzNet measurements, the other products overestimated. For example, the SMAP MOEA with average bias of  $0.057 \text{ m}^3 \text{ m}^{-3}$  had the most noticeable overestimation.

With the exception of SMAP VTCI and the Enhanced products, the other downscaled soil moisture products at 9 km showed a deterioration in the  $R^2$  when compared with the coarse original SMAP soil moisture products. For instance, the  $R^2$  of SMAP A/P was on average 0.12 less than that of SMAP PassiveA and PassiveD. Among the downscaled soil moisture products, the SMAP EnhancedA and EnhancedD downscaled soil moisture products maintained a similar RMSD to the coarse SMAP passive soil moisture products. It is to be noted that SMAP VTCI was the only downscaled product which outperformed the original coarse passive SMAP in terms of RMSD, hitting the lowest values of RMSD and ubRMSD. The DisPATChD could not improve the accuracy of non-downscaled SMOS PassiveD from which DisPATChD originated. However, the DisPATChD showed a close performance to that of SMOS PassiveD.

The SMAP EnhancedD with mean  $R^2$  of 0.81, mean RMSD of  $0.061 \text{ m}^3 \text{ m}^{-3}$  and mean bias of  $0.024 \text{ m}^3 \text{ m}^{-3}$  was found to have a slightly better performance than the SMAP EnhancedA. The performance of the Enhanced product, was generally consistent with that of products evaluated by Chan et al. (2018) who assessed the performance of the Enhanced products for the duration of April 1, 2015 to October 30, 2016 using *in situ* data from the SMAP mission core validation sites including Yanco. Chan et al. (2018) reported on the similarity between the performance of Enhanced products and that of SMAP passive soil moisture products. Based on their analysis, the SMAP EnhancedD data attained a mean  $R^2$  of 0.92 (correlation coefficient/ $R = 0.96$ ), mean RMSD of  $0.048 \text{ m}^3 \text{ m}^{-3}$  and mean bias of  $0.02 \text{ m}^3 \text{ m}^{-3}$  over the

Yanco region.

When compared against aggregated OzNet measurements at 1 km (Figure 4.6-a), the products were shown to have a poorer performance than the products at 9 km. Such a decrease in the performance of products at 1 km could be associated with the spatial-scale mismatch, which is expected to be larger for higher resolution products (van der Velde et al., 2012). Moreover, it has previously been noted by Yee et al. (2016) that the evaluation of soil moisture products against the OzNet stations in the Yanco region is more reliable for coarser

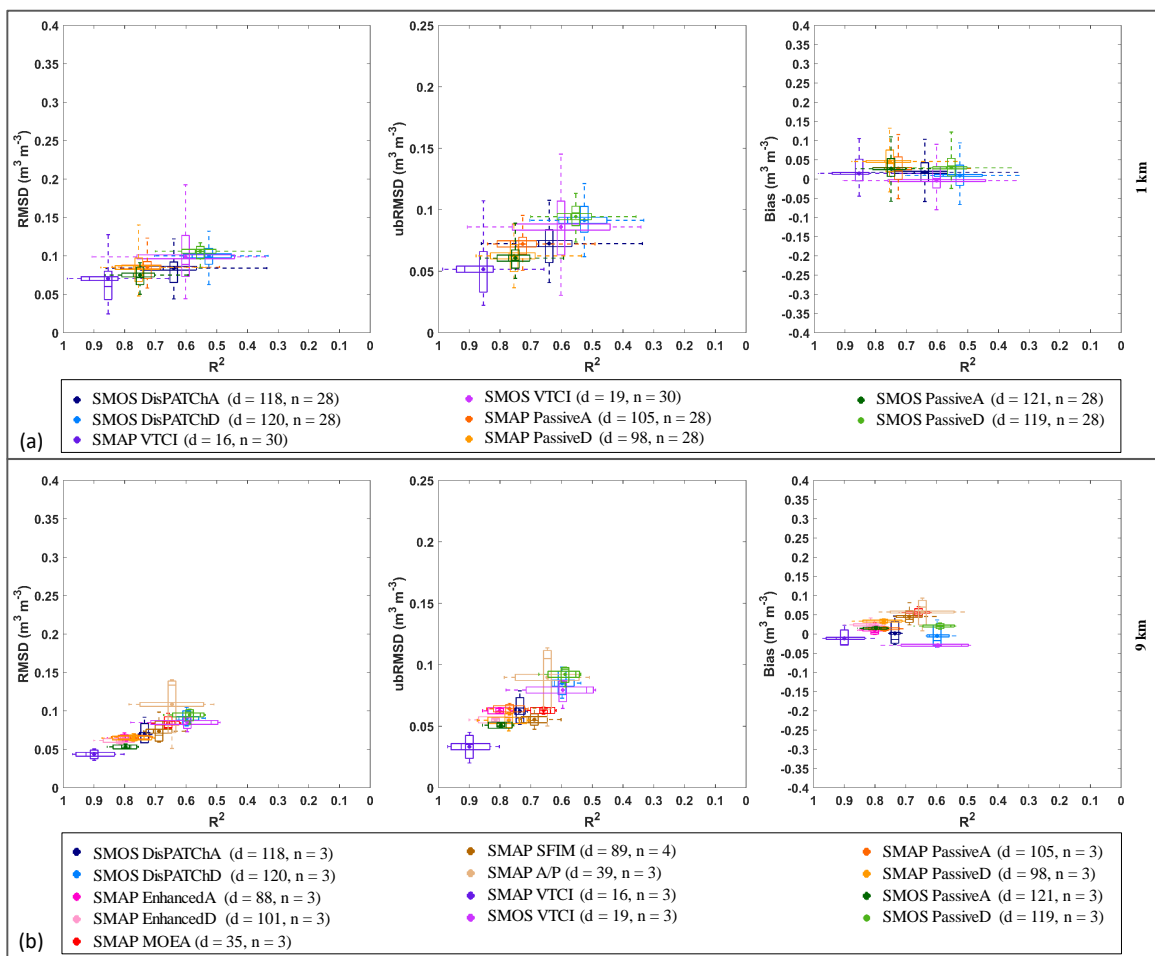


Figure 4.6: Summary of results obtained from temporal analysis of soil moisture products at (a) 1 km and (b) 9 km against the OzNet. For 9 km products, only pixels with the largest number of stations were chosen. Each boxplot displays the distribution of the accuracy statistics of different downscaled soil moisture products based on the interquartile range, the maximum and minimum range, and the statistics median (bar) associated with the mean (dot). d indicates the number of the downscaled soil moisture products that were used in this analysis and n indicates the number of statistical parameters that are summarized in this figure.

resolutions whereby multi-stations are aggregated for each pixel footprint.

The SMAP VTCI with mean  $R^2$  of 0.85 and mean RMSD of  $0.07 \text{ m}^3 \text{ m}^{-3}$  was found to have the best performance. The  $R^2$  of DisPATCh products at 1 km were observed to be slightly lower than that of DisPATCh products at 9 km. The same observation was made regarding the  $R^2$  of SMAP VTCI at 1 km, which did not change much in comparison with that of SMAP VTCI at 9 km; the  $R^2$  for 1 km scaled SMAP VTCI was on average 0.05 less than that of 9 km SMAP VTCI. Conversely, the  $R^2$  of SMOS VTCI at 1 km was observed to be roughly the same as that of SMOS VTCI at 9 km; similar results were obtained for the SMOS PassiveD from which SMOS VTCI originated. Except for SMOS VTCI at 1 km, which slightly underestimated the OzNet soil moisture by  $-0.004 \text{ m}^3 \text{ m}^{-3}$  on average, the remaining products overestimated by between 0.012 and  $0.046 \text{ m}^3 \text{ m}^{-3}$  on average. With the exception of SMAP VTCI, no improvement of statistical parameters was observed for the 1 km downscaled soil moisture products over the original coarse passive SMAP and SMOS soil moisture measurements. However, the accuracy of DisPATChD and SMOS VTCI were shown to be close to that of SMOS PassiveD.

An unequal number of soil moisture values were analysed for the different products included in the temporal analysis against the OzNet stations, due to the availability of product retrievals. This may raise a concern about the impact of the unequal number of data used in the estimation of statistical metrics, and thus the findings from the analysis. Consequently, the temporal analysis was also conducted for a consistent number of data by using only observations on the same dates (eight days only). This included comparison of SMAP EnhancedD, SMAP SFIM, SMAP PassiveD, SMOS PassiveD, SMAP VTCI and SMOS VTCI against the OzNet measurements. Findings from this analysis were consistent with the earlier results. However, the statistical metrics of the eight days only scenario were deteriorated compared to those summarized in Figure 4.6. Still, the SMAP VTCI at both 1 and 9 km were found to have the best performance. For the comparisons conducted at 1 km, the SMAP PassiveD followed closely the SMAP VTCI. Results obtained from the analysis of products at 9 km revealed that the performance of SMAP VTCI was followed by that of the SMAP EnhancedD and SMAP PassiveD.

As suggested by Merlin et al. (2015), the slope of linear regression between the downscaled soil moisture products and the OzNet *in situ* measurements was also considered as an evaluation metric for assessment of products at 1 and 9 km. The mean slope values of products at 1 km varied between 1 and 1.3, showing no difference in the performance of products. Similar to slope analysis for products at 1 km, there was no significant difference between the mean slope values for products at 9 km; with the range of mean slope being between 0.9 and 1.4. A slope larger than 1 could be attributed to the difference between the sensing depth of the downscaled soil moisture products (varying between 0 and 5 cm) and that of *in situ* measurements being 0-5 cm.

In the case of temporal analysis of the downscaled soil moisture products at 9 km against the OzNet (Figure 4.10), SMAP EnhancedA and EnhancedD products were generally superior to the other downscaled soil moisture products. Both reached the highest temporal correlation with the OzNet and had the lowest bias. SMAP VTCI at 1 km resolution also showed superiority to the remaining downscaled soil moisture products at 1 km.

#### **4.3.2 Temporal analysis against airborne PLMR soil moisture**

The temporal analysis of products was also carried out against the entire airborne PLMR soil moisture maps captured over the SMAPEX-4 and -5 airborne field campaigns. A summary of product accuracy statistics at 1 and 9 km resolution are presented as boxplots in Figures 4.7 and 4.8, respectively. When the same number of the downscaled and non-downscaled soil moisture maps at 1 km (Figure 4.7-a) were evaluated, descending SMAP and SMOS coarse passive products showed superiority in terms of accuracy when contrasted with the downscaled soil moisture products, having a mean  $R^2 \geq 0.6$  and mean RMSD of  $\sim 0.09 \text{ m}^3 \text{ m}^{-3}$ . The SMOS DisPATCHD maintained a similar accuracy to that of SMOS PassiveD, and performed the best among the downscaled soil moisture products. Generally, all products underestimated the airborne PLMR soil moisture; with the underestimation being greater in the SMAP PassiveA and SMOS DisPATCHA.

For the comparison against the SMAPEX-4 and -5 airborne field campaigns (Figure 4.7-c), SMOS VTCI at 1 km performed the best with  $R^2$  of 0.76, RMSD of  $0.084 \text{ m}^3 \text{ m}^{-3}$  and

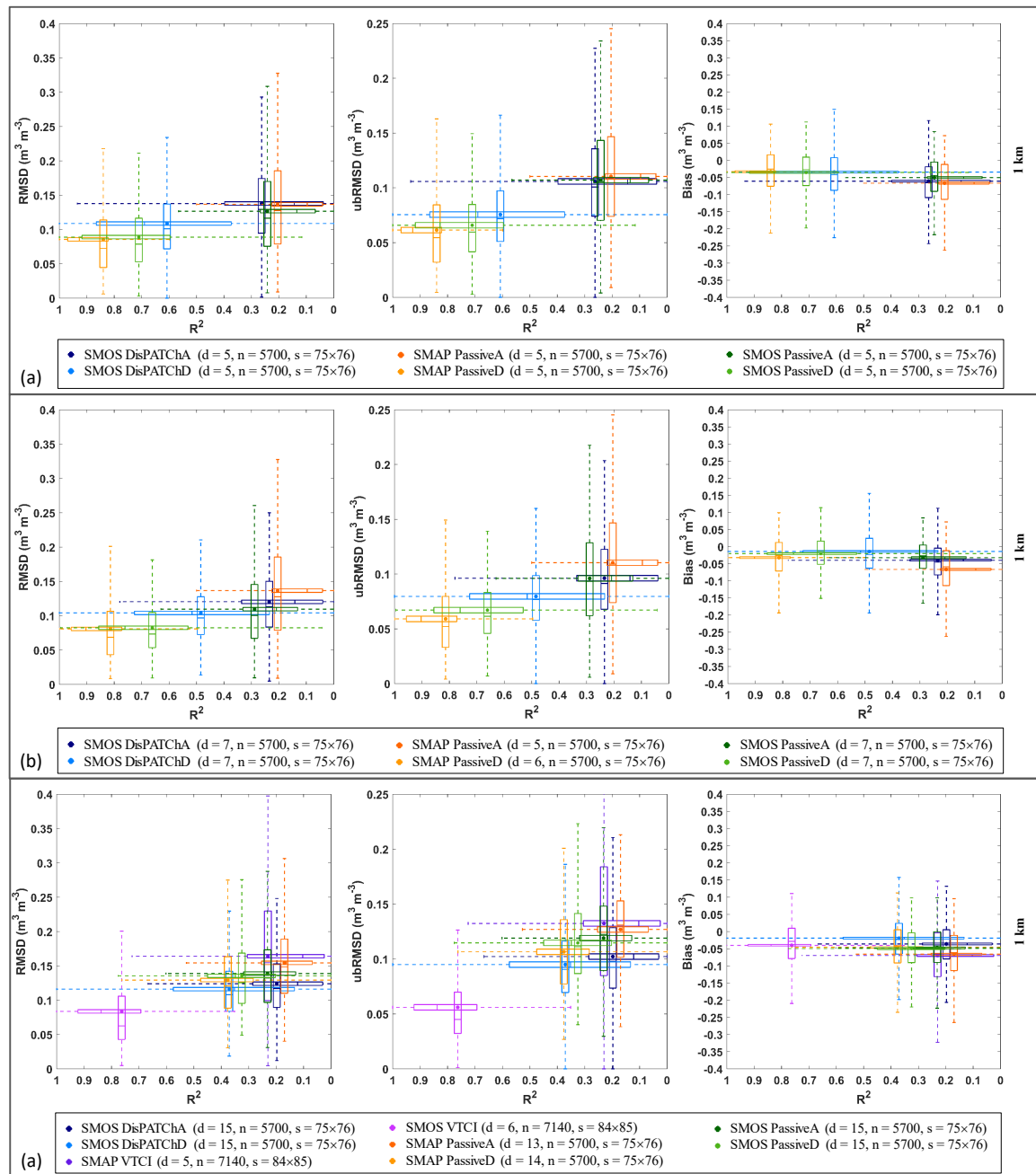


Figure 4.7: As for Figure 4.6 but for the comparison against airborne PLMR soil moisture at 1 km in which analysis was carried out for all the pixels covering the study area. These results are from different scenarios including: a) the equal number of downscaled soil moisture products captured during the SMAPEX-4, b) all available products during the SMAPEX-4, and c) products captured over the entire SMAPEX-4 and -5 airborne field campaigns' period. Here s stands for the dimension of analysis area arranged in row × column. Note: the performance analysis of the VTCI-based products was not possible for the SMAPEX-4 period as only one SMOS VTCI and two SMAP VTCI soil moisture maps were available.

ubRMSD of  $0.056 \text{ m}^3 \text{ m}^{-3}$ , which were better statistical metrics than for the other products. This was followed by the SMOS DisPATChD and SMAP PassiveD products which performed similarly; with a mean  $R^2$  close to 0.4, mean RMSD of about  $0.12 \text{ m}^3 \text{ m}^{-3}$  and mean bias between 0 and  $-0.05 \text{ m}^3 \text{ m}^{-3}$ . It is to be noted that the maximum  $R^2$  for both SMOS VTCI and DisPATChD was equal to 1, while other products could not reach this high level of temporal agreement with airborne PLMR soil moisture. The slope of the linear regression defined between the downscaled soil moisture products and PLMR soil moisture maps showed dependency to  $R^2$ . As anticipated, the slope values were small (close to zero) for products that had low  $R^2$ . The slope was mainly explained by the correlation, knowing that slope equals to  $(\text{correlation}) \times (\text{standard deviation of the downscaled soil moisture products} / \text{standard deviation of reference data})$ . Therefore, the standard deviation of the downscaled soil moisture products was rather similar across all products. Comparison of SMOS VTCI and SMOS DisPATCh as optical-based products has also been conducted for the SMAPEX-4 and -5 airborne field campaigns, by choosing the same dates. Based on this comparison, the performance of DisPATCh and VTCI was quite comparable.

In order to assess the seasonal impact on the performance of products at 1 km, the temporal analysis of products was also carried out for the SMAPEX-5 airborne field campaign conducted in the austral spring. During the SMAPEX-5 with wet soils, the products again underestimated the airborne PLMR soil moisture, being even more severe than for the SMAPEX-4. The performance of SMOS DisPATChD, SMAP EnhancedD, SMAP EnhancedA and SMAP PassiveD during the SMAPEX-5 showed a minor difference over their performance during the SMAPEX-4 in terms of  $R^2$  and ubRMSD. With the exception of SMOS PassiveD, whereby  $R^2$  decreased marginally from 0.66 (SMAPEX-4) to 0.57 (SMAPEX-5), the  $R^2$  of remaining products during the SMAPEX-5 increased by more than 0.5 compared to that of the SMAPEX-4. The SMAP PassiveA products experienced the largest increase (0.68) in terms of  $R^2$  and had the lowest agreement with the SMAPEX-4 PLMR soil moisture. Results from the comparison of SMOS VTCI and SMOS DisPATCh on the same dates during the SMAPEX-5 airborne field campaign revealed a similarity of DisPATCh and VTCI in terms of performance.

For the comparison against the SMAPEX-5 airborne field campaign data, with the exception

of SMOS PassiveD and DisPATChD with  $R^2$  less than 0.6, the remaining products were found to have an  $R^2$  greater than 0.75. The SMOS DisPATChA had a reasonable performance with an  $R^2$  of 0.77, a lower bias ( $-0.033 \text{ m}^3 \text{ m}^{-3}$ ) and a lower ubRMSD ( $0.044 \text{ m}^3 \text{ m}^{-3}$ ) than other products. This is unlike the SMOS VTCl, SMAP VTCl, SMAP PassiveA, SMAP PassiveD, and SMOS PassiveA, which with  $R^2 \geq 0.85$  could not meet the accuracy requirements in terms of bias and RMSD. For instance, the SMOS VTCl had the largest bias equal to  $-0.115 \text{ m}^3 \text{ m}^{-3}$  on average and the largest RMSD equal to  $0.143 \text{ m}^3 \text{ m}^{-3}$  on average.

At 9 km resolution for the scenario in which the same number of soil moisture maps were evaluated (Figure 4.8-a), the SMAP EnhancedA and EnhancedD products with average  $R^2$  of 0.92 and 0.94, respectively, surpassed the other downscaled soil moisture products in capturing the temporal evolution of airborne soil moisture estimates, followed by SMAP PassiveD, SFIM and MOEA. The SMOS PassiveD and SMAP A/P products also showed a good performance with  $R^2$  of 0.75 for the first and 0.73 for the later. The SMAP PassiveD without being downscaled was amongst the best results and yielded an  $R^2$  of 0.89 and ubRMSD of  $0.054 \text{ m}^3 \text{ m}^{-3}$ . Nevertheless, the SMAP EnhancedA was found to have the best agreement with airborne PLMR soil moisture. The SMAP EnhancedA not only had a high coefficient of determination but also low RMSD and/or ubRMSD. The DisPATChA at 9 km- retrieved from an optical-based downscaling technique - had the lowest agreement with airborne PLMR soil moisture. This is unlike the DisPATChD which was shown to have a moderate performance with  $R^2$  of 0.75. The DisPATChD yielded on average similar performance to the SMOS PassiveD. While it did not improve nor maintain the accuracy of SMOS PassiveD in terms of RMSD and ubRMSD, it deteriorated the  $R^2$  and bias relative to SMOS PassiveD. Nevertheless, the  $R^2$  of SMOS PassiveD was not significantly above that of DisPATChD. These findings are in agreement with those obtained from evaluation of all available soil moisture products during the SMAPEX-4 (Figure 4.8-b).

For the comparison against the SMAPEX-4 and -5 airborne field campaigns (Figure 4.8-c), SMOS VTCl at 9 km performed the best with a mean  $R^2$  of 0.91, mean bias of  $-0.04 \text{ m}^3 \text{ m}^{-3}$ , mean RMSD of  $0.061 \text{ m}^3 \text{ m}^{-3}$ , and mean ubRMSD of  $0.039 \text{ m}^3 \text{ m}^{-3}$  followed by SMAP MOEA and A/P, which were only available for the SMAPEX-4 period. The remaining products, with the exception of the SMAP VTCl, SMOS DisPATChA and SMAP PassiveA, had

similar performance with mean  $R^2$  between 0.2 and 0.5 and varying RMSD between 0.1 and  $0.13 \text{ m}^3 \text{ m}^{-3}$ .

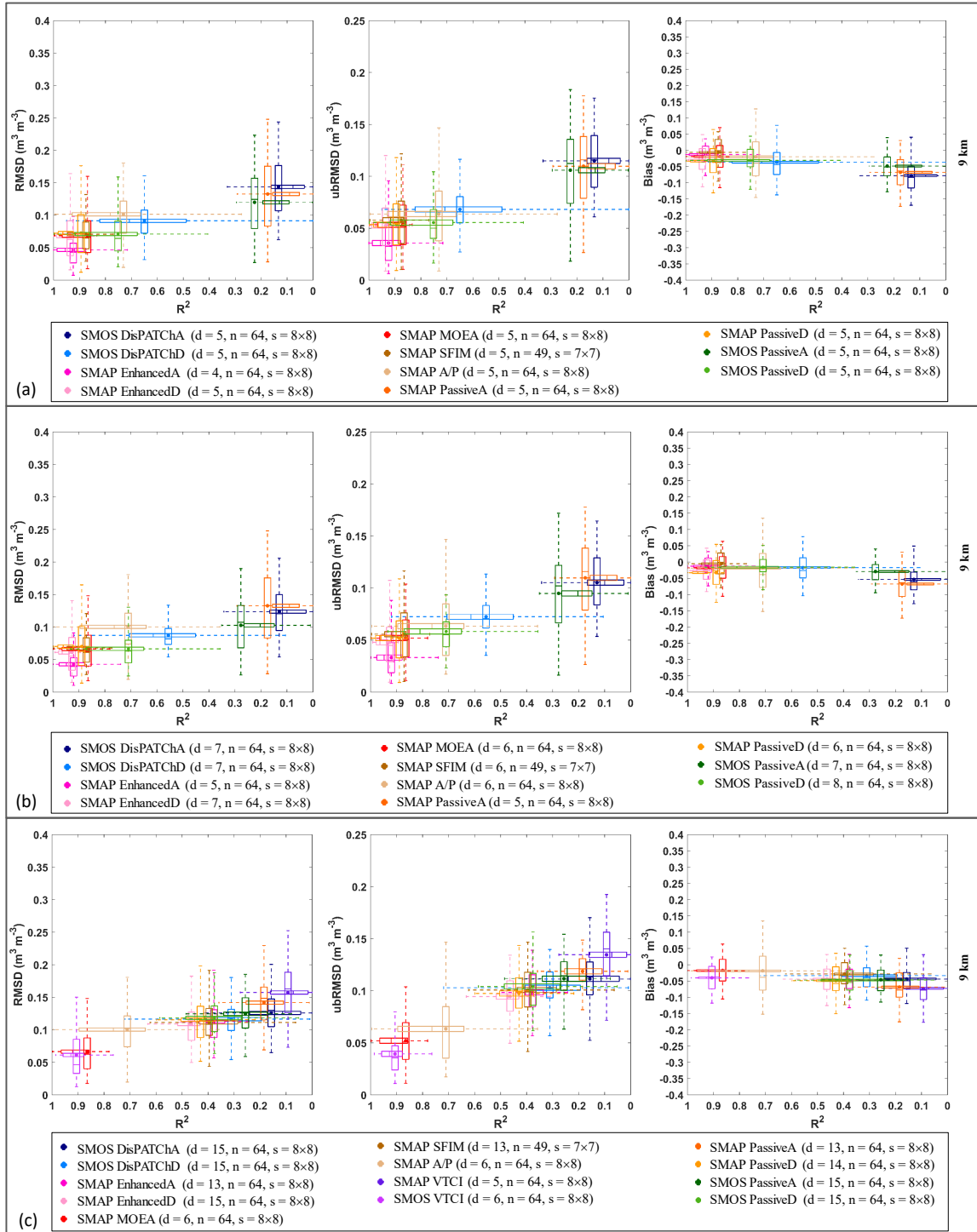


Figure 4.8: As for Figure 4.7 but for the comparison against airborne PLMR soil moisture at 9 km.

The seasonal performance assessment was also carried out for the products at 9 km. Based on this comparison, with the exception of SMOS PassiveD, SMOS DisPATChA and DisPATChD, the remaining products were superior with an  $R^2 \geq 0.9$ . This is not in line with the findings from the SMAPEX-4 in which SMOS PassiveA, SMOS DisPATChA and SMAP PassiveA had an  $R^2$  less than 0.3. Generally, the variation of RMSD, ubRMSD, and bias obtained from evaluation of 9 km products during the SMAPEX-5 was found to be smaller than that of products at 1 km. Still, the average of obtained statistical metrics for 9 km products was quite similar to that of products at 1 km.

Generally, a comparison of the temporal performance of DisPATCh products against airborne PLMR soil moisture showed that the accuracy of DisPATCh products was noticeably affected by that of the SMOS Passive products. While DisPATCh products were not superior to SMOS Passive products in terms of  $R^2$ , the DisPATCh products were shown to mimic the SMOS Passive  $R^2$ . For example, the SMOS PassiveA and SMOS PassiveD at 9 km had an average  $R^2$  of 0.9 and 0.63, respectively, during the SMAPEX-5, with DisPATChA and DisPATChD showing an average  $R^2$  of 0.8 and 0.5 for the former and latter. Results herein have also shown that DisPATCh products had a higher RMSD/ubRMSD than SMOS Passive products during the SMAPEX-4, which is opposite to the results obtained for the SMAPEX-5 period. During the SMAPEX-5 the RMSD of DisPATCh products were slightly lower than those of the SMOS Passive products.

Analysis of the downscaled soil moisture products against airborne PLMR soil moisture maps revealed the superiority of the oversampling-based technique in terms of delivering more frequent and accurate downscaled soil moisture products than the radar-, optical-and radiometer-based techniques. The SMAP Enhanced products not only had better performance and availability, but also showed improvement over coarse SMAP radiometer-only soil moisture products in terms of accuracy and spatial scale.

### **4.3.3 Spatial analysis against the airborne PLMR soil moisture**

Spatial analysis of soil moisture products was carried out against airborne PLMR soil moisture maps covering the entire study area during the SMAPEX-4 and -5 airborne field cam-

paigns. This spatial analysis involved evaluation of the daily maps of soil moisture estimates against the corresponding airborne PLMR maps in the same scenarios as in the temporal analysis. A summary of the spatial accuracy statistics of products at 1 and 9 km are presented as boxplots in Figures 4.9 and 4.10, respectively.

When the downscaled soil moisture maps at 1 km were evaluated (Figure 4.9), they showed low spatial correlation, denoted by  $R^2$ , with airborne PLMR maps. Such a low spatial correlation was followed by low linear regression slope. In the spatial analysis, the spatial correlation was very low for all products, with the slope mainly determined by the standard deviation of the downscaled soil moisture products in space. Furthermore, they underestimated the variability of the PLMR soil moisture with the range of average bias between  $-0.016$  and  $-0.075 \text{ m}^3 \text{ m}^{-3}$ . For the scenarios including: i) evaluation of the same number of products (Figure 4.9-a) and ii) evaluation of products during the SMAPEX-4 (Figure 4.9-b), the products had a mean  $R^2$  of less than 0.2 and the range of mean RMSD between  $0.083$  and  $0.146 \text{ m}^3 \text{ m}^{-3}$ . These results in general are not much different from those of comparisons against the SMAPEX-4 and -5 airborne field campaigns (Figure 4.9-c). However, results in Figure 4.9-c showed closer resemblance in the performance of products compared to Figure 4.9-a and b.

In the case of spatial pattern analysis of products at 9 km (Figure 4.10), generally, SMAP EnhancedA and EnhancedD products were superior to other products. Both reached the highest spatial correlation with airborne PLMR soil moisture and had the lowest bias. Nevertheless, the SMAP Enhanced products had mean  $R^2$  less than 0.5 and mean bias larger than  $0.04 \text{ m}^3 \text{ m}^{-3}$ . In addition, the slope of linear regression between SMAP Enhanced products and PLMR soil moisture was close to 0.1. The slope was mainly determined by the standard deviation of the downscaled soil moisture products in space, which is expected to be lower for coarser/lower resolutions. The SMAP A/P showed the highest variability in terms of slope range, and SMAP EnhancedA was one of the products with the lowest variability. Apart from the Enhanced products, the SFIM performance was shown to be one of the best during the short SMAPEX-4 period. When compared against the airborne PLMR at 9 km, the products were seen to have a slightly better spatial correlation than when compared against the airborne PLMR at 1 km. Such a difference in the performance of products could

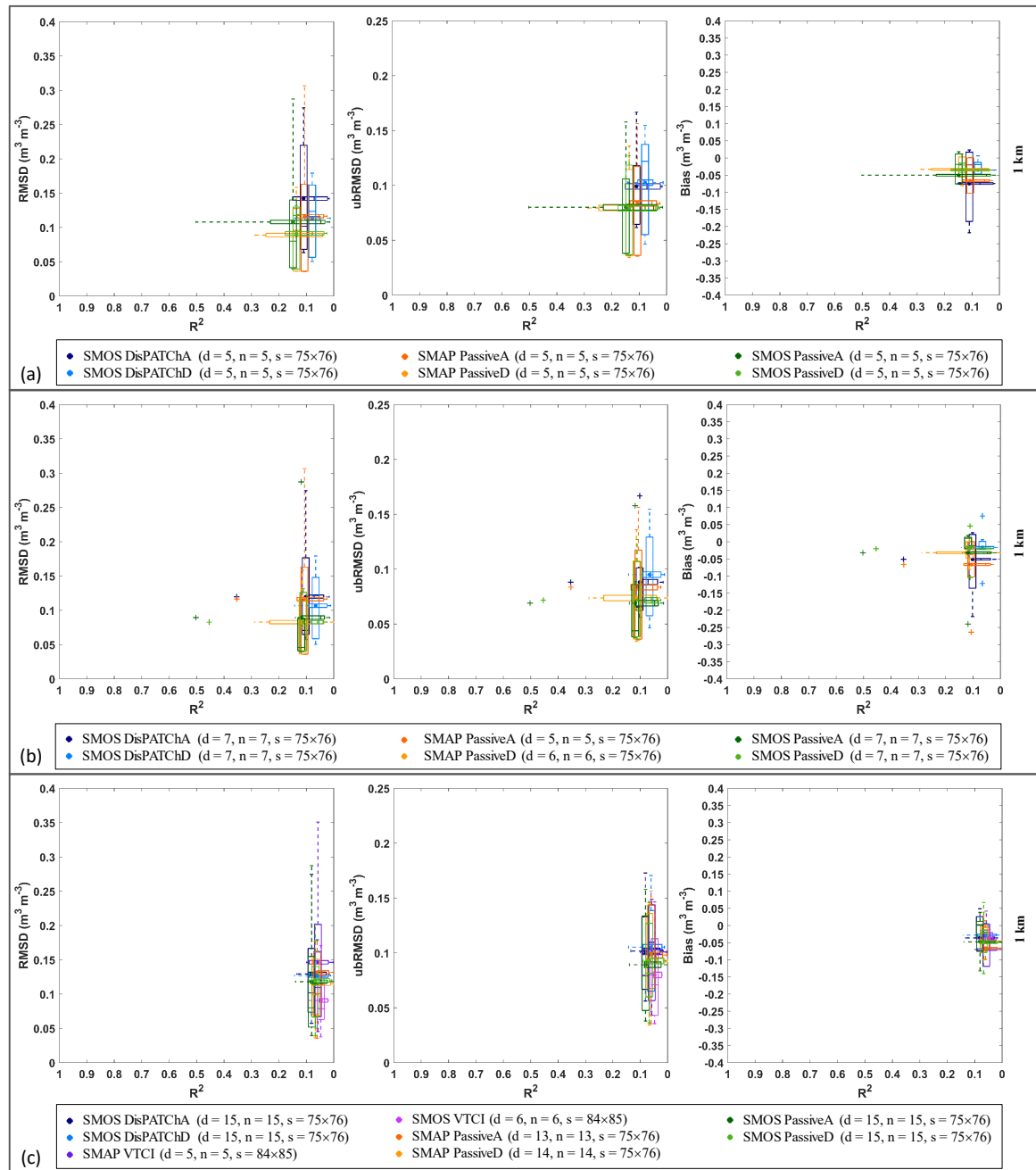


Figure 4.9: Summary of results obtained from spatial analysis of soil moisture products at 1 km against airborne PLMR soil moisture in which analysis was carried out for all the pixels covering the study area. These results are from different scenarios including: a) the equal number of the downscaled soil moisture products captured during the SMAPEx-4, b) all available products during the SMAPEx-4, and c) products captured over the entire SMAPEx-4 and -5 airborne field campaigns' period.

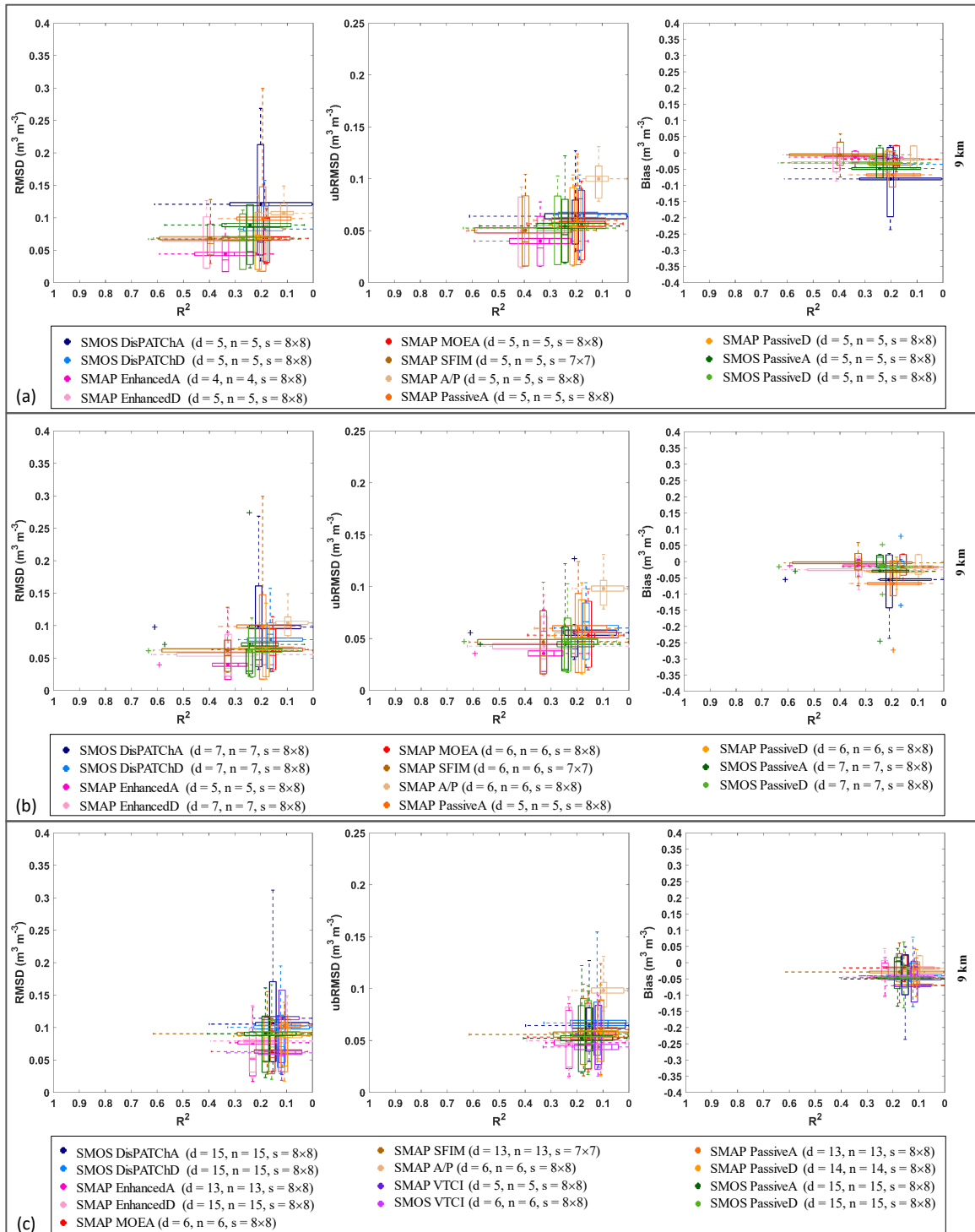


Figure 4.10: As for Figure 4.9 but for the spatial analysis at 9 km.

be associated with aggregation of more airborne soil moisture measurements for each pixel footprint at 9 km than those for each pixel footprint at 1 km, which may make comparison of products seemingly more reliable for 9 km products.

Comparison of the performance of products at 1 km during the SMAPE<sub>x</sub>-5 (austral spring) against that of products during the SMAPE<sub>x</sub>-4 (austral autumn) showed that there was no noticeable seasonal impact on the spatial performance of products. None of the products at 1 km could capture the spatial pattern of PLMR soil moisture with high correlation and low RMSD. Agreeing with findings from the evaluation of products during the SMAPE<sub>x</sub>-4 period, the mean  $R^2$  of products was generally less than 0.1 and mean RMSD was higher than  $0.09 \text{ m}^3 \text{ m}^{-3}$  for the SMAPE<sub>x</sub>-5. Regardless of season, there was an underestimation of PLMR soil moisture by products with a more noticeable error in the SMAPE<sub>x</sub>-5 period.

In contrast to the seasonal performance of products at 1 km, the seasonal impact on the spatial performance of products at 9 km was noticeable. Products at 9 km showed slightly better performance during the SMAPE<sub>x</sub>-4 than during the SMAPE<sub>x</sub>-5 when soils were wet. Comparison of the correlation of products with PLMR soil moisture during the SMAPE<sub>x</sub>-5 with that of products during the SMAPE<sub>x</sub>-4 showed a reduction of  $R^2$  for the SMAPE<sub>x</sub>-5, which was more pronounced for the SMAP SFIM. The SMAP SFIM was among products with the best performance during the SMAPE<sub>x</sub>-4, but among those with the poorest performance during the SMAPE<sub>x</sub>-5. The SMAP SFIM experienced a decrease in  $R^2$  from 0.33 in the SMAPE<sub>x</sub>-4 to 0.14 in the SMAPE<sub>x</sub>-5 and increase of RMSD from 0.062 to  $0.093 \text{ m}^3 \text{ m}^{-3}$ . Although the performance of SMAP EnhancedA was slightly poorer during the SMAPE<sub>x</sub>-5 than the SMAPE<sub>x</sub>-4, it still ranked the best with  $R^2$  of 0.18, RMSD of  $0.089 \text{ m}^3 \text{ m}^{-3}$  and ubRMSD of  $0.055 \text{ m}^3 \text{ m}^{-3}$ .

Based on results, none of the downscaled products could capture the spatial variability of PLMR soil moisture maps. Products at both 1 km and 9 km showed low spatial correlation, denoted by  $R^2$  values less than 0.5, with airborne PLMR maps. However, products at 1 km had lower spatial correlation than products at 9 km, with  $R^2$  values of  $\sim 0.1$ . While none of these methods met the accuracy expectations, the slightly better results at 9 km are expected to be an artifact of undertaking the evaluation at larger spatial scales where the high spatial

variability is smoothed by the averaging process.

#### 4.4 Discussion

This chapter has rigorously assessed the performance of a variety of available downscaled soil moisture products at resolutions between 1 and 10 km, to find approach(es) that is(are) applicable for multi-sensor soil moisture retrieval from the SMAP and SMOS. This assessment involved consistent inter-comparison of the downscaled soil moisture products, including radar-, optical-, radiometer- and oversampling-based retrievals against *in situ* and airborne reference data for a typical Australian landscape and climate. The performance of the original coarse radiometer-only products including SMAP and SMOS was analyzed to understand the extent of improvement of the downscaled soil moisture products over the coarse scale products in terms of accuracy and capability of capturing the spatio-temporal variability of soil moisture. A summary of accuracy statistics of the downscaled and non-downscaled soil moisture products at 9 km, evaluated against the airborne PLMR soil moisture during the SMAPEX-4 and -5 and OzNet *in situ* soil moisture measurements is provided in Table 4.1.

Based on the results, the downscaled soil moisture products showed a range of performance against different reference data sets and under differing spatial scale, weather and climate condition. This variation of performance between the downscaled soil moisture products could be influenced by the nature of utilized ancillary data for downscaling purpose. For example, in Figure 4.3 and 4.4 the optical-based products could not retrieve consistent time series of soil moisture maps under cloudy skies as optical observations are not captured under cloud coverage. This shortcoming reduces the functionality of optical-based techniques while the high temporal and spatial resolution of optical observations make them a promising ancillary data for soil moisture downscaling. Studies such as Zhao and Li (2013a), Peng et al. (2015), Piles et al. (2016), and Sabaghy et al. (2018) have suggested the use of geostationary based optical observations, instead of the optical imagery captured by polar orbiting counterparts, to overcome this issue. The geostationary sensors provide more frequent acquisitions and thus an opportunity for more cloud free observations.

Table 4.1: Averaged accuracy of the downscaled and non-downscaled soil moisture products at 9 km, evaluated against the airborne PLMR soil moisture and the OzNet *in situ* soil moisture measurements. Notes: i) the evaluation of SMAP MOEA and A/P was only carried out during the short SMAPEX-4 period due to radar availability, and ii) gray cells indicate the accuracy of products with superior performance to the other downscaled soil moisture products.

Downscaling Technique	Downscaled Product	Temporal analysis against airborne PLMR during SMAPEX-4 and -5					Spatial analysis against airborne PLMR during SMAPEX-4 and -5					Temporal analysis against OzNet				
		Bias ( $m^3 m^{-3}$ )	R <sup>2</sup>	RMSD ( $m^3 m^{-3}$ )	ubRMSD ( $m^3 m^{-3}$ )	ubRMSE ( $m^3 m^{-3}$ )	Bias ( $m^3 m^{-3}$ )	R <sup>2</sup>	RMSD ( $m^3 m^{-3}$ )	ubRMSD ( $m^3 m^{-3}$ )	ubRMSE ( $m^3 m^{-3}$ )	Bias ( $m^3 m^{-3}$ )	R <sup>2</sup>	RMSD ( $m^3 m^{-3}$ )	ubRMSD ( $m^3 m^{-3}$ )	ubRMSE ( $m^3 m^{-3}$ )
Radar-based	SMAP MOEA	-0.018	0.86	0.066	0.052	-0.016	0.16	0.063	0.053	0.084	0.055	0.66	0.084	0.063	0.063	
	SMAP A/P	-0.019	0.71	0.100	0.063	-0.018	0.10	0.104	0.098	0.108	0.057	0.65	0.108	0.090	0.090	
Optical-based	SMOS DisPATCHa	-0.044	0.16	0.126	0.111	-0.050	0.15	0.105	0.064	0.072	0.002	0.71	0.072	0.064	0.064	
	SMOS DisPATCHd	-0.034	0.31	0.116	0.103	-0.040	0.12	0.100	0.067	-0.005	0.60	0.090	0.090	0.085		
	SMAP VTCI	-0.073	0.09	0.157	0.135	-0.071	0.12	0.114	0.056	-0.011	0.90	0.044	0.033	0.033		
	SMOS VTCI	-0.040	0.91	0.061	0.039	-0.040	0.12	0.061	0.044	-0.029	0.60	0.085	0.079	0.079		
Radiometer-based	SMAP SFIM	-0.028	0.40	0.111	0.101	-0.029	0.17	0.090	0.056	0.046	0.69	0.074	0.055	0.055		
Oversampling-based	SMAP EnhancedA	-0.047	0.38	0.113	0.098	-0.047	0.23	0.077	0.048	0.012	0.85	0.060	0.057	0.057		
	SMAP EnhancedD	-0.044	0.46	0.109	0.094	-0.043	0.23	0.079	0.050	0.024	0.81	0.061	0.055	0.055		
	SMAP PassiveA	-0.069	0.19	0.142	0.119	-0.069	0.11	0.102	0.061	0.018	0.84	0.059	0.056	0.056		
N/A	SMAP PassiveD	-0.049	0.43	0.116	0.097	-0.048	0.11	0.087	0.057	0.034	0.77	0.065	0.055	0.055		
	SMOS PassiveA	-0.046	0.26	0.125	0.112	-0.046	0.18	0.090	0.052	0.017	0.79	0.054	0.051	0.051		
	SMOS PassiveD	-0.047	0.38	0.118	0.104	-0.047	0.16	0.091	0.056	0.020	0.63	0.090	0.088	0.088		

Unlike optical-based products, radar-, radiometer-, and oversampling-based downscaled soil moisture maps were available regardless of meteorological conditions. Oversampling-based products retrieved from optimal interpolation theory, which provides the closest observation to what could be measured by the radiometric instrument at the interpolation point, has the added advantage of not needing concurrent data from other sensors. This factor prevents data loss due to unavailability of required ancillary data for disaggregation.

The oversampling-based soil moisture products (SMAP EnhancedA and SMAP EnhancedD) best captured the temporal and spatial variability of soil moisture overall, though the SMAP MOEA and A/P had the better temporal agreement with PLMR during the short SMAPE<sub>x-4</sub> period. This superiority may lie in the characteristic of the L-band radiometer and radar data used for their soil moisture disaggregation. Especially, the oversampling-based soil moisture products with their disaggregation procedure based on the use of SMAP L-band radiometer imagery that are less affected by vegetation cover, surface roughness and meteorology condition.

The summary of accuracy statistics, in the review of temporal analysis of different downscaling techniques displayed in Figure 8 of Sabaghy et al. (2018), indicated that the radar-based technique was expected to deliver more accurate downscaled soil moisture products than optical-based techniques, with radar having been previously shown to have a greater sensitivity to soil moisture dynamics than optical observation and with a direct relation to soil moisture dynamics. Nevertheless, in this study the temporal analysis of products against the OzNet ground based soil moisture measurements revealed that optical-based products (SMAP VTCI at 9 km) performed the best, followed by the oversampling-based product (SMAP EnhancedD). The radiometer-based products which had the poorest performance in the review by Sabaghy et al. (2018), herein showed reasonable performance, being slightly higher than that of radar-based products (SMAP A/P and MOEA). Moreover, the temporal analysis of products against the airborne PLMR soil moisture during the SMAPE<sub>x-4</sub> and -5 revealed that SMOS VTCI at 9 km performed the best, followed by the radar-based products (SMAP A/P and MOEA). Differences observed between the temporal analysis of products against *in situ* and airborne soil moisture references suggest that relying only on *in situ* measurement is not appropriate for validation of soil moisture maps; basically *in situ*

measurements are not necessarily a great indicator of soil moisture variation in space. Furthermore, *in situ* measurements are not consistent and have station-to-station bias variations (Colliander et al., 2017).

Based on the temporal analysis of seasonal performance, the performance of SMOS PassiveA and DisPATChA products were noticeably affected by the season. The 9 km SMOS PassiveA and DisPATChA had mean  $R^2 < 0.3$  during the SMAPEX-4 and mean  $R^2 \geq 0.8$  during the SMAPEX-5, while the average RMSD/ubRMSD and bias of these products was approximately the same for both airborne field campaigns. Merlin et al. (2012) previously reported a similar impact of seasonal variations on the accuracy of DisPATCh products in capturing the spatial dynamic of soil moisture but with better temporal correlation of DisPATCh products against reference soil moisture for summer (semi-arid climate) than winter (temperate climate). The downscaled DisPATCh products were derived using the evaporative efficiency as the main downscaling factor, which has a higher level of coupling with surface soil moisture for the semi-arid rather than temperate climate (e.g. Colliander et al., 2017; Merlin et al., 2012); with evaporation being the primary control on soil wetness in semi-arid conditions. Results herein have shown that the  $R^2$  of DisPATChD during semi-arid (SMAPEX-4, austral spring) and temperate climate (SMAPEX-5, austral autumn) remained the same. Conversely, results from the analysis of DisPATChA products agree with the results of Merlin et al. (2012), being that the  $R^2$  of DisPATChA for the semi-arid climate was significantly higher than that of DisPATChA for the temperate climate. In order to avoid such a reduction of DisPATCh performance for wet soil conditions, Djamai et al. (2015) have recommended the use of a non-linear relationship between soil moisture and soil evaporative efficiency instead of the linear one used herein.

Results also showed that the seasonal performance of DisPATCh products was similar to that of passive soil moisture estimates from which the DisPATCh products originated. These findings suggest that the performance of DisPATCh is heavily influenced by the performance of the original passive soil moisture estimates. Therefore, the uncertainty of the original passive soil moisture products is dictating the accuracy of DisPATCh. These findings are not consistent with findings from Merlin et al. (2012) and Colliander et al. (2017), that proposed the coupling between soil moisture and evaporative efficiency as the main factor controlling

the accuracy of DisPATCh products. Improvement of the accuracy of passive coarse soil moisture products is therefore another requirement for improvement of DisPATCh products.

Based on the spatial analysis of seasonal performance, products at 1 km had similar performance for the SMAPE<sub>x</sub>-4 and SMAPE<sub>x</sub>-5 regardless of season. These results are contrasted against those obtained from spatial analysis of products at 9 km. In general, products at 9 km had slightly better performance during the SMAPE<sub>x</sub>-4 than the SMAPE<sub>x</sub>-5. The stark contrast of the performance of the downscaled soil moisture products during the SMAPE<sub>x</sub>-4 and SMAPE<sub>x</sub>-5, was specifically introduced for SMAP SFIM products. Reduced sensitivity of high frequency radiometer observations to soil moisture dynamics under increased vegetation cover and rainfall events during the SMAPE<sub>x</sub>-5 could be the key factor in accuracy reduction of SMAP SFIM in temperate climate.

#### **4.5 Chapter summary**

The objective of this study was to evaluate the radar-, optical-, radiometer- and oversampling-based downscaled soil moisture retrievals against the consistent SMAPE<sub>x</sub>-4 and -5 airborne field campaigns data and the OzNet *in situ* measurements. The evaluation included: i) temporal analysis against both the OzNet and airborne PLMR soil moisture, and ii) spatial analysis against the airborne PLMR soil moisture. The results showed that the oversampling-based soil moisture products (SMAP EnhancedA and SMAP EnhancedD) had the best agreement with reference soil moisture measurements. Oversampling-based products were also shown to have better performance, in terms of accuracy, than radiometer-only soil moisture retrievals. The radar-based downscaled soil moisture products (SMAP A/P and MOEA) captured the temporal change of the PLMR soil moisture better than the remaining downscaled soil moisture products during the SMAPE<sub>x</sub>-4.

## Chapter 5

### Combined downscaled soil moisture products

The previous chapter has undertaken an inter-comparison of a variety of downscaled soil moisture products against a comprehensive evaluation data set. Consequently, this chapter examines the performance of various combined downscaled soil moisture products. The technique used for the merging is a Gaussian algorithm, which takes the uncertainty of each downscaled soil moisture product into account when producing the spatio-temporal dynamics of soil moisture. Combined products were produced across different combination scenarios at 1 and 9 km spatial resolution, and compared against the same SMAPE<sub>x</sub> airborne soil moisture maps from PLMR and OzNet *in situ* soil moisture measurements that were presented in Chapter 3 and used in Chapter 4.

#### 5.1 Introduction

The current downscaled soil moisture products come with a range of accuracy, spatial resolutions and temporal repeats affected by the downscaling technique and ancillary data used for disaggregation (Chapter 2 and Chapter 4). Moreover, no single downscaled soil moisture alone could meet the application requirements in terms of accuracy and time interval. Therefore, providing accurate and frequent high resolution soil moisture products remains a challenge. Chapter 2 suggested that a merged ensemble of various downscaled soil moisture products, based on their strengths, may offer the opportunity to generate a soil moisture product that meets both the temporal and accuracy requirements.

The ESA CCI program used a Gaussian merging scheme, which combined various active

and passive microwave soil moisture products (e.g. Dorigo et al., 2012a,b, 2017; Liu et al., 2011, 2012) to produce a single long-term soil moisture data set. The approach taken by the ESA CCI was reported by Liu et al. (2012) to: i) preserve the temporal dynamic of the original soil moisture retrievals, and ii) improve the time interval of soil moisture maps. It is proposed here that the same merging algorithm used by the CCI could be applied in a similar way to combine downscaled soil moisture products. This technique, also known as the inverse variance weighted averaging approach, takes the statistical uncertainties in downscaled soil moisture contents into the soil moisture retrieval procedure. The expectation is to produce a soil moisture map with better temporal coverage over the study area, and having better agreement with reference data, than any individual downscaled soil moisture product alone.

This chapter merges the range of downscaled soil moisture products evaluated in Chapter 4, for the sake of performance assessment of the combined downscaled soil moisture product. A variety of combined soil moisture estimates were evaluated against the reference data set of Chapter 3, including the SMAPEX airborne PLMR soil moisture maps and OzNet *in situ* soil moisture measurements. This assessment was intended to evaluate the potential for a combined downscaled soil moisture product. This combination study is the first of its kind, offering a cutting-edge merged downscaled soil moisture product for better representation of soil moisture spatio-temporal variation. The accuracy of the combined product was also contrasted against the original and radiometer-only retrievals of SMAP and SMOS.

### **5.2 Combining methodology**

The merging procedure used in this chapter is summarised in Figure 5.1. Here the combined product was developed from merging the radar-, optical-, radiometer-, and oversampling-based downscaled soil moisture products. The combined products were evaluated against the reference data set to understand whether combining a variety of downscaled soil moisture products could provide better spatio-temporal representation of soil moisture at 1 and 9 km than the individual downscaled soil moisture products alone.

The combination procedure was applied to: i) SMOS DisPATCHD at 1 km as an optical-

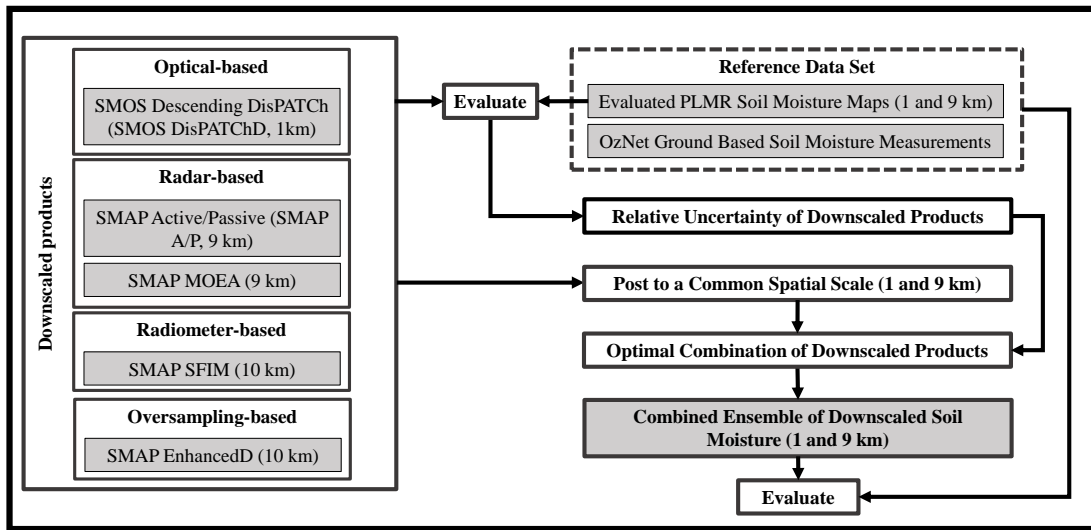


Figure 5.1: Schematic diagram showing the combination procedure.

based downscaled soil moisture, ii) the SMAP A/P and SMAP MOEA at 9 km as radar-based downscaled soil moisture product, iii) the SMAP SFIM at 10 km as a radiometer-based downscaled soil moisture products, and iv) the SMAP EnhancedD at 9 km as an oversampling-based downscaled soil moisture product. Available downscaled soil moisture products used for the combination are listed in Table 5.1.

Table 5.1: Availability of downscaled soil moisture products used for combination.

PLMR flight date	Products				
	SMOS DisPATChD	SMAP EnhancedD	SMAP A/P	SMAP MOEA	SMAP SFIM
03/05/2015	*	*	*	*	#
04/05/2015	*				
06/05/2015	*	*	*	*	*
11/05/2015	#	*	*	*	*
12/05/2015		*	*	*	*
14/05/2015	*	#			
20/05/2015	#	*	*	*	*
22/05/2015	*	*	*	*	*
09/09/2015	*	*			
11/09/2015	*	*			*
14/09/2015	*	*			*
17/09/2015	*	*			*
19/09/2015	*	*			
22/09/2015	*	*			*
24/09/2015	*	*			*
27/09/2015	*	*			*

Note: \* denotes availability of downscaled data on PLMR flight date and # shows nearest available downscaled data to PLMR flight date. The date of the nearest available observations is provided on the soil moisture plots as shown in Figure 4.3.

The SMOS DisPATCHD and SMAP EnhancedD products were used in the combination procedure since they had a better performance than SMOS DisPATCHA and SMAP EnhancedA products in terms of accuracy (Chapter 4). Moreover, the SMAP EnhancedA and SMOS DisPATCHA products were not included in the merging procedure, because of their relative dependency to the SMAP EnhancedD and SMOS DisPATCHD. Poor temporal coverage of VTCI product over the Yanco region restricted the VTCI from being used in the merging procedure. Different combination scenarios were created for evaluating the performance of combined downscaled soil moisture products, as listed in Table 5.2.

Prior to combination of products at 1 km, each downscaled soil moisture product at 9 and 10 km were mapped onto the same 1 km grid as that of the DisPATCH products. Rescaling the products from coarser to higher resolution involved assigning the value of each coarse pixel to the higher resolution pixels within the original coarse pixel. To combine products at 9 km resolution required all products to be mapped onto a 9 km grid; With the use of arithmetic average, downscaled soil moisture products at 1 km, herein SMOS DisPATCHD, were upscaled to the 9 km resolution of the SMAP A/P product. Mapping the SMAP SFIM product from 10 km to 9 km consisted of two steps: i) rescaling from 10 km to 1 km, and ii) upscaling 1 km products to 9 km.

The inverse variance weighted averaging approach (Lee et al., 2016) implemented in the ESA CCI SM v03.2 (Dorigo et al., 2017; Gruber et al., 2016) was used to combine downscaled soil moisture products. In this thesis, the relative weights are dynamic; if one product is not available on a specific date its' error variance is excluded.

$$\theta_{Combined} = \frac{\sum_{i=1}^n \frac{1}{\delta_{p_i}^2} \theta_{p_i}}{\sum_{i=1}^n \frac{1}{\delta_{p_i}^2}} \quad (5.1)$$

where  $\delta^2$  stands for error variance  $[(m^3 m^{-3})^2]$ ,  $\theta$  is the volumetric soil moisture  $[m^3 m^{-3}]$ , and  $p$  subscript indicates that the variable is representative for the specific downscaled soil moisture product ( $\{p_i\} = \{p_1, p_2, \dots, p_n\}$ ).

The uncertainty of downscaled soil moisture estimates, herein error variance, was calculated from evaluation of the alternative downscaled soil moisture products against the airborne

PLMR soil moisture maps (Chapter 4) during the SMAPEX-4 and SMAPEX-5 airborne field campaigns. Error values of each downscaled soil moisture products were calculated at their original scale on a daily basis for each SMAPEX campaign. Time series of error values were used to calculate the variance of daily errors for each pixel. The error variance for each downscaled soil moisture product during the SMAPEX-4 airborne field campaign are plotted in Figure 5.2. It is noted that when the downscaled soil moisture products were combined at 1 km resolution, the error variances at 9 km were mapped onto a 1 km grid. Likewise, for the combination of the downscaled soil moisture products at 9 km, the SMOS DisPATCHD error variance at 1 km and the SMAP SFIM error variance at 10 km were mapped onto a 9 km grid as described previously.

The temporal and spatial analysis described in Chapter 4 was used again here as the basis for evaluation of the combined retrievals. The main aim was to determine the best combination of downscaled soil moisture products for the period of the SMAPEX-4 airborne field campaign, during which the radar-based products (namely SMAP A/P and SMAP MOEA) were available. The S4 and S5 combinations were also derived and analysed during the SMAPEX-5 airborne field campaign.

Table 5.2: List of downscaled soil moisture product combination scenarios tested.

Combination scenarios	Combined products
<b>S1</b>	SMOS DisPATCHD, SMAP EnhancedD, SMAP A/P, SMAP MOEA and SMAP SFIM
<b>S2</b>	SMOS DisPATCHD, SMAP EnhancedD and SMAP MOEA
<b>S3</b>	SMOS DisPATCHD, SMAP EnhancedD and SMAP A/P
<b>S4</b>	SMOS DisPATCHD, SMAP EnhancedD and SMAP SFIM
<b>S5</b>	SMOS DisPATCHD and SMAP EnhancedD

Note: D stands for descending overpasses.

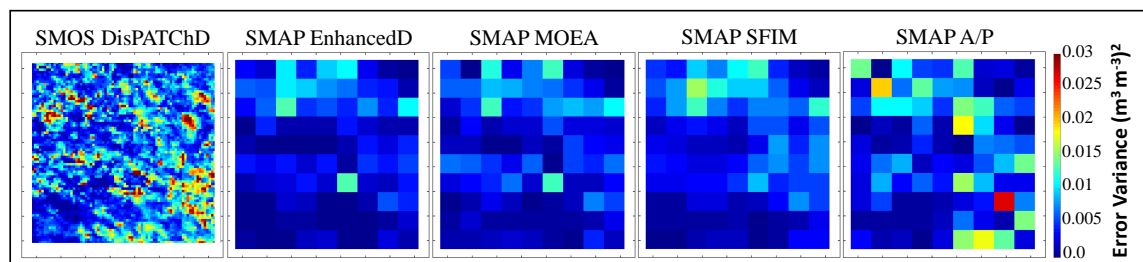


Figure 5.2: Error variance maps used for merging the downscaled soil moisture products during the SMAPEX-4 airborne field campaign.

The spatial correlation length of errors on daily basis was calculated for each individual downscaled soil moisture product to determine the presence of spatial correlation between the pixel uncertainty values; if data error estimates are spatially correlated, the effectiveness of merging algorithm may be reduced (Wang, 2012). Upon calculation of the spatial auto-correlation, which is summarised in Figure 5.3 as the average of daily analysis, the spatial independency of error characteristics was confirmed, as evidenced by the spatial correlation coefficient ( $R$ ) of uncertainty values being mainly between  $-0.2$  and  $+0.2$ . Consequently, there was no spatial correlation between the pixel uncertainty values, implying no negative impact of spatial error correlations on the merging algorithm performance.

### 5.3 Results

Figure 5.4 presents the qualitative inter-comparison of combined soil moisture maps together with the PLMR airborne soil moisture maps during the SMAPEX-4. Both PLMR and combined data are available at 1 and 9 km spatial resolution; the PLMR soil moisture

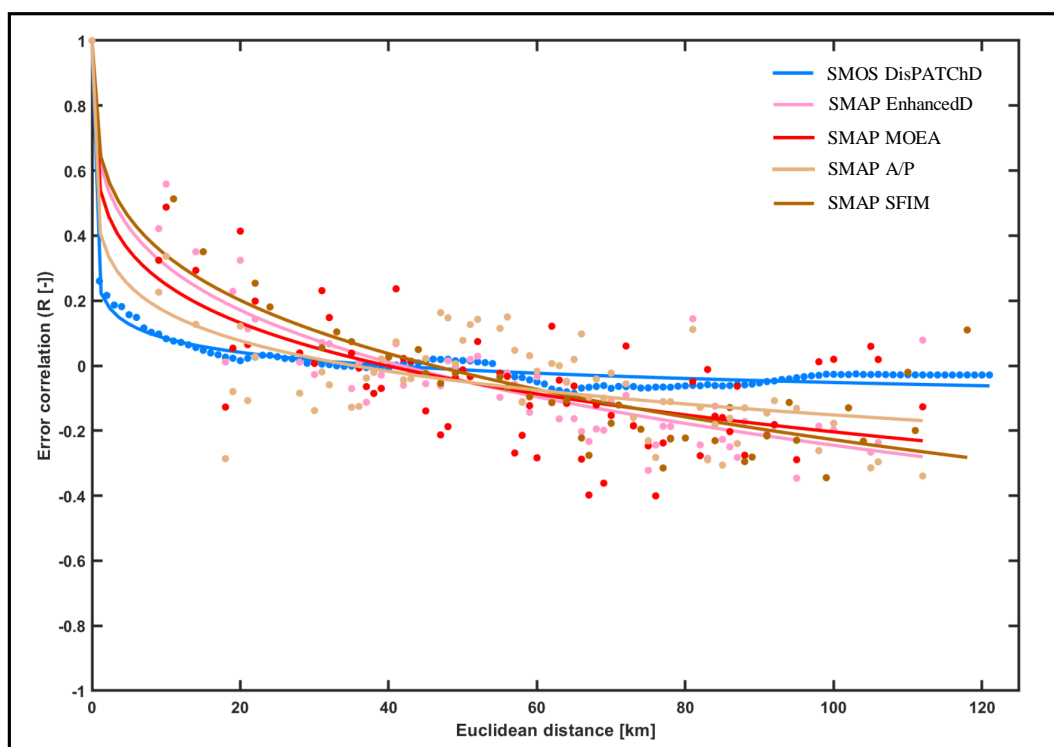


Figure 5.3: Averaged spatial auto-correlation analysis of relative uncertainty of downscaled soil moisture products.

estimates were mapped to 9 km resolution by averaging the 1 km PLMR estimates within the 9 km grid of the SMAP A/P downscaled soil moisture estimates. The qualitative inter-comparison of combined products during the SMAPEX-5 is shown in Figure 5.5.

As shown in Figure 5.4, temporal variation of the combined products matches well to that of the PLMR soil moisture estimates; they all captured the soil moisture increase due to the rain events that happened on 9 and 18 May 2015. However, a similar spatial pattern of soil moisture variation is represented by all combined products, and the pattern does not reflect that of the PLMR airborne soil moisture. The lack of ability to detect the spatial pattern of soil moisture was significant on 11th, 20th and 22nd May 2015. For instance, no combined product could represent the wet soil moisture conditions in the north-western part of the Yanco area on the 20th May.

Figure 5.5 shows the success of combined products in capturing the temporal pattern of PLMR soil moisture estimates during the dry-down period of the SMAPEX-5 airborne field campaign. Still, no agreement is seen between the spatial variation of combined products and that of the PLMR airborne soil moisture. Soil wetness associated to rainfall events on 9th, 11th and 14th September is not captured by any of the combined soil moisture products. Underestimation of PLMR soil moisture estimates by all the combined soil moisture products is also indicated. Comparing the temporal repeat of combined products with that of the individual downscaled soil moisture products shown in Figure 4.3 and Figure 4.4, shows that the combination of downscaled soil moisture products was able to deliver more frequent soil moisture maps than the individual downscaled soil moisture products alone during both the SMAPEX-4 and SMAPEX-5 airborne field campaigns.

The median and interquartile range of OzNet top 5 cm soil moisture measurements were also calculated across a sample pixel, being that with the largest number of OzNet stations (as shown in Figure 4.2). This is plotted as a time series against the combined soil moisture estimates at 9 km in Figure 5.6. Combined products were found to have similar temporal dynamics to the OzNet soil moisture measurements for this pixel. However, Figure 5.6 shows that combined soil moisture values underestimated PLMR airborne soil moisture estimates, while overestimating the median OzNet top 5 cm soil moisture measurements. Still,

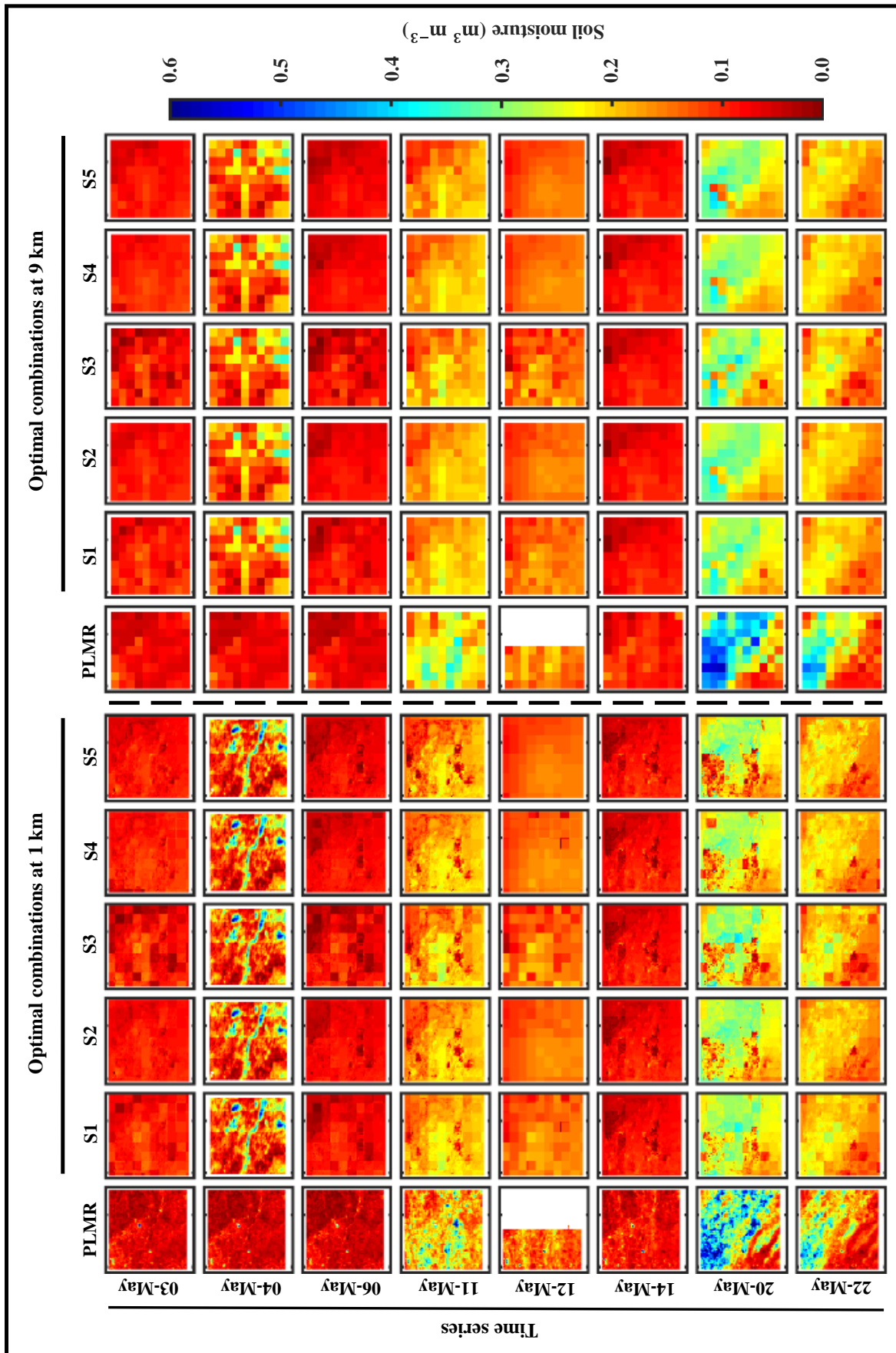


Figure 5.4: Time sequence plots of the combinations of downscaled soil moisture products from the five different combination scenarios described in Table 5.2 across the SMAPEX-4 airborne field campaign. Note: Missing data are shown in white colour.

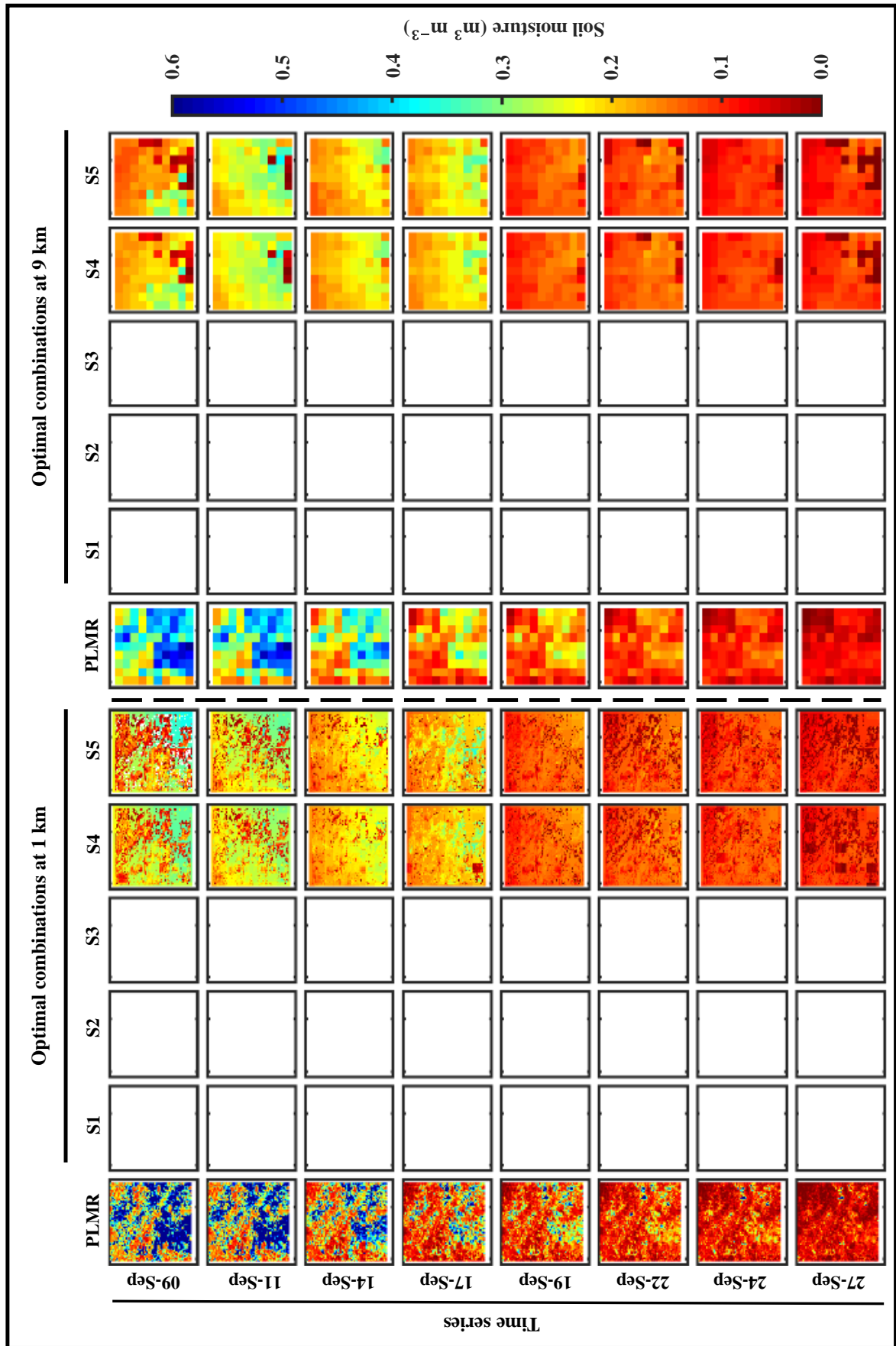


Figure 5.5: As for Figure 5.4 but across the SMAPEx-5 airborne field campaign.

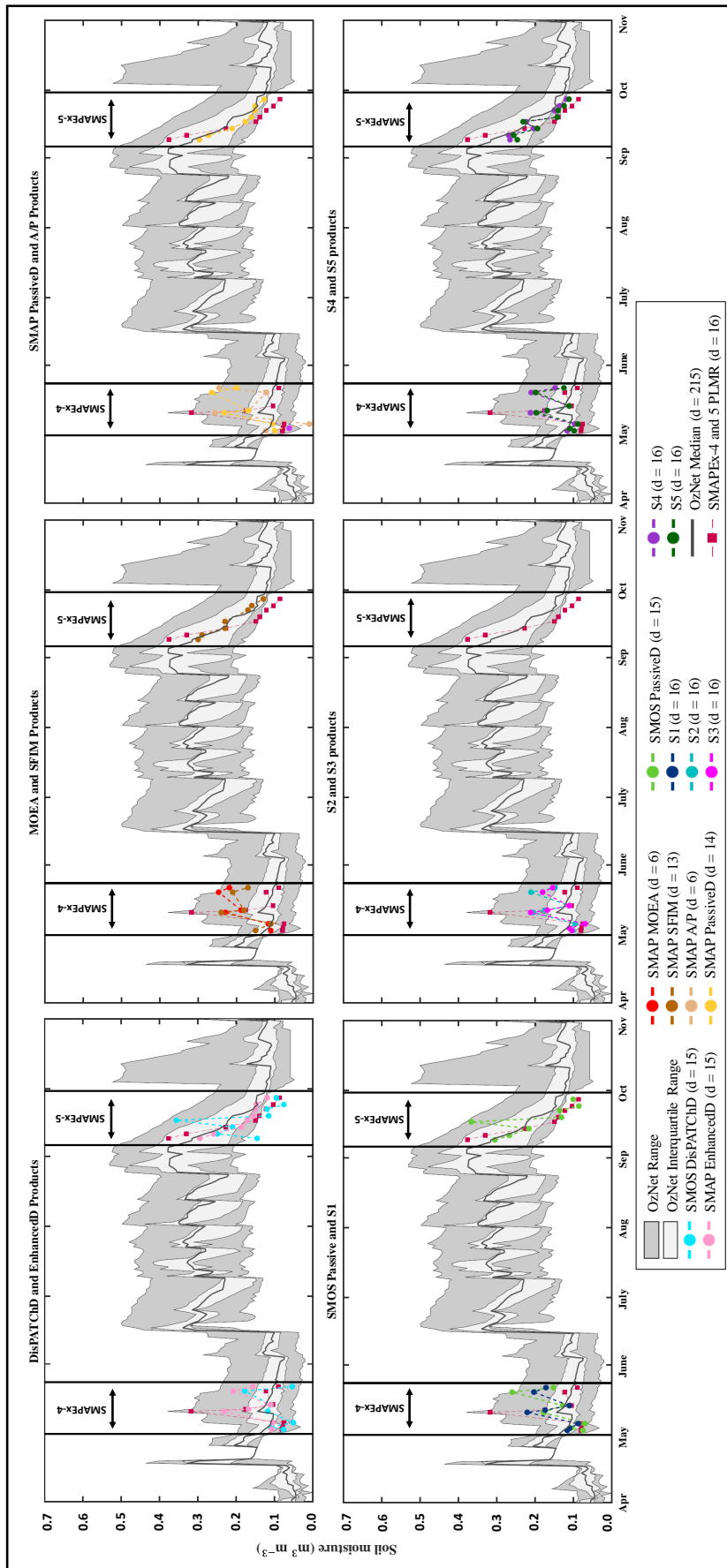


Figure 5.6: Sample of PLMR airborne time series of soil moisture estimates for the 9 km pixel having the largest number of OzNet stations (shown in Figure 4.2). Shown here is the median of measurements from the OzNet stations, coarse SMAP and SMOS soil moisture retrievals posted to 9 km without any downscaling technique being applied, and combination scenarios for the Yanco region during the SMAPEX-4 and -5 airborne field campaigns' period. This temporal evolution is generated for 9 and 10 km pixels (shown in Figure 4.2) having the largest *in situ* monitoring stations. Note: d indicates the number of days for which soil moisture products were available over the SMAPEX-4 and -5 flight area.

combined values did not move out of range of the OzNet measurements. To understand whether the time series of combined products were improved in capturing the temporal dynamics of the PLMR soil moisture estimates and/or the OzNet *in situ* measurements, temporal analysis of the combined products required comparison against the individual downscaled soil moisture products. This section is followed by the temporal analysis of combined products against the airborne PLMR and OzNet *in situ* soil moisture estimates.

### 5.3.1 Temporal analysis against the OzNet

The combined products from the five combination scenarios in Table 5.2 were retrieved at both 1 and 9 km spatial resolution. The accuracy of these combined products was quantified against both the PLMR airborne and OzNet top 5 cm soil moisture measurements, as the reference soil moisture data set. Bias,  $R^2$ , RMSD and ubRMSD were used as a measure of quality, as shown in Figure 5.7, 5.8, 5.9, and 5.10.

For the analysis of combined products against the OzNet measurements during the SMAPEX-4 airborne field campaign, the RMSD and ubRMSD across the combined products at 1 and 9 km showed improvement over the individual downscaled soil moisture products alone. For example, the average RMSD of SMOS DisPATCHD at 1 km was  $0.095 \text{ m}^3 \text{ m}^{-3}$ , while the average RMSD of combined products at 1 km varied between 0.07 and  $0.075 \text{ m}^3 \text{ m}^{-3}$ . The  $R^2$  of combined products was similar to that of SMOS DisPATCHD at 1 km alone, but lower than for the radiometer-only products, herein SMAP PassiveD and SMOS PassiveD. However, the bias of combined products at 1 km was on average  $0.02 \text{ m}^3 \text{ m}^{-3}$  larger than the SMOS DisPATCHD bias of  $0.003 \text{ m}^3 \text{ m}^{-3}$ . In comparison, combined products at 9 km had a lower bias compared to downscaled soil moisture products with positive bias. The S4 and S5 combined products were also analysed against the OzNet soil moisture measured on the SMAPEX-5 flight dates as summarised in Figure 5.8. Based on this analysis, while the S4 and S5 combined products at 1 km showed improved performance over the individual downscaled soil moisture products, the S4 and S5 products at 9 km could not reach the high level of performance for the individual downscaled soil moisture products at 9 km spatial resolution.

### 5.3.2 Temporal analysis against the airborne PLMR soil moisture

From the temporal analysis of combined products at 1 km against PLMR airborne soil moisture in Figure 5.9, the combined products were found to have a better temporal match with the PLMR soil moisture during the SMAPEX-4 airborne field campaign than the individual downscaled soil moisture products. The S1 product had the highest temporal correlation with a mean  $R^2$  of 0.63. However, the high correlation of S1 does not imply superiority to the remaining combined products; all combined products had similar RMSD, with the

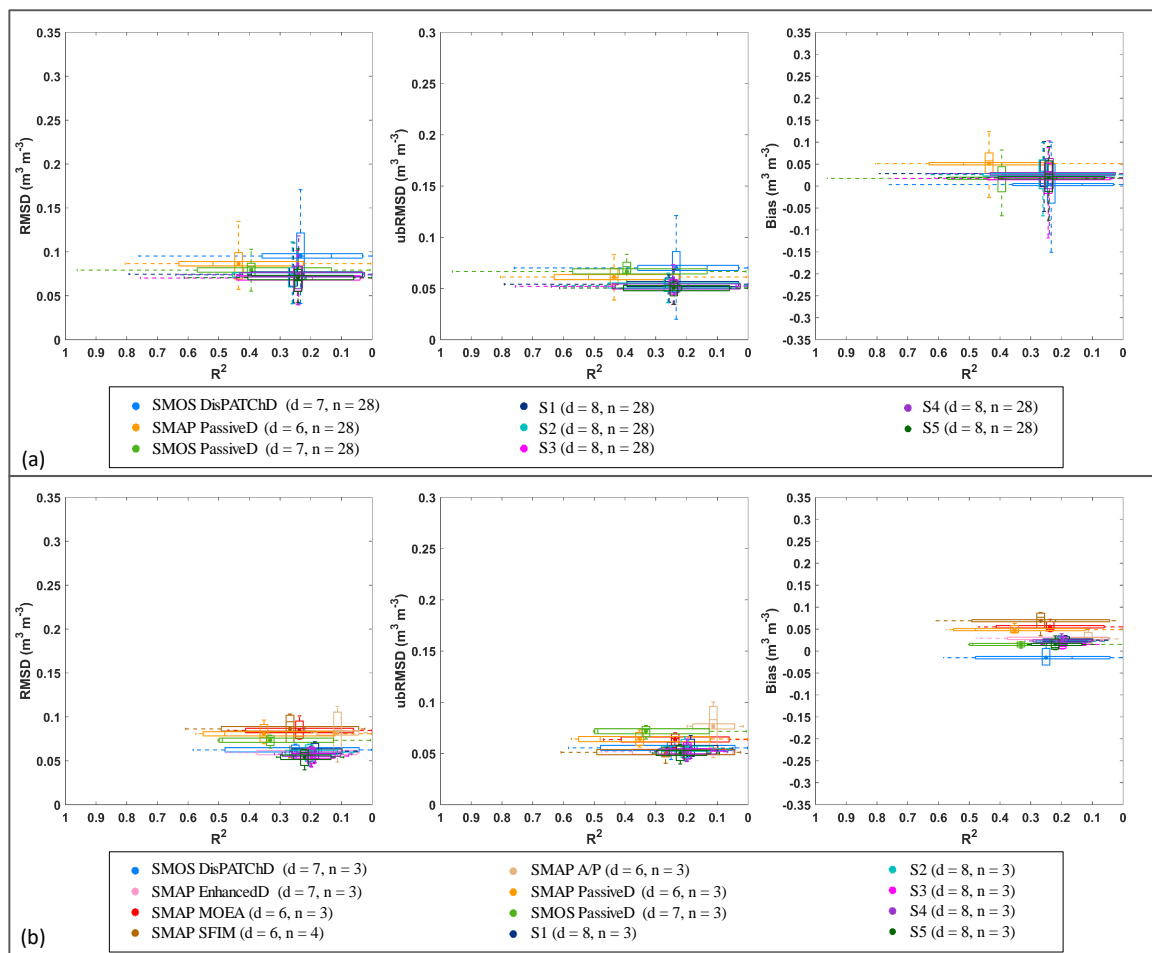


Figure 5.7: Boxplots summarising the interquartile range, the maximum and minimum range, and the median (bar) associated with the mean (dot) of statistical results obtained from temporal analysis of combined soil moisture products at (a) 1 km and (b) 9 km against OzNet *in situ* measurements for the SMAPEX-4 airborne field campaign. For 9 and 10 km products, only pixels with largest number of stations (see Figure 4.2) were chosen. d indicates the number of downscaled soil moisture products that were used in this analysis and n indicates the number of statistical parameters that are summarised in this figure.

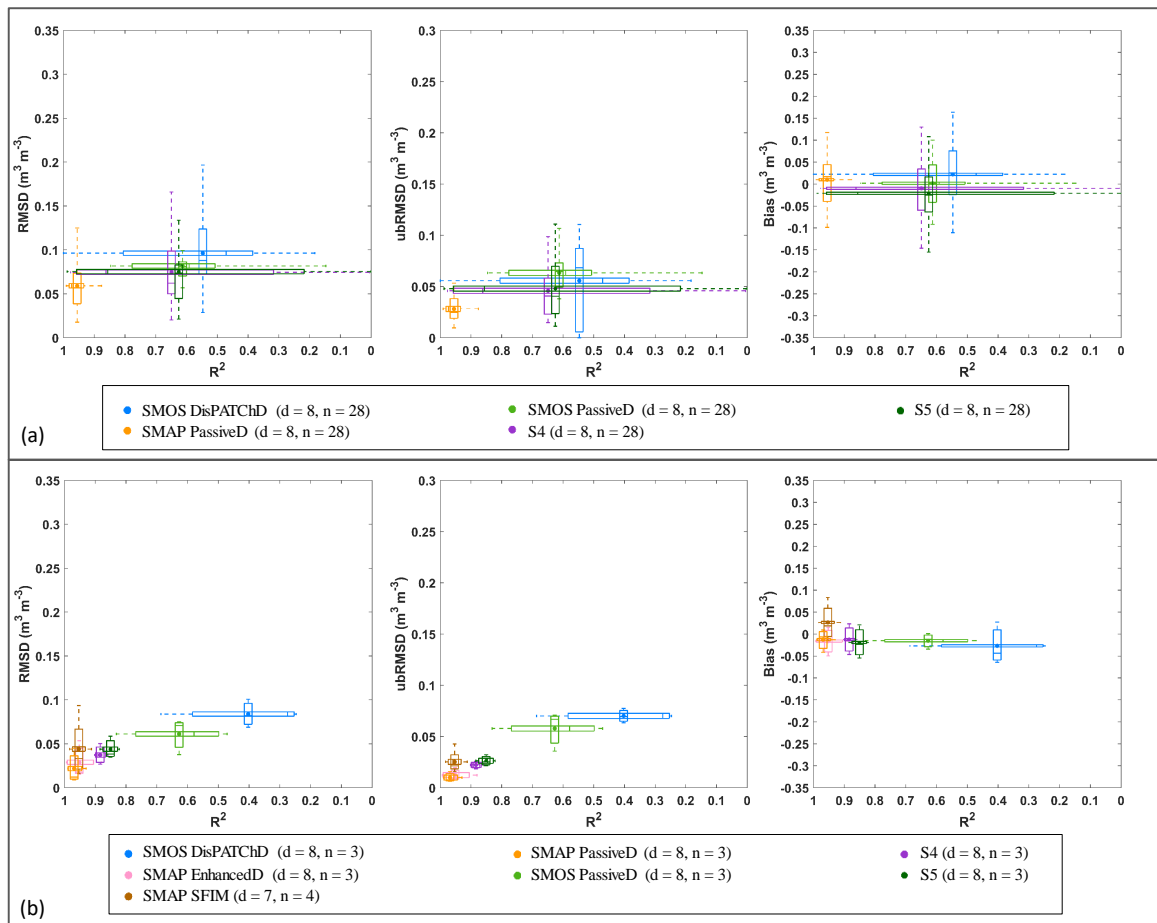


Figure 5.8: As for Figure 5.7 but for the SMAPEX-5 airborne field campaign flight dates.

lowest mean  $R^2$  of 0.57 obtained for S5. A summary of accuracy statistics of the combined products at 1 km, evaluated against the airborne PLMR soil moisture maps during the SMAPEX-4 and OzNet *in situ* soil moisture measurements, is provided in Table 5.3. All combined products at 1 km showed poor performance when assessed against the airborne PLMR soil moisture maps and OzNet *in situ* soil moisture measurements. As expected, all combined products underestimated the airborne PLMR soil moisture; this underestimation of PLMR soil moisture was also identified for the downscaled soil moisture products alone in Chapter 4.

Performance assessment of the S4 and S5 products at 1 km during the SMAPEX-5 airborne field campaign showed inferiority of combined products to the downscaled product alone, in terms of RMSD, ubRMSD and bias. Both these combined products had an RMSD of higher than  $0.15 \text{ m}^3 \text{ m}^{-3}$  and ubRMSD of  $\sim 0.1 \text{ m}^3 \text{ m}^{-3}$ . However, the  $R^2$  of the combined products

was  $\sim 0.1$  higher than that of the downscaled soil moisture products alone. Both the S4 and S5 products underestimated the airborne PLMR soil moisture, being even more severe than for the SMAPE<sub>x</sub>-4 period. Results from the comparison of the S4 and S5 combined products against coarse SMOS and SMAP passive microwave soil moisture products during the SMAPE<sub>x</sub>-5 airborne field campaign revealed deterioration of combined products in terms of performance. The dense vegetation cover during the SMAPE<sub>x</sub>-5 may have had a negative impact on the performance of the combining algorithm; the original downscaled soil moisture products during the SMAPE<sub>x</sub>-4 and SMAPE<sub>x</sub>-5 airborne field campaigns showed a similar performance in terms of accuracy (Chapter 4) which support this hypothesis.

According to the temporal evaluations at 9 km in Figure 5.10, all of the combined products had a tendency to underestimate PLMR soil moisture with a mean bias ranging from -0.01 to -0.02  $\text{m}^3 \text{m}^{-3}$ , which was less than that for the majority of downscaled soil moisture products alone, with a mean bias ranging from -0.02 to -0.03  $\text{m}^3 \text{m}^{-3}$ . However, they yielded similar  $R^2$  and RMSD values of approximately 0.7 and 0.07  $\text{m}^3 \text{m}^{-3}$ . Nonetheless, when the combined products were evaluated across 5 days only (3, 6, 11, 20 and 22 May), being when all downscaled soil moisture products were available, the combined products showed better  $R^2$  than the analysis of all available combined products during the SMAPE<sub>x</sub>-4.

The temporal analysis of the S4 and S5 combined products at 9 km were also conducted against the airborne PLMR soil moisture during the SMAPE<sub>x</sub>-5 airborne field campaign. Based on these analyses, the combined products could not yield soil moisture estimates as accurate as the downscaled soil moisture products alone. The  $R^2$  of accurate downscaled soil moisture products was above 0.9, while the S4 and S5 combined products had an average  $R^2$  of 0.58 and 0.66, respectively. However, the S5 combined soil moisture estimates showed lower bias (-0.028  $\text{m}^3 \text{m}^{-3}$ ) than the remaining soil moisture estimates, including the individual downscaled and combined ones.

Overall, the temporal analysis of combined products at 1 and 9 km against the airborne PLMR soil moisture maps showed that the  $R^2$  of combined products at both 1 and 9 km was on average  $\sim 0.6$ , being similar to the retrievals of the machine learning- and radar-based

Table 5.3: Averaged accuracy of the combined products at 1 km, evaluated against the airborne PLMR soil moisture and OzNet *in situ* soil moisture measurements. Gray cells indicate the accuracy of products with slightly better performance than the other combined products.

Combined product	Temporal analysis against airborne PLMR soil moisture during SMAPEX-4				Spatial analysis against airborne PLMR soil moisture during SMAPEX-4				Temporal analysis against <i>in situ</i> OzNet soil moisture during SMAPEX-4			
	Bias (m <sup>3</sup> m <sup>-3</sup> )	R <sup>2</sup>	RMSD (m <sup>3</sup> m <sup>-3</sup> )	ubRMSD (m <sup>3</sup> m <sup>-3</sup> )	Bias (m <sup>3</sup> m <sup>-3</sup> )	R <sup>2</sup>	RMSD (m <sup>3</sup> m <sup>-3</sup> )	ubRMSD (m <sup>3</sup> m <sup>-3</sup> )	Bias (m <sup>3</sup> m <sup>-3</sup> )	R <sup>2</sup>	RMSD (m <sup>3</sup> m <sup>-3</sup> )	ubRMSD (m <sup>3</sup> m <sup>-3</sup> )
S1	-0.014	0.63	0.084	0.070	-0.021	0.09	0.088	0.076	0.028	0.26	0.075	0.054
S2	-0.018	0.62	0.086	0.071	-0.017	0.08	0.087	0.074	0.026	0.26	0.074	0.053
S3	-0.021	0.59	0.088	0.072	-0.023	0.09	0.088	0.075	0.017	0.24	0.070	0.052
S4	-0.017	0.58	0.088	0.074	-0.032	0.11	0.083	0.074	0.028	0.24	0.074	0.052
S5	-0.023	0.57	0.090	0.075	-0.020	0.11	0.083	0.072	0.019	0.24	0.071	0.050

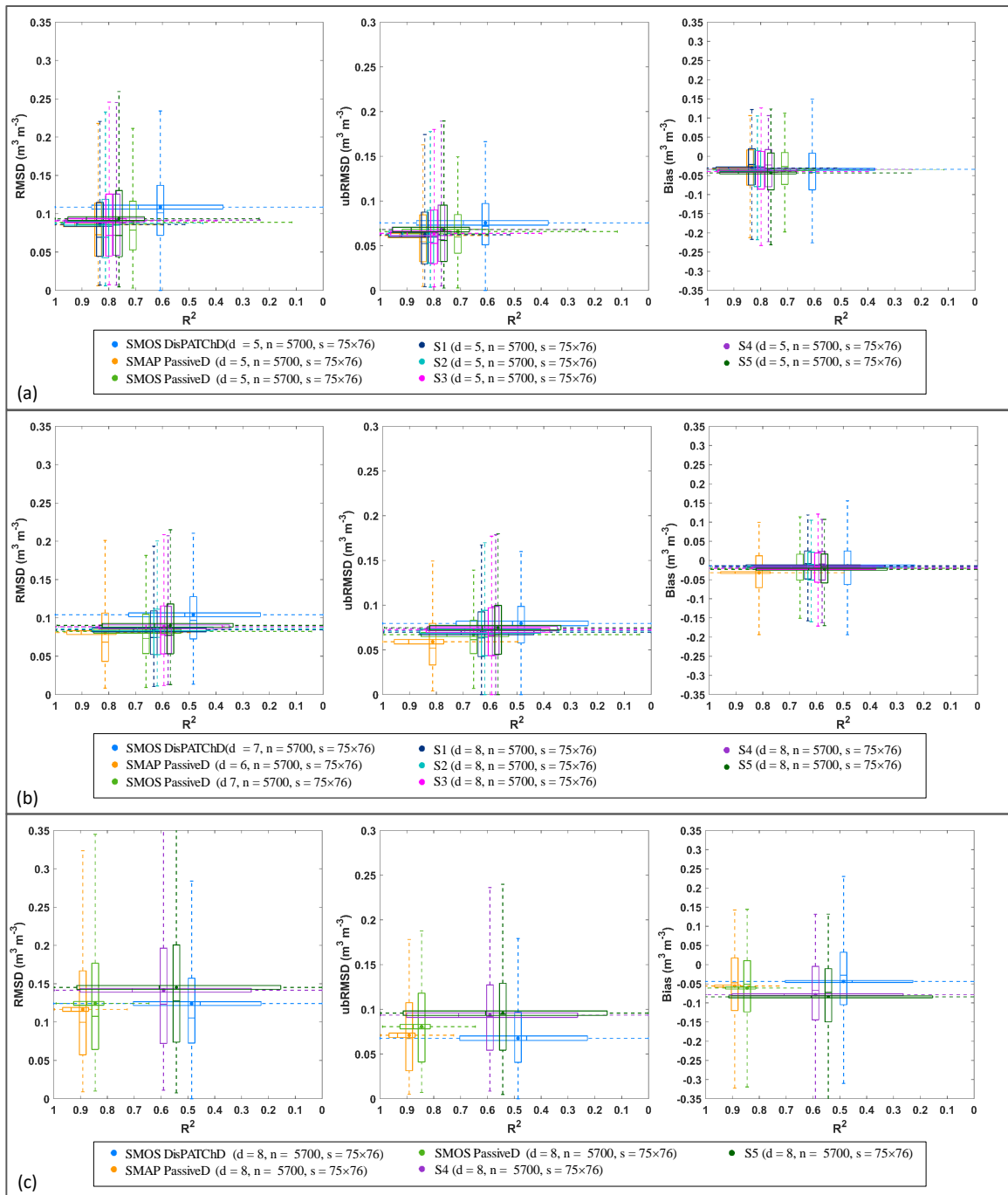


Figure 5.9: As for Figure 5.7 but for the comparison against airborne PLMR soil moisture at 1 km in which analysis was carried out for all the pixels covering the study area. These results are from the different scenarios including: a) combined products across 5 days when all downscaled soil moisture products were available on the same date during the SMAPEX-4, b) all available products during the SMAPEX-4, and c) all available products during the SMAPEX-5. Here s stands for the dimension of analysis area arranged in rows  $\times$  column. Please be noted that the maximum RMSD obtained for S4 and S5 products during the SMAPEX-5 was 0.55 and 0.56  $m^3 m^{-3}$ , respectively

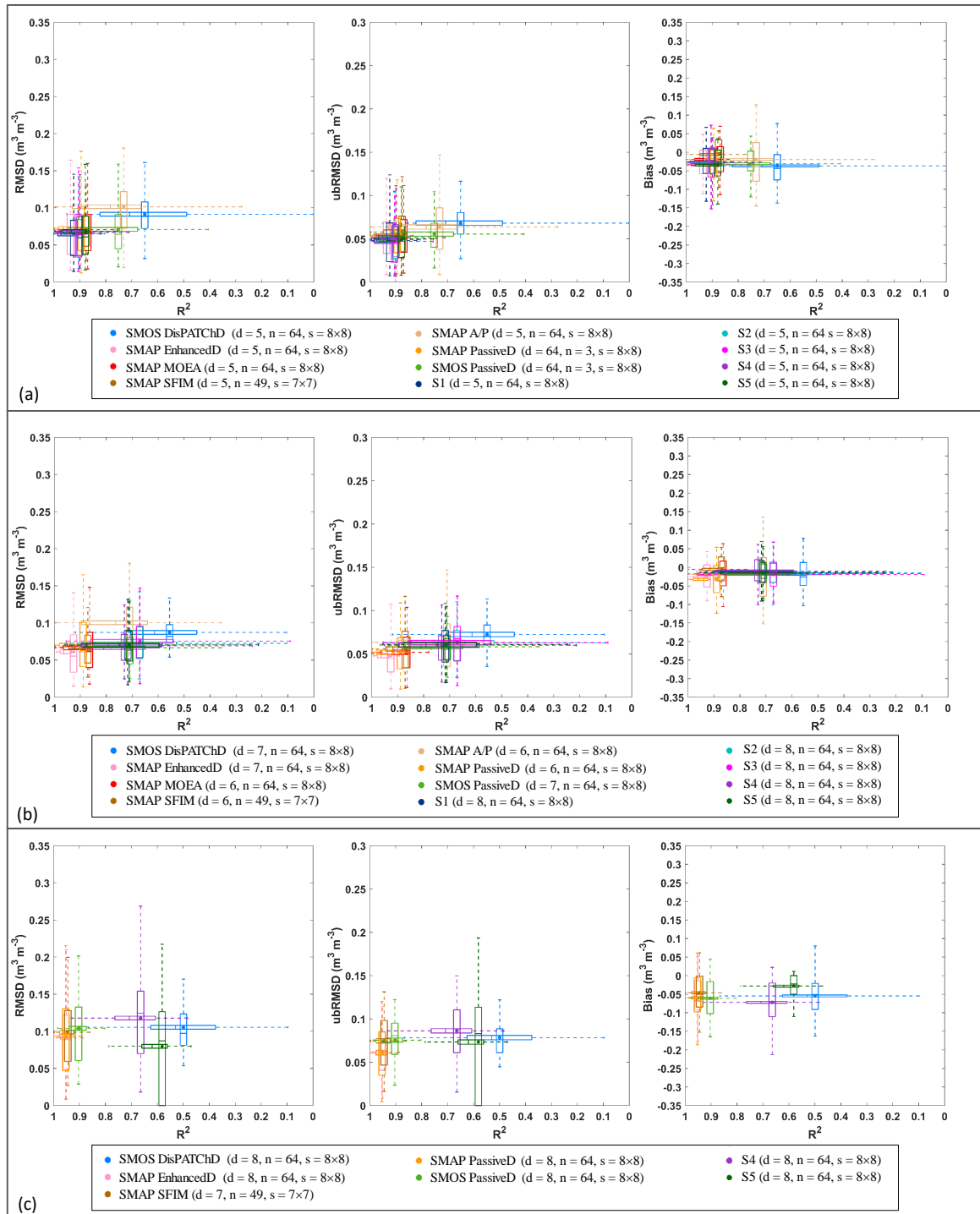


Figure 5.10: As for Figure 5.9 but for the comparison of combined products at 9 km against airborne PLMR soil moisture.

downscaling techniques analysed in Chapter 2, having the highest temporal correlation with reference soil moisture estimates. Based on the summary of results in Table 5.4, the RMSD of combined products at 1 km was on average 0.1 which is poorer than the average RMSD of all the downscaling techniques in Chapter 2, but still in minimum and maximum range of their RMSD values. The RMSD results for the combined products at 9 km were close to the average RMSD values of 0.07 and 0.08  $\text{m}^3 \text{m}^{-3}$  reported for the data assimilation- and optical-based downscaling techniques, respectively. Consequently, the combination method could not produce soil moisture estimates with comparable RMSD to the radar- and soil surface attribute-based downscaled soil moisture products, which had the lowest averaged RMSD of  $\sim 0.04$  and  $0.03 \text{m}^3 \text{m}^{-3}$ , respectively.

### 5.3.3 Spatial analysis against the airborne PLMR soil moisture

Apart from the temporal analysis, the combined products were spatially analysed using the PLMR airborne soil moisture measurements. Bias,  $R^2$ , RMSD and ubRMSD were also calculated for each combined product, in order to investigate which combined product best

Table 5.4: Comparison of results from the combined products with the downscaled soil moisture products based on literature review.

Results	Products	RMSD ( $\text{m}^3 \text{m}^{-3}$ )			$R^2$		
		minimum	maximum	average	minimum	maximum	average
Literature	Optical-based	0.012	0.210	0.072	0.00	0.81	0.38
	Radar-based	0.010	0.120	0.042	0.03	0.99	0.59
	Radiometer-based	0.054	0.130	0.078	0.28	0.41	0.35
	Soil surface attribute-based	0.024	0.033	0.028	0.02	0.86	0.45
	Machine learning-based	0.006	0.160	0.056	0.37	0.96	0.65
	Data assimilation-based	0.030	0.090	0.064	0.22	0.86	0.50
SMAPE <sub>x</sub> -4 (1 km)	S1	0.105	0.404	0.084	0.00	1.00	0.63
	S2	0.011	0.415	0.086	0.00	0.99	0.62
	S3	0.012	0.396	0.089	0.00	1.00	0.59
	S4	0.013	0.416	0.088	0.00	0.99	0.58
	S5	0.013	0.419	0.09	0.00	0.99	0.57
SMAPE <sub>x</sub> -4 (9 km)	S1	0.017	0.132	0.071	0.10	0.95	0.72
	S2	0.025	0.142	0.073	0.10	0.95	0.67
	S3	0.018	0.147	0.076	0.09	0.95	0.67
	S4	0.025	0.163	0.069	0.10	0.97	0.73
	S5	0.022	0.185	0.071	0.11	0.96	0.71
SMAPE <sub>x</sub> -5 (1 km)	S4	0.011	0.554	0.142	0.00	1.00	0.59
	S5	0.008	0.559	0.15	0.00	1.00	0.54
SMAPE <sub>x</sub> -5 (9 km)	S4	0.018	0.269	0.118	0.00	0.93	0.66
	S5	0.000	0.217	0.080	0.10	0.79	0.58

captured the spatial pattern of soil moisture. Results from this spatial analysis are summarised in Figure 5.11 and 5.12. In the spatial analysis, daily maps of combined estimates were compared against the corresponding PLMR airborne soil moisture maps. Similar comparisons of the S4 and S5 combined products against the SMAPEX-5 PLMR soil moisture maps can be found at the bottom of Figure 5.11 and 5.12.

In the spatial analysis, combined products at 1 and 9 km showed minor difference in terms of performance for both the SMAPEX-4 and -5 campaigns. During the SMAPEX-4 period, the combined products at 1 km showed better correlation than the only downscaled soil moisture product available at 1 km, the SMOS DisPATCHD. It is noted though that all of the combined products at 1 km had  $R^2$  values lower than 0.2. But in general the combination of downscaled soil moisture products, resulted in a reduction of RMSD and ubRMSD compared to the downscaled soil moisture products alone. These results are opposite of the findings for the SMAPEX-5 airborne field campaign, where combining downscaled soil moisture products resulted in decreased accuracy of soil moisture estimates.

For combined products at 9 km the RMSD and ubRMSD remained similar to that of individual downscaled soil moisture products. Furthermore, none of the combined products at 9 km could surpass the retrieval accuracy of the SMAP SFIM and EnhancedD products on their own. These results were found to be similar for different analysis scenarios including: i) only the 5 days when all the downscaled soil moisture products were available, ii) all available combined products during the SMAPEX-4 airborne field campaign period, and iii) all available combined products during the SMAPEX-5 airborne field campaign period. However, combined products at 9 km in general showed better temporal coverage over the study area.

### **5.4 Discussion**

Comparing different combination of downscaled soil moisture products, showed indifference between their performance. The accuracy of merged products depends on the error estimate (herein error variance) of downscaled soil moisture data, which was used inversely as a factor reflecting the weight of each downscaled soil moisture product. Because the

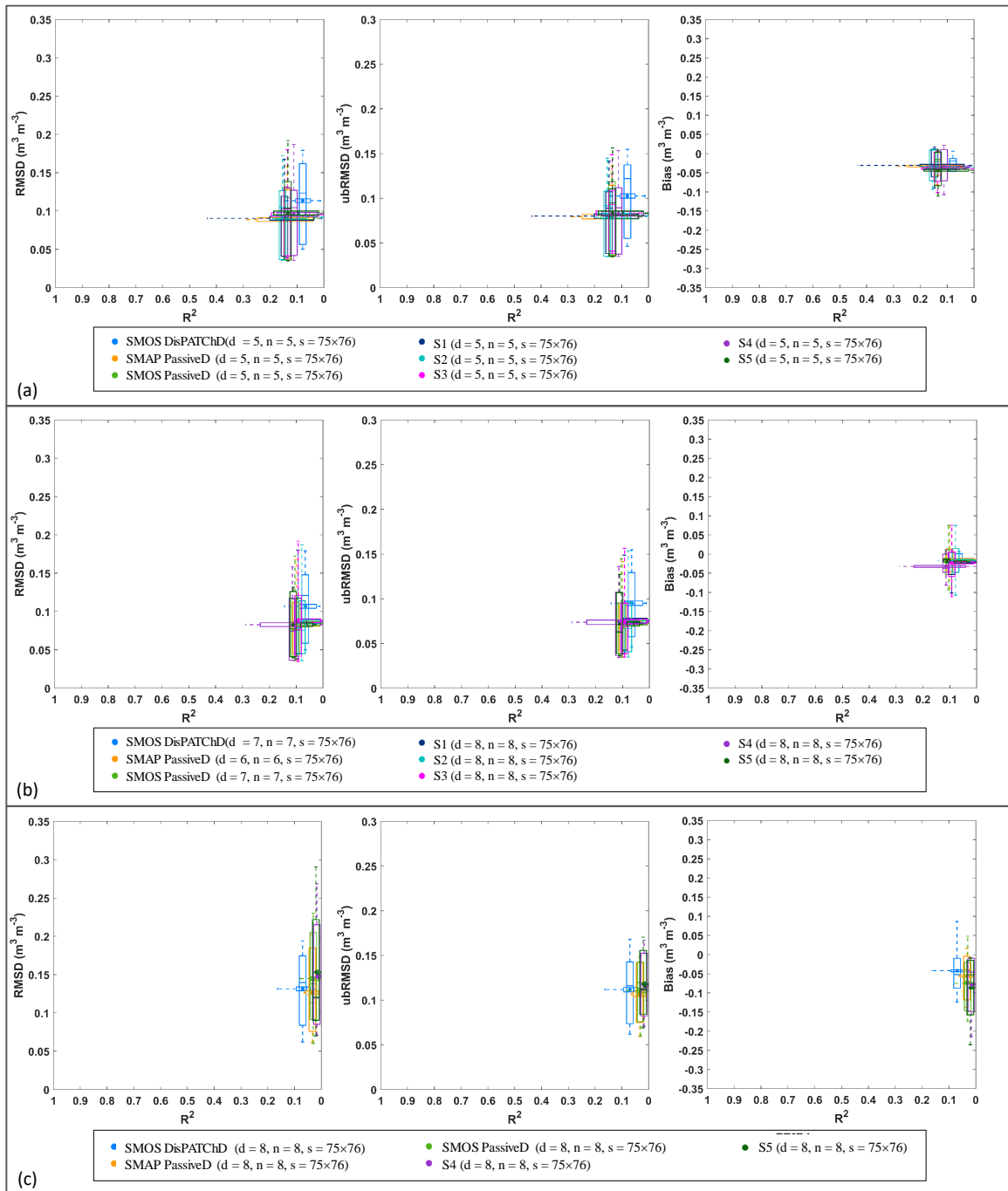


Figure 5.11: Boxplots summarising the interquartile range, the maximum and minimum range, and the statistics median (bar) associated with the mean (dot) of statistical results obtained from spatial analysis of combined soil moisture products at 1 km. These results are from the different scenarios including: a) combined products across 5 days when all downscaled soil moisture product were available on the same date during the SMAPEX-4, b) all available products during the SMAPEX-4, and c) all available products during the SMAPEX-5.

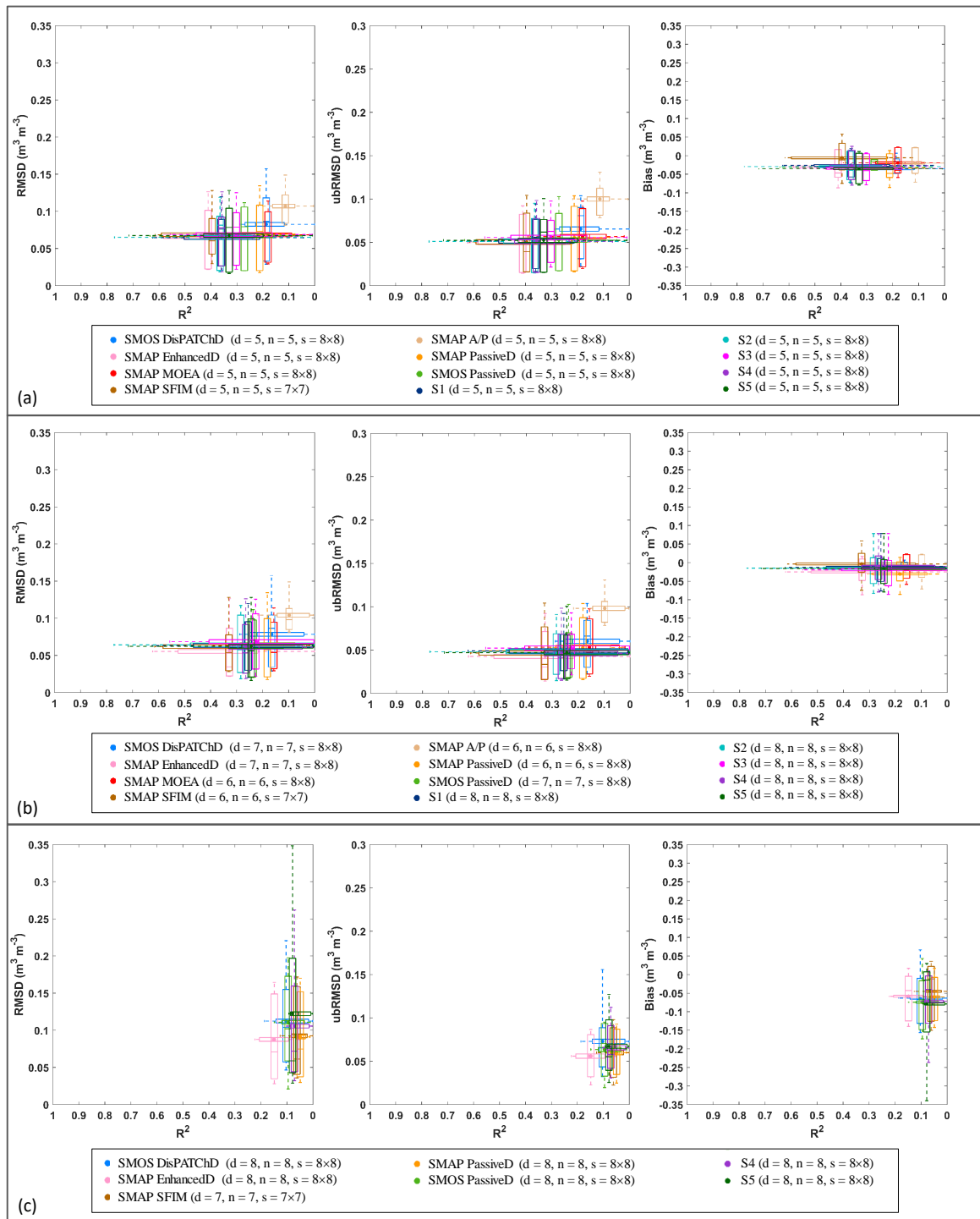


Figure 5.12: As for Figure 5.11 but for the comparison of combined products at 9 km against airborne PLMR soil moisture.

merging model gives similar results in terms of accuracy and performance, the error estimates of downscaled soil moisture products may be correlated. Therefore, the correlation of daily error estimates was calculated between different pairs of downscaled soil moisture products mapped onto the same grid. For this purpose, daily error values of each downscaled soil moisture product at their original spatial resolution was calculated by comparing them against the concurrent PLMR soil moisture observations.

To calculate error correlations at 1 km resolution, all daily error estimates were mapped onto a 1 km grid, excepting the daily error estimates of the SMOS DisPATCHD, being originally scaled at 1 km resolution; pixels at 1 km resolution within the coarse 9/10 km resolution pixels were assigned the same value of that coarse pixel. Daily error estimates were also mapped onto a 9 km grid to calculate the error correlation at 9 km. Therefore, the 1 km error estimates of those SMOS DisPATCHD pixels lying within the coarse 9 km pixel were averaged to the 9 km spatial resolution of SMAP A/P. Similarly to the mapping of the SMAP SFIM products from 10 to 9 km, two steps were followed, including: i) rescaling error estimates from 10 km to 1 km, and ii) upscaling the 1 km error estimates to 9 km. The error correlation for each pixel (either 1 or 9 km) was calculated when 5 or more coincident errors of downscaled soil moisture products were available.

Figure 5.13 and 5.14 show the correlation coefficient maps generated during the SMAPEX-4 airborne field campaign using daily error estimates of downscaled soil moisture products at 1 and 9 km, respectively. Error correlation maps of downscaled soil moisture products at 9 km which were mapped onto 1 km grid were similar to those generated between downscaled soil moisture products at 9 km, but at higher resolution. Therefore, these correlation maps are not provided in Figure 5.13.

Values of correlation coefficients mapped in 5.13 and 5.14 show strong correlation between different pairs of downscaled soil moisture products. Pixels in the medium to dark red colour indicate the positive correlation, while pixels in the medium to dark blue colour represent negative correlation. For example, the SMAP EnhancedD and SMAP SFIM paired error estimates are positively correlated with their R values generally larger than 0.5 (Figure 5.14).

A summary of the correlation values obtained for the daily error estimates of downscaled

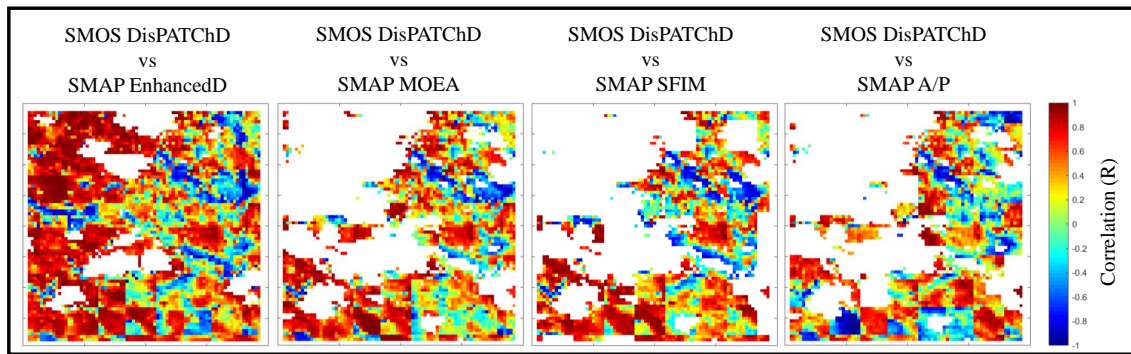


Figure 5.13: The correlation coefficient maps generated between time series of error estimates of downscaled soil moisture products at 1 km during the SMAPEX-4 airborne field campaign. Note: missing data shown in white colour are pixels for which less than 5 pairs of coincident error estimates were available.

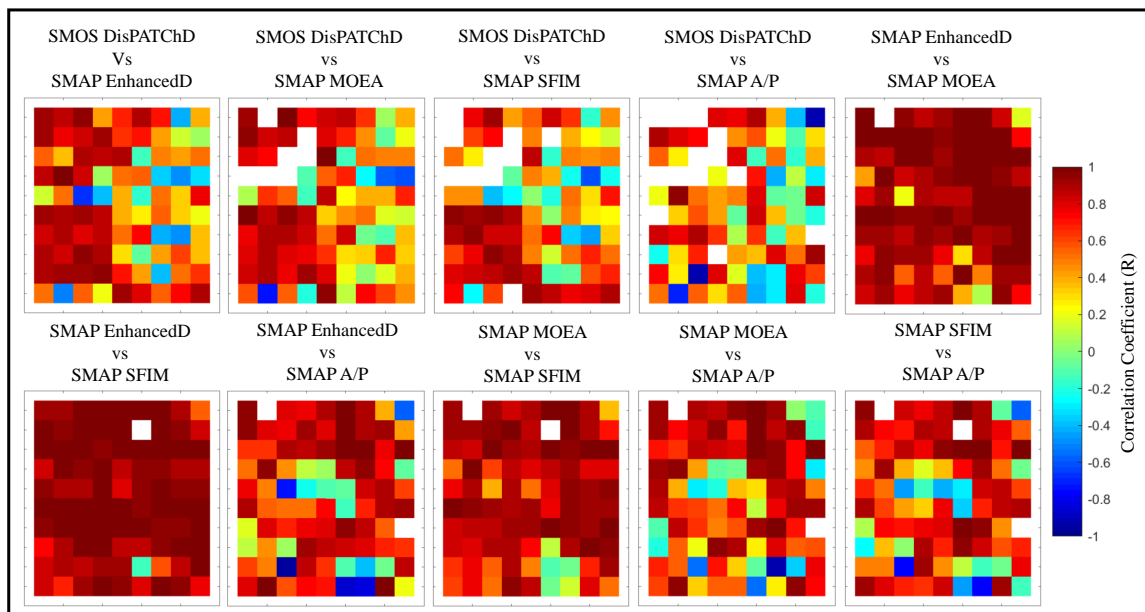


Figure 5.14: As for Figure 5.13 but for the downscaled soil moisture products originally at 9 km or mapped into a 9 km grid.

products at 1 and 9 km spatial resolution is provided in Figure 5.15 as boxplots dropping the outliers. The error correlations for those pairs including the daily error estimates of the SMOS DisPATCHd show a wide range of variation in the error correlations; the SMOS DisPATCHd comes already at a higher resolution than the other downscaled soil moisture products used in the merging process, which explains the higher variability of its daily error estimates and thus the correlations of SMOS DisPATCHd daily error with the other downscaled soil moisture products. Based on Figure 5.15, the median of the error correlations is identified to be equal to or above 0.4, excepting the SMOS DisPATCHd versus SMAP A/P

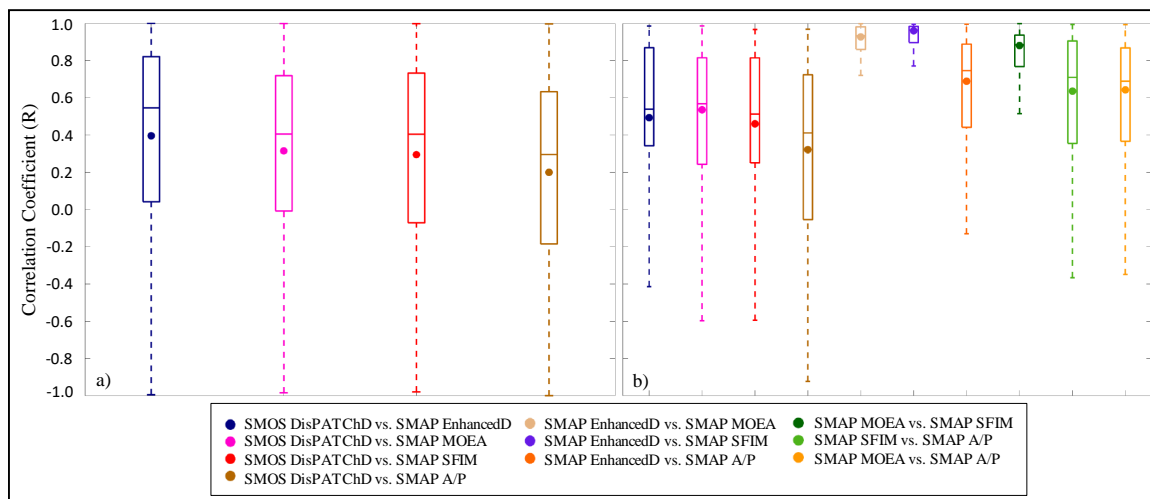


Figure 5.15: Boxplots summarising the interquartile range, the maximum and minimum range, and the statistics median and average (bar and dot, respectively) associated with the mean of correlation coefficients obtained from comparison of error estimates of downscaled soil moisture products at a) 1 km and b) 9 km.

at 1 km resolution. Such high error correlations explain why merging different downscaled soil moisture products could end up having similar results.

## 5.5 Chapter summary

This chapter has evaluated the effectiveness of merging individual downscaled soil moisture products for improving soil moisture mapping reliability and temporal availability. The theoretical basis of a merging candidate technique has been briefly discussed and the approach demonstrated. Five different combinations based on data availability were tested to provide an analysis of the combined downscaled soil moisture products that could be used for high resolution soil moisture mapping with the data available.

This chapter demonstrated that a combination of downscaled soil moisture products can deliver more frequent soil moisture maps than the individual downscaled soil moisture products. While the accuracy of combined products at 1 km was superior to the downscaled soil moisture product originally scaled at 1 km during the SMAPEX-4 airborne field campaign, the combining procedure could not deliver more accurate soil moisture estimates than the downscaled only products at 1 km during the SMAPEX-5 airborne field campaign. During

the SMAPE<sub>x</sub>-5 the vegetation cover was denser than during the SMAPE<sub>x</sub>-4, which might be the reason for a poorer merging performance. Similarity of performance for the original downscaled products during the SMAPE<sub>x</sub>-4 and SMAPE<sub>x</sub>-5 airborne field campaigns, (see Chapter 4), supports this statement. The combined products at 9 km did not surpass the individual products in terms of accuracy during both the SMAPE<sub>x</sub>-4 and -5 airborne field campaigns. However, combined products at 9 km were found to increase the temporal availability of soil moisture maps from single downscaling approach. Moreover, the difference between individual combined products was marginal, regardless of the combination scenarios.



# Chapter 6

## Conclusions and future work

### 6.1 Conclusions

The thesis has assessed the performance of current downscaled soil moisture products. In particular, there has been an extensive evaluation against a common reference data set, including the SMAPE<sub>x-4</sub> and -5 airborne PLMR soil moisture maps and OzNet *in situ* measurements, to determine a preferred method for soil moisture downscaling. Downscaled soil moisture products derived from radar-, optical-, radiometer-, and oversampling-based downscaling techniques have been evaluated. Previously these downscaled soil moisture products have been independently analysed and tested for different climate conditions. Therefore, the main contribution of this research was a comparative analysis of alternative downscaled soil moisture products based on: i) literature, and ii) with an extensive reference data set for a specific landscape and climate condition, followed by iii) development of a combined downscaled soil moisture retrieval as a step towards producing a harmonious multi-sensor soil moisture product from SMOS and SMAP. The key conclusions for each contribution are as follows.

#### 6.1.1 Review of spatially enhanced passive microwave derived soil moisture

Downscaling techniques can deliver substantially greater spatial detail about soil moisture spatial variability, as compared to the original remotely sensed passive microwave data, to meet the requirements of a growing number of applications. Moreover, the combining of remotely sensed land surface features with passive microwave observations has been shown

to derive fine-scaled soil moisture with reasonable accuracy. A considerable contribution to combined techniques was made by the optical acquisitions that are available at high resolution on a daily basis, but cloudy skies and seasonality significantly affect the functionality of optical-based downscaling methods. Moreover, combined L-band radar and radiometer (radar-based) downscaling approaches have demonstrated the best success in deriving multi-sensor soil moisture maps (as shown in Figure fig:Accuracy), but at a resolution of approximately 10 km.

Utilizing the soil surface attributes and structure, including topography and soil texture, is also beneficial to the space-time scaling of soil moisture. Topography and soil texture impacts the soil water dynamic and thus distribution of soil moisture. Both soil water dynamics and storage capacity exert effective impact on soil moisture variation. However, the limited access to such data imposes a limit on the application and development of these downscaling techniques for global soil moisture monitoring.

Alternative downscaling approaches that use high resolution model predictions together with data assimilation of coarse scale observations - and/or machine learning-based techniques - provide an opportunity to overcome issues related to the lack of concurrent overpasses by required satellites or lost data due to cloud coverage. However, there is considerably more work required to increase the accuracy of high resolution soil moisture prediction models, the computational efficiency of these innovative techniques, and the global training required for the machine learning technique.

Soil moisture downscaling to spatial resolutions higher than 1 km should also be considered an issue for advancing the practical use of soil moisture in agriculture and water resources management. These must also be provided at the time scale of 1 to 3 days in order to provide information about the temporal dynamics of soil moisture. The development of applicable downscaling techniques under all weather and climate conditions and across all current passive microwave observations will fill this gap. Prior to reaching this milestone, the merger of multi satellite soil moisture products should reach a level of maturity. Thus, harmonized downscaled soil moisture products from different downscaling techniques could be able to produce a consistent time series of high resolution soil moisture.

### 6.1.2 Inter-comparison of alternative downscaled soil moisture products

The first ever inter-comparison analysis of the alternative downscaled soil moisture products currently available against a common reference data set has been undertaken, to assess their suitability for the applications requiring soil moisture products at resolutions higher than 10 km. While cloudy skies limit the application of optical-based downscaled soil moisture products, the SMAP and SMOS VTCI optical-based products had the highest level of temporal agreement with OzNet and airborne PLMR soil moisture, respectively. However, they could not meet the temporal requirements for applications being 3 days or better. The use of geostationary based optical sensors which collect data at about 30 minute time intervals may help to overcome this shortcoming by increasing the chance of capturing cloud-free observations.

The oversampling-based soil moisture products (SMAP EnhancedA and SMAP EnhancedD) best captured the temporal and spatial variability of soil moisture overall, though the SMAP MOEA and A/P had a better temporal agreement with PLMR during the short SMAPE<sub>x-4</sub> period. The SMAP Enhanced products not only surpassed the other downscaled soil moisture products in terms of performance and accuracy, but also in terms of availability under all weather conditions and improvement of soil moisture retrieval over the coarse passive microwave retrievals. Furthermore, the interpolation technique used for the Enhanced soil moisture production does not require any concurrent data from other satellites.

The difference between temporal analysis of products against *in situ* and airborne soil moisture reference data sets also pointed to the fact that relying on *in situ* measurement alone is not appropriate for validation of high resolution soil moisture maps; basically *in situ* measurements that are site specific and sparsely distributed ignore the short scale spatial variation of soil moisture. Furthermore, the difference between temporal and spatial analysis of products against the airborne PLMR soil moisture maps suggests that dependence on temporal analysis is not ideal for assessing the performance of spatial variation in soil moisture products. Based on the purpose of the soil moisture application, spatial analysis should be conducted to quantify the performance of the soil moisture products in capturing the variability of soil moisture in space.

### 6.1.3 Combined downscaled soil moisture products

Application of a Gaussian merging algorithm, which accounts for uncertainties in input data, was evaluated for combining downscaled soil moisture products. The Gaussian merging algorithm is an inverse variance weighted averaging system, which combines independent input data that can be approximated by normal random variables. The precision of combined retrievals from the Gaussian technique depends on the error estimates and availability of downscaled data. Therefore, different combination scenarios were developed to investigate the combination of downscaled soil moisture products.

While different combination scenarios were tested, it was shown that the accuracy of combined products did not vary considerably. Combined products from each combination scenarios showed similar results in terms of accuracy, as well as spatio-temporal patterns.

This analysis is the first step in combining alternative downscaled soil moisture products. The results so far suggest the usefulness of merging products at 1 km, as combined products at 1 km illustrated improvement in temporal correlation and RMSD/ubRMSD over the single downscaled soil moisture products. In contrast, results from merged downscaled soil moisture products at 9 km did not justify the use of a merging procedure for enhancing the accuracy of the derived soil moisture maps, but increasing the temporal availability of soil moisture maps at 9 km does make the effort of merging worth while.

### 6.1.4 Comparison of results from this study with literature

The temporal analysis of downscaling techniques in Chapter 2 showed that while the radar-based downscaling techniques delivered more accurate soil moisture estimates than the optical- and radiometer-based downscaling techniques, the radiometer-based downscaled soil moisture products had the poorest performance. These findings are in contrast with the results in Chapter 4 from the temporal analysis of downscaled soil moisture products conducted against the OzNet *in situ* soil moisture measurements, which revealed that the optical-based downscaled soil moisture product (in this study SMAP VTCI at 9 km) had the best performance. Based on the findings of Chapter 4, the SMAP SFIM product de-

rived from the radiometer-based downscaling technique had a slightly better performance than that of the radar-based downscaled soil moisture products (SMAP A/P and MOEA). The higher sensitivity of radar backscatter to surface roughness and vegetation than the radiometric emissions, makes it acceptable to have better soil moisture estimates from the radiometer-based downscaling technique than radar-based ones; except some would argue there is no soil moisture signal in Ka-band observations which were used in the SMAP SFIM retrieval procedure. Such difference between findings emphasizes the need for direct evaluation of the downscaled soil moisture products against each other using a common reference data set for specific climate and landscape conditions.

The performance of SMOS VTCI at 9 km during the SMAPEX-4 and -5 airborne field campaign also showed superiority to the radar-based downscaled soil moisture products (SMAP A/P and MOEA), in terms of capturing the temporal dynamics of the airborne PLMR soil moisture estimates. These results were not expected because radar in general has: i) a better sensitivity to soil moisture dynamics than optical observation and, ii) a more direct relation to soil moisture dynamics.

The temporal analysis of the combined products at 1 and 9 km against the airborne PLMR soil moisture maps showed that the combination of the downscaled soil moisture products can reach the highest degree of correlation obtained by the machine learning- and radar-based downscaling techniques as reported in Chapter 2. However, the combined products could not meet the highest accuracy of radar- and soil surface attribute-based in terms of RMSD.

### **6.2 Future work**

Currently available downscaled soil moisture products retrieved from the radar-, optical-, oversampling-, and radiometer-based downscaling techniques were inter-compared in this thesis through performance analysis using soil moisture measurements from the Australian airborne campaign and soil moisture monitoring network. In addition, a merging technique was developed and tested to combine downscaled soil moisture products for improving estimates of soil moisture in space and time. Future works that are identified to expand this

research are as follows:

- The thesis focused on an analysis of the performance of downscaled soil moisture products for a typical Australian landscape and climate. Deep insight into the performance of downscaled soil moisture products requires similar inter-comparisons be undertaken for different climate conditions and landscapes. Consequently, the progression from this research is to conduct downscaled soil moisture inter-comparison over different evaluation sites around the globe.
- This thesis analysed the accuracy of downscaled soil moisture products regardless of land cover types across the Yanco region. Hence, an extensive assessment of downscaled soil moisture products may be conducted to analyse the impact of land cover types on the radar-, optical-, radiometer-, and oversampling-based downscaling algorithms. Relative errors in soil moisture estimates should be differentiated according to land cover types, including cropping, forested, and the grassland areas. Moreover, assuming that downscaled soil moisture products perform similarly for different land cover types excepting forested areas, downscaled soil moisture products may be analysed for the entire Yanco region excluding the forested area.
- Development of alternative downscaling approaches should be investigated as an expansion to this research. Since none of the tested methods had a high correlation in terms of spatial pattern, the main focus of interest in the new downscaling method should be the representation of soil moisture patterns in space. Perhaps high resolution information on land cover conditions and precipitation data could be involved in optical-based downscaling procedures. Another approach could be using more physical-based interpretation of SAR data than the empiricism of the SMAP active/passive baseline algorithm.
- Apart from the Gaussian merging technique, alternative combining techniques should be developed and tested to merge downscaled soil moisture products. The inclusion of alternative merging techniques, such as the Bayesian merging method, may result in determining the most pragmatic technique(s) for the accuracy improvement of combined products in terms of estimating temporal and spatial variability of reference soil

moisture data.

- When combining products it may also be advantageous to rescale products using a Cumulative Distribution Function (CDF) matching technique. The use of CDF matching is expected to result in adjusting downscaled soil moisture products to the same range and distribution, so that the accuracy of combined products is not deteriorated because of possible systematic differences between downscaled soil moisture products.



## References

- R. Akbar and M. Moghaddam. A combined active-passive soil moisture estimation algorithm with adaptive regularization in support of SMAP. *IEEE Transactions on Geoscience and Remote Sensing*, 53(6):3312–3324, 2015.
- R. Akbar, S. Chan, N. Das, S. Kim, D. Entekhabi, and M. Moghaddam. A multi-objective optimization approach to combined radar-radiometer soil moisture estimation. In *IEEE International Geoscience and Remote Sensing Symposium (IGARSS)*, pages 3074–3077, July 2016.
- M. C. Anderson, J. M. Norman, G. R. Diak, W. P. Kustas, and J. R. Mecikalski. A two-source time-integrated model for estimating surface fluxes using thermal infrared remote sensing. *Remote Sensing of Environment*, 60(2):195–216, 1997.
- M. C. Anderson, J. M. Norman, J. R. Mecikalski, J. A. Otkin, and W. P. Kustas. A climatological study of evapotranspiration and moisture stress across the continental united states based on thermal remote sensing: 1. model formulation. *Journal of Geophysical Research: Atmospheres*, 112(D10), 2007.
- G. Backus and F. Gilbert. Uniqueness in the inversion of inaccurate gross earth data. *Philosophical Transactions of the Royal Society of London A: Mathematical, Physical and Engineering Sciences*, 266(1173):123–192, 1970.
- G. E. Backus and J. Gilbert. Numerical applications of a formalism for geophysical inverse problems. *Geophysical Journal International*, 13(1-3):247–276, 1967.
- G. Balsamo, F. Bouyssel, and J. Noilhan. A simplified bi-dimensional variational analysis of soil moisture from screen-level observations in a mesoscale numerical weather-prediction

---

model. 130:895 – 915, 12 2006.

R. Bindlish and A. P. Barros. Subpixel variability of remotely sensed soil moisture: an inter-comparison study of sar and estar. *IEEE Transactions on Geoscience and Remote Sensing*, 40(2):326–337, 2002.

R. Bindlish, T. Jackson, M. Cosh, S. Ruijing, S. Yueh, and S. Dinardo. Combined passive and active soil moisture observations during clasic. In *IEEE International Geoscience and Remote Sensing Symposium (IGARSS)*, volume 2, pages II–237–II–240, 2008.

H. F. Blaney and W. D. Criddle. *Determining water requirements in irrigated areas from climatological and irrigation data*. USDA SCS-TP-96, U.S. Dept. of Agric., Washington, D. C, 1950.

J. D. Bolten, W. T. Crow, X. Zhan, T. J. Jackson, and C. A. Reynolds. Evaluating the utility of remotely sensed soil moisture retrievals for operational agricultural drought monitoring. *IEEE Journal of Selected Topics in Applied Earth Observations and Remote Sensing*, 3(1):57–66, 2010.

Bureau of Meterology. Climate statistics for Australian locations. Australian Government, 2018. URL <http://www.bom.gov.au/climate/data/>.

F. A. Busch, J. D. Niemann, and M. Coleman. Evaluation of an empirical orthogonal function-based method to downscale soil moisture patterns based on topographical attributes. *Hydrological Processes*, 26(18):2696–2709, 2012.

J.-C. Calvet, J.-P. Wigneron, J. Walker, F. Karbou, A. Chanzy, and C. Albergel. Sensitivity of passive microwave observations to soil moisture and vegetation water content: L-band to W-band. *IEEE Transactions on Geoscience and Remote Sensing*, 49(4):1190–1199, 2011.

A. Camps, M. Vall-llossera, M. Piles, F. Torres, I. Corbella, and N. Duffo. Improving the spatial resolution of synthetic aperture radiometer imagery using auxiliary information: Application to the SMOS mission. In *IEEE International Geoscience and Remote Sensing Symposium (IGARSS)*, volume 3, pages 411– 414, 2008.

- 
- T. N. Carlson, R. R. Gillies, and E. M. Perry. A method to make use of thermal infrared temperature and ndvi measurements to infer surface soil water content and fractional vegetation cover. *Remote Sensing Reviews*, 9(1-2):161–173, 1994.
- L. M. Castro, J. Gironás, and B. Fernández. Spatial estimation of daily precipitation in regions with complex relief and scarce data using terrain orientation. *Journal of Hydrology*, 517:481–492, 2014.
- S. Chai, J. P. Walker, B. Veenendaal, and G. West. An artificial neural network model for downscaling of passive microwave soil moisture. In *6th IASME/WSEAS International Conference on Water Resources, Hydraulics & Hydrology (WHH'11)*, pages 26–31. WSEAS Press-World Scientific and Engineering Academy and Society, 2011.
- S. S. Chai and K. L. Goh. Neural network ensembles: Combining multiple models for downscaling of soil moisture. *International Journal of Emerging Science and Engineering (IJESE)*, 2:46–50, 2013.
- S.-S. Chai, J. Walker, O. Makarynsky, M. Kuhn, B. Veenendaal, and G. West. Use of soil moisture variability in artificial neural network retrieval of soil moisture. *Remote Sensing*, 2(1):166–190, 2009.
- S. Chakrabarti, T. Bongiovanni, J. Judge, K. Nagarajan, and J. C. Principe. Downscaling satellite-based soil moisture in heterogeneous regions using high-resolution remote sensing products and information theory: A synthetic study. *IEEE Transactions on Geoscience and Remote Sensing*, 53(1):85–101, 2015.
- S. Chakrabarti, J. Judge, T. Bongiovanni, A. Rangarajan, and S. Ranka. Disaggregation of remotely sensed soil moisture in heterogeneous landscapes using holistic structure-based models. *IEEE Transactions on Geoscience and Remote Sensing*, 54(8):4629–4641, 2016.
- S. Chan, R. Bindlish, P. O’Neill, T. Jackson, E. Njoku, S. Dunbar, J. Chaubell, J. Piepmeier, S. Yueh, D. Entekhabi, A. Colliander, F. Chen, M. Cosh, T. Caldwell, J. Walker, A. Berg, H. McNairn, M. Thibeault, J. Martínez-Fernández, F. Uldall, M. Seyfried, D. Bosch, P. Starks, C. H. Collins, J. Prueger, R. van der Velde, J. Asanuma, M. Palecki, E. Small, M. Zreda, J. Calvet, W. Crow, and Y. Kerr. Development and assessment of the SMAP

- 
- enhanced passive soil moisture product. *Remote Sensing of Environment*, 204:931–941, 2018.
- S. K. Chan, R. Bindlish, P. E. O. Neill, E. Njoku, T. Jackson, A. Colliander, F. Chen, M. Burgin, S. Dunbar, J. Piepmeier, S. Yueh, D. Entekhabi, M. H. Cosh, T. Caldwell, J. Walker, X. Wu, A. Berg, T. Rowlandson, A. Pacheco, H. McNairn, M. Thibeault, J. Martínez-Fernández, G.-Z. Á, M. Seyfried, D. Bosch, P. Starks, D. Goodrich, J. Prueger, M. Palecki, E. E. Small, M. Zreda, J. C. Calvet, W. T. Crow, and Y. Kerr. Assessment of the SMAP passive soil moisture product. *IEEE Transactions on Geoscience and Remote Sensing*, 54(8):4994–5007, 2016.
- J. Chaubell. SMAP algorithm theoretical basis document: SMAP L1B enhancement radiometer brightness temperature data product. Jet Propulsion Laboratory, 2016.
- N. S. Chauhan. Soil moisture estimation under a vegetation cover: Combined active passive microwave remote sensing approach. *International Journal of Remote Sensing*, 18(5):1079–1097, 1997.
- N. S. Chauhan, S. Miller, and P. Ardanuy. Spaceborne soil moisture estimation at high resolution: a microwave-optical/IR synergistic approach. *International Journal of Remote Sensing*, 24(22):4599–4622, 2003.
- N. Chen, Y. He, and Z. Xiang. NIR-red spectra-based disaggregation of SMAP soil moisture to 250 m resolution based on SMAPEX-4/5 in southeastern Australia. *Remote Sensing*, 9:51, 2017.
- M. Choi and Y. Hur. A microwave-optical/infrared disaggregation for improving spatial representation of soil moisture using AMSR-E and MODIS products. *Remote Sensing of Environment*, 124:259–269, 2012.
- B. J. Choudhury, C. J. Tucker, R. E. Golus, and W. W. Newcomb. Monitoring vegetation using Nimbus-7 scanning multichannel microwave radiometer’s data. *International Journal of Remote Sensing*, 8(3):533–538, 1987.
- M. L. Coleman and J. D. Niemann. Controls on topographic dependence and temporal

- 
- instability in catchment-scale soil moisture patterns. *Water Resources Research*, 49(3): 1625–1642, 2013.
- A. Colliander, J. B. Fisher, G. Halverson, O. Merlin, S. Misra, R. Bindlish, T. J. Jackson, and S. Yueh. Spatial downscaling of SMAP soil moisture using MODIS land surface temperature and NDVI during SMAPVEX15. *IEEE Geoscience and Remote Sensing Letters*, 14(11):2107–2111, 2017.
- A. Coppola, A. Basile, M. Menenti, M. Buonanno, J. Colin, R. De Mascellis, M. Esposito, U. Lazzaro, V. Magliulo, and P. Manna. Spatial distribution and structure of remotely sensed surface water content estimated by a thermal inertia approach. In *Remote Sensing for Environmental Monitoring and Change Detection Symposium*, volume 316, page 3, 2007.
- C. Corradini. Soil moisture in the development of hydrological processes and its determination at different spatial scales. *Journal of Hydrology*, 516:1 – 5, 2014.
- G. S. Cowley, J. D. Niemann, T. R. Green, M. S. Seyfried, A. S. Jones, and P. J. Grazaitis. Impacts of precipitation and potential evapotranspiration patterns on downscaling soil moisture in regions with large topographic relief. *Water Resources Research*, 53(2):1553–1574, 2017.
- R. Crago and W. Brutsaert. Daytime evaporation and the self-preservation of the evaporative fraction and the bowen ratio. *Journal of Hydrology*, 178(1–4):241–255, 1996.
- W. T. Crow, A. A. Berg, M. H. Cosh, A. Loew, B. P. Mohanty, R. Panciera, P. Rosnay, D. Ryu, and J. P. Walker. Upscaling sparse ground-based soil moisture observations for the validation of coarse-resolution satellite soil moisture products. *Reviews of Geophysics*, 50(2), 2012.
- R. Dalal and R. Henry. Simultaneous determination of moisture, organic carbon, and total nitrogen by near infrared reflectance spectrophotometry. *Soil Science Society of America Journal*, 50(1):120–123, 1986.
- N. N. Das, D. Entekhabi, and E. G. Njoku. An algorithm for merging SMAP radiometer and

- 
- radar data for high-resolution soil-moisture retrieval. *IEEE Transactions on Geoscience and Remote Sensing*, 49(5):1504–1512, 2011.
- N. N. Das, D. Entekhabi, E. G. Njoku, J. J. C. Shi, J. T. Johnson, and A. Colliander. Tests of the SMAP combined radar and radiometer algorithm using airborne field campaign observations and simulated data. *IEEE Transactions on Geoscience and Remote Sensing*, 52(4):2018–2028, 2014.
- R. A. M. de Jeu, T. R. H. Holmes, R. M. Parinussa, and M. Owe. A spatially coherent global soil moisture product with improved temporal resolution. *Journal of Hydrology*, 516(0):284–296, 2014.
- G. J. De Lannoy, R. H. Reichle, P. R. Houser, V. Pauwels, and N. E. Verhoest. Correcting for forecast bias in soil moisture assimilation with the ensemble Kalman filter. *Water Resources Research*, 43(9), 2007.
- G. J. M. De Lannoy and R. H. Reichle. Assimilation of SMOS brightness temperatures or soil moisture retrievals into a land surface model. *Hydrology and Earth System Sciences*, 20(12):4895–4911, 2016a.
- G. J. M. De Lannoy and R. H. Reichle. Global assimilation of multiangle and multipolarization SMOS brightness temperature observations into the GEOS-5 catchment land surface model for soil moisture estimation. *Journal of Hydrometeorology*, 17(2):669–691, 2016b.
- N. Djamai, R. Magagi, K. Goita, O. Merlin, Y. Kerr, and A. Walker. Disaggregation of SMOS soil moisture over the Canadian Prairies. *Remote Sensing of Environment*, 170:255–268, 2015.
- N. Djamai, R. Magagi, K. Goita, O. Merlin, Y. Kerr, and A. Roy. A combination of DISPATCH downscaling algorithm with CLASS land surface scheme for soil moisture estimation at fine scale during cloudy days. *Remote Sensing of Environment*, 184:1–14, 2016.
- M. C. Dobson and F. T. Ulaby. Active microwave soil moisture research. *IEEE Transactions on Geoscience and Remote Sensing*, GE-24(1):23–36, 1986.

- 
- W. Dorigo, R. de Jeu, D. Chung, R. Parinussa, Y. Liu, W. Wagner, and D. Fernández-Prieto. Evaluating global trends (1988–2010) in harmonized multi-satellite surface soil moisture. *Geophysical Research Letters*, 39(18):L18405, 2012a.
- W. Dorigo, W. Wagner, B. Bauer-Marschallinger, D. Chung, R. de Jeu, R. Parinussa, and L. Yi. Constructing and analyzing a 32-years climate data record of remotely sensed soil moisture. In *IEEE International Geoscience and Remote Sensing Symposium (IGARSS)*, pages 2028–2031, 2012b.
- W. Dorigo, W. Wagner, C. Albergel, F. Albrecht, G. Balsamo, L. Brocca, D. Chung, M. Ertl, M. Forkel, A. Gruber, E. Haas, P. D. Hamer, M. Hirschi, J. Ikonen, R. de Jeu, R. Kidd, W. Lahoz, Y. Y. Liu, D. Miralles, T. Mistelbauer, N. Nicolai-Shaw, R. Parinussa, C. Prato, C. Reimer, R. van der Schalie, S. I. Seneviratne, T. Smolander, and P. Lecomte. ESA CCI soil moisture for improved earth system understanding: State-of-the art and future directions. *Remote Sensing of Environment*, 203:185 – 215, 2017. Earth Observation of Essential Climate Variables.
- C. Draper and R. Reichle. The impact of near-surface soil moisture assimilation at subseasonal, seasonal, and inter-annual timescales. *Hydrology and Earth System Sciences*, 19(12):4831–4844, 2015.
- C. S. Draper, J. F. Mahfouf, and J. P. Walker. An EKF assimilation of AMSR-E soil moisture into the ISBA land surface scheme. *Journal of Geophysical Research: Atmospheres*, 114(D20), 2009.
- Y. Du, F. T. Ulaby, and M. C. Dobson. Sensitivity to soil moisture by active and passive microwave sensors. *IEEE Transactions on Geoscience and Remote Sensing*, 38(1):105–114, 2000.
- E. T. Engman and N. Chauhan. Status of microwave soil moisture measurements with remote sensing. *Remote Sensing of Environment*, 51(1):189–198, 1995.
- D. Entekhabi. Recent advances in land-atmosphere interaction research. *Reviews of Geophysics*, 33(S2):995–1003, 1995.

- 
- D. Entekhabi, I. Rodriguez-Iturbe, and F. Castelli. Mutual interaction of soil moisture state and atmospheric processes. *Journal of Hydrology*, 184(1–2):3–17, 1996.
- D. Entekhabi, G. R. Asrar, A. K. Betts, K. J. Beven, R. L. Bras, C. J. Duffy, T. Dunne, R. D. Koster, D. P. Lettenmaier, D. B. McLaughlin, W. J. Shuttleworth, M. T. van Genuchten, M.-Y. Wei, and E. F. Wood. An agenda for land surface hydrology research and a call for the second international hydrological decade. *Bulletin of the American Meteorological Society*, 80(10):2043–2058, 1999.
- D. Entekhabi, T. J. Jackson, E. Njoku, P. O’Neill, and J. Entin. Soil Moisture Active/Passive (SMAP) Mission concept. volume 7085, 2008a.
- D. Entekhabi, E. Njoku, P. O’Neill, M. Spencer, T. Jackson, J. Entin, E. Im, and K. Kellogg. The Soil Moisture Active/Passive Mission (SMAP). In *IEEE International Geoscience and Remote Sensing Symposium (IGARSS)*, volume 3, 2008b.
- D. Entekhabi, E. G. Njoku, P. E. O’Neill, K. H. Kellogg, W. T. Crow, W. N. Edelstein, J. K. Entin, S. D. Goodman, T. J. Jackson, J. Johnson, J. Kimball, J. R. Piepmeier, R. D. Koster, N. Martin, K. C. McDonald, M. Moghaddam, S. Moran, R. Reichle, J. C. Shi, M. W. Spencer, S. W. Thurman, T. Leung, and J. Van Zyl. The Soil Moisture Active Passive (SMAP) Mission. *Proceedings of the IEEE*, 98(5):704–716, 2010.
- B. Fang and V. Lakshmi. AMSR-E soil moisture disaggregation using MODIS and NLDAS data. In *Remote Sensing of the Terrestrial Water Cycle*, pages 277–304. John Wiley & Sons, Inc, 2014a.
- B. Fang and V. Lakshmi. Soil moisture at watershed scale: Remote sensing techniques. *Journal of Hydrology*, 516(0):258–272, 2014b.
- B. Fang, V. Lakshmi, R. Bindlish, T. J. Jackson, M. Cosh, and J. Basara. Passive microwave soil moisture downscaling using vegetation index and skin surface temperature. *Vadose Zone Journal*, 12(3), 2013.
- J. Franke, J. Häntzschel, V. Goldberg, and C. Bernhofer. Application of a trigonometric approach to the regionalization of precipitation for a complex small-scale terrain in a GIS

- 
- environment. *Meteorological Applications*, 15(4):483–490, 2008.
- M. A. Friedl and F. W. Davis. Sources of variation in radiometric surface temperature over a tallgrass prairie. *Remote Sensing of Environment*, 48(1):1–17, 1994.
- B.-C. Gao. NDWI—a normalized difference water index for remote sensing of vegetation liquid water from space. *Remote sensing of environment*, 58(3):257–266, 1996.
- Y. Gao, J. P. Walker, M. Allahmoradi, A. Monerris, R. Dongryeol, and T. J. Jackson. Optical sensing of vegetation water content: A synthesis study. *IEEE Journal of Selected Topics in Applied Earth Observations and Remote Sensing*, 8(4):1456–1464, 2015.
- M. Garcia, N. Fernández, L. Villagarcía, F. Domingo, J. Puigdefábregas, and I. Sandholt. Accuracy of the temperature–vegetation dryness index using MODIS under water-limited vs. energy-limited evapotranspiration conditions. *Remote Sensing of Environment*, 149: 100–117, 2014.
- D. Geudtner. Sentinel-1 system overview and performance. *Proc. SPIE 8528, Earth Observing Missions and Sensors: Development, Implementation, and Characterization II*, 2012.
- D. Geudtner and R. Torres. Sentinel-1 system overview and performance. In *IEEE Transactions on Geoscience and Remote Sensing Symposium (IGARSS)*, pages 1719–1721. IEEE, 2012. ISBN 1467311596.
- A. I. Gevaert, R. M. Parinussa, L. J. Renzullo, A. I. J. M. van Dijk, and R. A. M. de Jeu. Spatio-temporal evaluation of resolution enhancement for passive microwave soil moisture and vegetation optical depth. *International Journal of Applied Earth Observation and Geoinformation*, 2015.
- R. R. Gillies and T. N. Carlson. Thermal remote sensing of surface soil water content with partial vegetation cover for incorporation into climate models. *Journal of Applied Meteorology*, 34(4):745–756, 1995.
- S. N. Goward, Y. Xue, and K. P. Czajkowski. Evaluating land surface moisture conditions from the remotely sensed temperature/vegetation index measurements: An exploration

- 
- with the simplified simple biosphere model. *Remote sensing of environment*, 79(2):225–242, 2002.
- J. P. Grant, K. Saleh-Contell, J. P. Wigneron, M. Guglielmetti, Y. H. Kerr, M. Schwank, N. Skou, and A. A. V. de Griend. Calibration of the L-MEB model over a coniferous and a deciduous forest. *IEEE Transactions on Geoscience and Remote Sensing*, 46(3): 808–818, 2008.
- A. Gruber, C.-H. Su, S. Zwieback, W. Crow, W. Dorigo, and W. Wagner. Recent advances in (soil moisture) triple collocation analysis. *International Journal of Applied Earth Observation and Geoinformation*, 45:200 – 211, 2016. Advances in the Validation and Application of Remotely Sensed Soil Moisture - Part 1.
- C. R. Hain, J. R. Mecikalski, and M. C. Anderson. Retrieval of an available water-based soil moisture proxy from thermal infrared remote sensing. part i: Methodology and validation. *Journal of Hydrometeorology*, 10(3):665–683, 2009.
- L. K. Hansen and P. Salamon. Neural network ensembles. *IEEE Transactions on Pattern Analysis & Machine Intelligence*, (10):993–1001, 1990.
- C. L. Hanson. Distribution and stochastic generation of annual and monthly precipitation on a mountainous watershed in southwest Idaho. *JAWRA Journal of the American Water Resources Association*, 18(5):875–883, 1982.
- M. Hemakumara, J. Kalma, J. Walker, and G. Willgoose. Downscaling of low resolution passive microwave soil moisture observations. In *Proceedings of the 2nd International CAHMDA Workshop on: The Terrestrial Water Cycle: Modeling and Data Assimilation Across Catchment Scales*, pages 25–27, 2004.
- M. Hirschi, S. I. Seneviratne, V. Alexandrov, F. Boberg, C. Boroneant, O. B. Christensen, H. Formayer, B. Orłowsky, and P. Stepanek. Observational evidence for soil-moisture impact on hot extremes in southeastern Europe. *Nature Geosci*, 4(1):17–21, 2011.
- D. C. Hoehn, J. D. Niemann, T. R. Green, A. S. Jones, and P. J. Grazaitis. Downscaling soil moisture over regions that include multiple coarse-resolution grid cells. *Remote Sensing*

- 
- of Environment*, 199:187–200, 2017.
- A. Huete, R. Jackson, and D. Post. Spectral response of a plant canopy with different soil backgrounds. *Remote sensing of environment*, 17(1):37–53, 1985.
- J. Im, S. Park, J. Rhee, J. Baik, and M. Choi. Downscaling of AMSR-E soil moisture with MODIS products using machine learning approaches. *Environmental Earth Sciences*, 75(15):1120, 2016.
- A. V. M. Ines, B. P. Mohanty, and Y. Shin. An unmixing algorithm for remotely sensed soil moisture. *Water Resources Research*, 49(1):408–425, 2013.
- T. J. Jackson. Iii. measuring surface soil moisture using passive microwave remote sensing. *Hydrological Processes*, 7(2):139–152, 1993.
- T. J. Jackson and T. J. Schmugge. Passive microwave remote sensing system for soil moisture: some supporting research. *IEEE Transactions on Geoscience and Remote Sensing*, 27(2):225–235, 1989. ISSN 0196-2892.
- R. B. Jana. *Scaling characteristics of soil hydraulic parameters at varying spatial resolutions*. Texas A&M University, 2010.
- H. Jiang, H. Shen, H. Li, F. Lei, W. Gan, and L. Zhang. Evaluation of multiple downscaled microwave soil moisture products over the central Tibetan Plateau. *Remote Sensing*, 9(5):402, 2017.
- L. Jiang and S. Islam. An intercomparison of regional latent heat flux estimation using remote sensing data. *International Journal of Remote Sensing*, 24(11):2221–2236, 2003.
- M. Jung, M. Reichstein, P. Ciais, S. I. Seneviratne, J. Sheffield, M. L. Goulden, G. Bonan, A. Cescatti, J. Chen, R. de Jeu, A. J. Dolman, W. Eugster, D. Gerten, D. Gianelle, N. Gobron, J. Heinke, J. Kimball, B. E. Law, L. Montagnani, Q. Mu, B. Mueller, K. Oleson, D. Papale, A. D. Richardson, O. Roupsard, S. Running, E. Tomelleri, N. Viovy, U. Weber, C. Williams, E. Wood, S. Zaehle, and K. Zhang. Recent decline in the global land evapotranspiration trend due to limited moisture supply. *Nature*, 467(7318):951–954, 2010.

- 
- Y. H. Kaheil, M. K. Gill, M. McKee, L. A. Bastidas, and E. Rosero. Downscaling and assimilation of surface soil moisture using ground truth measurements. *IEEE Transactions on Geoscience and Remote Sensing*, 46(5):1375–1384, 2008.
- Y. Kerr, J. Wigneron, A. Al Bitar, A. Mialon, and P. Srivastava. Soil moisture from space: Techniques and limitations. *Satellite Soil Moisture Retrieval: Techniques and Applications*, page 1, 2016.
- Y. H. Kerr, P. Waldteufel, J. P. Wigneron, J. Martinuzzi, J. Font, and M. Berger. Soil moisture retrieval from space: the Soil Moisture and Ocean Salinity (SMOS) mission. *IEEE Transactions on Geoscience and Remote Sensing*, 39(8):1729–1735, 2001.
- Y. H. Kerr, P. Waldteufel, P. Richaume, J. P. Wigneron, P. Ferrazzoli, A. Mahmoodi, A. A. Bitar, F. Cabot, C. Gruhier, S. E. Juglea, D. Leroux, A. Mialon, and S. Delwart. The SMOS soil moisture retrieval algorithm. *IEEE Transactions on Geoscience and Remote Sensing*, 50(5):1384–1403, 2012.
- G. Kim and A. P. Barros. Downscaling of remotely sensed soil moisture with a modified fractal interpolation method using contraction mapping and ancillary data. *Remote Sensing of Environment*, 83(3):400–413, 2002a.
- G. Kim and A. P. Barros. Space–time characterization of soil moisture from passive microwave remotely sensed imagery and ancillary data. *Remote Sensing of Environment*, 81(2–3):393–403, 8// 2002b. ISSN 0034-4257.
- J. Kim and T. S. Hogue. Improving spatial soil moisture representation through integration of AMSR-E and MODIS products. *IEEE Transactions on Geoscience and Remote Sensing*, 50(2):446–460, 2012.
- S. Kim, K. Balakrishnan, Y. Liu, F. Johnson, and A. Sharma. Spatial disaggregation of coarse soil moisture data by using high-resolution remotely sensed vegetation products. *IEEE Geoscience and Remote Sensing Letters*, 14(9):1604–1608, 2017.
- K. C. Kornelsen, M. H. Cosh, and P. Coulibaly. Potential of bias correction for downscaling passive microwave and soil moisture data. *Journal of Geophysical Research*:

---

*Atmospheres*, 120(13):6460–6479, 2015.

- R. D. Koster, M. J. Suarez, A. Ducharne, M. Stieglitz, and P. Kumar. A catchment-based approach to modeling land surface processes in a general circulation model: 1. model structure. *Journal of Geophysical Research: Atmospheres*, 105(D20):24809–24822, 2000.
- R. D. Koster, P. A. Dirmeyer, Z. Guo, G. Bonan, E. Chan, P. Cox, C. T. Gordon, S. Kanae, E. Kowalczyk, D. Lawrence, P. Liu, C.-H. Lu, S. Malyshev, B. McAvaney, K. Mitchell, D. Mocko, T. Oki, K. Oleson, A. Pitman, Y. C. Sud, C. M. Taylor, D. Verseghy, R. Vasic, Y. Xue, and T. Yamada. Regions of strong coupling between soil moisture and precipitation. *Science*, 305(5687):1138–1140, 2004.
- R. D. Koster, S. P., P. M., T. J. Yamada, G. Balsamo, A. A. Berg, M. Boissarie, P. A. Dirmeyer, F. Doblas-Reyes, G. Drewitt, C. T. Gordon, Z. Guo, J. . Jeong, D. M. Lawrence, W. . Lee, Z. Li, L. Luo, S. Malyshev, W. J. Merryfield, S. I. Seneviratne, T. Stanelle, B. J., J. M. v. d. H., F. Vitart, and E. F. Wood. Contribution of land surface initialization to subseasonal forecast skill: First results from a multi-model experiment. *Geophysical Research Letters*, 37(2), 2010.
- P. C. Kyriakidis, J. Kim, and N. L. Miller. Geostatistical mapping of precipitation from rain gauge data using atmospheric and terrain characteristics. *Journal of Applied Meteorology*, 40(11):1855–1877, 2001.
- V. Lakshmi. Remote sensing of soil moisture. *ISRN Soil Science*, 2013:33, 2013.
- C. H. Lee, S. Cook, J. Sung Lee, and B. Han. Comparison of two meta-analysis methods: Inverse-variance-weighted average and weighted sum of z-scores. *Genomics & Informatics*, 14:173, 2016.
- T. J. Lee and R. A. Pielke. Estimating the soil surface specific humidity. *Journal of Applied Meteorology*, 31(5):480–484, 1992.
- A. P. Leone and S. Sommer. Multivariate analysis of laboratory spectra for the assessment of soil development and soil degradation in the southern Apennines (Italy). *Remote Sensing of Environment*, 72(3):346–359, 2000.

- 
- X. Liang, D. P. Lettenmaier, E. F. Wood, and S. J. Burges. A simple hydrologically based model of land surface water and energy fluxes for general circulation models. *Journal of Geophysical Research: Atmospheres*, 99(D7):14415–14428, 1994.
- X. Liang, E. F. Wood, and D. P. Lettenmaier. Surface soil moisture parameterization of the vic-2l model: Evaluation and modification. *Global and Planetary Change*, 13(1): 195–206, 1996.
- X. Liang, E. F. Wood, and D. P. Lettenmaier. Modeling ground heat flux in land surface parameterization schemes. *Journal of Geophysical Research: Atmospheres*, 104(D8): 9581–9600, 1999.
- H. Lievens, S. K. Tomer, A. Al Bitar, G. J. M. De Lannoy, M. Drusch, G. Dumedah, H. J. Hendricks Franssen, Y. H. Kerr, B. Martens, M. Pan, J. K. Roundy, H. Vereecken, J. P. Walker, E. F. Wood, N. E. C. Verhoest, and V. R. N. Pauwels. SMOS soil moisture assimilation for improved hydrologic simulation in the Murray Darling Basin, Australia. *Remote Sensing of Environment*, 168:146–162, 2015.
- H. Lievens, R. H. Reichle, Q. Liu, G. J. M. De Lannoy, R. S. Dunbar, S. B. Kim, N. N. Das, M. Cosh, J. P. Walker, and W. Wagner. Joint Sentinel-1 and SMAP data assimilation to improve soil moisture estimates. *Geophysical Research Letters*, 44(12):6145–6153, 2017.
- J. G. Liu. Smoothing filter-based intensity modulation: A spectral preserve image fusion technique for improving spatial details. *International Journal of Remote Sensing*, 21(18): 3461–3472, 2000.
- W. Liu, F. Baret, G. Xingfa, T. Qingxi, Z. Lanfen, and Z. Bing. Relating soil surface moisture to reflectance. *Remote Sensing of Environment*, 81(2–3):238–246, 2002.
- Y. Y. Liu, R. M. Parinussa, W. A. Dorigo, R. A. M. De Jeu, W. Wagner, A. I. J. M. van Dijk, M. F. McCabe, and J. P. Evans. Developing an improved soil moisture dataset by blending passive and active microwave satellite-based retrievals. *Hydrology and Earth System Sciences*, 15(2):425–436, 2011.

- 
- Y. Y. Liu, W. A. Dorigo, R. M. Parinussa, R. A. M. de Jeu, W. Wagner, M. F. McCabe, J. P. Evans, and A. I. J. M. van Dijk. Trend-preserving blending of passive and active microwave soil moisture retrievals. *Remote Sensing of Environment*, 123(0):280–297, 2012.
- C. D. Lloyd. Assessing the effect of integrating elevation data into the estimation of monthly precipitation in great britain. *Journal of Hydrology*, 308(1):128–150, 2005.
- A. Loew and W. Mauser. On the disaggregation of passive microwave soil moisture data using a priori knowledge of temporally persistent soil moisture fields. *IEEE Transactions on Geoscience and Remote Sensing*, 46(3):819–834, 2008.
- D. G. Long. Reconstruction and resolution enhancement techniques for microwave sensors. 2003.
- D. G. Long and D. L. Daum. Spatial resolution enhancement of SSM/I data. *IEEE Transactions on Geoscience and Remote Sensing*, 36(2):407–417, 1998.
- J.-F. Mahfouf, K. Bergaoui, C. Draper, F. Bouyssel, F. Taillefer, and L. Taseva. A comparison of two off-line soil analysis schemes for assimilation of screen level observations. 114, 04 2009.
- Y. Malbêteau, O. Merlin, B. Molero, C. Rüdiger, and S. Bacon. DisPATCH as a tool to evaluate coarse-scale remotely sensed soil moisture using localized in situ measurements: Application to SMOS and AMSR-E data in southeastern Australia. *International Journal of Applied Earth Observation and Geoinformation*, 2016.
- K. Mallick, B. K. Bhattacharya, and N. K. Patel. Estimating volumetric surface moisture content for cropped soils using a soil wetness index based on surface temperature and NDVI. *Agricultural and Forest Meteorology*, 149(8):1327–1342, 2009.
- A. Maltese, P. Bates, F. Capodici, M. Cannarozzo, G. Ciruolo, and G. La Loggia. Critical analysis of thermal inertia approaches for surface soil water content retrieval. *Hydrological Sciences Journal*, 58(5):1144–1161, 2013.
- K.-b. Mao, Y. Ma, L. Xia, H.-j. Tang, and L.-j. Han. The monitoring analysis for the drought

- 
- in China by using an improved MPI method. *Journal of Integrative Agriculture*, 11(6): 1048–1058, 2012.
- G. Mascaro, E. R. Vivoni, and R. Deidda. Downscaling soil moisture in the southern Great Plains through a calibrated multifractal model for land surface modeling applications. *Water Resources Research*, 46(8), 2010.
- G. Mascaro, E. R. Vivoni, and R. Deidda. Soil moisture downscaling across climate regions and its emergent properties. *Journal of Geophysical Research: Atmospheres*, 116(D22): n/a–n/a, 2011.
- M. J. McFarland, R. L. Miller, and C. M. U. Neale. Land surface temperature derived from the SSM/I passive microwave brightness temperatures. *IEEE Transactions on Geoscience and Remote Sensing*, 28(5):839–845, 1990. ISSN 0196-2892.
- J. R. Mecikalski, G. R. Diak, M. C. Anderson, and J. M. Norman. Estimating fluxes on continental scales using remotely sensed data in an atmospheric–land exchange model. *Journal of Applied Meteorology*, 38(9):1352–1369, 1999.
- A. G. C. A. Meesters, R. A. M. D. Jeu, and M. Owe. Analytical derivation of the vegetation optical depth from the microwave polarization difference index. *IEEE Geoscience and Remote Sensing Letters*, 2(2):121–123, 2005.
- O. Merlin, A. G. Chehbouni, Y. H. Kerr, E. G. Njoku, and D. Entekhabi. A combined modeling and multispectral/multiresolution remote sensing approach for disaggregation of surface soil moisture: application to SMOS configuration. *IEEE Transactions on Geoscience and Remote Sensing*, 43(9):2036–2050, 2005.
- O. Merlin, A. Chehbouni, Y. H. Kerr, and D. C. Goodrich. A downscaling method for distributing surface soil moisture within a microwave pixel: Application to the monsoon '90 data. *Remote Sensing of Environment*, 101(3):379–389, 2006.
- O. Merlin, J. P. Walker, R. Panciera, J. D. Young, R. K., and E. J. Kim. Calibration of a soil moisture sensor in heterogeneous terrain with the national airborne field experiment (NAFE) data. In *MODSIM 2007 International Congress on Modelling and Simulation*.

---

*Modelling and Simulation Society of Australia and New Zealand, 2007.*

- O. Merlin, A. Chehbouni, J. P. Walker, R. Panciera, and Y. H. Kerr. A simple method to disaggregate passive microwave-based soil moisture. *IEEE Transactions on Geoscience and Remote Sensing*, 46(3):786–796, 2008a.
- O. Merlin, J. P. Walker, A. Chehbouni, and Y. Kerr. Towards deterministic downscaling of SMOS soil moisture using MODIS derived soil evaporative efficiency. *Remote Sensing of Environment*, 112(10):3935–3946, 2008b.
- O. Merlin, A. Al Bitar, J. P. Walker, and Y. Kerr. A sequential model for disaggregating near-surface soil moisture observations using multi-resolution thermal sensors. *Remote Sensing of Environment*, 113(10):2275–2284, 2009.
- O. Merlin, A. Al Bitar, J. P. Walker, and Y. Kerr. An improved algorithm for disaggregating microwave-derived soil moisture based on red, near-infrared and thermal-infrared data. *Remote Sensing of Environment*, 114(10):2305–2316, 2010.
- O. Merlin, C. Rudiger, A. Al Bitar, P. Richaume, J. P. Walker, and Y. H. Kerr. Disaggregation of SMOS soil moisture in southeastern Australia. *IEEE Transactions on Geoscience and Remote Sensing*, 50(5):1556–1571, 2012.
- O. Merlin, M. J. Escorihuela, M. A. Mayoral, O. Hagolle, A. Al Bitar, and Y. Kerr. Self-calibrated evaporation-based disaggregation of SMOS soil moisture: An evaluation study at 3km and 100m resolution in Catalunya, Spain. *Remote Sensing of Environment*, 130(0):25–38, 2013.
- O. Merlin, Y. Malbêteau, Y. Notfi, S. Bacon, S. Khabba, and L. Jarlan. Performance metrics for soil moisture downscaling methods: Application to dispatch data in central morocco. *Remote Sensing*, 7(4):3783–3807, 2015.
- M. Minacapilli, M. Iovino, and F. Blanda. High resolution remote estimation of soil surface water content by a thermal inertia approach. *Journal of Hydrology*, 379(3–4):229–238, 2009.
- B. P. Mohanty, M. H. Cosh, V. Lakshmi, and C. Montzka. Soil moisture remote sensing:

---

State-of-the-science. *Vadose Zone Journal*, 16(1), 2017.

- B. Molero, O. Merlin, Y. Malbêteau, A. Al Bitar, F. Cabot, V. Stefan, Y. Kerr, S. Bacon, M. H. Cosh, R. Bindlish, and T. J. Jackson. SMOS disaggregated soil moisture product at 1 km resolution: Processor overview and first validation results. *Remote Sensing of Environment*, 180:361–376, 2016.
- C. Montzka, S. Hasan, H. Bogaena, I. Hajnsek, R. Horn, T. Jagdhuber, A. Reigber, N. Hermes, C. Rüdiger, and H. Vereecken. Active and passive airborne microwave remote sensing for soil moisture retrieval in the Rur catchment, Germany. In *IEEE International Geoscience and Remote Sensing Symposium*, pages 6956–6959, 22-27 July 2012.
- C. Montzka, T. Jagdhuber, R. Horn, H. R. Bogaena, I. Hajnsek, A. Reigber, and H. Vereecken. Investigation of SMAP fusion algorithms with airborne active and passive L-band microwave remote sensing. *IEEE Transactions on Geoscience and Remote Sensing*, 54(7): 3878–3889, 2016.
- M. S. Moran, T. R. Clarke, Y. Inoue, and A. Vidal. Estimating crop water deficit using the relation between surface-air temperature and spectral vegetation index. *Remote Sensing of Environment*, 49(3):246–263, 1994.
- M. S. Moran, D. C. Hymer, J. Qi, and E. E. Sano. Soil moisture evaluation using multi-temporal Synthetic Aperture Radar (SAR) in semiarid rangeland. *Agricultural and Forest Meteorology*, 105(1–3):69–80, 2000.
- E. Muller and H. Décamps. Modeling soil moisture–reflectance. *Remote Sensing of Environment*, 76(2):173–180, 2001.
- U. Narayan and V. Lakshmi. Characterizing subpixel variability of low resolution radiometer derived soil moisture using high resolution radar data. *Water Resources Research*, 44(6), 2008.
- U. Narayan, V. Lakshmi, and T. J. Jackson. High-resolution change estimation of soil moisture using L-band radiometer and radar observations made during the SMEX02 experiments. *IEEE Transactions on Geoscience and Remote Sensing*, 44(6):1545–1554, 2006.

- 
- C. M. U. Neale, M. J. McFarland, and K. Chang. Land-surface-type classification using microwave brightness temperatures from the special sensor microwave/imager. *IEEE Transactions on Geoscience and Remote Sensing*, 28(5):829–838, 1990.
- R. Nemani, L. Pierce, S. Running, and S. Goward. Developing satellite-derived estimates of surface moisture status. *Journal of Applied Meteorology*, 32(3):548–557, 1993.
- E. Njoku, K. Yunjin, M. Spencer, Y. Rahmat-Samii, and M. W. Thomson. A spaceborne L-band radiometer-radar concept for land and ocean surface monitoring. In *Aerospace Conference, IEEE Proceedings.*, volume 4, pages 4/1841–4/1848 vol.4, 2001.
- E. G. Njoku and D. Entekhabi. Passive microwave remote sensing of soil moisture. *Journal of Hydrology*, 184(1–2):101–129, 1996.
- E. G. Njoku, W. J. Wilson, S. H. Yueh, and Y. Rahmat-Samii. A large-antenna microwave radiometer-scatterometer concept for ocean salinity and soil moisture sensing. *IEEE Transactions on Geoscience and Remote Sensing*, 38(6):2645–2655, 2000.
- E. G. Njoku, W. J. Wilson, S. H. Yueh, S. J. Dinardo, K. L. Fuk, T. J. Jackson, V. Lakshmi, and J. Bolten. Observations of soil moisture using a passive and active low-frequency microwave airborne sensor during SGP99. *IEEE Transactions on Geoscience and Remote Sensing*, 40(12):2659–2673, 2002.
- J. Noilhan and S. Planton. A simple parameterization of land surface processes for meteorological models. *Monthly Weather Review*, 117(3):536–549, 1989.
- C. Notarnicola, M. Angiulli, and F. Posa. Soil moisture retrieval from remotely sensed data: Neural network approach versus bayesian method. *IEEE Transactions on Geoscience and Remote Sensing*, 46(2):547–557, 2008.
- P. O’Neill, D. Entekhabi, E. Njoku, and K. Kellogg. The NASA Soil Moisture Active Passive (SMAP) mission: Overview. In *IEEE International Geoscience and Remote Sensing Symposium (IGARSS)*, pages 3236–3239, 2010.
- P. O’Neill, R. Bindlish, S. Chan, E. Njoku, and T. Jackson. Algorithm theoretical basis document, Level 2 and 3 soil moisture (passive) data products, 2018.

- 
- P. E. O'Neill and N. Chauhan. Synergistic use of active and passive microwave in soil moisture estimation. In *International Geoscience and Remote Sensing Symposium, 1992. IGARSS '92.*, volume 1, pages 492–494, 26-29 May 1992 1992.
- P. E. O'Neill, N. S. Chauhan, and T. J. Jackson. Use of active and passive microwave remote sensing for soil moisture estimation through corn. *International Journal of Remote Sensing*, 17(10):1851–1865, 1996.
- M. Owe and A. A. Van de Griend. Comparison of soil moisture penetration depths for several bare soils at two microwave frequencies and implications for remote sensing. *Water Resources Research*, 34(9):2319–2327, 1998.
- M. Owe, R. de Jeu, and J. Walker. A methodology for surface soil moisture and vegetation optical depth retrieval using the microwave polarization difference index. 39:1643 – 1654, 09 2001.
- M. Owe, R. de Jeu, and T. Holmes. Multisensor historical climatology of satellite-derived global land surface moisture. *Journal of Geophysical Research: Earth Surface*, 113(F1), 2008.
- S. Paloscia, S. Pettinato, E. Santi, C. Notarnicola, L. Pasolli, and A. Reppucci. Soil moisture mapping using Sentinel-1 images: Algorithm and preliminary validation. *Remote Sensing of Environment*, 134:234–248, 2013.
- P. Pampaloni and S. Paloscia. Experimental relationships between microwave emission and vegetation features. *International Journal of Remote Sensing*, 6(2):315–323, 1985.
- R. Panciera, J. P. Walker, J. D. Kalma, E. J. Kim, J. M. Hacker, O. Merlin, M. Berger, and N. Skou. The NAFE'05/CoSMOS data set: Toward SMOS soil moisture retrieval, downscaling, and assimilation. *IEEE Transactions on Geoscience and Remote Sensing*, 46(3):736–745, 2008.
- R. Panciera, J. P. Walker, J. D. Kalma, E. J. Kim, K. Saleh, and J.-P. Wigneron. Evaluation of the SMOS L-MEB passive microwave soil moisture retrieval algorithm. *Remote Sensing of Environment*, 113(2):435–444, 2009.

- 
- R. Panciera, J. P. Walker, T. J. Jackson, D. A. Gray, M. A. Tanase, D. Ryu, A. Monerris, H. Yardley, C. Rüdiger, X. Wu, Y. Gao, and J. M. Hacker. The soil moisture active passive experiments (SMAPEX): Toward soil moisture retrieval from the SMAP mission. *IEEE Transactions on Geoscience and Remote Sensing*, 52(1):490–507, 2014.
- L. M. Parada and X. Liang. A downscaling framework for l band radiobrightness temperature imagery. *Journal of Geophysical Research: Atmospheres*, 108(D22), 2003.
- R. M. Parinussa, M. T. Yilmaz, M. C. Anderson, C. R. Hain, and R. A. M. de Jeu. An intercomparison of remotely sensed soil moisture products at various spatial scales over the Iberian Peninsula. *Hydrological Processes*, 28(18):4865–4876, 2014.
- S. Park, J. Im, S. Park, and J. Rhee. AMSR2 soil moisture downscaling using multisensor products through machine learning approach. In *2015 IEEE International Geoscience and Remote Sensing Symposium (IGARSS)*, pages 1984–1987, 26-31 July 2015.
- N. R. Patel, R. Anapashsha, S. Kumar, S. K. Saha, and V. K. Dadhwal. Assessing potential of MODIS derived temperature/vegetation condition index (TVDI) to infer soil moisture status. *International Journal of Remote Sensing*, 30(1):23–39, 2009.
- J. Pellenq, J. Kalma, G. Boulet, G. M. Saulnier, S. Wooldridge, Y. Kerr, and A. Chehbouni. A disaggregation scheme for soil moisture based on topography and soil depth. *Journal of Hydrology*, 276(1–4):112–127, 2003.
- J. Peng, J. Niesel, and A. Loew. Evaluation of soil moisture downscaling using a simple thermal-based proxy – the REMEDHUS network (Spain) example. *Hydrology and Earth System Sciences*, 19(12):4765–4782, 2015.
- J. Peng, A. Loew, Z. Shiqiang, W. Jie, and J. Niesel. Spatial downscaling of satellite soil moisture data using a vegetation temperature condition index. *IEEE Transactions on Geoscience and Remote Sensing*, 54(1):558–566, 2016.
- J. Peng, A. Loew, O. Merlin, and N. E. C. Verhoest. A review of spatial downscaling of satellite remotely sensed soil moisture. *Reviews of Geophysics*, 2017.
- M. A. Perry and J. D. Niemann. Analysis and estimation of soil moisture at the catchment

- 
- scale using eofs. *Journal of Hydrology*, 334(3):388–404, 2007.
- M. A. Perry and J. D. Niemann. Generation of soil moisture patterns at the catchment scale by EOF interpolation. *Hydrology and Earth System Sciences*, 12(1):39–53, 2008.
- G. P. Petropoulos, G. Ireland, and B. Barrett. Surface soil moisture retrievals from remote sensing: Current status, products & future trends. *Physics and Chemistry of the Earth, Parts A/B/C*, (0), 2015.
- M. Piles, A. Camps, M. Vall-llossera, and M. Talone. Spatial-resolution enhancement of SMOS data: A deconvolution-based approach. *IEEE Transactions on Geoscience and Remote Sensing*, 47(7):2182–2192, 2009a.
- M. Piles, D. Entekhabi, and A. Camps. A change detection algorithm for retrieving high-resolution soil moisture from SMAP radar and radiometer observations. *IEEE Transactions on Geoscience and Remote Sensing*, 47(12):4125–4131, 2009b.
- M. Piles, A. Camps, M. Vall-llossera, I. Corbella, R. Panciera, C. Rudiger, Y. H. Kerr, and J. Walker. Downscaling SMOS-derived soil moisture using MODIS visible/infrared data. *IEEE Transactions on Geoscience and Remote Sensing*, 49(9):3156–3166, 2011.
- M. Piles, M. Vall-llossera, L. Laguna, and A. Camps. A downscaling approach to combine SMOS multi-angular and full-polarimetric observations with MODIS VIS/IR data into high resolution soil moisture maps. In *IEEE International Geoscience and Remote Sensing Symposium (IGARSS)*, pages 1247–1250, 22-27 July 2012. ISBN 2153-6996.
- M. Piles, M. Vall-llossera, A. Camps, N. Sánchez, J. Martínez-Fernández, J. Martínez, V. González-Gambau, and R. Riera. On the synergy of SMOS and Terra/Aqua MODIS: High resolution soil moisture maps in near real-time. In *IEEE International Geoscience and Remote Sensing Symposium (IGARSS)*, pages 3423–3426, 21-26 July 2013. ISBN 2153-6996.
- M. Piles, N. Sanchez, M. Vall-llossera, A. Camps, J. Martinez-Fernandez, J. Martinez, and V. Gonzalez-Gambau. A downscaling approach for SMOS land observations: Evaluation of high-resolution soil moisture maps over the Iberian Peninsula. *IEEE Journal of Se-*

- 
- lected Topics in Applied Earth Observations and Remote Sensing*, 7(9):3845–3857, 2014.
- M. Piles, G. P. Petropoulos, N. Sánchez, n. González-Zamora, and G. Ireland. Towards improved spatio-temporal resolution soil moisture retrievals from the synergy of SMOS and MSG SEVIRI spaceborne observations. *Remote Sensing of Environment*, 180:403–417, 2016.
- G. A. Poe. Optimum interpolation of imaging microwave radiometer data. *IEEE Transactions on geoscience and remote sensing*, 28(5):800–810, 1990.
- A. Quesney, S. Le Hégarat-Masclé, O. Taconet, D. Vidal-Madjar, J. P. Wigneron, C. Loumagne, and M. Normand. Estimation of watershed soil moisture index from ERS/SAR data. *Remote Sensing of Environment*, 72(3):290–303, 2000.
- K. J. Ranney, J. D. Niemann, B. M. Lehman, T. R. Green, and A. S. Jones. A method to downscale soil moisture to fine resolutions using topographic, vegetation, and soil data. *Advances in Water Resources*, 76:81–96, 2015.
- C. Rüdiger, C. H. Su, D. Ryu, and W. Wagner. Disaggregation of low-resolution L-band radiometry using C-band radar data. *IEEE Geoscience and Remote Sensing Letters*, 13(10):1425–1429, 2016.
- R. Reichle, R. Koster, G. De Lannoy, W. Crow, and J. Kimball. SMAP Algorithm Theoretical Basis Document (ATBD): Level 4 surface and root zone soil moisture data product. Jet Propulsion Lab, 2014.
- R. H. Reichle, D. Entekhabi, and D. B. McLaughlin. Downscaling of radio brightness measurements for soil moisture estimation: A four-dimensional variational data assimilation approach. *Water Resources Research*, 37(9):2353–2364, 2001.
- R. H. Reichle, G. J. M. De Lannoy, Q. Liu, J. V. Ardizzone, A. Colliander, A. Conaty, W. Crow, T. J. Jackson, L. A. Jones, J. S. Kimball, R. D. Koster, S. P. Mahanama, E. B. Smith, A. Berg, S. Bircher, D. Bosch, T. G. Caldwell, M. Cosh, n. González-Zamora, C. D. Holifield Collins, K. H. Jensen, S. Livingston, E. Lopez-Baeza, J. Martínez-Fernández, H. McNairn, M. Moghaddam, A. Pacheco, T. Pellarin, J. Prueger, T. Row-

- 
- landson, M. Seyfried, P. Starks, Z. Su, M. Thibeault, R. van der Velde, J. Walker, X. Wu, and Y. Zeng. Assessment of the SMAP level-4 surface and root-zone soil moisture product using in situ measurements. *Journal of Hydrometeorology*, 18(10):2621–2645, 2017.
- R. Remesan, M. A. Shamim, D. Han, and J. Mathew. Runoff prediction using an integrated hybrid modelling scheme. *Journal of Hydrology*, 372(1–4):48–60, 2009.
- A. J. Richardson and C. Wiegand. Distinguishing vegetation from soil background information. *Photogrammetric Engineering and Remote Sensing*, 43(12):1541–1552, 1977.
- D. Robinson, C. Campbell, J. Hopmans, B. Hornbuckle, S. B. Jones, R. Knight, F. Ogden, J. Selker, and O. Wendroth. Soil moisture measurement for ecological and hydrological watershed-scale observatories: A review. *Vadose Zone Journal*, 7(1):358–389, 2008.
- J. W. Rouse, R. Haas, J. Schell, and D. Deering. Monitoring vegetation systems in the great plains with erts. 1974.
- S. Sabaghy, J. P. Walker, L. J. Renzullo, and T. J. Jackson. Spatially enhanced passive microwave derived soil moisture: Capabilities and opportunities. *Remote Sensing of Environment*, 209:551 – 580, 2018.
- A. K. Sahoo, G. J. M. De Lannoy, R. H. Reichle, and P. R. Houser. Assimilation and downscaling of satellite observed soil moisture over the little river experimental watershed in Georgia, USA. *Advances in Water Resources*, 52(0):19–33, 2013.
- M. Salvia, F. Grings, P. Ferrazzoli, V. Barraza, V. Douna, P. Perna, C. Bruscantini, and H. Karszenbaum. Estimating flooded area and mean water level using active and passive microwaves: the example of paraná river delta floodplain. *Hydrology and Earth System Sciences*, 15(8):2679–2692, 2011.
- I. Sandholt, K. Rasmussen, and J. Andersen. A simple interpretation of the surface temperature/vegetation index space for assessment of surface moisture status. *Remote Sensing of Environment*, 79(2–3):213–224, 2002.
- E. Santi. An application of the SFIM technique to enhance the spatial resolution of spaceborne microwave radiometers. *International Journal of Remote Sensing*, 31(9):2419–

---

2428, 2010.

- T. Schmugge, P. Gloersen, T. Wilheit, and F. Geiger. Remote sensing of soil moisture with microwave radiometers. *Journal of Geophysical Research*, 79(2):317–323, 1974.
- T. Schmugge, T. Jackson, and H. McKim. Survey of methods for soil moisture determination. *Water Resources Research*, 16(6):961–979, 1980.
- T. J. Schmugge, W. P. Kustas, J. C. Ritchie, T. J. Jackson, and A. Rango. Remote sensing in hydrology. *Advances in Water Resources*, 25(8–12):1367–1385, 2002.
- S. I. Seneviratne, T. Corti, E. L. Davin, M. Hirschi, E. B. Jaeger, I. Lehner, B. Orlowsky, and A. J. Teuling. Investigating soil moisture–climate interactions in a changing climate: A review. *Earth-Science Reviews*, 99(3–4):125–161, 2010.
- L. Shevenell. Regional potential evapotranspiration in arid climates based on temperature, topography and calculated solar radiation. *Hydrological Processes*, 13(4):577–596, 1999.
- H. Shi, X. Fu, J. Chen, G. Wang, and T. Li. Spatial distribution of monthly potential evaporation over mountainous regions: case of the Lhasa River basin, China. *Hydrological Sciences Journal*, 59(10):1856–1871, 2014a.
- J. Shi, P. Guo, T. Zhao, and J. Du. Soil moisture downscaling algorithm for combining radar and radiometer observations for SMAP mission. In *URSI General Assembly and Scientific Symposium (URSI GASS)*, pages 1–4, 16-23 Aug. 2014b.
- Y. Shin and B. P. Mohanty. Development of a deterministic downscaling algorithm for remote sensing soil moisture footprint using soil and vegetation classifications. *Water Resources Research*, 49(10):6208–6228, 2013.
- A. B. Smith, J. P. Walker, A. W. Western, R. I. Young, K. M. Ellett, R. C. Pipunic, R. B. Grayson, L. Siriwidena, F. H. S. Chiew, and H. Richter. The Murrumbidgee soil moisture monitoring network data set. *Water Resources Research*, 48(W07701):6pp., 2012.
- S. Sánchez-Ruiz, M. Piles, N. Sánchez, J. Martínez-Fernández, M. Vall-llossera, and A. Camps. Combining SMOS with visible and near/shortwave/thermal infrared satellite

- 
- data for high resolution soil moisture estimates. *Journal of Hydrology*, 516(0):273–283, 2014.
- C. Song, L. Jia, and M. Menenti. Retrieving high-resolution surface soil moisture by downscaling AMSR-E brightness temperature using MODIS LST and NDVI data. *IEEE Journal of Selected Topics in Applied Earth Observations and Remote Sensing*, 7(3):935–942, 2014.
- P. Srivastava, D. Han, M. Ramirez, and T. Islam. Machine learning techniques for downscaling SMOS satellite soil moisture using MODIS land surface temperature for hydrological application. *Water Resources Management*, 27(8):3127–3144, 2013.
- S. Stisen, I. Sandholt, A. Nørgaard, R. Fensholt, and K. H. Jensen. Combining the triangle method with thermal inertia to estimate regional evapotranspiration—applied to MSG-SEVIRI data in the Senegal river basin. *Remote Sensing of Environment*, 112(3):1242–1255, 2008.
- C. M. Taylor. Detecting soil moisture impacts on convective initiation in Europe. *Geophysical Research Letters*, 42(11):4631–4638, 2015.
- M. Temimi, R. Leconte, F. Brissette, and N. Chaouch. Flood and soil wetness monitoring over the Mackenzie river basin using AMSR-E 37 GHz brightness temperature. *Journal of Hydrology*, 333(2–4):317–328, 2007.
- M. Temimi, R. Leconte, N. Chaouch, P. Sukumal, R. Khanbilvardi, and F. Brissette. A combination of remote sensing data and topographic attributes for the spatial and temporal monitoring of soil wetness. *Journal of Hydrology*, 388(1–2):28–40, 2010.
- S. W. Theis, B. J. Blanchard, and A. J. Blanchard. Utilization of active microwave roughness measurements to improve passive microwave soil moisture estimates over bare soils. *IEEE Transactions on Geoscience and Remote Sensing*, GE-24(3):334–339, 1986.
- R. Torres, P. Snoeij, D. Geudtner, D. Bibby, M. Davidson, E. Attema, P. Potin, B. Rommen, N. Floury, M. Brown, I. N. Traver, P. Deghaye, B. Duesmann, B. Rosich, N. Miranda, C. Bruno, M. L’Abbate, R. Croci, A. Pietropaolo, M. Huchler, and F. Rostan. GMES

- 
- Sentinel-1 mission. *Remote Sensing of Environment*, 120:9–24, 2012.
- S. E. Tuttle and G. D. Salvucci. A new approach for validating satellite estimates of soil moisture using large-scale precipitation: Comparing AMSR-E products. *Remote Sensing of Environment*, 142:207 – 222, 2014.
- F. T. Ulaby, R. K. Moore, and A. K. Fung. Microwave remote sensing: Active and passive. volume 1-microwave remote sensing fundamentals and radiometry. 1981.
- F. T. Ulaby, R. K. Moore, and A. K. Fung. *Microwave remote sensing: Active and passive, in Radar Remote Sensing and Surface Scattering and Emission Theory*, volume 2. Addison-Wesley, Reading, MA, USA, 1982.
- F. T. Ulaby, M. C. Dobson, and D. R. Brunfeldt. Improvement of moisture estimation accuracy of vegetation-covered soil by combined active/passive microwave remote sensing. *IEEE Transactions on Geoscience and Remote Sensing*, GE-21(3):300–307, 1983.
- F. T. Ulaby, P. C. Dubois, and J. van Zyl. Radar mapping of surface soil moisture. *Journal of Hydrology*, 184(1–2):57–84, 1996.
- K. van der Linden, J. V. Giráldez, and M. V. Meirvenne. Spatial estimation of reference evapotranspiration in Andalusia, Spain. *Journal of Hydrometeorology*, 9(2):242–255, 2008.
- R. van der Velde, M. S. Salama, M. D. van Helvoirt, Z. Su, and Y. Ma. Decomposition of uncertainties between coarse MM5–Noah-simulated and fine ASAR-retrieved soil moisture over Central Tibet. *Journal of Hydrometeorology*, 13(6):1925–1938, 2012.
- J. van Doninck, J. Peters, B. De Baets, E. M. De Clercq, E. Ducheyne, and N. E. C. Verhoest. The potential of multitemporal Aqua and Terra MODIS apparent thermal inertia as a soil moisture indicator. *International Journal of Applied Earth Observation and Geoinformation*, 13(6):934–941, 2011.
- H. Vereecken, J. A. Huisman, H. Bogaen, J. Vanderborght, J. A. Vrugt, and J. W. Hopmans. On the value of soil moisture measurements in vadose zone hydrology: A review. *Water Resources Research*, 44(4), 2008.

- 
- A. Verhoef, B. J. J. M. van den Hurk, A. F. G. Jacobs, and B. G. Heusinkveld. Thermal soil properties for vineyard (EFEDA-I) and Savanna (HAPEX-Sahel) sites. *Agricultural and Forest Meteorology*, 78(1–2):1–18, 1996.
- N. E. C. Verhoest, M. J. van den Berg, B. Martens, H. Lievens, E. F. Wood, P. Ming, Y. H. Kerr, A. Al Bitar, S. K. Tomer, M. Drusch, H. Vernieuwe, B. De Baets, J. P. Walker, G. Dumedah, and V. R. N. Pauwels. Copula-based downscaling of coarse-scale soil moisture observations with implicit bias correction. *IEEE Transactions on Geoscience and Remote Sensing*, 53(6):3507–3521, 2015.
- W. Wagner and K. Scipal. Large-scale soil moisture mapping in western Africa using the ERS scatterometer. *IEEE Transactions on Geoscience and Remote Sensing*, 38(4):1777–1782, 2000.
- W. Wagner, G. Lemoine, and H. Rott. A method for estimating soil moisture from ERS scatterometer and soil data. *Remote sensing of environment*, 70(2):191–207, 1999.
- W. Wagner, D. Sabel, M. Doubkova, A. Bartsch, and C. Pathe. The potential of Sentinel-1 for monitoring soil moisture with a high spatial resolution at global scale. In *Symposium of Earth Observation and Water Cycle Science*, 2009.
- W. Wagner, W. Dorigo, R. de Jeu, D. Fernandez, J. Benveniste, E. Haas, and M. Ertl. Fusion of active and passive microwave observations to create an essential climate variable data record on soil moisture. *ISPRS Annals of the Photogrammetry, Remote Sensing and Spatial Information Sciences*, (1-7):315–321, 2012.
- W. Wagner, S. Hahn, R. Kidd, T. Melzer, Z. Bartalis, S. Hasenauer, J. Figa-Saldaña, P. de Rosnay, A. Jann, S. Schneider, J. Komma, G. Kubu, K. Brugger, C. Aubrecht, J. Züger, U. Gangkofner, S. Kienberger, L. Brocca, Y. Wang, G. Blöschl, J. Eitzinger, K. Steinnocher, P. Zeil, and F. Rubel. The ASCAT soil moisture product: A review of its specifications, validation results, and emerging applications. *Meteorologische Zeitschrift*, 22(1):5–33, / 2013.
- J. P. Walker and P. R. Houser. Requirements of a global near-surface soil moisture satellite mission: accuracy, repeat time, and spatial resolution. *Advances in water resources*, 27

- 
- (8):785–801, 2004.
- J. P. Walker, G. R. Willgoose, and J. D. Kalma. One-dimensional soil moisture profile retrieval by assimilation of near-surface measurements: A simplified soil moisture model and field application. *Journal of Hydrometeorology*, 2(4):356–373, 2001.
- J. P. Walker, P. R. Houser, and G. R. Willgoose. Active microwave remote sensing for soil moisture measurement: a field evaluation using ers-2. *Hydrological Processes*, 18(11):1975–1997, 2004.
- J. Wang, Z. Ling, Y. Wang, and H. Zeng. Improving spatial representation of soil moisture by integration of microwave observations and the temperature–vegetation–drought index derived from MODIS products. *ISPRS Journal of Photogrammetry and Remote Sensing*, 113:144–154, 2016.
- L. Wang and J. J. Qu. NMDI: A normalized multi-band drought index for monitoring soil and vegetation moisture with satellite remote sensing. *Geophysical Research Letters*, 34(20), 2007.
- L. Wang and J. J. Qu. Satellite remote sensing applications for surface soil moisture monitoring: A review. *Frontiers of Earth Science in China*, 3(2):237–247, 2009.
- P.-X. Wang, X.-W. Li, J.-Y. Gong, and C. Song. Vegetation temperature condition index and its application for drought monitoring. In *IEEE International Geoscience and Remote Sensing Symposium (IGARSS)*, volume 1, pages 141–143, 2001.
- S. Wang. *Assessments of multiscale precipitation data fusion and soil moisture data assimilation and their roles in hydrological forecasts*. PhD thesis, 2012.
- K. L. Werbylo and J. D. Niemann. Evaluation of sampling techniques to characterize topographically-dependent variability for soil moisture downscaling. *Journal of Hydrology*, 516(0):304–316, 2014.
- A. W. Western, R. B. Grayson, and G. Blöschl. Scaling of soil moisture: A hydrologic perspective. *Annual Review of Earth and Planetary Sciences*, 30(1):149–180, 2002.

- 
- J. P. Wigneron, Y. Kerr, P. Waldteufel, K. Saleh, M. J. Escorihuela, P. Richaume, P. Ferrazoli, P. de Rosnay, R. Gurney, J. C. Calvet, J. P. Grant, M. Guglielmetti, B. Hornbuckle, C. Mätzler, T. Pellarin, and M. Schwank. L-band microwave emission of the biosphere (L-MEB) model: Description and calibration against experimental data sets over crop fields. *Remote Sensing of Environment*, 107(4):639–655, 2007.
- D. J. Wilson, A. W. Western, and R. B. Grayson. A terrain and data-based method for generating the spatial distribution of soil moisture. *Advances in Water Resources*, 28(1): 43–54, 2005.
- X. Wu, J. P. Walker, N. N. Das, R. Panciera, and C. Rüdiger. Evaluation of the SMAP brightness temperature downscaling algorithm using active–passive microwave observations. *Remote Sensing of Environment*, 155(0):210–221, 2014.
- X. Wu, J. P. Walker, C. Rudiger, R. Panciera, and D. A. Gray. Simulation of the SMAP data stream from SMAPEX field campaigns in Australia. *IEEE Transactions on Geoscience and Remote Sensing*, 53(4):1921–1934, 2015.
- X. Wu, J. P. Walker, C. Rüdiger, R. Panciera, and Y. Gao. Intercomparison of alternate soil moisture downscaling algorithms using active–passive microwave observations. *IEEE Geoscience and Remote Sensing Letters*, PP(99):1–5, 2016.
- X. Wu, J. Walker, C. Rudiger, and Y. Gao. Medium-resolution soil moisture retrieval using bayesian merging method. *IEEE Geoscience and Remote Sensing Letters*, 2017.
- Y. Xia, J. Sheffield, M. B. Ek, J. Dong, N. Chaney, H. Wei, J. Meng, and E. F. Wood. Evaluation of multi-model simulated soil moisture in NLDAS-2. *Journal of Hydrology*, 512:107 – 125, 2014.
- N. Ye, J. P. Walker, and C. Rüdiger. A cumulative distribution function method for normalizing variable-angle microwave observations. *IEEE Transactions on Geoscience and Remote Sensing*, 53(7):3906–3916, 2015.
- N. Ye, J. P. Walker, X. Wu, R. d. Jeu, D. Entekhabi, Y. Gao, T. J. Jackson, F. Jonard, E. Kim, O. Merlin, V. Pauwels, L. Renzullo, C. Rüdiger, S. Sabaghy, C. v. H. e, S. H. Yueh, and

- 
- L. Z. a. The soil moisture active passive experiments: Towards calibration and validation of the SMAP mission. *IEEE Transactions on Geoscience and Remote Sensing*, in review.
- M. Yee, J. P. Walker, C. Rüdiger, R. M. Parinussa, T. Koike, and Y. H. Kerr. A comparison of SMOS and AMSR-2 soil moisture using representative sites of the OzNet monitoring network. *Remote Sensing of Environment*, 2017.
- M. S. Yee, J. P. Walker, A. Monerris, C. Rüdiger, and T. J. Jackson. On the identification of representative in situ soil moisture monitoring stations for the validation of SMAP soil moisture products in Australia. *Journal of Hydrology*, 537:367 – 381, 2016.
- X. Zhan, S. Miller, N. Chauhan, L. Di, P. Ardanuy, and S. Running. Soil moisture visible/infrared imager/radiometer suite algorithm theoretical basis document. 2002.
- X. Zhan, P. R. Houser, J. P. Walker, and W. T. Crow. A method for retrieving high-resolution surface soil moisture from hydros l-band radiometer and radar observations. *IEEE Transactions on Geoscience and Remote Sensing*, 44(6):1534–1544, 2006.
- D. Zhang, R. Tang, W. Zhao, B. Tang, H. Wu, K. Shao, and Z.-L. Li. Surface soil water content estimation from thermal remote sensing based on the temporal variation of land surface temperature. *Remote Sensing*, 6(4):3170, 2014.
- Y. Zhang and M. Wegehenkel. Integration of MODIS data into a simple model for the spatial distributed simulation of soil water content and evapotranspiration. *Remote Sensing of Environment*, 104(4):393–408, 10/30/ 2006.
- W. Zhao and A. Li. A downscaling method for improving the spatial resolution of AMSR-E derived soil moisture product based on MSG-SEVIRI data. *Remote Sensing*, 5(12):6790, 2013a.
- W. Zhao and Z.-L. Li. Sensitivity study of soil moisture on the temporal evolution of surface temperature over bare surfaces. *International Journal of Remote Sensing*, 34(9-10):3314–3331, 2013b.